Development and Mechanism of Action of Antimicrobial Coatings

Saeed Behzadinasab

Dissertation submitted to the faculty of the Virginia Polytechnic Institute and State University in partial fulfillment of the requirements for the degree of

Doctor of Philosophy

In

Chemical Engineering

William A. Ducker, Chair

Joseph O. Falkinham, III

Abby R. Whittington

Richey M. Davis

April 24th, 2023

Blacksburg, VA

Keywords: antimicrobial, coatings, functional, surface, copper, cuprous oxide, Cu_2O, antibacterial, mechanism

Copyright 2023 Saeed Behzadinasab

All Rights Reserved

CC BY-NC-ND

Abstract

Development and Mechanism of Action of Antimicrobial Coatings

Saeed Behzadinasab

Microbial diseases infect hundreds of millions of people each year and lead to the death of millions. Infections can also complicate other medical conditions. Some pathogens can transfer from inanimate solid surfaces to humans and thereby cause illnesses. The ability of microbes to survive for long periods of time on such surfaces means that infections from solids are problematic. This dissertation describes the development of 6 different antimicrobial coatings that rapidly inactivate or kill various pathogens. The coatings have various properties that are customized for particular applications. For example, some of the coatings are opaque while some of them are transparent for use on objects, such as cell phone screens, where transparency of the coating is required for the functionality of the object. Some of them are hydrophilic, while others are hydrophobic. Some are deliberately porous to achieve a faster kill, while others are non-porous. Our coatings rapidly kill antibiotics-resistant bacteria, SARS-CoV-2 virus (which is the causative virus for COVID-19 disease), mycobacteria, and fungi. Additionally, our coatings are fabricated using inexpensive and safe ingredients, and the process to prepare the coatings is relatively non-technical.

We developed the first anti-SARS-CoV-2 virus during the global COVID-19 pandemic. This coating used cuprous oxide (Cu_2O) particles as the active ingredient and polyurethane (PU) as the binder. The coating (Cu_2O/PU) caused a reduction of >99.9% of

SARS-CoV-2 within 1 hr, and its effectivity was not lost after the coating was stored in water for 13 days, or repeatedly exposed to the virus. Additionally, we tested the coating against 12 other microorganisms, including Gram-positive (such as methicillin-resistant *Staphylococcus aureus* (MRSA)) and Gram-negative (such as *Pseudomonas aeruginosa (P. aeruginosa*)) bacteria, mycobacteria, fungi, and yeast and we showed the coating kills them rapidly.

We also developed two transparent surfaces using polydopamine (PDA) and copper (Cu) or Cu_2O. One of the coatings was fabricated using a single step co-deposition of Cu_2O particles in dopamine solution. The dopamine self-polymerizes into a conformal layer and maintained the particles in place on the surface. The coating killed *P. aeruginosa* (>99.9%) and MRSA (~97%) within 10 minutes, and inactivated ~99.9% of SARS-CoV-2 in 1 hr. Another transparent coating was prepared using an initial deposition of PDA, followed by electroless deposition of a thin Cu layer. This coating killed >99.9% of *P. aeruginosa* and ~99% of MRSA in 10 minutes, and inactivated >99.9% of COVID-19 virus in 1 hr.

While the EPA standard for an antimicrobial coating is to achieve 99.9% reduction in 1-2 hours, individuals share items at a much faster scale, typically in minutes, so the appropriate time scale for killing is minutes. We developed a porous antimicrobial coating for this purpose. Our porous antimicrobial coating was prepared by fabricating a porous PMMA scaffold via heat treatment of PMMA particles, then depositing a conformal PDA layer, followed by electroless deposition of copper. The coating was also hydrophilic to allow infiltration of microbial droplets and hence very

fast inactivation of the suspended pathogens. The coating killed >99.9% of drug-resistant bacteria in only 5 minutes, achieving a half-life of 21 second.

An important challenge in turning regular surfaces into antimicrobials is that the process is typically too difficult for a non-technical people. Also, over time coatings will wear out and get covered with oil and other debris that will reduce its potency against pathogens. We developed methods for easily coating regular surfaces with antimicrobial coatings. The antimicrobial coating was deposited on a commercial wrap that has an adhesive-backing of the type that is commonly used by consumers on kitchen drawers. Without any tools, the antimicrobial wrap can be placed on any solid surface or removed from it to restore the original surface. We fabricated two wraps: PU/Cu_2O and PDA/Cu_2O. Both antimicrobial wraps killed ~99.9% of human pathogen in 10 min.

In addition, a hydrophilic coating using the tetrapod morphology of zinc oxide (ZnO-T) and a PU layer was developed. This coating soaked in the microbial droplets and caused a 99.9% reduction of SARS-CoV-2 virus compared to the uncoated surface in 1 hr.

To understand how exactly our coatings kill pathogens, we extensively studied the antimicrobial mechanism of Cu_2O-containing coatings against *P. aeruginosa*. We found the leaching of copper species from Cu_2O particles is strongly dependent upon the leaching medium. For example, little copper leaches into phosphate buffer saline (PBS) while large quantities of that leaches into Dulbecco's Modified Eagle Medium (DMEM). Therefore the results of antimicrobial tests and efficacy in the field may depend on the medium in which the pathogen is suspended. We demonstrated that there is a strong

correlation between the concentration of leached copper and the killing of *P. aeruginosa*, and that the contact between pathogenic cells and solid antimicrobial surface is not required, while the proximity of the two is crucial. We also showed that the generation of Reactive Oxygen Species (ROSs) is not involved in the mechanism of action of the coatings.

Additionally, we investigated the transfer of SARS-CoV-2 virus from various solids to skin. Using a very small microbial droplet and a light force of contact between the surface and the skin, we found 13–16% (0.8–0.9 log less than the input droplet) of the virus transferred from non-porous solids to skin when the virus-containing droplet was still wet, and 3–9 % transferred when the droplet had dried. Also, very little quantities of the virus transferred to the skin from hydrophilic porous surfaces, presumably due to to viral deposition on interior pore spaces.

Also, this dissertation will discuss the effects of surface properties on microbial survival, particularly SARS-CoV-2, along with the challenges and opportunities that face the field of antimicrobial coatings.

Abstract (General Audience)

Development and Mechanism of Action of Antimicrobial Coatings

Saeed Behzadinasab

Antimicrobial coatings can inhibit the spread, via surfaces, of various diseases that infect humans. Antimicrobial coatings are useful because they can continue to kill pathogens (germs) for a long time after the surface is coated. This is a big improvement over use of common disinfectants that must be applied continuously. The main goal of this dissertation research is to develop various surface coatings that are antimicrobial and can provide a rapid killing of germs. We demonstrate 6 different antimicrobial coatings that rapidly inactivate a wide variety of pathogens, such as the most recent coronavirus, drug-resistant bacteria, or fungi. The antimicrobial coatings were composed of a variety of adhesives and active antimicrobial ingredients. Traditional adhesives and recently-invented adhesives were incorporated into the coatings, and active ingredients included copper, copper oxide, or zinc oxide. In short, our coatings provide a short killing period of a few minutes to one hour.

Additionally, we investigated the mechanism of action of copper oxide surface coatings, and determined that the proximity of microbial cells to an antimicrobial surface is the key to inactivation or killing of the pathogen.

Also, we measured the transfer of the most recent coronavirus from solid surfaces to skin under various conditions. We found that a substantial quantity of the virus is transferred to skin. More specifically, when the virus-infected droplet is still wet, a higher

percentage is transferred from the solid to skin. In addition, we composed a review of the scientific literature on antimicrobial coatings with a focus on coatings and methods that inactivate the coronavirus.

Dedication

To my mother, Homa

To my father, Mohammad

To my spouse, Yasaman

To my brother, Masoud

For their endless love, support,

Sacrifice, care, and encouragement.

Acknowledgements

First, I would like to express my deepest gratitude to my family. I am grateful to my parents, Mohammad and Homa, whose continuous care, support, and encouragement has enabled me to be where I am today. To my soulmate, Yasaman, you entered my life at a time when I needed you the most. You bring purpose, joy, and happiness in my life. I am incredibly grateful and lucky that I am married to you. I would also like to thank my brother, who instilled in me the importance of diligent study and encouraged me to pursue graduate studies in the US.

I would like to thank the teachers who played important roles in my educational journey since elementary school. Additionally, I owe a debt of gratitude to the professors during my undergraduate studies at Shiraz University from whom I learned the fundamentals of science and engineering. The insights and teachings that I learned from them, particularly, Payam Setoodeh, Sona Raeissi, Ali Shariati, and Mohammad Farsi, will follow me in my life. I am also indebted to my M.Sc. advisor, Julie Albert, for teaching me invaluable laboratory techniques and the fundamentals of polymer science.

During my Ph.D. years at Virginia Tech, I had the opportunity to work with many exceptional individuals. I would like to acknowledge my colleagues at the Ducker's lab: Jimmy Ritter, who helped me with challenging statistics concepts, Zechen Zhang, who taught me some basic laboratory techniques, Saurabh Sharma, who taught me the basic microbiology techniques, Mohsen Hosseini, and Zach Benmamoun. Also, I am thankful to Xu Feng, Stephen McCartney, McAlister Council-Troche, for their technical support with XPS, SEM/EDS, and ICP-MS equipment. Moreover, I would like to thank the undergraduate students, Jared Arkfeld, Mete Aktuglu, and Chris Stolls, whom I mentored and supervised. I enjoyed working with all of you.

Additionally, I thank Kevin Holshouser for his help in manufacturing some laboratory equipment.

During my research at Virginia Tech, I enjoyed collaborating with many scientists in other fields and I extend my sincere gratitude to each of them, namely, Leo Poon, Alex Chin, Irving Allen, and Hannah Ivester. I, also, express my deepest gratitude to Joseph Falkinham and Myra Williams for their unwavering and invaluable collaboration. As a result, we were able to achieve substantial research milestones. Additionally, I learned a lot from Joeseph Falkinham who is a role model for hard work and tireless dedication.

I extend my heartfelt appreciation to my dissertation committee members, Abby Whittington, Richey Davis, and Joseph Falkinham, for their review and valuable insights provided for this dissertation. Their informative comments have improved the quality of this work.

I extend my thanks to the following for financially supporting me over the past few years: the Department of Chemical Engineering for supporting most of my doctorate program via various Graduate Teaching Assistantships (GTAs), Macromolecules Innovation Institution through a Graduate Research Assistantship (GRA), the College of Engineering via a GRA, and William Ducker by a GRA supported via his various grant fundings. During my GTA assignments, I enjoyed helping Abby Whittington, John Hassler, and William Ducker as their GTA in different courses.

Life during graduate school can be challenging and demanding and I am incredibly thankful to my friends, who have been a source of support and companionship throughout this journey. I am grateful to Ali, Mohammad, Homayoun, and Mona among many others who are

too many to individually name. Your friendship has brought joy and laughter I had amazing times hanging out and enjoying life with all of you.

Lastly, but not least, I want to express my sincere gratitude to my Ph.D. advisor, William Ducker, for his scholarly support, guidance, advice, and feedback during my Ph.D. journey. I am deeply appreciative of his time, expertise, and guidance throughout this process. I learned a lot from him in research and scientific topics, particularly in the field of surface science and colloids, and the lessons and skills I have acquired under his mentorship will be with me throughout my future endeavors.

Table of Contents

Abstract ii

Abstract (General Audience) vi

Dedications viii

Acknowledgements ix

CHAPTER 1. INTRODUCTION 1

1.1. CFU AND $TCID_{50}$ METHODOLOGY 4
1.2. CALCULATION OF MICROBIAL SURVIVAL AND REDUCTION 6
1.3. ACTIVE INGREDIENTS 7
1.4. COPPER AS AN ANTIMICROBIAL 9
1.5. SURFACE ROUGHNESS 13
1.6. MECHANISM OF CELLULAR DEATH BY COPPER 14
REFERENCES 15

CHAPTER 2. A SURFACE COATING THAT RAPIDLY INACTIVATES SARS-COV-2 32

2.1. ABSTRACT 33
2.2. INTRODUCTION 34
2.3. MATERIALS AND METHODS 36
2.3.1. Materials 36
2.3.2. Fabrication of the Films 36
2.3.3. Characterization of the Cu_2O Films 38
2.3.4. Characterization of the Cationic Films 38
2.3.5. Inactivation of SARS-CoV-2 39
2.4. RESULTS AND DISCUSSION 40
2.4.1. The Cu2O/PU Film Rapidly Inactivates SARS-CoV-2 40
2.4.2. The Cu_2O/PU Film Remains Potent after Multiple Exposures to Virus or Storage under Water 44
2.4.3. The Cu_2O/PU Film is Robust 45
2.4.4. A Coating of a Cationic Polymer Coating Did Not Speed Inactivation of SARS-CoV-19 46
2.5. CONCLUSIONS 46
REFERENCES 49
2.6. SUPPORTING INFORMATION 53
2.6.1. Alternative methods for preparing the Cu_2O/PU film. 64
References 81

CHAPTER 3. TRANSPARENT AND SPRAYABLE SURFACE COATINGS THAT KILL DRUG-RESISTANT BACTERIA WITHIN MINUTES AND INACTIVATE SARS-COV-2 VIRUS 82

3.1. ABSTRACT 84
3.2. INTRODUCTION 85
3.3. RESULTS AND DISCUSSION 88

3.3.1. The antimicrobial coatings are transparent *88*
3.3.2. Other characterization of the coatings *90*
3.3.3. Inactivation of microbes *92*
3.3.3.1. Both transparent coatings kill bacteria in 10 minutes 92
3.3.3.2. Both coatings rapidly inactivate SARS-CoV-2 94
3.3.4. Mechanism of action *96*
3.3.5. The PDA/Cu_2O coating is sprayable *96*
3.3.6. Other aspects of the coatings *97*
3.4. CONCLUSION 98
3.5. EXPERIMENTAL SECTION 99
3.5.1. Materials *99*
3.5.2. Fabrication of the surface coatings *99*
3.5.2.1. Fabrication of PDA/Cu coating 99
3.5.2.2. Fabrication of PDA/Cu_2O coating 100
3.5.3. Characterization *101*
3.5.4. Antibacterial assay *101*
3.5.5. SARS-CoV-2 assay *103*
3.5.6. Calculation of microbe Survival and Reduction *103*
3.5.7. Statistical analysis *104*
REFERENCES 107
3.6. SUPPORTING INFORMATION 117
3.6.1. Additional materials and methods: *118*
3.6.1.1. Antibacterial assay 118
3.6.1.2. Abrasion tests 118
3.6.2. Additional characterizations *120*
3.6.3. Characterization of PDA/Cu2O coating that was prepared by spray-coating *129*
3.6.4. Data tables of bacterial and viral tests *130*
References *137*

CHAPTER 4. POROUS ANTIMICROBIAL COATINGS FOR KILLING MICROBES WITHIN MINUTES 138

4.1. ABSTRACT 139
4.2. INTRODUCTION 140
4.3. RESULTS AND DISCUSSION 144
4.3.1. The pore structure is retained after addition of the PDA/Cu layer *144*
4.3.2. The porous PDA/Cu coating allows for very rapid imbibition and drying of droplets *145*
4.3.3. Porous PDA/Cu stainless steel is highly antimicrobial *146*
4.3.4. Our assay is effective at extracting bacteria from the porous coating *149*
4.3.5. Porous antimicrobial polymer coating *151*
4.3.6. Abrasion Resistance *154*
4.3.7. Other Characteristics of the PMMA Coating *155*
4.4. CONCLUSION 156
4.5. EXPERIMENTAL SECTION 158
4.5.1. Materials *158*
4.5.2. Fabrication of porous PMMA scaffold test samples *158*
4.5.3. Deposition of antimicrobial PDA/Cu surface coating *159*

4.5.4. Characterization *160*
4.5.5. Antibacterial Assay *160*
4.5.5.1. Choice of Microbial Strain. 160
4.5.5.2. Growth of Microbial Strains. 160
4.5.5.3. Preparation of Microbial Strains for Testing. 161
4.5.5.4. Measurement of Viable Cell Number. 161
4.5.5.5. Measurement of Surface-Killing. 161
4.5.6. Abrasion tests *162*
4.5.7. Statistical Analysis *163*
4.5.8. Calculation of Microbial Reduction *163*
REFERENCES 167
4.6. SUPPORTING INFORMATION 176
4.6.1. Supplementary methods *177*
4.6.1.1. Abrasion tests 177
4.6.2. Supplementary Results *179*
4.6.2.1. SEM images of uncoated porous SS scaffold 179
4.6.2.2. XPS, EDS, and SEM images of coated porous SS 180
4.6.2.3. SEM image of flat SS surfaces 183
4.6.2.4. Extraction of bacteria from porous and non-porous solids 184
4.6.2.5. SEM images of porous PMMA scaffold 186
4.6.2.6. CFU measurements for flat or porous PMMA scaffolds 188
4.6.2.7. Photographs of water droplet absorbing into PDA/Cu-coated porous PMMA. 189
4.6.2.8. Porous PMMA scaffold does not possess antimicrobial properties. 190
References *191*

CHAPTER 5. ANTIMICROBIAL ACTIVITY OF CUPROUS OXIDE AND CUPRIC OXIDE-COATED SURFACES 192

5.1. STRUCTURE SUMMARY 193
5.1.1. Background *193*
5.1.2. Aims *193*
5.1.3. Methods *193*
5.1.4. FINDINGS *194*
5.1.5. Conclusion *194*
5.2. INTRODUCTION 195
5.3. MATERIALS AND METHODS 197
5.3.1. Materials *197*
5.3.1.1. Materials for Preparation of Antimicrobial Copper Surfaces 197
5.3.1.2. Fabrication of Cu_2O/PU coating[27] 198
5.3.1.3. Fabrication of partially-sintered CuO coating[29] 198
5.3.2. Measurement of Antimicrobial Activity *198*
5.3.2.1. Growth of Microbial Strains 198
5.3.2.2. Preparation of Microbial Cells for Surface Killing Measurements 199
5.3.2.3. Measurement of Surface-Killing 200
5.3.3. Cytotoxicity study *200*
5.4. RESULTS 201
5.4.1. Controls and Validation *201*

5.4.2. Both Cu_2O/PU and Sintered CuO Coatings have broad-spectrum antimicrobial activity *201*
5.4.3. Repeated Disinfection/Cleaning of the Cu_2O/PU Coating with ethanol over 20-weeks Did Not Reduce Killing *204*
5.4.4. The PU/Cu2O and Sintered CuO coatings are Not Cytotoxic Against Human Monocytes and Murine Fibroblasts *205*
5.4.5. Antimicrobial Activity of Cu_2O/PU Coating Survive Abrasion *206*
5.5. DISCUSSION 208
5.5.1. Are Cells Killed or Are They Simply Trapped in the Matrix? *208*
5.5.2. Widespread application of the Cu_2O/PU coating *210*
5.6. CONCLUSION 210
REFERENCES 212
5.7. SUPPLEMENTARY MATERIAL 219
5.7.1. Supplementary Materials and Methods *220*
5.7.1.1. Abrasion Tests 220
5.7.1.2. Statistical Analysis 220
5.7.1.3. Cytotoxicity Experiments 221
5.7.2. Supplementary Results and Discussion *222*
5.7.2.1. Characterization of Coatings 222
5.7.2.2. Tests of Microbial Survival on Surfaces 225
5.7.2.3. Survival of P. aeruginosa and S. aureus at Higher Cell Densities 235
5.7.2.4. Bacterial Killing as a Function of Cell Density 236
5.7.2.5. Cu_2O/PU Coating Kills Bacteria Rapidly 238
5.7.2.6. Comparison of killing of S. aureus and Methicillin-resistant S. aureus by Sintered CuO Coating at 0 Time Point 240
5.7.2.7. Survival of bacteria on uncoated stainless-steel control 241
References *242*

CHAPTER 6. FACILE IMPLEMENTATION OF ANTIMICROBIAL COATINGS THROUGH ADHESIVE FILMS (WRAPS) DEMONSTRATED WITH CUPROUS OXIDE COATINGS 243

6.1. ABSTRACT 244
6.2. INTRODUCTION 245
6.3. RESULTS 248
6.3.1. Preparation and Characterization of the Antimicrobial Wraps *248*
6.3.2. The Wraps are Highly Antimicrobial *249*
6.3.3. The Antimicrobial Wraps is Easy to Replace *253*
6.3.4. Other Characteristics of the Coating *254*
6.4. CONCLUSION 255
6.5. MATERIALS AND METHODS 256
6.5.1. Materials *256*
6.5.2. Fabrication of antimicrobial PU/Cu2O Wrap *257*
6.5.3. Fabrication of Antimicrobial PDA/Cu2O Wrap *257*
6.5.4. Characterization of Test Solids *258*
6.5.5. Antibacterial Assay *258*
6.5.5.1. Choice of Microbial Strain 258
6.5.5.2. Growth of Microbial Strains 258

6.5.5.3. Preparation of Microbial Strains for Testing 258
6.5.5.4. Measurement of Viable Cell Number 259
6.5.5.5. Measurement of Surface-Killing 259
6.5.6. Statistical Analysis *260*
6.5.7. Calculation of Microbial Survival and Reduction *260*
REFERENCES 264

CHAPTER 7. REDUCTION OF INFECTIVITY OF SARS-COV-2 BY ZINC OXIDE COATINGS 272

7.1. ABSTRACT 273
7.2. INTRODUCTION 274
7.3. RESULTS 277
7.3.1. Characterization *277*
7.3.2. ZnO Coatings Reduce Infectivity of SARS-CoV-2 ..... *279*
7.4. DISCUSSION 281
7.5. CONCLUSIONS 286
REFERENCES 290
7.6. SUPPORTING INFORMATION 298
7.6.1. Materials and Methods *299*
7.6.1.1. Materials 299
7.6.1.2. Fabrication of ZnO/Silica 299
7.6.1.3. Fabrication of ZnO-T/PU 300
7.6.1.4. Fabrication of porous glass surfaces 301
7.6.1.5. Characterization 301
7.6.1.6. Preparation of SARS-CoV-2 culture 302
7.6.1.7. Inactivation of SARS-CoV-2 302
7.6.1.8. ASTM D3359 adhesion test 303
7.6.1.9. Statistical Tests 303
References *316*

CHAPTER 8. ANTIMICROBIAL MECHANISM OF CUPROUS OXIDE (Cu_2O) COATINGS 318

8.1. ABSTRACT 320
8.2. INTRODUCTION 321
8.3. RESULTS AND DISCUSSION 326
8.3.1. The Concentration of Dissolved Copper Species is a Strong Function of the Solution Composition. *326*
8.3.2. Leaching and Drying Can Alter the Oxidation State of Copper *329*
8.3.3. Killing of P. aeruginosa Depends on the Buffer and is Correlated with the Buffer Copper Content. *331*
8.3.4. Cu_2O Solid Surfaces Kill Bacteria in PBS. *335*
8.3.5. Direct Contact with Cu_2O is not Necessary for Killing by Cu_2O *336*
8.3.6. Generation of ROSs is not Involved in the Mechanism *338*
8.3.7. Effect of Light on the ability of Cu2O to Kill P. aeruginosa *340*
8.4. CONCLUSION 342
8.5. MATERIALS AND METHODS 344
8.5.1. Materials *344*

8.5.2. Light/Dark Experiments ... *345*
8.5.3. Preparation of the Antimicrobial Cu_2O/PU Coating ... *345*
8.5.4. Preparation of CMC-coated Cu_2O/PU ... *346*
8.5.5. Characterization of Coatings ... *346*
8.5.6. Preparation of Solutions for Ion Leaching Experiments ... *346*
8.5.7. Preparation of ICP-MS Samples ... *347*
8.5.8. Measurement of Antimicrobial Activity ... *347*
8.5.8.1. Growth of Microbial Strains ... 347
8.5.8.2. Preparation of Microbial Cells ... 348
8.5.8.3. Measurement of Killing by Leached Copper ... 348
8.5.8.4. Measurement of Surface-Killing ... 349
8.5.9. Statistical Analysis ... *349*
8.5.10. Calculation of Microbial Reduction ... *349*
REFERENCES ... 352
8.6. SUPPORTING INFORMATION ... 366
8.6.1. Composition of DMEM ... *367*
8.6.2. Supplementary Results ... *369*
8.6.2.1. Supplementary ICP-MS data ... 369
8.6.2.2. Supplementary XPS data ... 370
8.6.2.3. Addition of BCCA to Cu_2O leachates ... 371
8.6.2.4. SEM images of CMC coating ... 372
8.6.2.5. Supplementary XPS data ... 373
References ... *374*

CHAPTER 9. SARS-COV-2 VIRUS TRANSFERS TO SKIN THROUGH CONTACT WITH CONTAMINATED SOLIDS ... 375

9.1. ABSTRACT ... 376
9.2. INTRODUCTION ... 377
9.3. MATERIALS AND METHODS ... 378
9.3.1. Artificial Skin ... *378*
9.3.2. Artificial Finger ... *379*
9.3.3. Transfer Experiment ... *379*
9.3.4. SARS-CoV-2 Assay ... *380*
9.3.5. Statistical analysis ... *381*
9.4. RESULTS ... 381
9.5. DISCUSSION ... 389
9.6. CONCLUSIONS ... 390
REFERENCES ... 392
9.7. SUPPLEMENTARY INFORMATION ... 398
Supplementary Materials and Methods ... *399*
9.7.1. Materials ... *399*
9.7.2. Methods ... *400*
9.7.2.1. Characterization ... 400
9.7.2.2. Fabrication of porous glass test solids ... 400
9.7.2.3. Preparation of SARS-CoV-2 culture ... 401
9.7.2.4. SARS-CoV-2 assay ... 401
9.7.2.5. qPCR test ... 402

9.7.3. Characterization of Samples ... *403*
9.7.3.1. Vitro-Skin® ... 403
9.7.3.2. Porous Glass ... 406
9.7.4. Transfer Apparatus ... *407*
9.7.5. Data Analysis ... *408*
9.7.6. Mass Balance for Transfer Efficiency ... *409*
9.7.7. Calculation of the transfer ratio by another method. ... *412*
9.7.8. Data tables ... *413*
9.7.9. Additional figures ... *416*
References ... *423*

CHAPTER 10. THE VIABILITY OF SARS-COV-2 ON SOLID SURFACES ... 424

10.1. Abstract ... 425
10.2. Introduction ... 426
10.3. SARS-CoV-2 RNA on public surfaces ... 431
10.4. Pioneering studies of the Longevity of SARS-CoV-2 on Solids ... 433
10.5. Effect of Environmental Conditions ... 434
10.6. Stability on Common Solids ... 435
10.7. Stability on Antimicrobial Coatings ... 437
10.8. Mechanism of action against SARS-CoV-2 ... 440
10.8.1. Attack of the virus by dissolved Cu(I) or Cu(II) species. ... *441*
10.8.2. Generation of reactive oxygen species (ROS) at the solid–liquid interface or by dissolved species ... *441*
10.8.3. Contact-killing ... *442*
10.8.4. Adsorption ... *443*
10.8.5. Surface Wettability ... *444*
10.8.6. Drying of the respiratory droplet in contact with the solid ... *444*
10.9. Inactivation of the SARS-COV-2 virus in suspensions ... 446
10.10. Other Methods for Inactivating SARS-CoV-2 at Surfaces ... 448
10.11. Facemasks and Clothing ... 450
10.12. Future Perspectives ... 454
10.12.1. Characterization of Surfaces ... *454*
10.12.2. Porosity ... *455*
10.12.3. Active ingredients ... *455*
10.12.4. Multiple Organisms. ... *455*
10.12.5. Transfer from Surfaces to Humans ... *456*
10.12.6. The mechanism of the inactivation of SARS-CoV-2 ... *456*
10.13. Summary ... 456
References ... 458

CHAPTER 11. CONCLUSIONS AND FUTURE WORK ... 470

11.1. Conclusions ... 470
11.2. Future Work ... 471
References ... 473

Table of Figures

Figure 2-1. Cross section view of the Cu_2O/polyurethane film. 39
Figure 2-2. Time course of viable titer of SARS-CoV-2 on solids, with and without a coating of cuprous oxide microparticles bound with polyurethane (Cu_2O/PU). Note that the vertical axis in on a log10 scale. Data is shown for coated glass and coated stainless steel. Individual circular data points represent each independent measurement and the × symbol represents the mean of the log of independent measurements. The detection limit was 90 TCID50/mL (shown with a dotted line). Experimental results where virus was not detected are plotted at 90 TCID50/mL and are included in the average as 90 TCID50/mL. SARS-CoV-2 is inactivated much more rapidly on the coated surface than on the bare surface. 43
Figure 2-3. Time course of viable titer of SARS-CoV-2 on glass coated in Cu2O/PU that was subjected to 5 cycles of exposure to SARS-CoV-2 plus soaking in 70% ethanol. The uncoated glass was also subjected to the disinfection cycles. 45
Figure 3-1. A) and C) photographs of PDA/Cu and PDA/Cu_2O coatings, respectively, held in front of a computer monitor. Both coatings are transparent and allow all colors to be seen in transmission. B) and D) visible spectra of the coatings. B) Transmission spectra of PDA, and the PDA/Cu coating. Data for PDA is from the PDA that was prepared in the first step of making the PDA/Cu coating (designated as PDA_{Cu}). D) Transmission spectra of PDA, and the PDA/Cu coating. The PDA was prepared by the same method as the PDA/Cu_2O coating, but without adding the Cu_2O particles (designated as PDA_{Cu2O}). The spectra of the two PDAs (i.e. PDA_{Cu} and PDA_{Cu2O}) are similar. To ensure that coatings formed on one side only for the optical measurements, the PDA_{Cu} and PDA/Cu coatings were prepared with tape covering one side of the glass. The tape was removed prior to spectrometry. The background for the visible spectra is glass 89
Figure 3-2. Plan view SEM images of the coatings. A) PDA-only from an intermediate step in fabrication of the PDA/Cu coating. B) PDA/Cu coating. The copper coating is apparent from the slight roughening of the coating as well as the filling of depressions compared to A. C) plan view PDA/Cu_2O coating. D) 50-degree tilt of magnified view of PDA/Cu_2O coating. The PDA meniscus that holds Cu_2O particles is shown with a white arrow. Further images are shown in Supporting Information Figure S3-3 & Figure S3-4 91
Figure 3-3. Time course of survival of *P. aeruginosa* (PA) and methicillin-resistant staphylococcus aureus (MRSA) on transparent PDA/Cu (left) and PDA/Cu_2O (right) coatings. Survival was calculated with Equation 3-3 so zero represents the CFU in the initial droplet. For the coatings, each symbol represents the average of 3 separate samples, the error bar is the comparison interval from ANOVA, and the detection limit for each bacterium is shown with a dotted line. Compared to glass control, within 10 minutes, the PDA/Cu coating caused a Reduction of more than 99.99% of *P. aeruginosa* and 99.18% of MRSA, and the PDA/Cu_2O caused a Reduction of more than 99.94% of *P. aeruginosa* and 96.82% of MRSA. We performed a 3-way ANOVA with each of the coatings: factor 1 = surface type (glass vs each coating), factor 2 = time, factor 3 = bacteria type (*P. aeruginosa* and MRSA). The *p*-values for surface type were $< 10^{-10}$ for PDA/Cu and $< 10^{-9}$ for PDA/Cu_2O. 93
Figure 3-4. Time course of SARS-CoV-2 titer for transparent PDA/Cu (left) and PDA/Cu_2O (right) coatings. Each marker shows the average of 3 independent samples and the error bars are the comparison interval from ANOVA. The detection limit was 90 TCID50/mL (shown with

dotted line). When data was below the detection limit, the point was plotted at the detection limit. PDA/Cu reduces the infectivity of SARS-CoV-2 by 99.98% and PDA/Cu_2O reduces the infectivity by 99.88% in 1 hour. We performed a 2-way ANOVA with each of the coatings: factor 1 = surface type (glass vs each coating), factor 2 = time. The *p*-value for coating was $< 10^{-8}$ for PDA/Cu and $< 10^{-6}$ for PDA/Cu_2O. 95
Figure 4-1. Cross-section SEM images of the porous stainless steel A) without and B) with the PDA/Cu coating. 145
Figure 4-2. Photographs showing the time for a 10 μL water droplet to imbibe into the PDA/Cu-coated porous stainless steel structure. 146
Figure 4-3. Time course of P. aeruginosa on flat PDA/Cu and porous PDA/Cu coatings. Compared to the control SS, the porous PDA/Cu coating causes a reduction of 99.83% of P. aeruginosa within only 3 minutes, while the same coating in a flat configuration causes a 77.82% reduction (see Equation 4-3 in the Experimental Section for the equation for reduction). The bacteria input on the coatings and the detection limit for the bacterium is shown with dotted lines. Each symbol represents the average of two independent samples. A 3-way ANOVA gave the following p values: porosity (porous vs flat), $p = 0.008$; surface type (uncoated vs coated sample), $p < 10^{-6}$; and time, $p < 10^{-4}$. The 2-way interactions are as follows: $p_{\text{surface type and time}} < 10^{-4}$, $p_{\text{surface type and porosity}} = 0.0135$, $p_{\text{time and porosity}} = 0.0436$. The 3-way interaction p-value between all three factors is 0.038, which indicates that over time, the porosity makes a difference if the antimicrobial coating is present. 147
Figure 4-4. CFUs of P. aeruginosa extracted from solids compared to the CFUs input on the solid. A very high percentage of bacteria is extracted from the porous coating. The detection limit is 50 CFU. There is a small, but not significant ($p = 0.071$) decrease in the CFU for porous stainless steel compared to the input, but this also occurs for flat stainless steel (see Figure 4-3 and Figure S4-5). After the porous structure was coated with PDA, the bacteria were still extracted ($p = 0.44$ comparing input and extracted). 150
Figure 4-5. SEM images of porous PMMA scaffold fabricated by partial sintering of PMMA particles through 2 h of heat treatment at 125ºC (above T_g). (A) Image showing the retained porosity and (B) Image showing the formation of polymer “necks” or frozen mensci. Further images are in Figure S4-7. 151
Figure 4-6. SEM images of porous antimicrobial coating (scaffold = PMMA). The antimicrobial layer (PDA/Cu) was successfully prepared inside the pores of the porous PMMA scaffold. 153
Figure 4-7. Time course of bacteria on uncoated flat PMMA (control) and PDA/Cu-coated porous PMMA. Porous PDA/Cu coating is highly effective. The porous PDA/Cu causes a reduction of >99.99% of P. aeruginosa in 5 minutes compared to the uncoated sample ($p = 0.009$). Each symbol represents the average of two separate samples, and the error bars are standard deviation. The bacteria input on the coatings and the detection limit for the bacterium is shown with dotted lines. To determine the effect of porosity, we compared the PDA/Cu-coated porous material to the flat PDA/Cu material on SS, assuming that the underlying support was not important. For a 2-way ANOVA with factors of sample ($p < 0.001$), time ($p < 0.001$), and the sample-time ($p < 0.001$), were significant, providing additional support for the hypothesis that porosity speeds the killing of P. aeruginosa. 153
Figure 4-8. Bacteria tests with abraded porous PDA/Cu coating. The abraded coatings kill 99.9% of bacteria within 5 minutes. The detection limit (i.e., all bacteria were dead) is 50 CFU. (* represents $p < 0.05$; ns represents $p > 0.05$) 155

Figure 5-1. Cytotoxicity study of the coatings. Cell lysis caused by Cu2O/PU or sintered CuO coatings was negligible compared to full lysis. 206
Figure 6-1. (**A**) Plan-view and (**B**) cross-section SEM images of PU/Cu_2O wrap. The thickness of the coating was approximately 12 μm. For SEM imaging, the coating was prepared on glass. 248
Figure 6-2. SEM images of PDA/Cu2O wrap. (A) Plan-view SEM image and (B) 50 degree tilt image. The coating was prepared on glass..... 249
Figure 6-3. Survival of *P. aeruginosa* on PU/Cu_2O wrap. The PU/Cu_2O wrap caused a reduction of 99.97% and >99.99% of *P. aeruginosa* in 10 and 20 min, respectively, compared to the uncoated wrap. Survival was calculated using Equation 6-1. Each point in this and subsequent figures of survival represents the average of three independent measurements, and the error bars represent the standard deviation. Some error bars are smaller than the size of the symbols..... 251
Figure 6-4. Survival of *P. aeruginosa* on PU/Cu_2O wrap that was not heat-treated or plasma-treated. The wrap caused a reduction of 96.81% and >99.99% of *P. aeruginosa* in 10 and 20 min, respectively. Some error bars are smaller than the size of the symbols. 252
Figure 6-5. Survival of *P. aeruginosa* on PDA/Cu_2O wrap. The PDA/Cu_2O wrap caused a reduction of 99.80% and >99.99% of *P. aeruginosa* in 10 and 20 min, respectively. The reduction compared to the uncoated wrap was >99.9% ($p < 0.001$) again for 20 min exposure. 253
Figure 6-6. Series of photographs demonstrating the ability to apply, remove, and reapply an antimicrobial wrap to stainless steel (SS). (**A**) Bare SS. (**B**) Initial application of antimicrobial wrap to SS. (**C**) After removal of wrap. (**D**) After application of a new antimicrobial wrap to the same SS. Removal and replacement of the wraps took less than one minute. 254
Figure 6-7. Survival of *P. aeruginosa* on an aged PU/Cu_2O wrap (no heat or plasma treatments). The antimicrobial wrap was 3.5 months old at the time it was tested. The aged wrap caused a reduction of >99.99% of *P. aeruginosa* in 20 min. Some error bars are smaller than the size of the symbols. 255
Figure 7-1. Photograph of A) ZnO/Silica coating and B) ZnO-T/PU coating. SEM images of C) the surface ZnO/Silica, D) the surface ZnO-T/PU, E) Cross-section of ZnO/Silica coating, F) Cross-section of ZnO-T/PU coating, G) Silica menisci (necks) between ZnO particles in ZnO/Silica coating and H) Higher resolution cross-sectional image of ZnO-T/PU sample. Arrows point to regions where the coating is amorphous and therefore there is a large volume fraction of PU. Other regions have a lower volume fraction of PU and hence greater porosity. Note scale difference for ZnO/Silica compared to ZnO-T/PU SEM images. 278
Figure 7-2. Decay of SARS-CoV-2 TCID50 titer on A) ZnO/Silica and B) ZnO-T/PU coatings on glass. Diamonds and circles show independent titer measurements, × represents the average of the log titer at each time, and the dashed line shows the detection limit of the assay (90 TCID50/mL). The error bars are the 95% confidence interval. In comparison to uncoated glass, the virus titer has a 99.98% Reduction on ZnO/Silica (p = 10-3, one tail, unpaired) and 99.97% Reduction on ZnO-T/PU after one hour (p = 7×10-5, one tail, unpaired). 281
Figure 7-3. Decay of SARS-CoV-2 TCID50 titer on porous glass compared to flat glass. The two glass surfaces are soda-lime glass, and have similar chemistry (See XPS in Figure S7-9). Diamonds and circles show independent titer measurements, × represents the average of the log titer at each time, the dashed line shows the detection limit of the assay (90 TCID50/mL), and the error bars are the 95% confidence interval. The virus titer on porous glass at 0 and 1 hr time

points are not statistically different (p = 0.33, one tail, unpaired) confirming its inactive nature against SARS-CoV-2. 285
Figure 8-1. XPS spectra of an aqueous droplet dried onto polyethylene (red lines). Each droplet contained leachate from Cu_2O into DMEM (top) or DI water (bottom). For DMEM, the leachates are Cu^+, whereas for DI water, the leachates are a mixture of Cu^+ and Cu^{2+}. Blue lines are fitted Cu(I) spectra and the green lines are fitted Cu(II) spectra. 330
Figure 8-2. Effect of leachate solution on bacterial kill. Aqueous solution where indicated. Kill was measured by CFU and copper concentrations were measured by ICP-MS. Points labelled Cu were prepared form solid Cu compounds; no leaching was done. The kill depends strongly on the leaching solution and there is a linear relationship between log kill and the log soluble copper (slope = 1.3 ± 0.4, excluding Cu(II) points). The copper solutions were CuCl and $CuCl_2$. Higher concentrations of Cu^+ could not be prepared from CuCl because of the solubility limit. 332
Figure 8-3. Bacterial (P. aeruginosa) test with leached copper at various conditions. The sodium bicarbonate concentration was 88 mM and the DMEM included 2% v/v FBS. The detection limit (i.e., all bacteria are dead) is log CFU = 1.7. 333
Figure 8-4. Effect of 10 equivalents of BCCA chelating agent on the antimicrobial activity of Cu_2O leachate. The concentration of BCCA used was 10 times the amount of copper that was measured by ICP-MS in that solution. BCCA reduces the antimicrobial effect of the leachate into both DMEM and bicarbonate (44 mM), which suggests that Cu^+ is the potent antimicrobial that leaches from Cu_2O. Data for 1.5 equivalents of BCCA is shown in Figure S8-2. 334
Figure 8-5. Killing of P. aeruginosa from droplets on Cu_2O-coated surfaces. The Cu_2O/PU coating causes a reduction of 99.16% in 10 min (p = 0.0069). The detection limit is log CFU = 1.7. 336
Figure 8-6. Effect of a CMC layer on the ability of Cu_2O/PU coatings to kill of P. aeruginosa. The Cu_2O/PU coating is good at killing, whether or not it is coated in CMC. With the CMC layer, the Cu_2O/PU caused a reduction of 99.2% and without the CMC layer, there was a reduction of 99.6% in 10 min and we did not resolve a difference (p = 0.739). The detection limit is log CFU = 1.7. 2-way ANOVA resulted in the following p-values: $p_{time} < 10^{-9}$, $p_{coating} < 10^{-7}$, and $p_{interaction} < 10^{-7}$. 338
Figure 8-7. Effect of illumination on the antimicrobial properties of Cu_2O. The coating kills *P. aeruginosa* very well under the three light conditions we studied. The bottom dotted line shows the detection limit, which was 50 CFU. 341
Figure 9-1. Mean percentage transfer to an artificial finger from various solid material during a 5 sec contact with a 3 N (300 g) load with no lateral motion (i.e., no rubbing). Error bars are the comparison intervals from ANOVA with two factors: the material and the time, which corresponds to wet or evaporated. The error bar is asymmetric because of the exponential distribution of measurement residuals. When the upper bound is off-scale, it is indicated by a number. The time to adsorb the droplet on porous surfaces was as follows: tissue and porous glass, immediate; wood, 1-2 min; and paper, 2.5 min. Note that the transfer is high for non-porous solids and is measurable when the 1 μL test drop is wet (10 sec) or has evaporated (30 min). Each data point was obtained from three independent measurements that are tabulated in Supplementary Table 9-1. 385
Figure 9-2. Log($TCID_{50}$/mL) values (x) and population marginal means (o) on artificial skin after transfer from various solids. The population marginal means were calculated from Post Hoc comparison using N-way ANOVA (two factors: material and wet/evaporated) in MATLAB using the Dunn-Sidák's approach. The bars represent the comparison interval; two groups are

statistically different if their intervals do not overlap. Transfer is detectable for all solids, except tissue, wood (dry), porous glass (dry), and paper (dry), and these data points have been plotted on the detection limit of 90. Transfer is greater for wet solids than for dry and there is no significant difference among common non-porous solids. 388
Figure 10-1. A. Infection via a fomite. B. Engineered coating to reduce infection. 427
Figure 10-2. Possible mechanisms of inactivation of SARS-COV-2 on solids. 440
Figure 10-3. The effect of droplet drying on the surface. The concentration of dissolved species increases, and diffusion times get shorter. Passage of the air-liquid interface subjects adsorbed virus to a tension that may damage the virus. 446

Table of Tables

Table 2-1. Average reduction of SARS-CoV-2 titer on Cu2O/PU coated solid in 1 h compared to titer on uncoated solid in 1h. 42
Table 5-1. Relative Survival of microbes on cuprous oxide/polyurethane (Cu2O/PU) or sintered cupric oxide (CuO) coatings compared to on stainless steel. *Time since contact of the droplet with the sample; in practice, time = zero is actually a few minutes processing time. "<" indicates that no colonies were formed on the coated sample and the number following is the % if 1 colony were formed on the agar plate. †The difference in results for the two S. aureus strains for CuO at zero time was large. To test whether the difference was significant, we performed a second round of experiments, described in Supporting Materials, 2.5, and concluded that there was not a significant difference. ‡Data for stainless steel in Table S5-10. 203
Table 5-2. Repeated killing of S. aureus and P. aeruginosa on rinsed and disinfected Cu2O/PU coating. The contact time between bacteria and the coating was 1 h, except in week 20, when it was 1.5 h 205
Table 5-3. Survival of P. aeruginosa on fresh and abraded Cu_2O/PU coatings. Abraded coupons are as effective as the fresh ones. Two-tailed heteroscedastic P-value for log(CFU_{coated}) of fresh vs abraded coatings is 0.42, i.e., we found no significant effect of the rubbing. 207
Table 8-1. Total copper concentration as measured by ICP-MS. The medium has a strong effect on the equilibrium copper concentration. The error is the standard deviation rounded to one significant figure. The final entry in the table is for leaching from CMC-coated particles into PBS solution. Additional data is shown in Table S8-2. 329
Table 8-2. Total Effect of ascorbic acid on the CFUs of *P. aeruginosa* that were placed in suspension on Cu_2O. The addition of ascorbic acid in bacteria suspension did not impact the killing of bacteria in 10 min, which suggests that ROSs were not important for killing. 339
Table 8-3. Total Control experiments for ROSs mechanism Data shows CFU of *P. aeruginosa* after various treatments of Cu_2O/PU. Treatment with H_2O_2, ascorbic acid, or a mixture of the two does not affect the killing of bacteria. 340
Table 9-1. Mean water contact angle measurements of test solids. The figure after ± sign is the 95% confidence interval. The contact angle was measured 10 seconds after the droplet was placed on the solid. 386

Attributions

This dissertation includes copies of our scientific articles that are published or manuscripts that are pending for publication. All published papers are reproduced with permission. Below is listed the citations for each publication along with details of author contributions.

Chapter 2

Full citation: **Behzadinasab, S.**, Chin, A., Hosseini, M., Poon, L., & Ducker, W.A. (2020). A Surface Coating that Rapidly Inactivates SARS-CoV-2. *ACS Applied Materials & Interfaces*, 12(31), 34723-34727, https://doi.org/10.1021/acsami.0c11425

Author Contribution: W.D. conceived of the experiments. W.D. and S.B. prepared the samples. S.B. characterized the samples unless otherwise noted. M.H. performed the cross-hatch test. The preparation of SARS-CoV-2 and experiments containing the virus were done by A.W.H.C. Analysis of data was done by W.D., S.B, A.W.H.C., and L.L.M.P. Supervision was done by W.D. and L.L.M.P. The original manuscript was written by W.D. The manuscript was edited by W.D., S.B., A.W.H.C., and L.L.M.P, and it was reviewed by all authors.

Chapter 3

Full citation: **Behzadinasab, S.**, Williams, M., Hosseini, M., Poon, L.L.M., Chin, A.W.H., Falkinham III, J.O., & Ducker, W.A. (2021). Transparent and Sprayable Surface Coatings that Kill Drug Resistant Bacteria and Inactivate SARS-CoV-2 Virus Within

Minutes, *ACS Applied Materials & Interfaces*, 13(46), 54706–54714, https://doi.org/10.1021/acsami.1c15505

Author Contribution: S.B. conceived of the experiments. S.B. and W.D. designed the methodology. S.B. performed all experiments unless otherwise noted. The experiments containing bacteria and SARS-CoV-2 virus were done by M.W, and A.W.H.C, respectively. Analysis of data was done by S.B. and W.D. Supervision was done by W.D., J.F, and L.L.M.P. The original manuscript was written by S.B. The manuscript was edited by S.B., W.D., J.F., A.W.H.C, and L.L.M.P, and it was reviewed by all authors.

Chapter 4

Full citation: Behzadinasab, S., Williams, M.D., Aktuglu, M., Falkinham III, J.O., & Ducker, W.A. (2023). Porous Antimicrobial Coatings for Killing Microbes within Minutes, *ACS Applied Materials & Interfaces*, 15(12), 15120–15128, https://doi.org/10.1021/acsami.2c22240

Author Contribution: W.D. and S.B. conceived of the experiments. S.B. and W.D. designed the methodology. S.B. performed all experiments unless otherwise noted. M.A. was an undergraduate student working under the supervision of S.B. M.A. helped prepare some of the recipe for porous PMMA scaffolds. The experiments containing bacteria were done by M.W. Analysis of data was done by S.B. and W.D. Supervision was done by W.D. and J.F. The original manuscript was written by S.B. The manuscript was edited by S.B., W.D., and J.F., and it was reviewed by all authors.

Chapter 5

Full citation: **Behzadinasab, S.**, Hosseini, M., Williams, M.D., Ivester, H.M., Allen, I.C., Falkinham III, J.O., & Ducker, W.A. (2022). Antimicrobial Activity of Cuprous Oxide- and Cupric Oxide-Coated Surfaces, *Journal of Hospital Infection*, 129, 58-64, https://doi.org/10.1016/j.jhin.2022.07.022

Author Contribution: W.D. conceived of the experiments. S.B. performed all the experiments unless otherwise noted. M.H. prepared the cupric oxide samples. The preparation of microorganisms and experiments containing them were done by M.W. and J.F. Analysis of data was done by J.F., S.B., and W.D. Supervision was done by W.D. and J.F. The original manuscript was written by S.B. The manuscript was edited by S.B., W.D., and J.F., and it was reviewed by all authors.

Chapter 6

Full citation: **Behzadinasab, S.**, Williams, M.D., Falkinham III, J.O., & Ducker, W.A. (2023). Facile Implementation of Antimicrobial Coatings through Adhesive Films (Wraps) demonstrated with Cuprous Oxide Coatings, *Antibiotics,* 12(5), 920, https://doi.org/10.3390/antibiotics12050920

Author Contribution: S.B. conceptualized and designed the project. S.B. and W.D. designed the methodology. S.B., W.D., J.F. validated the experiments. S.B., and W.D analyzed the data formally. S.B., W.D., J.F., and M.W. investigated the experiments and details. The original manuscript was written by S.B. The manuscript was edited by S.B., W.D., J.F., and M.W., and reviewed by all authors. Supervision was done by W.D. and J.F.

Project administration was done by W.D., and funding acquisition was done by W.D. and J.F.

Chapter 7

Full citation: Hosseini, M., **Behzadinasab, S.**, Chin, A.W.H., Poon, L.L.M., & Ducker, W.A. (2021). The Inactivation of SARS-CoV-2 virus by Zinc Oxide Coatings, *ACS Biomaterials Science & Engineering*, 7(11), 5022–5027, https://doi.org/10.1021/acsbiomaterials.1c01076

(co-first authorship)

Author Contribution: S.B. and M.H. contributed equally to this article. W.D., S.B., and M.H. developed the methodology. S.B. prepared and characterized ZnO-T samples. M.H. performed similarly for ZnO samples. The experiments containing SARS-CoV-2 virus were done by A.W.H.C. Analysis of data was done by S.B, M.H., and W.D. Supervision was done by W.D. and L.L.M.P. The original manuscript was written by M.H. The manuscript was edited by M.H., W.D., S.B., A.W.H.C., and L.L.M.P, and it was reviewed by all authors.

Chapter 8

Full citation: Behzadinasab, S., Williams, M.D., Falkinham III, J.O., & Ducker, W.A. Antimicrobial Mechanism of Cuprous Oxide (Cu_2O) Coatings, *ACS Applied Materials & Interfaces*, *submitted*

Author Contribution: W.D. and S.B. conceived of the experiments. S.B. and W.D. developed the methodology. S.B. performed all experiments unless otherwise noted. The

experiments containing bacteria were done by M.W. Analysis of data was done by S.B. and W.D. Supervision was done by W.D. and J.F. The original manuscript was written by S.B. The manuscript was edited by S.B., W.D., and J.F., and it was reviewed by all authors.

Chapter 9

Full citation: **Behzadinasab, S.**, Chin, A.W.H., Hosseini, M., Poon, L.L.M., & Ducker, W.A. (2021). SARS-CoV-2 Virus Transfers to Skin Through Contact with Contaminated Solids, *Scientific Reports*, 11(1), 1-7, https://doi.org/10.1038/s41598-021-00843-0

Author Contribution: W.D. and L.L.M.P. conceived of the experiments and W.D. designed the transfer apparatus. W.D. and S.B. designed the artificial finger and designed the experiments. S.B. prepared and characterized the samples unless otherwise noted. M.H. fabricated the porous glass samples. Analysis of data was done by W.D., S.B., A.W.H.C., and L.L.M.P. The preparation of SARS-CoV-2 and experiments containing the virus were done by A.W.H.C. Supervision was done by W.D. and L.L.M.P. The manuscript was written by S.B. and W.D. with input from all authors.

Chapter 10

Full citation: Hosseini, M., **Behzadinasab, S.**, Benmamoun, Z., & Ducker, W.A. (2021). The Viability of SARS-COV-2 on Solid Surfaces. *Current Opinion in Colloid & Interface Science*, 101481, https://doi.org/10.1016/j.cocis.2021.101481

(co-first authorship)

Author Contribution: S.B. and M.H. contributed equally to this article. W.D. conceived of the article. Supervision was done by W.D. The original manuscript was written by W.D., M.H., S.B., and Z.B. The manuscript was edited and reviewed by all authors.

Additionally, below is the list of publications that I have contributed to. They are not, however, included in this dissertation.

1. **Full citation:** Hosseini, M., Chin, A.W.H., **Behzadinasab, S.**, Poon, L.L.M., & Ducker, W.A. (2021). Cupric Oxide Coating That Rapidly Reduces Infection by SARS-CoV-2 via Solids. *ACS Applied Materials & Interfaces*, 13(5), 5919-5928, https://doi.org/10.1021/acsami.0c19465
2. **Full citation:** Hosseini, M., Chin, A.W.H., Williams, M., **Behzadinasab, S.**, Falkinham III, J.O., Poon, L.L.M., & Ducker, W.A. (2022). Transparent Anti-SARS-CoV-2 and Antibacterial Silver Oxide Coatings, *ACS Applied Materials & Interfaces*, 14(7), 8718–8727, https://doi.org/10.1021/acsami.1c20872

Chapter 1. Introduction

More than 1,400 pathogens are known to exist that can cause diseases in humans, and 150 of which have the "potential to cause epidemic or endemic disease".[1] It is also likely that in the future, new pathogens will arise, as evidenced by the COVID-19 pandemic. Microbial diseases cause hundreds of millions of infections in the world annually, and as a result, unfortunately millions of the infected individuals die.[2-3] A report by the World Health Organization (WHO) indicated that every year more than 17 million people die as a result of infectious diseases.[4] In addition, billions of dollars are required to treat such infections. These diseases can spread to humans through a variety of ways: by airborne droplets,[5-6] contaminated foods or drinks,[7] contaminated solid surfaces (i.e. "fomites"),[8-12] bloodborne,[13] and so on.

Various microbes, including parasites, viruses, bacteria, and fungi can cause acute illness in humans.[14] Microbes that cause diseases are called pathogens. Microbes may also induce or contribute to chronic diseases. For example, hepatitis B virus HBV can trigger chronic hepatitis,[15] or pneumonia bacteria can worsen or cause cardiovascular diseases.[16]

Among microbial diseases, drug-resistant pathogens are most troublesome. A recent report indicated that annually 1.2 million people die solely due to antibiotic-resistant bacteria.[17] Antibiotic-resistance has been called the "silent pandemic" as it causes a very high level of mortality and morbidity while receiving little attention by the media.[18] Additionally, the number of approvals for new antibiotics by the U.S. has declined in the last few decades,[19] and scientists have been calling on pharmaceutical companies to start research and development of new antibiotic medicine. The US Centers for Disease Control and Prevention (CDC) recently reported[20-21] during the global COVID-19 pandemic, antibiotic-resistant infections has rose.

Additionally, drug-resistant diseases can occur in the general community as well as in hospitals.[22]

Two particularly problematic antibiotic-resistant bacteria are methicillin-resistant *Staphylococcus aureus* (*S. aureus*), also known as MRSA, and multidrug-resistant *Pseudomonas aeruginosa* (*P. aeruginosa*). MRSA is a strain of *S. aureus* that has developed or acquired drug resistance to beta-lactam antibiotics, a group that includes some derivatives of penicillin including methicillin.[23] Multidrug-resistant *Pseudomonas aeruginosa* (*P. aeruginosa*), as the name suggests, are the strains of *P. aeruginosa* that have obtained resistance to multiple antibiotics[24], such as tobramycin, aminopenicillin, penicillin G, cephalosporins, piperacillin, cefepime and tazobactam, ceftazidime. *P. aeruginosa* is particularly worrisome because it has a strong ability to develop resistance to new antibiotics, by adapting to the environment.[25]

Both of MRSA and *P. aeruginosa* bacteria have been declared a "Serious Threat" by the CDC in 2017 and 2019,[26-28] and they can cause a wide range of infections in blood, in lung, on skin, etc.[29] As a result, they cause high incidence of disease in both healthcare settings as well as the general community, and thus they are both Healthcare-Associated Infections (HAIs) and Community-Associated Infections (CAIs).[30-31] Each of these bacteria can survive on solid surfaces for very long periods of time,[32] and form biofilms on solids.[33] The survival of the bacteria depends upon the type of surface, but it ranges from 7 days to 7 months for MRSA, and a period of 6 hr up to 16 months for *P. aeruginosa*.[32] Both bacteria are known to spread to humans via contact with contaminated surfaces or skins.[34-35] To stop surface transmission, it would be very helpful to kill the bacteria shortly after they land on solids.

The important point is that it would be better to prevent an infection than to cure it. Obviously an infection that does not happen does not cause human suffering. In addition, the main treatment of bacterial infections is via antibiotics, and such treatments cause antibiotic resistance, and side effects. It is hoped that by reducing the rate of infections, fewer antibiotic treatments will be needed and fewer antibiotic resistant bacteria will arise.

Another disease that has severely impacted life is the global COVID-19 pandemic: between early 2020 to March 2023, it *officially* caused nearly 700 million infections and 6.9 million deaths,[36] while it is estimated the actual mortality was 3 times as high for the first 1.5 years.[37] The financial cost to the Unites States was approximately 16 trillion dollars in the first year alone.[38] This viral disease is caused by severe acute respiratory syndrome coronavirus 2 (SARS-CoV-2), which is similar to severe acute respiratory syndrome coronavirus (SARS-CoV) that caused an outbreak in 2003. Another similar virus (MERS-CoV) caused the outbreaks in 2012, 2015, and 2018. However, neither of SARS-CoV or MERS-CoV caused such widespread chaos and high mortality and morbidity rates as SARS-CoV-2.

While the primary method of disease transmission for SARS-CoV-2 is believed to be via airborne droplets, the virus can also spread by contaminated surfaces.[39] As the World Health Organization mentions: “fomite transmission is considered a likely mode of transmission for SARS-CoV-2”.[39] Experimental work also shows that the virus can be transferred substantially from solids to skin.[40] A study on hamsters showed inhalation of infectious droplets is the main cause of disease spread, but also one of three of the hamsters got infected when they were exposed to infected solids only.[41] Mathematical modelling the disease also indicated that fomite transmission makes up for up to 25% of disease transmission.[42] The COVID-19 virus also remains infectious up to 7 days on solid surfaces.[43] At room temperature it is stable for up to 9 hr

on a dead human skin model[44], or up to 4 days on dead pig skin.[45] Thus, there has been fear of touching communal objects, and authorities recommended frequent handwashing to help reduce disease transmission.

Typical disinfectants such as 70% alcohol are useful chemicals to disinfect solid surfaces to reduce spread of disease. However, a major problem is that minutes after the alcohol is evaporated, recontamination can occur. Another problem is that some disinfectants, such as bleach, are dangerous and hazardous to human health.[46] An efficient method is to use antimicrobial surface coatings that provide a continuous kill, and to apply them to solid surfaces. It has been shown that antimicrobial coatings are effective in a healthcare setting;[47] for example, after an antimicrobial coating was applied in a hospital, the quantity of bacteria on solids and the number of healthcare-acquired infections were reduced.[47] Also, using antimicrobial coatings on hospital surfaces correlated with a reduction in infections [48]. Several antimicrobial surface coating have been developed for such a purpose, against bacteria[49-52] or viruses[49, 52-57], and have been reviewed recently[58-60]. The criteria set by the US Environmental Protection Agency (EPA) standard for antimicrobial coatings is that they should achieve a reduction of 99.9% of the test microbes in 1-2 hour.[61-62]

1.1. CFU AND $TCID_{50}$ METHODOLOGY

Microorganisms are quantified by various methods. In this work, the quantification of bacteria was done via counting Colony Forming Units (CFUs) on plates, while in our viral assays, 50% Tissue Culture Infectious Dose ($TCID_{50}$) methodology was employed. Both methods are explained in detail below.

The CFU counting method is based on the fact that CFUs are formed by viable bacteria cells, with each cell forming one CFU. Bacteria cells multiply and increase in number under favorable conditions. For example, at very low temperatures, bacteria cells freeze, and their metabolic activity slows down. Therefore, they cannot reproduce and multiply to form colonies. In this dissertation, a temperature of 37 °C was used to grow bacteria. 37 °C is the optimized temperature which allows obtaining data with the highest resolution.

In the CFU counting methodology, a bacteria suspension is serially diluted with specific ratios, and each dilution is plated on an agar plate (agar plates provide required nutrition for growth of cells). Subsequently, the plates are incubated at 37 °C overnight to allow sufficient time for growth of CFUs. Then, a plate with a colony count between 30 and 300 is chosen and the colonies are counted. The dilution of the plate is then incorporated, and the CFU/mL of the bacteria suspension is calculated.

Viruses are metabolically inactive microorganisms and they cannot reproduce on their own. Therefore, they need a cell as a host to be able to multiply, reproduce, and cause an infection. As a result, $TCID_{50}$ is a measure of the infectivity of a virus. In the $TCID_{50}$ assay used in this work, Vero E6 cells as a surrogate for human cells were employed. Vero E6 cells are a standard cell line that was isolated from the kidney of an African green monkey and they lack antiviral activity, making an ideal host for viruses.

The $TCID_{50}$ assay involves introducing a serially diluted virus suspension in a well-plate where each well contains the same quantity of the host cells. After incubating the well-plate under optimal conditions for 5 days, the cells are carefully inspected for signs of infection. The

well with 50% infected cells is identified, the dilution of the well's virus suspension is incorporated, and the $TCID_{50}$/mL of the original viral suspension is calculated.

1.2. Calculation of Microbial Survival and Reduction

As mentioned, the CFU counting method includes cells that are viable and form colonies. Therefore, the term "kill" is used to quantify the cells that cannot reproduce. Log kill and % kill are calculated as follows:

$$\log \text{kill} = \text{mean}\left[\log_{10}\left(\frac{\text{input titer}}{\text{units}}\right)\right] - \text{mean}\left[\log_{10}\left(\frac{\text{sample titer}}{\text{units}}\right)\right] \quad \text{Equation 1-1}$$

$$\% \text{ kill} = \left[1 - 10^{-\log \text{kill}}\right] \times 100 \quad \text{Equation 1-2}$$

Some pathogens are gradually killed or inactivated on their own overtime. To account for this gradual inactivation, the term "reduction" is used. Log reduction and % reduction are calculated according to the below equations:

$$\log \text{reduction} = \text{mean}\left[\log_{10}\left(\frac{\text{uncoated sample titer}}{\text{units}}\right)\right] - \text{mean}\left[\log_{10}\left(\frac{\text{antimicrobial sample titer}}{\text{units}}\right)\right] \quad \text{Equation 1-3}$$

$$\% \text{ reduction} = \left[1 - 10^{-\log \text{Reduction}}\right] \times 100 \qquad \text{Equation 1-4}$$

1.3. Active Ingredients

To prepare an antimicrobial surface coating, an active ingredient is necessary. Some metals and metal oxides have been shown to have useful antimicrobial properties.[63-69] Copper (Cu)[70], cuprous oxide (Cu_2O)[63], cupric oxide (CuO)[71], silver (Ag)[72], silver oxide (Ag_2O)[69], zinc (Zn)[73], zinc oxide (ZnO)[64], gold (Au)[74], titanium oxide (TiO_2)[75], cadmium (Cd)[76], and others, are examples of such antimicrobials. Also, some organic materials, polymers, and peptides possess antimicrobial properties. Quaternary ammonium[77], polyethylenimine[78], layer by layer structures by polycation and polyanions[79], human cathelicidin[80], Magainin I[81], bovine lactoferrin[82] are among those. In addition, it is possible to achieve antimicrobial properties by texturizing surfaces.[83-85]

For example, in a publication by Dhabarde et al.[86] studied the development of an antimicrobial coating using titania (TiO_2) nanotubes. Titania is a photocatalyst that causes oxidation. In that work, titania nanotubes with a range of morphologies and aspect ratios (the ratio of length to diameter) were synthesized by an anodization process. Both human coronavirus and SARS-CoV-2 virus were tested and the authors found the coating caused complete inactivation of the viruses after 30 sec of UV-C of illumination. It was also shown that illumination of UV-C alone caused a ~4 log reduction (uncoated control titer minus sample titer) in the viral titer, but with the coating it caused ~2 more logs. However, UV-C is a very dangerous and hazardous light and cannot be illuminated while living organisms are nearby.

In a study by Fu et al.[87], an antiviral surface coating was prepared using thin films of TiO_2 with various compositions. The coatings were transparent (~75% transmittance with visible light), hydrophilic (contact angle up to 40 degrees), and smooth (average roughness of < 100 nm). While illuminated with 365 nm UV light, the coating with the highest antiviral characteristic caused a 5.5 log reduction of MS2 bacteriophage in 90 min, which was used as a surrogate for SARS-CoV-2.

Heo et al.[88] discussed a light-activated antimicrobial coating made through sol-gel. The coating used a photosensitizer (crystal violet) and silica-alumina sol-gel to produce singlet oxygen, which is a Reactive Oxygen Species (ROS), thus killing bacteria. The coating caused a ~3 log reduction of bacteria while visible light was illuminated, but when it was tested in the dark, nearly no killing of bacteria was resulted. Additionally, some performance tests, such as scratch test, abrasion, pencil test, tape adhesion, or immersion in water, were conducted on the coating and the coating passed all tests. Also, the coating's cytotoxicity against human cells was evaluated and the researchers concluded the coating has no adverse effect against the cells.

Zhang et al.[89] prepared an antimicrobial coating by incorporating polyhexamethylene guanidine molybdate in an epoxy coating to prevent bacterial biofilms from forming. They noted the antimicrobial coating stays potent in long term with no biofilm on the coating after 120 days. Also, the coating was immersed in seawater and fewer fouling microorganisms were present on the coating after the same time period.

1.4. Copper as an Antimicrobial

Among antimicrobials, copper has attracted more attention because it has other desirable practical characteristics: copper is inexpensive (~$7 per kilogram), while silver costs nearly $900/kg. Copper has excellent and broad antimicrobial properties against bacteria, viruses, fungi, and other microbes. Also copper is relatively safe; copper (oxide)-containing textiles used in clinical and animal studies have been shown no adverse effects on skin.[90] The environmental Protection Agency (EPA) concludes that[91]: "Current available literature and studies do not indicate any systemic toxicity associated with copper exposure. … There are no residential or occupational risks of concern resulting from exposure to copper products." As a result, some antibacterial coatings using copper or copper oxide have been developed previously.[70, 92-94] Our group has developed surface coatings using copper and copper oxide that will be discussed further in this dissertation.[49, 53, 95-96]

The first anti-COVID-19 surface coating was developed as part of my dissertation work, but here some of the later coatings are described. Our anti-SARS-CoV-2 coating does not require any costly lab instrumentation and is rapidly prepared.[53] To prepare the coating, Cu_2O (cuprous oxide) particles were added to a thin layer of commercial polyurethane (PU), and the coating (called Cu_2O/PU) is cured for 2 hours.[53] In this dissertation, the work will be discussed in detail.

Hutasoit et al.[54] prepared an anti-COVID-19 surface coating using a cold spray method. The coating was prepared by spraying micron-sized copper particles using a specialized spray system, where a high temperature was required to deposit the particles. This was followed by a secondary thermal annealing process to the films, and then polishing to obtain a uniform surface. After monitoring the viral reduction over time, they found that the annealed sample caused a

reduction of 96%, while the as-deposited sample decreased SARS-CoV-2 infectivity by 92%. For a 5-hr contact time, the annealed coating caused a 99.2% reduction. The authors speculated that release of cuprous ions from the coating, as well as contact killing caused the inactivation of SARS-CoV-2. However, this study uses specialized cold spraying methods that are expensive and specialized.

Jampa et al.[97] studied the effectivity of Cu_2O in zeolite nanoparticles. While the weight of the Cu_2O compared to the whole zeolite system was relatively low (up to 9 wt%), the zeolite/ Cu_2O showed high thermal stability compared to Cu_2O nanoparticles. The researchers conducted tests against Gram-positive and Gram-negative bacteria, SARS-CoV-2, and porcine coronavirus and showed the coating inactive 99.9% of each microbe. Also, the coating's cytotoxicity was determined on an embryo (zebrafish) and the authors concluded the cytotoxicity was lower than Cu_2O alone. Similar results were found when performing a skin irritation test with human epidermis.

In a publication by Gonçalves et al.[98], the scientists incorporated Cu_2O or copper nanoparticles on the surface and they found the antimicrobial surface kills bacteria in 45 sec. *S. aureus* (Gram-positive), *K. pneumoniae* (Gram-negative), and *P. aeruginosa* (Gram-negative) were tested in that study and the coating was effective against all 3 microorganisms, showing broad antimicrobial efficacy of copper against microbes. DNA degradation and fragmentation was found after bacteria was killed by the surface, and therefore the authors concluded the mechanism of action was oxidative stress by the Cu/Cu_2O nanoparticles.

Shigetoh et al.[99] investigated the nanostructured Cu, Cu_2O, and CuO thin films prepared by a sputtering method. The antimicrobial surfaces were tested against bacteriophage Φ6

(enveloped) and bacteriophage Qβ (non-enveloped), and it was reported the resulted in 5 logs, 3 logs, and <1 log inactivation of the bacteriophage for Cu, Cu_2O, and CuO surfaces, respectively, in 30 minutes. It was shown Cu or Cu_2O have much higher antimicrobial characteristics than CuO. While the researchers showed the surfaces were still active after 1 month of exposure to the atmospheric air, some of their antimicrobial properties decreased.

In a work by Alhussein et al.[100], 316 SS surfaces were sputtered with copper (oxide). The SS surface was initially mechanically treated to enhance its roughness for the Cu/Cu_2O layer. The authors noted that the coating killed 3-4 logs of bacterial (*E. coli*) cells within 30 minutes. However, in the study, sputtering occurred at ~10^{-5} Pa. Additionally, a pure copper target and an inert Ar environment were needed for the process. The requirements of vacuum and Ar environments can significantly limit the application of this method.

Foffa et al.[101] reported the preparation of a spray coating based on copper nanoparticles and polyurethane. They synthesized Cu nanoparticles (diameter <100 nm), mixed them with polyurethane that was dissolved in THF (tetrahydrofuran) and dioxane, and sprayed the suspension onto the surface. They allowed the coating to dry for 3 hr at 40 °C and subsequently illuminated with UV light for 2 hr. The authors reported 92% and 99% inactivation of SARS-CoV-2 virus in 5 and 30 minutes respectively.

Liu et al.[102] fabricated an antimicrobial stainless steel (SS) by sintering a mixture of SS and copper particles at 900 °C and 50 MPa. The antimicrobial surface achieved a 99.75% inactivation of SARS-CoV-2 titer in 3 hr. Also, the surface inactivated >99.99% of *E coli.* or H1N1 virus over 6 hr. While the SS showed relatively acceptable antimicrobial properties, the temperature and pressure requirements limit its wide-spread use. Additionally, in a similar

system, the researchers incorporated silver instead of copper in the SS but they reported no significant inactivation of SARS-CoV-2 was observed, concluding that silver does not have antiviral properties against the coronavirus.

In a research by Saud et al.[103], a Cu^{2+}-releasing coating for inactivation of the COVID-19 virus was developed. The authors used a pigment that released Cu^{2+} in an organic coating, and they showed the antimicrobial coating caused a 6-log reduction of SARS-CoV-2 titer in 4 hr. The authors investigated various weight ratios of Cu^{2+}-releasing pigment to organic materials and they concluded to have great efficiency, the Cu^{2+}-releasing pigment needs to make up of at least 50 wt% of the whole coating. They, however, noted that the presence of fouling proteins decreases the efficacy of the coating.

In addition to the presence of antimicrobial ingredients, other factors may also affect stability of pathogens on surfaces. For example, the temperature or relative humidity affect the survival of microorganisms.[104-106] Multiple studies have proven that the SARS-CoV-2 virus is inactivated on its own more rapidly with increasing temperature.[104-106] An impactful paper by Chin et al.[43] demonstrated that the virus was inactivated naturally at higher temperatures: at a commercial refrigerator temperature (4 °C) the virus infectivity decayed little over a 2-week test period, while no active virus was detected after only 5 minutes at 70 °C. This shows that temperature is clearly a strong factor. One may consider increasing temperature as a mean of disinfecting surfaces, but heat treating all surfaces is impractical, and heating has the same weakness as liquid disinfectants (e.g.,70% ethanol solution): once the solids cool down to the room temperature, re-contamination can shortly occur.

1.5. Surface Roughness

Surface roughness is another important factor that can affect antimicrobial activity of coatings and surfaces.[85] In a publication by Hasan et al [107], the authors made a nanostructured aluminum for this purpose. Specifically, the aluminum was etched by sodium hydroxide to fabricate 'ridges' that were ~20 nm wide. The authors noted that this etching process increased the root mean square roughness 1000-fold, from <1 nm to ~1 μm. The static contact angle decreased from 96.3° to 17.7°. Comparing the stability of microbes on etched sample and smooth surfaces, they showed that the etched surface was able to cause a 99.999% reduction in 6 hours and >99% reduction in 3 hours, while it took the flat aluminum 48 hours to cause a similar reduction. They attributed the enhanced inactivation to adsorption of the virions within the nanostructure texture.[107] The study showed that the increasing of roughness inactivates viruses much faster. Additionally, a similar phenomenon has been shown previously for killing of bacteria. Ivanova et al.[84] demonstrated a cicada wing kill bacteria due to its micro scale roughness.

Luanghane and Pewnim[108] modified the surface of 304 stainless steel (SS) to nanostructures for antimicrobial characteristics. The authors chose SS because it is a widely used material in facilities, such as hospitals, where bacterial contamination is likely to happen. Several SS surfaces were modified using an electrochemical process with various parameters that resulted in creation of nano morphologies on the surfaces. They reported the surface with the most antimicrobial properties showed a ~50% reduction in bacteria adhesion after 24 hr. However, 50% reduction in a long time such as 24 hr is very mild compared to the other results in this summary and is unlikely to be of practical use.

1.6. Mechanism of Cellular Death by Copper

Upon the contact between pathogenic cells and copper or cuprous oxide surface coatings, various parts of the cells can be damaged. It has been shown that the morphology of cellular wall or membrane might be compromised, resulting in cellular death.[109] The membrane may experience rupture, allowing for release of content of the cell, which leads to the death of the cell.[110-111] Furthermore, copper uptake in a cell can affect different proteins, which will cause inhibition or alteration of vital cellular functions and ultimately leads to the death or inactivation of the microorganism's cell.[112-113] Additionally, the DNA or RNA of the cell can be damaged by the dissolved copper species that infiltrate the microorganism cell.[114]

This dissertation demonstrates the development of several antimicrobial surface coatings that are easily and rapidly prepared, and each quickly kills or inactivates microbes. This document first discusses our antimicrobial coatings (Cu_2O/PU[53, 95], ZnO-T/PU[57], transparent PDA/ Cu_2O[49], transparent PDA/Cu[49], porous PDA/Cu[96], and antimicrobial wraps,[115], followed by the study of antimicrobial mechanism of Cu_2O surfaces[116]. Subsequently, our research on the transfer of SARS-CoV-2 virus from contaminated solids is discussed, which is followed by our review of the literature on the stability of the COVID-19 virus on surfaces and challenges and opportunities facing the field of antimicrobial coatings.

REFERENCES

(1) Mack, A.; Choffnes, E. R.; Hamburg, M. A.; Relman, D. A. *Microbial Evolution and Co-Adaptation: A Tribute to the Life and Scientific Legacies of Joshua Lederberg: Workshop Summary*, National Academies Press: 2009.

(2) Piret, J.; Boivin, G. Pandemics Throughout History. *Front. Microbiol.* **2021,** *11*, 631736.

(3) Scheld, W. M. Introduction to Microbial Disease: Host-Pathogen Interactions. *Goldman's Cecil Medicine* **2012**, 1761.

(4) World Health Organization Infectious Diseases Kill over 17 Million People a Year: Who Warns of Global Crisis. https://www.who.int/news/item/01-01-1996-infectious-diseases-kill-over-17-million-people-a-year-who-warns-of-global-crisis (accessed Mar 20, 2023).

(5) Eames, I.; Tang, J.; Li, Y.; Wilson, P. Airborne Transmission of Disease in Hospitals. *J R Soc Interface* **2009,** *6* (suppl_6), S697-S702.

(6) La Rosa, G.; Fratini, M.; Libera, S. D.; Iaconelli, M.; Muscillo, M. Viral Infections Acquired Indoors through Airborne, Droplet or Contact Transmission. *Ann. Ist. Super. Sanita* **2013,** *49*, 124-132.

(7) Shikanai-Yasuda, M. A.; Carvalho, N. B. Oral Transmission of Chagas Disease. *Clin. Infect. Dis.* **2012,** *54* (6), 845-852.

(8) Boone, S. A.; Gerba, C. P. Significance of Fomites in the Spread of Respiratory and Enteric Viral Disease. *Appl. Environ. Microbiol.* **2007,** *73* (6), 1687-1696.

(9) Bausch, D. G.; Towner, J. S.; Dowell, S. F.; Kaducu, F.; Lukwiya, M.; Sanchez, A.; Nichol, S. T.; Ksiazek, T. G.; Rollin, P. E. Assessment of the Risk of Ebola Virus Transmission from Bodily Fluids and Fomites. *J. Infect. Dis.* **2007,** *196* (Supplement_2

The Journal of infectious diseases), S142-S147.

(10) Mubareka, S.; Lowen, A. C.; Steel, J.; Coates, A. L.; García-Sastre, A.; Palese, P. Transmission of Influenza Virus Via Aerosols and Fomites in the Guinea Pig Model. *J. Infect. Dis.* **2009,** *199* (6), 858-865.

(11) Abad, F. X.; Pinto, R. M.; Bosch, A. Survival of Enteric Viruses on Environmental Fomites. *Appl. Environ. Microbiol.* **1994,** *60* (10), 3704-3710.

(12) Stephens, B.; Azimi, P.; Thoemmes, M. S.; Heidarinejad, M.; Allen, J. G.; Gilbert, J. A. Microbial Exchange Via Fomites and Implications for Human Health. *Curr. Pollut. Rep.* **2019,** *5* (4), 198-213.

(13) Fry, D. E. Occupational Blood-Borne Diseases in Surgery. *Am. J. Surg.* **2005,** *190* (2), 249-254.

(14) O'Connor, S. M.; Taylor, C. E.; Hughes, J. M. Emerging Infectious Determinants of Chronic Diseases. *Emerg. Infect. Dis.* **2006,** *12* (7), 1051.

(15) Carbone, K. M.; Luftig, R. B.; Buckley, M., Microbial Triggers of Chronic Human Illness. Am Soc Microbiol: 2005.

(16) Restrepo, M. I.; Reyes, L. F. Pneumonia as a Cardiovascular Disease. *Respirol* **2018,** *23* (3), 250-259.

(17) Murray, C. J.; Ikuta, K. S.; Sharara, F.; Swetschinski, L.; Aguilar, G. R.; Gray, A.; Han, C.; Bisignano, C.; Rao, P.; Wool, E. Global Burden of Bacterial Antimicrobial Resistance in 2019: A Systematic Analysis. *The Lancet* **2022,** *399* (10325), 629-655.

(18) Mahoney, A. R.; Safaee, M. M.; Wuest, W. M.; Furst, A. L. The Silent Pandemic: Emergent Antibiotic Resistances Following the Global Response to Sars-Cov-2. *Iscience* **2021,** *24* (4), 102304.

(19) Plackett, B. Why Big Pharma Has Abandoned Antibiotics. *Nature* **2020,** *586* (7830), S50-S50.

(20) Centers for Disease Control and Prevention Covid-19: U.S. Impact on Antimicrobial Resistance, Special Report 2022. https://www.cdc.gov/drugresistance/pdf/covid19-impact-report-508.pdf (accessed Mar 25, 2023).

(21) Centers for Disease Control and Prevention Covid-19 & Antibiotic Resistance. https://www.cdc.gov/drugresistance/covid19.html (accessed Mar 28, 2023).

(22) Centers for Disease Control and Prevention Hai and Antibiotic Use Prevalence Survey. https://www.cdc.gov/hai/eip/antibiotic-use.html (accessed Mar 24, 2023).

(23) Gurusamy, K. S.; Koti, R.; Toon, C. D.; Wilson, P.; Davidson, B. R. Antibiotic Therapy for the Treatment of Methicillin-Resistant Staphylococcus Aureus (Mrsa) Infections in Surgical Wounds. *Cochrane Database Syst. Rev.* **2013,** (8).

(24) Yayan, J.; Ghebremedhin, B.; Rasche, K. Antibiotic Resistance of Pseudomonas Aeruginosa in Pneumonia at a Single University Hospital Center in Germany over a 10-Year Period. *PLoS One* **2015,** *10* (10), e0139836.

(25) Pang, Z.; Raudonis, R.; Glick, B. R.; Lin, T.-J.; Cheng, Z. Antibiotic Resistance in Pseudomonas Aeruginosa: Mechanisms and Alternative Therapeutic Strategies. *Biotechnol. Adv.* **2019,** *37* (1), 177-192.

(26) CDC 2019 Ar Threats Report. https://www.cdc.gov/drugresistance/biggest-threats.html (accessed Mar 22, 2023).

(27) Centers for Disease Control and Prevention Multidrug-Resistant Pseudomonas Aeruginosa https://www.cdc.gov/drugresistance/pdf/threats-report/pseudomonas-aeruginosa-508.pdf (accessed Mar 20, 2023).

(28) Centers for Disease Control and Prevention Methicillin-Resistant Staphylococcus Aureus (Mrsa). https://www.cdc.gov/drugresistance/pdf/threats-report/mrsa-508.pdf (accessed Mar 20, 2023).

(29) Doron, S.; Gorbach, S. Bacterial Infections: Overview. *International Encyclopedia of Public Health* **2008**, 273.

(30) Maree, C. L.; Daum, R. S.; Boyle-Vavra, S.; Matayoshi, K.; Miller, L. G. Community-Associated Methicillin-Resistant Staphylococcus Aureus Isolates and Healthcare-Associated Infections. *Emerg. Infect. Dis.* **2007,** *13* (2), 236.

(31) David, M. Z.; Daum, R. S. Community-Associated Methicillin-Resistant Staphylococcus Aureus: Epidemiology and Clinical Consequences of an Emerging Epidemic. *Clin. Microbiol. Rev.* **2010,** *23* (3), 616-687.

(32) Kramer, A.; Schwebke, I.; Kampf, G. How Long Do Nosocomial Pathogens Persist on Inanimate Surfaces? A Systematic Review. *BMC Infect. Dis.* **2006,** *6* (1), 1-8.

(33) Mulcahy, L. R.; Isabella, V. M.; Lewis, K. Pseudomonas Aeruginosa Biofilms in Disease. *Microb. Ecol.* **2014,** *68*, 1-12.

(34) Vos, M. C.; Verbrugh, H. A. Mrsa: We Can Overcome, but Who Will Lead the Battle? *Infect. Control Hosp. Epidemiol.* **2005,** *26* (2), 117-120.

(35) de Abreu, P. M.; Farias, P. G.; Paiva, G. S.; Almeida, A. M.; Morais, P. V. Persistence of Microbial Communities Including Pseudomonas Aeruginosa in a Hospital Environment: A Potential Health Hazard. *BMC Microbiol.* **2014,** *14* (1), 1-10.

(36) Covid-19 Dashboard by the Center for Systems Science and Engineering (Csse) at Johns Hopkins University (Jhu). https://coronavirus.jhu.edu/map.html (accessed March 6, 2023).

(37) Wang, H.; Paulson, K. R.; Pease, S. A.; Watson, S.; Comfort, H.; Zheng, P.; Aravkin, A. Y.; Bisignano, C.; Barber, R. M.; Alam, T. Estimating Excess Mortality Due to the Covid-19 Pandemic: A Systematic Analysis of Covid-19-Related Mortality, 2020–21. *The Lancet* **2022**.

(38) Cutler, D. M.; Summers, L. H. The Covid-19 Pandemic and the $16 Trillion Virus. *JAMA* **2020,** *324* (15), 1495-1496.

(39) World Health Organization Transmission of Sars-Cov-2: Implications for Infection Prevention Precautions. https://www.who.int/news-room/commentaries/detail/transmission-of-sars-cov-2-implications-for-infection-prevention-precautions (accessed Feb 28, 2023).

(40) Behzadinasab, S.; Chin, A. W. H.; Hosseini, M.; Poon, L. L. M.; Ducker, W. A. Sars-Cov-2 Virus Transfers to Skin through Contact with Contaminated Solids. *Sci. Rep.* **2021,** *11* (1), 22868, DOI: https://doi.org/10.1038/s41598-021-00843-0.

(41) Sia, S. F.; Yan, L.-M.; Chin, A. W.; Fung, K.; Choy, K.-T.; Wong, A. Y.; Kaewpreedee, P.; Perera, R. A.; Poon, L. L.; Nicholls, J. M. Pathogenesis and Transmission of Sars-Cov-2 in Golden Hamsters. *Nature* **2020,** *583* (7818), 834-838.

(42) Meiksin, A. Dynamics of Covid-19 Transmission Including Indirect Transmission Mechanisms: A Mathematical Analysis. *Epidemiol. Infect.* **2020,** *148*, e257, DOI: 10.1017/S0950268820002563.

(43) Chin, A. W. H.; Chu, J. T. S.; Perera, M. R. A.; Hui, K. P. Y.; Yen, H.-L.; Chan, M. C. W.; Peiris, M.; Poon, L. L. M. Stability of Sars-Cov-2 in Different Environmental Conditions. *The Lancet Microbe* **2020,** *1* (1), e10, DOI: 10.1016/S2666-5247(20)30003-3.

(44) Hirose, R.; Ikegaya, H.; Naito, Y.; Watanabe, N.; Yoshida, T.; Bandou, R.; Daidoji, T.; Itoh, Y.; Nakaya, T. Survival of Severe Acute Respiratory Syndrome Coronavirus 2 (Sars-Cov-2) and Influenza Virus on Human Skin: Importance of Hand Hygiene in Coronavirus Disease 2019 (Covid-19). *Clin. Infect. Dis.* **2020**, DOI: 10.1093/cid/ciaa1517.

(45) Harbourt, D. E.; Haddow, A. D.; Piper, A. E.; Bloomfield, H.; Kearney, B. J.; Fetterer, D.; Gibson, K.; Minogue, T. Modeling the Stability of Severe Acute Respiratory Syndrome

Coronavirus 2 (Sars-Cov-2) on Skin, Currency, and Clothing. *PLoS Negl. Trop. Dis.* **2020,** *14* (11), e0008831.

(46) Rutala, W. A.; Weber, D. J. Uses of Inorganic Hypochlorite (Bleach) in Health-Care Facilities. *Clin. Microbiol. Rev.* **1997,** *10* (4), 597-610.

(47) Ellingson, K. D.; Pogreba-Brown, K.; Gerba, C. P.; Elliott, S. P. Impact of a Novel Antimicrobial Surface Coating on Health Care–Associated Infections and Environmental Bioburden at 2 Urban Hospitals. *Clin. Infect. Dis.* **2020,** *71* (8), 1807-1813.

(48) Marik, P.; Shankaran, S.; King, L. The Effect of Copper-Oxide-Treated Soft and Hard Surfaces on the Incidence of Healthcare-Associated Infections: A Two-Phase Study. *J. Hosp. Infect.* **2020,** *105* (2), 265-271.

(49) Behzadinasab, S.; Williams, M. D.; Hosseini, M.; Poon, L. L.; Chin, A. W.; Falkinham III, J. O.; Ducker, W. A. Transparent and Sprayable Surface Coatings That Kill Drug-Resistant Bacteria within Minutes and Inactivate Sars-Cov-2 Virus. *ACS Appl. Mater. Interfaces* **2021,** *13* (46), 54706-54714, DOI: https://doi.org/10.1021/acsami.1c15505.

(50) Cloutier, M.; Mantovani, D.; Rosei, F. Antibacterial Coatings: Challenges, Perspectives, and Opportunities. *Trends Biotechnol.* **2015,** *33* (11), 637-652.

(51) Salwiczek, M.; Qu, Y.; Gardiner, J.; Strugnell, R. A.; Lithgow, T.; McLean, K. M.; Thissen, H. Emerging Rules for Effective Antimicrobial Coatings. *Trends Biotechnol.* **2014,** *32* (2), 82-90.

(52) Hosseini, M.; Chin, A. W.; Williams, M. D.; Behzadinasab, S.; Falkinham III, J. O.; Poon, L. L.; Ducker, W. A. Transparent Anti-Sars-Cov-2 and Antibacterial Silver Oxide Coatings. *ACS Appl. Mater. Interfaces* **2022,** *14* (7), 8718-8727.

(53) Behzadinasab, S.; Chin, A.; Hosseini, M.; Poon, L.; Ducker, W. A. A Surface Coating That Rapidly Inactivates Sars-Cov-2. *ACS Appl. Mater. Interfaces* **2020,** *12* (31), 34723-34727, DOI: https://doi.org/10.1021/acsami.0c11425.

(54) Hutasoit, N.; Kennedy, B.; Hamilton, S.; Luttick, A.; Rashid, R. A. R.; Palanisamy, S. Sars-Cov-2 (Covid-19) Inactivation Capability of Copper-Coated Touch Surface Fabricated by Cold-Spray Technology. *Manuf. Lett.* **2020,** *25*, 93-97.

(55) Hosseini, M.; Chin, A. W.; Behzadinasab, S.; Poon, L. L.; Ducker, W. A. Cupric Oxide Coating That Rapidly Reduces Infection by Sars-Cov-2 Via Solids. *ACS Appl. Mater. Interfaces* **2021,** *13* (5), 5919-5928.

(56) Sousa, B. C.; Cote, D. L. Antimicrobial Copper Cold Spray Coatings and Sars-Cov-2 Surface Inactivation. *MRS Adv.* **2020,** *5* (56), 2873-2880.

(57) Hosseini, M.; Behzadinasab, S.; Chin, A. W.; Poon, L. L.; Ducker, W. A. Reduction of Infectivity of Sars-Cov-2 by Zinc Oxide Coatings. *ACS Biomater. Sci. Eng.* **2021,** *7* (11), 5022-5027.

(58) Rakowska, P. D.; Tiddia, M.; Faruqui, N.; Bankier, C.; Pei, Y.; Pollard, A. J.; Zhang, J.; Gilmore, I. S. Antiviral Surfaces and Coatings and Their Mechanisms of Action. *Commun. Mat.* **2021,** *2* (1), 1-19.

(59) Hosseini, M.; Behzadinasab, S.; Benmamoun, Z.; Ducker, W. A. The Viability of Sars-Cov-2 on Solid Surfaces. *Curr. Opin. Colloid Interface Sci.* **2021**, 101481.

(60) Singha, P.; Locklin, J.; Handa, H. A Review of the Recent Advances in Antimicrobial Coatings for Urinary Catheters. *Acta Biomater.* **2017,** *50*, 20-40.

(61) Environmental Protection Agency Antimicrobial Testing Methods & Procedures: Interim Method for Evaluating the Efficacy of Antimicrobial Surface Coatings https://www.epa.gov/pesticide-analytical-methods/antimicrobial-testing-methods-procedures-interim-method-evaluating (accessed Sep 2, 2022).

(62) Environmental Protection Agency Protocol for the Evaluation of Bactericidal Activity of Hard, Non-Porous Copper Containing Surface Products. https://www.epa.gov/sites/production/files/2016-02/documents/copper_and_copper-alloy_surface_protocol_revised_012916.pdf (accessed Sep 2, 2022).

(63) Sunada, K.; Minoshima, M.; Hashimoto, K. Highly Efficient Antiviral and Antibacterial Activities of Solid-State Cuprous Compounds. *J. Hazard. Mater.* **2012,** *235*, 265-270.

(64) Aydin Sevinç, B.; Hanley, L. Antibacterial Activity of Dental Composites Containing Zinc Oxide Nanoparticles. *J. Biomed. Mater. Res. B Appl. Biomater.* **2010,** *94* (1), 22-31.

(65) Pasquet, J.; Chevalier, Y.; Pelletier, J.; Couval, E.; Bouvier, D.; Bolzinger, M.-A. The Contribution of Zinc Ions to the Antimicrobial Activity of Zinc Oxide. *Colloids Surf. Physicochem. Eng. Aspects* **2014,** *457*, 263-274.

(66) Young, M.; Ozcan, A.; Myers, M. E.; Johnson, E. G.; Graham, J. H.; Santra, S. Multimodal Generally Recognized as Safe Zno/Nanocopper Composite: A Novel Antimicrobial Material for the Management of Citrus Phytopathogens. *J. Agric. Food Chem.* **2017,** *66* (26), 6604-6608.

(67) El Saeed, A. M.; Abd El-Fattah, M.; Azzam, A. M.; Dardir, M. M.; Bader, M. M. Synthesis of Cuprous Oxide Epoxy Nanocomposite as an Environmentally Antimicrobial Coating. *Int. J. Biol. Macromol.* **2016,** *89*, 190-197.

(68) Akiyama, T.; Miyamoto, H.; Yonekura, Y.; Tsukamoto, M.; Ando, Y.; Noda, I.; Sonohata, M.; Mawatari, M. Silver Oxide-Containing Hydroxyapatite Coating Has in Vivo Antibacterial Activity in the Rat Tibia. *J. Orthop. Res.* **2013,** *31* (8), 1195-1200.

(69) Johnson, J. R.; Roberts, P. L.; Olsen, R. J.; Moyer, K. A.; Stamm, W. E. Prevention of Catheter-Associated Urinary Tract Infection with a Silver Oxide-Coated Urinary Catheter: Clinical and Microbiologic Correlates. *J. Infect. Dis.* **1990,** *162* (5), 1145-1150.

(70) Grass, G.; Rensing, C.; Solioz, M. Metallic Copper as an Antimicrobial Surface. *Appl. Environ. Microbiol.* **2011,** *77* (5), 1541-1547.

(71) Ren, G.; Hu, D.; Cheng, E. W.; Vargas-Reus, M. A.; Reip, P.; Allaker, R. P. Characterisation of Copper Oxide Nanoparticles for Antimicrobial Applications. *Int. J. Antimicrob. Agents* **2009,** *33* (6), 587-590.

(72) Song, Y.; Jiang, H.; Wang, B.; Kong, Y.; Chen, J. Silver-Incorporated Mussel-Inspired Polydopamine Coatings on Mesoporous Silica as an Efficient Nanocatalyst and Antimicrobial Agent. *ACS Appl. Mater. Interfaces* **2018,** *10* (2), 1792-1801.

(73) Gopal, V.; Nilsson-Payant, B. E.; French, H.; Siegers, J. Y.; Yung, W.-s.; Hardwick, M.; Te Velthuis, A. J. Zinc-Embedded Polyamide Fabrics Inactivate Sars-Cov-2 and Influenza a Virus. *ACS Appl. Mater. Interfaces* **2021,** *13* (26), 30317-30325.

(74) Zhang, Y.; Shareena Dasari, T. P.; Deng, H.; Yu, H. Antimicrobial Activity of Gold Nanoparticles and Ionic Gold. *J. Environ. Sci. Health, Pt. C* **2015,** *33* (3), 286-327.

(75) Mlcochova, P.; Chadha, A.; Hesselhoj, T.; Fraternali, F.; Ramsden, J.; Gupta, R. Extended in Vitro Inactivation of Sars-Cov-2 by Titanium Dioxide Surface Coating. *bioRxiv* **2020**.

(76) Gaarenstroom, S.; Winograd, N. Initial and Final State Effects in the Esca Spectra of Cadmium and Silver Oxides. *J. Chem. Phys.* **1977,** *67* (8), 3500-3506.

(77) Gottenbos, B.; van der Mei, H. C.; Klatter, F.; Nieuwenhuis, P.; Busscher, H. J. In Vitro and in Vivo Antimicrobial Activity of Covalently Coupled Quaternary Ammonium Silane Coatings on Silicone Rubber. *Biomaterials* **2002,** *23* (6), 1417-1423.

(78) Beyth, N.; Houri-Haddad, Y.; Baraness-Hadar, L.; Yudovin-Farber, I.; Domb, A. J.; Weiss, E. I. Surface Antimicrobial Activity and Biocompatibility of Incorporated Polyethylenimine Nanoparticles. *Biomaterials* **2008,** *29* (31), 4157-4163.

(79) Wong, S. Y.; Li, Q.; Veselinovic, J.; Kim, B.-S.; Klibanov, A. M.; Hammond, P. T. Bactericidal and Virucidal Ultrathin Films Assembled Layer by Layer from Polycationic N-Alkylated Polyethylenimines and Polyanions. *Biomaterials* **2010,** *31* (14), 4079-4087, DOI: 10.1016/j.biomaterials.2010.01.119.

(80) Gabriel, M.; Nazmi, K.; Veerman, E. C.; Nieuw Amerongen, A. V.; Zentner, A. Preparation of Ll-37-Grafted Titanium Surfaces with Bactericidal Activity. *Bioconjugate chemistry* **2006,** *17* (2), 548-550.

(81) Glinel, K.; Jonas, A. M.; Jouenne, T.; Leprince, J.; Galas, L.; Huck, W. T. Antibacterial and Antifouling Polymer Brushes Incorporating Antimicrobial Peptide. *Bioconjugate chemistry* **2009,** *20* (1), 71-77.

(82) Wang, Q.; Uzunoglu, E.; Wu, Y.; Libera, M. Self-Assembled Poly (Ethylene Glycol)-Co-Acrylic Acid Microgels to Inhibit Bacterial Colonization of Synthetic Surfaces. *ACS Appl. Mater. Interfaces* **2012,** *4* (5), 2498-2506.

(83) Reddy, S. T.; Chung, K. K.; McDaniel, C. J.; Darouiche, R. O.; Landman, J.; Brennan, A. B. Micropatterned Surfaces for Reducing the Risk of Catheter-Associated Urinary Tract Infection: An in Vitro Study on the Effect of Sharklet Micropatterned Surfaces to Inhibit Bacterial Colonization and Migration of Uropathogenic Escherichia Coli. *J. Endourol.* **2011,** *25* (9), 1547-1552.

(84) Ivanova, E. P.; Hasan, J.; Webb, H. K.; Truong, V. K.; Watson, G. S.; Watson, J. A.; Baulin, V. A.; Pogodin, S.; Wang, J. Y.; Tobin, M. J. Natural Bactericidal Surfaces: Mechanical Rupture of Pseudomonas Aeruginosa Cells by Cicada Wings. *Small* **2012,** *8* (16), 2489-2494.

(85) Hasan, J.; Xu, Y.; Yarlagadda, T.; Schuetz, M.; Spann, K.; Yarlagadda, P. K. Antiviral and Antibacterial Nanostructured Surfaces with Excellent Mechanical Properties for Hospital Applications. *ACS Biomater. Sci. Eng.* **2020,** *6* (6), 3608-3618.

(86) Dhabarde, N.; Khaiboullina, S.; Uppal, T.; Adhikari, K.; Verma, S. C.; Subramanian, V. R. Inactivation of Sars-Cov-2 and Other Human Coronaviruses Aided by Photocatalytic One-Dimensional Titania Nanotube Films as a Self-Disinfecting Surface. *ACS Appl. Mater. Interfaces* **2022,** *14* (45), 50463-50474.

(87) Fu, H.; Yaniv, V.; Betzalel, Y.; Mamane, H.; Gray, K. A. Creating Anti-Viral High-Touch Surfaces Using Photocatalytic Transparent Films. *Chemosphere* **2023**, 138280.

(88) Heo, K. J.; Lee, D. U.; Shin, J. H.; Park, J.; Lee, B. J.; Shin, J.; Jeong, S. B.; Hwang, G. B.; MacRobert, A. J.; Parkin, I. P. Transparent, Robust, and Photochemical Antibacterial Surface Based on Hydrogen Bonding between a Si-Al and Cationic Dye. *ACS Appl. Mater. Interfaces* **2022,** *14* (47), 53285-53297.

(89) Zhang, T.; Wan, H.; Xu, Z.; Zhang, Y.; Dai, J.; Liu, H. Polyhexamethylene Guanidine Molybdate as an Efficient Antibacterial Filler in Epoxy Coating for Inhibiting Sulfate Reducing Bacteria Biofilm. *Prog. Org. Coat.* **2023,** *176*, 107401.

(90) Borkow, G. Safety of Using Copper Oxide in Medical Devices and Consumer Products. *Curr. Chem. Biol.* **2012,** *6* (1), 86-92.

(91) Environmental Protection Agency Reregistration Eligibility Decision (Red) for Coppers. https://www3.epa.gov/pesticides/chem_search/reg_actions/reregistration/red_G-26_26-May-09.pdf (accessed June 2nd 2021).

(92) Faúndez, G.; Troncoso, M.; Navarrete, P.; Figueroa, G. Antimicrobial Activity of Copper Surfaces against Suspensions of Salmonella Enterica and Campylobacter Jejuni. *BMC Microbiol.* **2004,** *4* (1), 1-7.

(93) Mehtar, S.; Wiid, I.; Todorov, S. The Antimicrobial Activity of Copper and Copper Alloys against Nosocomial Pathogens and Mycobacterium Tuberculosis Isolated from Healthcare Facilities in the Western Cape: An in-Vitro Study. *J. Hosp. Infect.* **2008,** *68* (1), 45-51.

(94) Noyce, J.; Michels, H.; Keevil, C. Potential Use of Copper Surfaces to Reduce Survival of Epidemic Meticillin-Resistant Staphylococcus Aureus in the Healthcare Environment. *J. Hosp. Infect.* **2006,** *63* (3), 289-297.

(95) Behzadinasab, S.; Hosseini, M.; Williams, M.; Ivester, H.; Allen, I.; Falkinham III, J.; Ducker, W. Antimicrobial Activity of Cuprous Oxide-Coated and Cupric Oxide-Coated Surfaces. *J. Hosp. Infect.* **2022,** *129*, 58-64, DOI: https://doi.org/10.1016/j.jhin.2022.07.022.

(96) Behzadinasab, S.; Williams, M. D.; Aktuglu, M.; Falkinham III, J. O.; Ducker, W. A. Porous Antimicrobial Coatings for Killing Microbes within Minutes. *ACS Appl. Mater. Interfaces* **2023,** *15* (12), 15120–15128, DOI: https://doi.org/10.1021/acsami.2c22240.

(97) Jampa, S.; Ratanatawanate, C.; Pimtong, W.; Aueviriyavit, S.; Chantho, V.; Sillapaprayoon, S.; Kunyanee, C.; Warin, C.; Gamonchuang, J.; Kumnorkaew, P. Transparent Anti-Sars Cov-2 Film from Copper (I) Oxide Incorporated in Zeolite Nanoparticles. *ACS Appl. Mater. Interfaces* **2022,** *14* (46), 52334-52346.

(98) Gonçalves, R. A.; Ku, J. W.; Zhang, H.; Salim, T.; Oo, G.; Zinn, A. A.; Boothroyd, C.; Tang, R. M.; Gan, C. L.; Gan, Y.-H. Copper-Nanoparticle-Coated Fabrics for Rapid and Sustained Antibacterial Activity Applications. *ACS Appl. Nano Mater.* **2022,** *5* (9), 12876-12886.

(99) Shigetoh, K.; Hirao, R.; Ishida, N. Durability and Surface Oxidation States of Antiviral Nano-Columnar Copper Thin Films. *ACS Appl. Mater. Interfaces* **2023**.

(100) Alhussein, A.; Aouchiche, L.; Hmima, A.; Retraint, D.; Rtimi, S. Distinctive Effects of Surface Roughness and Ions Release on the Bacterial Adhesion and Inactivation of Textured Copper Oxide Surfaces. *Coatings* **2023,** *13* (2), 454.

(101) Foffa, I.; Losi, P.; Quaranta, P.; Cara, A.; Al Kayal, T.; D'Acunto, M.; Presciuttini, G.; Pistello, M.; Soldani, G. A Copper Nanoparticles-Based Polymeric Spray Coating: Nanoshield against Sars-Cov-2. *J. Appl. Biomater. Funct. Mater.* **2022,** *20*, 22808000221076326.

(102) Liu, L.; Chin, A.; Yu, P.; Poon, L.; Huang, M. Anti-Pathogen Stainless Steel Combating Covid-19. *Chem. Eng. J.* **2022,** *433*, 133783.

(103) Saud, Z.; Richards, C. A.; Williams, G.; Stanton, R. J. Anti-Viral Organic Coatings for High Touch Surfaces Based on Smart-Release, Cu2+ Containing Pigments. *Prog. Org. Coat.* **2022,** *172*, 107135.

(104) Biryukov, J.; Boydston, J. A.; Dunning, R. A.; Yeager, J. J.; Wood, S.; Reese, A. L.; Ferris, A.; Miller, D.; Weaver, W.; Zeitouni, N. E. Increasing Temperature and Relative Humidity Accelerates Inactivation of Sars-Cov-2 on Surfaces. *MSphere* **2020,** *5* (4).

(105) Matson, M. J.; Yinda, C. K.; Seifert, S. N.; Bushmaker, T.; Fischer, R. J.; van Doremalen, N.; Lloyd-Smith, J. O.; Munster, V. J. Effect of Environmental Conditions on Sars-Cov-2 Stability in Human Nasal Mucus and Sputum. *Emerg. Infect. Dis.* **2020,** *26* (9), 2276.

(106) Riddell, S.; Goldie, S.; Hill, A.; Eagles, D.; Drew, T. W. The Effect of Temperature on Persistence of Sars-Cov-2 on Common Surfaces. *Virol J.* **2020,** *17* (1), 1-7.

(107) Hasan, J.; Pyke, A.; Nair, N.; Yarlagadda, T.; Will, G.; Spann, K.; Yarlagadda, P. K. Antiviral Nanostructured Surfaces Reduce the Viability of Sars-Cov-2. *ACS Biomater. Sci. Eng.* **2020,** *6* (9), 4858-4861.

(108) Luanghane, L.; Pewnim, N. Electrochemical Modification of High Contact Stainless Steel 304 Surfaces for Antimicrobial Applications. *Materials Today: Proceedings* **2022,** *65*, 2432-2435.

(109) Raffi, M.; Mehrwan, S.; Bhatti, T. M.; Akhter, J. I.; Hameed, A.; Yawar, W. Investigations into the Antibacterial Behavior of Copper Nanoparticles against Escherichia Coli. *Ann. Microbiol.* **2010,** *60* (1), 75-80.

(110) Lemire, J. A.; Harrison, J. J.; Turner, R. J. Antimicrobial Activity of Metals: Mechanisms, Molecular Targets and Applications. *Nature Reviews Microbiology* **2013,** *11* (6), 371-384.

(111) Warnes, S.; Caves, V.; Keevil, C. Mechanism of Copper Surface Toxicity in Escherichia Coli O157: H7 and Salmonella Involves Immediate Membrane Depolarization Followed by Slower Rate of DNA Destruction Which Differs from That Observed for Gram-Positive Bacteria. *Environ. Microbiol.* **2012,** *14* (7), 1730-1743.

(112) Kim, J.-H.; Cho, H.; Ryu, S.-E.; Choi, M.-U. Effects of Metal Ions on the Activity of Protein Tyrosine Phosphatase Vhr: Highly Potent and Reversible Oxidative Inactivation by Cu2+ Ion. *Archives of Biochemistry and Biophysics* **2000,** *382* (1), 72-80.

(113) Macomber, L.; Imlay, J. A. The Iron-Sulfur Clusters of Dehydratases Are Primary Intracellular Targets of Copper Toxicity. *Proceedings of the National Academy of Sciences* **2009,** *106* (20), 8344-8349.

(114) Warnes, S.; Green, S.; Michels, H.; Keevil, C. Biocidal Efficacy of Copper Alloys against Pathogenic Enterococci Involves Degradation of Genomic and Plasmid Dnas. *Appl. Environ. Microbiol.* **2010,** *76* (16), 5390-5401.

(115) Behzadinasab, S.; Williams, M. D.; Falkinham III, J. O.; Ducker, W. A. Facile Implementation of Antimicrobial Coatings through Adhesive Films (Wraps) Demonstrated with Cuprous Oxide Coatings. *Antibiotics* **2023,** *12* (5), 920.

(116) Behzadinasab, S.; Williams, M. D.; Falkinham III, J. O.; Ducker, W. A. Antimicrobial Mechanism of Cuprous Oxide (Cu2o) Coatings. *submitted*.

Chapter 2. A Surface Coating that Rapidly Inactivates SARS-CoV-2

Saeed Behzadinasab[†1], Alex Chin[†2], Mohsen Hosseini[1], Leo Poon*[2,3], and William Ducker*[1]

[†] These authors contributed equally

*Corresponding Authors' Email: Leo Poon llmpoon@hku.hk; William Ducker wducker@vt.edu

[1]Dept. of Chemical Engineering and Center for Soft Matter and Biological Physics, Virginia Tech, VA, 24061, USA

[2]School of Public Health, LKS Faculty of Medicine, The University of Hong Kong, Hong Kong Special Administrative Region, China.

[3]HKU-Pasteur Research Pole, LKS Faculty of Medicine, The University of Hong Kong, Hong Kong, China

ORCID

Saeed Behzadinasab: 0000-0002-6271-2623

Mohsen Hosseini: 0000-0002-9482-0215

William A. Ducker: 0000-0002-8207-768X

Keywords: SARS-CoV-2, coronavirus, coating, Cu_2O, cuprous oxide, virucidal, COVID-19

2.1. ABSTRACT

SARS-CoV-2, the virus that causes the disease COVID-19, remains viable on solids for periods of up to one week, so one potential route for human infection is via exposure to an infectious dose from a solid. We have fabricated and tested a coating that is designed to reduce the longevity of SARS-CoV-2 on solids. The coating consists of cuprous oxide (Cu_2O) particles bound with polyurethane. After one hour on coated glass or stainless steel, the viral titer was reduced by about 99.9% on average compared to the uncoated sample. An advantage of a polyurethane-based coating is that polyurethane is already used to coat a large number of everyday objects. Our coating adheres well to glass and stainless steel, as well as everyday items that people may fear to touch during a pandemic, such as a doorknob, a pen, and a credit card keypad button. The coating performs well in the cross-hatch durability test and remains intact and active after 13 days immersed in water, or after exposure to multiple cycles of exposure to virus and disinfection.

2.2. Introduction

COVID-19 has caused widespread human morbidity and mortality, as well as disruption to our economy and our way of life. The disease is spread through the virus, SARS-CoV-2, which is known to remain viable on some solids for periods of up to one week.[1-2] One potential route of human infection occurs when a person comes into contact with a solid that is contaminated with the virus (a fomite), so one method of reducing transmission would be to reduce the period of human vulnerability to infection by reducing the period of viability of SARS-CoV-2 on solids. In this report, we describe the fabrication and testing of an anti-SARS-CoV-2 coating. Our ultimate goal is to produce a coating that (1) inactivates the virus quickly, (2) can be coated on many solids, and (3) is sufficiently robust that it retains virucidal potency during consumer use. Such a film could be used on many household, commercial, medical, and manufacturing surfaces, such as doorknobs, credit card buttons, and cell phone covers. These are objects that a person might touch only minutes after deposition of respiratory droplets. Our hope is that widespread use of such a coating could reduce transmission of SARS-CoV-2 and also reduce fear of touching objects.

At our starting point, it was unknown which chemical groups inactivated SARS-CoV-2. We tested three films. Two of the films were monolayers of cationic polymer: cationic groups are known to inactivate other viruses[3-4] (and bacteria[3-5]), and the mechanism is believed to be that the high density of charge disrupts the self-assembly of the pathogen. These films did not have a significant effect. We chose cuprous oxide (Cu_2O) as the active ingredient of the third film. Prior work demonstrated that SARS-CoV-2 had a short period of viability on Cu metal,[1] and the surface layer of Cu metal readily oxidizes to Cu_2O.[6] Cu_2O has shown activity against two

other viruses: a bacteriophage by exposure to unbound particles[7] and hepatitis C by exposure of the virus to suspended nanoparticles.[8]

Cuprous oxide is used as pesticide and is rated as Toxicity Category III by the EPA which means that it is slightly toxic and slightly irritating.[9] It is also used as marine antifoulant and it known to have an adverse effect on marine organisms.[10-11] However, a review of clinical and animal studies of textiles containing copper oxide by Borkow reports no effects on human skin.[12] For copper pesticide products more generally, according to an 2009 EPA report:[9] "Current available literature and studies do not indicate any systemic toxicity associated with copper exposure. … There are no residential or occupational risks of concern resulting from exposure to copper products." Likewise, immune response to copper is rare, whereas contact with copper in coins, intrauterine devices and other applications is common.[12]

In this work, we describe the time-course of inactivation of SARS-CoV-2 on Cu_2O particles bound into a thin (10–16 μm) film with a commercial polyurethane (PU) (Figure 2-1). The commercial polyurethane is already formulated to be hard-wearing and easy to apply to many materials. Our results show that the Cu_2O/Pu coating inactivates the virus very quickly: viable viral counts drop by an average of about 99.9 % in 1 h. The film is robust and retains its potency to SARS-CoV-2 after multiple cycles of exposure to the virus followed by disinfection.

2.3. Materials And Methods

2.3.1. Materials

Cu_2O particles (Chem Copp HP III Type UltraFine -5) were purchased from American Chemet Corporation. The chemical composition and particle size distribution information are described in Table S2-1 and Figure S2-1. Polyurethane (Miniwax, Fast-Drying Polyurethane, clear satin) was purchased from Lowes Home Improvement Store. The following chemicals were purchased from Sigma Aldrich: (3-glycidyloxypropyl)trimethoxysilane (GOPTS) (>98%), poly(diallyldimethylammonium chloride)(PDADMAC) (average M_W = 400 000-500 000, 20 wt% in water). Polyallylamine (PA) in freebase form (MW = 15 000, 15% in water) was purchased from Polysciences. The following items were obtained from VWR: glass slides (25 × 75 × 1 mm), toluene (ACS grade), ethanol 200 PROOF, nitric acid (70%, ACS grade), sodium chloride (ACS grade). Stainless steel 301 shim (thickness 0.25 mm, McMaster Carr) was cut into 13 × 13 mm pieces, washed with soap and water, and rinsed with water. Water was purified by a Barnstead EASY pure II unit.

2.3.2. Fabrication of the Films

The Cu_2O/PU coating was fabricated as follows**.** A very thin layer of PU was applied to a glass slide using a sponge and then left to dry for approximately 8 minutes to allow partial curing of the polymer. At this time, the film showed only slight or zero marking when touched with a gloved hand. 10% Cu_2O in ethanol suspension was sonicated for 3 min. and then 1 mL was applied to the PU film and left to partially dry for about 5 minutes at room temperature. The film

was then heated in an oven at 120 °C for 2 hours to finish the cure, forcefully blown with compressed nitrogen gas, washed thoroughly with DI water, and dried with a stream of nitrogen gas. At this point the film had a high advancing contact angle for water, approximately 130º. The glass film was broken into ≈ 12×12 mm pieces. Each piece of glass or stainless steel was then cleaned with argon plasma to remove excess polyurethane (See Figure S2-2). For the plasma cleaning, the sample was placed in vacuum, twice purged in argon gas for 10 minutes, then exposed to argon plasma for 3 min at 100 W and <200 mTorr. After plasma cleaning, the film was wetted by water, but the advancing water contact angle was recovered after one day. This is the state in which SARS-CoV-2 inactivation was tested and all other tests were performed unless otherwise specified. The films showed no visible change after immersion in water for 7 weeks or ethanol for one month. When we replaced the oven treatment with 24 h of cure, the outer layer of the film was less stable but a robust layer remained on the solid (See Supporting Information).

The PA film was prepared as described previously.[5] Briefly, the glass was rinsed three times with DI water, soaked in 70% ethanol for 15 min, and rinsed 3 times with DI water. Subsequently, the glass was immersed in 6 M nitric acid for 20 min, then thoroughly rinsed in DI water. The glass was then exposed to oxygen plasma, treated with pure GOPTS at 37°C for 60 minutes, and then with 15% PA in water (pH = 11) and left to react at 75°C for 36 h in a closed container. Subsequently the films was rinsed with DI water (10 times) to remove unattached polymer chains, and dried with nitrogen gas.[5] For the PDADMAC surface, the cleaned glass was immersed in 1 mM PDADMAC / 10 mM NaCl for 3 h and then gently rinsed in DI water and dried with nitrogen gas.[13]

2.3.3. Characterization of the Cu_2O Films

An SEM image of the film in cross-section is shown in Figure 2-1 and a plan view is shown in Figure S2-2 along with images of a film before plasma treatment. As a result of fabrication from a polydisperse particle distribution, the final film has a distribution of particle sizes, and is rough; the thickness ranged from 10–16 μm. Contact angles were measured using a First Ten Angstroms FTA125. Water contact angles of the film one week after fabrication were advancing: 120 º, receding: < 10º, and sessile in the range 80–120º. The chemical composition of the film was investigated by X-ray photoelectron spectroscopy (XPS, PHI VersaProbe III with a monochromatic Al Kα source of 1486.6 eV) as well as Electron Dispersive X-ray Spectroscopy (EDX, Bruker Quantax) and Scanning Electron Microscopy (SEM, FEI Quanta 600 FE-ESEM). Results confirmed the chemical identity of the Cu_2O particles in the film, and are contained in Supporting Information, Figure S2-3. and Table S2-2. The robustness of the film was measured by the cross-hatch test ASTM D3359 Method B and peel test ASTM D1876.

2.3.4. Characterization of the Cationic Films

The PA and PDADMAC film contact angles were < 10º, and the chemical compositions and XPS (Figure S2-4 and Figure S2-5) were consistent with the chemical composition.

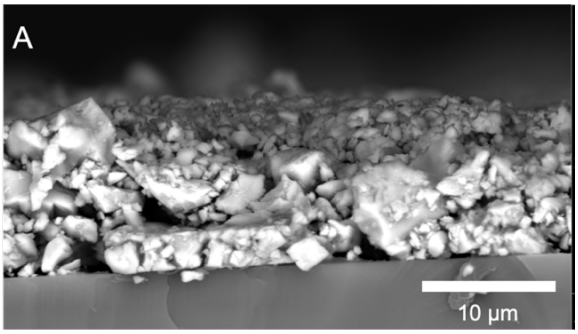


Figure 2-1. Cross section view of the Cu_2O/polyurethane film.

2.3.5. Inactivation of SARS-CoV-2

Biological testing methods are described in Chin et al's prior work.[2] Briefly, before testing with SARS-CoV-2, the film was disinfected with 70% ethanol in water and air dried at 37 ºC overnight, unless otherwise stated. SARS-CoV-2 was isolated from the index case of Hong Kong. Stock virus was prepared by Vero-E6 cells cultured in Dulbecco's Modified Eagle Medium supplemented with 2% fetal bovine serum and 1%v/v penicillin-streptomycin at 37°C with 5% CO_2. A 5 µL test droplet containing 6.2 x 10^7 (7.8 log unit) $TCID_{50}$/ml SARS-CoV-2 was placed on the test solid at 60–70% humidity and 22–23°C and was observed to dry in about 15 min for more hydrophilic samples and about 30 min for more hydrophobic samples. After a prescribed time, the solid was soaked in 300 µL of viral transport medium (Earle's balanced salt solution supplemented with 0.5%(w/v) bovine serum albumin and 0.1%(w/v) glucose, pH 7.4) at room temperature (≈22°C) to elute the virus. The eluted virus was titrated by 50% tissue culture infective dose ($TCID_{50}$) assay in Vero E6 cells.[14-15] In brief, confluent Vero E6 cells on 96-well plates were infected with serially diluted virus in quadruplicates. The infected cells were incubated at 37°C with 5% CO_2. On day 5 post-infection, the cells were examined for a cytopathic effect. The $TCID_{50}$/ml is the dilution that caused a cytopathic effect in 50% of treated

Vero E6 cell cultures (N=4 per each dilution; Reed-Muench method[16]). Three independent tests were done at each condition, except for the data in Figure S2-8, where there were 6 independent measurements. Error residuals were approximately normally distributed after a log transformation (Figure S2-6), so all averages were calculated from the log of the titers. Because reductions in titer were very large, we make use the "log reduction" terminology of biology:

$$\text{log reduction} = \text{mean}\left[\log_{10}\left(\frac{\text{uncoated titer}}{\text{units}}\right)\right] - \text{mean}\left[\log_{10}\left(\frac{\text{coated titer}}{\text{units}}\right)\right] \quad \text{Equation 2-1}$$

$$\%\ \text{reduction} = \left[1 - 10^{-\log \text{reduction}}\right] \times 100 \quad \text{Equation 2-2}$$

For example, a 99.9 % reduction is the same as a 3-log reduction.

2.4. Results And Discussion

2.4.1. The Cu2O/PU Film Rapidly Inactivates SARS-CoV-2

Inactivation of the virus by the Cu_2O/PU coating is swift and dramatic, typically a reduction of 99.9% of the viral titer in 1h (Figure 2-2). The virus is slowly inactivated even on glass or stainless steel, so in Equation 2-1 we always use as our basis of comparison the titer on the uncoated sample at the same time point. Clearly, the numerical reductions would be even greater if we were to compare to the viral titer at time zero.

On glass, the SARS-CoV-2 titer was below the detection limit after 1h for all three samples, and at all further times, so the reduction is at least 99.98% (Table 2-1). The 95% confidence interval is the range greater than 99.5%. On stainless steel the reduction was 99.90%

after one hour. The reductions in titer on glass and stainless steel are very similar because the virus interacts with the coating, not the underlying material. Films were fabricated by hand so some variation may be due to differences in sample preparation as well as in testing. Numerical values of data points are in Table S2-3 to Table S2-10. The effects of polyurethane-only coating were not resolved (p >0.05 at 1 h), demonstrating that Cu_2O is a necessary ingredient in the film. Figure S2-7 shows the time course of viral titer on polyurethane.

Several Mechanisms for the biocidal activity of cuprous oxide compounds have been proposed, and the mechanism may vary according to the microbe. Fujimori reported that the mechanism was dissolution of Cu^+ followed by production of reactive oxygen species (ROS), e.g., OH·. These ROS would then go on to degrade viral proteins.[17-18] In contrast, Sunada et al. reported that direct contact with Cu_2O with a virus was required for virucidal activity,[7] and Hang report that Cu_2O can inhibit infection by preventing virus entry.[8] The inhibitory mechanism of Cu_2O on SARS-CoV-2 is beyond the scope of this study, but further investigation on this topic is warranted.

It is interesting to note that time course of inactivation appeared to be affected by the wettability of the Cu_2O/PU film. The first batch of coating that we made produced high sessile contact angles of viral culture medium, >90º (possibly due to some polyurethane on the surface), whereas later batches had lower angles, ≈45º (precise measurement not available in the BSL-3 lab.). XPS and SEM characterizations are from the later batches. When the angle was high, we were able to detect a small amount of virus at 1 h on some replicates (See Figure S2-8) We rationalize this effect in terms of higher contact area between the viral suspension and the coating and/or faster transport within the liquid that were able to partially penetrate the film.

Condition	Comparison	% reduction	Log reduction	95% CI*	*p*-value	Figure no.
Cu_2O/PU coating on glass	glass	>99.98	>3.64	99.95	5×10^{-4}	Figure 2-2
Cu_2O/PU coating on stainless steel	stainless steel	99.90	2.97	98.51	8×10^{-3}	Figure 2-2
PU coating on glass	glass	10	0.04	-164	0.22	Figure S2-7
Cu_2O/PU on glass, stored 13 days underwater	glass†	99.96	3.39	99.56	8×10^{-4}	Figure S2-10
Cu_2O/PU glass, high contact angle	glass	99.89	2.97	99.22	2×10^{-6}	Figure S2-8
Cu_2O/PU glass, 5× disinfection	glass	99.89	2.95	99.79	4×10^{-8}	Figure 2-3

* 95% confidence limit lower bound. Upper bound set at 100%. Calculated for one-tail, assuming heteroscedastic.

† Comparison sample not stored under water.

p-values for Student's t-test calculated for one-tail, assuming heteroscedastic.

Table 2-1. Average reduction of SARS-CoV-2 titer on Cu2O/PU coated solid in 1 h compared to titer on uncoated solid in 1h.

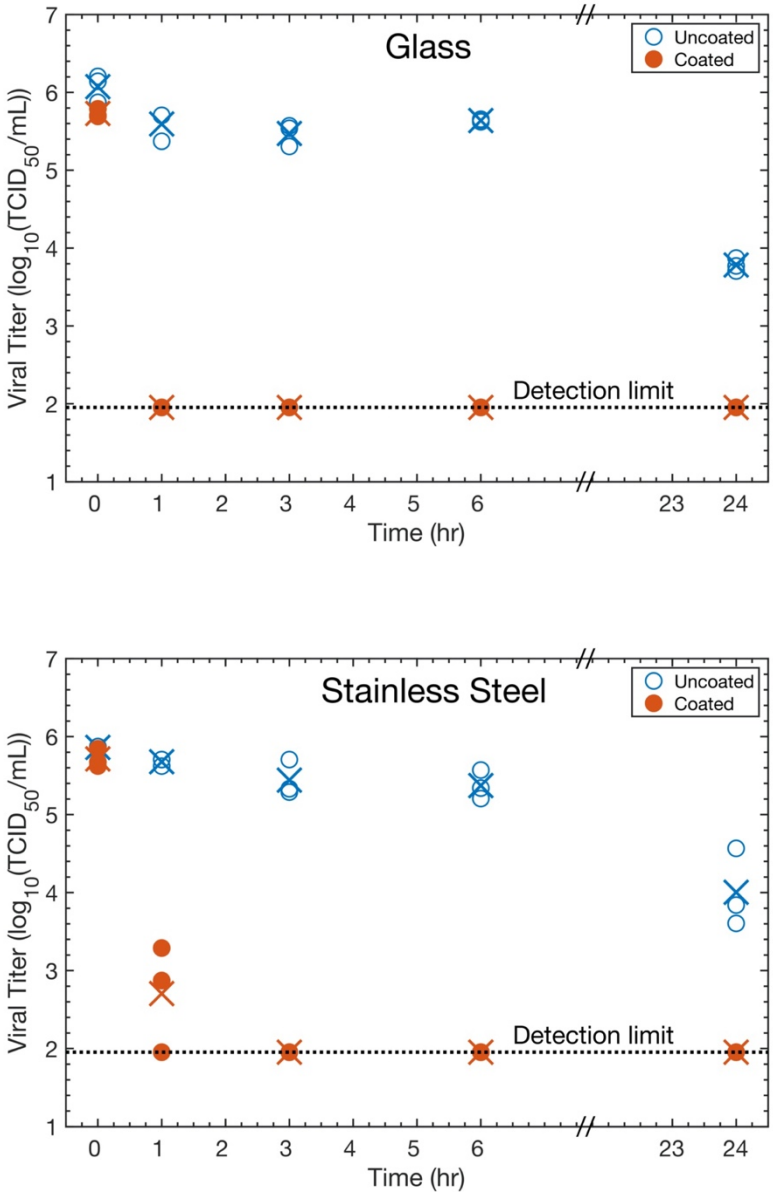


Figure 2-2. Time course of viable titer of SARS-CoV-2 on solids, with and without a coating of cuprous oxide microparticles bound with polyurethane (Cu_2O/PU). Note that the vertical axis in on a log10 scale. Data is shown for coated glass and coated stainless steel. Individual circular data points represent each independent measurement and the × symbol represents the mean of the log of independent measurements. The detection limit was 90 TCID50/mL (shown with a dotted line). Experimental results where virus was not detected are plotted at 90 TCID50/mL and are included in the average as 90 TCID50/mL. SARS-CoV-2 is inactivated much more rapidly on the coated surface than on the bare surface.

The coating is easy to apply to everyday objects because the first stage of the coating procedure is to paint with a commercial polyurethane, which has been formulated to adhere to a variety of surfaces. The Supporting Information (Figure S2-9) shows images of various items – a doorknob, a credit card reader "Enter" button, a pen and a supermarket cart handle – coated in the Cu_2O/PU film.

We also note that there was no cytopathic effect to the Vero-E6 cells after exposure to the viral transport medium that had been in contact with the Cu_2O/PU film, consistent with low toxicity of the film.

2.4.2. The Cu_2O/PU Film Remains Potent after Multiple Exposures to Virus or Storage under Water

To determine the potency of the film for inactivating virus after multiple exposure to virus, we applied a 5 µL droplet of SARS-CoV-2 to a Cu_2O/PU-coated surface and allowed the droplet and then its dry residue to stand for 24 h to ensure inactivation of virus. The coated solid was then cleaned by soaking in 70% ethanol. After air drying, another 5 µL virus droplet was applied on the same spot of the surface. These procedures were repeated 5 times and then we tested the ability of the coating to inactivate SARS-CoV-2 as described in the methods section. The film remained potent for inactivating SARS-CoV-2: after 5 exposure/disinfection cycles, the film still reduced the viral titer by about 99.89% in 1 h (see Figure 2-3), which is similar to the potency of the same films prior the disinfection cycles (99.88%) (See Figure S2-8).

Samples were also stored under water for 13 days and then then tested. The coating retained its virucidal ability for SARS-CoV-2 (See Figure S2-10).

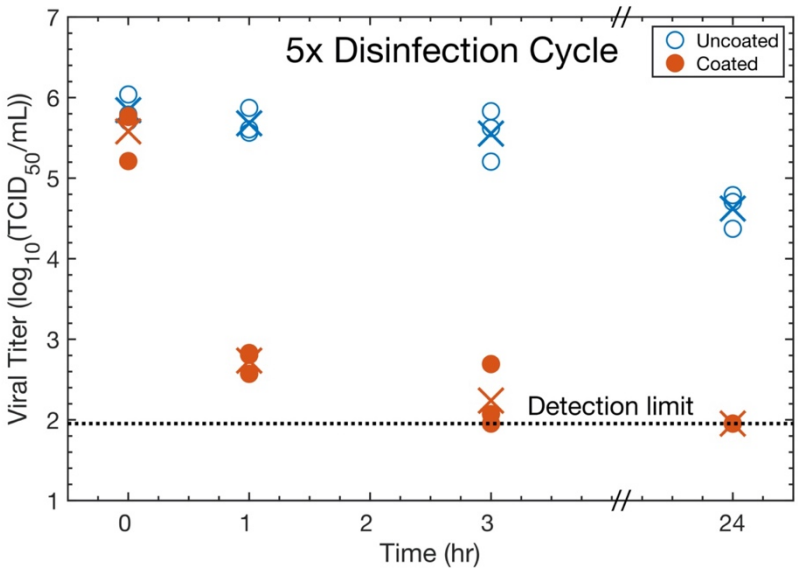


Figure 2-3. Time course of viable titer of SARS-CoV-2 on glass coated in Cu2O/PU that was subjected to 5 cycles of exposure to SARS-CoV-2 plus soaking in 70% ethanol. The uncoated glass was also subjected to the disinfection cycles.

2.4.3. The Cu_2O/PU Film is Robust

The Cu_2O/PU film is not noticeably scratched when handled with tweezers, although it can be removed by heavy, deliberate scratching. Five samples of the Cu_2O/PU film on stainless steel were scratched through to the steel with a razor blade in an 11 × 11, 1 mm square grid and then an attempt was made to remove each of the 100 small pieces of coating with tape (ASTM cross-hatch test ASTM D3359). For three independent samples, on average only 2.4 of the 100 squares were affected, with a standard deviation of 0.8, corresponding to a 4B rating in the ASTM standard (See Figure S2-11). When tape was used to pull off the top layer of particles

from an unscratched sample (a variant of ASTM D1876 Peel test[19]), there was a 0.25% loss of coverage ($p = 0.007$, six samples); visual inspection of the images showed that only a few particles were removed (see Figure S2-12). These results indicate that the film has durability.

2.4.4. A Coating of a Cationic Polymer Coating Did Not Speed Inactivation of SARS-CoV-19

Two cationic polymer films were examined. A Film of PA (mainly primary amines) and a film of PDADMAC (quaternary ammonium). Both films were designed such that the polymer retained flexibility. The PA was tethered by covalent linkages and prior force measurements showed that chains could extend up 200 nm from the solid in solution.[5] PDADMAC chains could extend up to 10 nm from the solid.[13] This chain flexibility was designed to assist contact with a larger area of the curved virus. The cationic coatings did not, however, lead to greater inactivation of the virus for the first 24 h for PDADMAC or for the first 48 h for PA (See Figure S2-13 and Figure S2-14).

2.5. Conclusions

A porous coating of Cu_2O/PU causes a swift and dramatic reduction of the infective titer of SARS-CoV-2. After one hour, a typical reduction is 99.9% compared to the uncoated sample. The coating retains its potency after multiple exposures to virus followed by washing with 70% ethanol in water, or after immersion in water for 13 days. The coating retains its mechanical integrity after being cut with a razor blade. Amine and ammonium-based polymers did not inactivate the virus under the conditions tested.

ACKNOWLEDGEMENTS

The authors thank Stephen McCartney for capturing the SEM images and acknowledge use of Electron Microscopy facilities within the Nanoscale Characterization and Fabrication Laboratory at Virginia Polytechnic Institute. We also thank Xu Fang for capturing the XPS spectra and acknowledge the use of Surface Analysis Laboratory in Department of Chemistry at Virginia Tech, which is supported by the National Science Foundation under Grant No. CHE-1531834. We also thank Matthew Ducker for help with statistical analysis, Dr. Dave Dillard for advice on the cross-hatch test, and Dr. Ayman Karim for the loan of an argon cylinder. Cu_2O chemical composition and size distribution was provided by American Chemet Corporation. This work was supported by the National Science Foundation under Grant No. CBET-1902364, the Health and Medical Research Fund (COVID190116), and the National Institute of Allergy and Infectious Diseases (contract HHSN272201400006C)

Supporting Information

Table S2-1. Chemical Composition of Cu2O particles.

Table S2-2. Elemental Composition of the Cu2O/PU film measured by EDS.

Table S2-3 to Table S2-10. Virus titration data.

Alternative methods for preparing the Cu_2O/PU film.

Figure S2-1. Particle Size Distribution of Cu_2O particles.

Figure S2-2. SEM Images of the Cu_2O/PU coating before and after plasma cleaning.

Figure S2-3. XPS results for Cu_2O/PU.

Figure S2-4. XPS results for the PA polymer films.

Figure S2-5. XPS results for the PDADMAC polymer films.

Figure S2-6. Histogram of Residuals for virus titer.

Figure S2-7. Viral titer for polyurethane film.

Figure S2-8. Viral titer for high-contact-angle sample.

Figure S2-9. Images of various items coated in Cu_2O/PU.

Figure S2-10. Viral titer for samples stored under water for 13 days.

Figure S2-11. Cross-Hatch test results for Cu_2O/PU on stainless steel.

Figure S2-12. Peel test results.

Figure S2-13. Viral titer for PA (Polyallylamine).

Figure S2-14. Viral titer for PDADMAC.

REFERENCES

1. van Doremalen, N.; Bushmaker, T.; Morris, D. H.; Holbrook, M. G.; Gamble, A.; Williamson, B. N.; Tamin, A.; Harcourt, J. L.; Thornburg, N. J.; Gerber, S. I. Aerosol and Surface Stability of SARS-CoV-2 as Compared with SARS-CoV-1. *N. Engl. J. Med.* **2020,** *382* (16), 1564-1567.

2. Chin, A.; Chu, J.; Perera, M.; Hui, K.; Yen, H.-L.; Chan, M.; Peiris, M.; Poon, L. Stability of SARS-CoV-2 in Different Environmental Conditions. *Lancet Microbe,* **2020**, 1, e10.

3. Wong, S. Y.; Li, Q.; Veselinovic, J.; Kim, B.-S.; Klibanov, A. M.; Hammond, P. T. Bactericidal and Virucidal Ultrathin Films Assembled Layer by Layer From Polycationic N-Alkylated Polyethylenimines and Polyanions. *Biomaterials* **2010,** *31* (14), 4079-4087.

4. Haldar, J.; An, D.; de Cienfuegos, L. A.; Chen, J.; Klibanov, A. M. Polymeric Coatings that Inactivate both Influenza Virus and Pathogenic **b**acteria. *Proc. Natl. Acad. Sci* **2006,** *103* (47), 17667-17671.

5. Iarikov, D. D.; Kargar, M.; Sahari, A.; Russel, L.; Gause, K. T.; Behkam, B.; Ducker, W. A. Antimicrobial Surfaces Using Covalently Bound Polyallylamine. *Biomacromolecules* **2014,** *15* (1), 169-176.

6. Chang, R. C. *Chemistry*; Fourth ed.; McGraw Hill: New York, 1991, page 803.

7. Sunada, K.; Minoshima, M.; Hashimoto, K. Highly Efficient Antiviral and Antibacterial Activities of Solid-State Cuprous Compounds. *J. Hazard. Mater.* **2012,** *235*, 265-270.

8. Hang, X.; Peng, H.; Song, H.; Qi, Z.; Miao, X.; Xu, W. Antiviral Activity of Cuprous Oxide Nanoparticles against Hepatitis C Virus in Vitro. *J. Virol. Methods* **2015,** *222*, 150-157.

9. EPA. *Reregistration Eligibility Decision (RED) for Coppers ttps://www3.epa.gov/pesticides/chem_search/reg_actions/reregistration/red_G-26_26-May-09.pdf*2009.

10. Chen, D.; Zhang, D.; Jimmy, C. Y.; Chan, K. M. Effects of Cu2O Nanoparticle and CuCl2 on Zebrafish Larvae and a Liver Cell-line. *Aquat. Toxicol.* **2011,** *105* (3-4), 344-354.

11. Amara, I.; Miled, W.; Slama, R. B.; Ladhari, N. Antifouling Processes and Toxicity Effects of Antifouling Paints on Marine Environment. A Review. *Environ. Toxicol. Pharmacol.* **2018,** *57*, 115-130.

12. Borkow, G. Safety of Using Copper Oxide in Medical Devices and Consumer Products. *Curr. Chem. Biol.* **2012,** *6* (1), 86-92.

13. Liu, J. F.; Min, G.; Ducker, W. A. AFM study of adsorption of cationic surfactants and cationic polyelectrolytes at the silica-water interface. *Langmuir* **2001,** *17*, 4895-4903.

14. Chan, K.; Lai, S.; Poon, L.; Guan, Y.; Yuen, K.; Peiris, J. Analytical Sensitivity of Rapid Influenza Antigen Detection Tests for Swine-origin Influenza Virus (H1N1). *J. Clin. Virol.* **2009,** *45* (3), 205-207.

15. Malenovska, H. Virus Quantitation by Transmission Electron Microscopy, TCID50, and the Role of Timing Virus Harvesting: A Case Study of hree Animal Viruses. *J. Virol. Methods* **2013,** *191* (2), 136-140.

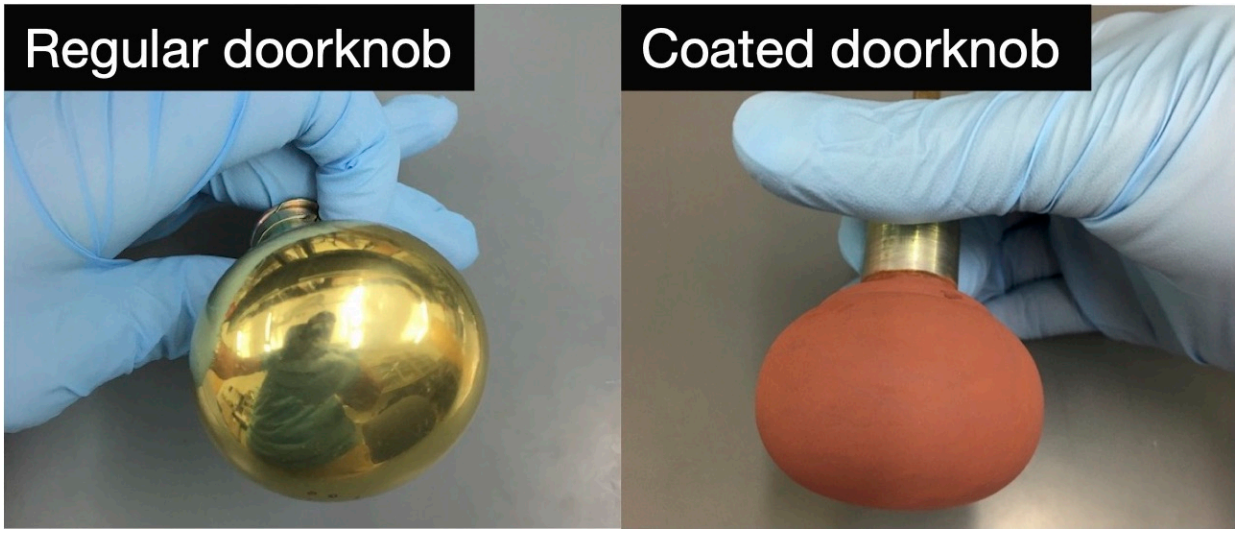
16. Reed, L. J.; Muench, H. A Simple Method of Estimating Fifty per cent Endpoints. *Am. J. Epidemiol.* **1938,** *27* (3), 493-497.

17. Fujimori, Y.; Sato, T.; Hayata, T.; Nagao, T.; Nakayama, M.; Nakayama, T.; Sugamata, R.; Suzuki, K. Novel Antiviral Characteristics of Nanosized Copper (I) Iodide Particles Showing Inactivation Activity against 2009 Pandemic H1N1 Influenza Virus. *Appl. Environ. Microbiol.* **2012,** *78* (4), 951-955.

18. Hans, M.; Mathews, S.; Mücklich, F.; Solioz, M. Physicochemical Properties of Copper Important for its Antibacterial Activity and Development of a Unified Model. *Biointerphases* **2016,** *11* (1), 018902.

19. Chang, Y.-R.; Taylor, S.; Duncan, S.; Mazilu, D. A.; Ritter, A. L.; Ducker, W. A. Fabrication of Stabilized Colloidal Crystal Monolayers. *Colloids Surf., A: Physicochem. Eng. Aspects* **2017,** *514*, 185-191.

Table of Contents Graphic



2.6. SUPPORTING INFORMATION

A Surface Coating that Rapidly Inactivates SARS-CoV-2

Saeed Behzadinasab[†], Alex Chin[†], Mohsen Hosseini, Leo Poon*, and William Ducker*

[†] These authors contributed equally

*Corresponding Authors' Email: Leo Poon llmpoon@hku.hk; William Ducker wducker@vt.edu

[1]Dept. of Chemical Engineering and Center for Soft Matter and Biological Physics, Virginia Tech, VA, 24061, USA

[2]School of Public Health, LKS Faculty of Medicine, The University of Hong Kong, Hong Kong Special Administrative Region, China.

Copper Compounds	**%**
Cuprous Oxide (Cu_2O)	95.6
Cupric Oxide (CuO)	3.2
Metallic Cu	0.1
Trace Metals	**ppb**
Lead	60
Cadmium	0
Arsenic	1

Table S2-1. Chemical Composition of Cu_2O particles. The lot number is 2696. This information was provided by American Chemet Corporation.

		Cu:O ratio
Before plasma treatment	top	1.4:1
	cross section	2:1
After 3 min plasma treatment	top	5:1
	Cross section	2:1

Table S2-2. Elemental Composition of the Particles in the film measured by EDS. EDS is sensitive to about 1 μm of surface layer. Before plasma treatment the top of the film was less rich in Cu than expected for Cu_2O, presumably because part of the surface was covered in PU. After plasma treatment, the film is more rich in copper than expected.

Material	Time	$TCID_{50}$/ml				log ($TCID_{50}$/ml)		
Nil (virus input control)	0	692703.4	1606690	472804.9		5.840547	6.205932	5.674682
Glass	0	1606690	745759.2	1391336		6.205932	5.872599	6.143432
	1 h	508079.8	508079.8	235829.8		5.705932	5.705932	5.372599
	3 h	202270.2	372663.3	346150.8		5.305932	5.571317	5.539265
	6 h	434260.3	452826.6	419371.2		5.63775	5.655932	5.622599
	1 day	5911.823	5080.798	7457.592		3.771721	3.705932	3.872599
Cu_2O on glass	0	492917.3	615552.8	508079.8		5.692774	5.789265	5.705932
	1 h	<	<	<		<	<	<
	3 h	<	<	<		<	<	<
	6 h	<	<	<		<	<	<
	1 day	<	<	<		<	<	<

Table S2-3. Virus titration data of SARS-CoV-2 for the Cu_2O coating on glass and its control (glass). < represents that the measurement was less than the minimum detectable value of 90 TCID50/ml. This data appears in Figure 2-2.

Material	Time	$TCID_{50}$/ml				log ($TCID_{50}$/ml)		
Nil (virus input control)	0	1166925	492917.3	1606690		6.067043	5.692774	6.205932
Stainless steel	0	692703.4	745759.2	745759.2		5.840547	5.872599	5.872599
	1 h	508079.8	419371.2	508079.8		5.705932	5.622599	5.705932
	3 h	194654.9	508079.8	214255.5		5.289265	5.705932	5.330932
	6 h	160669	219052.1	372663.3		5.205932	5.340547	5.571317
	1 day	4035.822	6927.034	36901.42		3.605932	3.840547	4.567043
Cu_2O on stainless steel	0	419371.2	472804.9	699553.4		5.622599	5.674682	5.844821
	1 h	<	745.7592	1946.549		<	2.872599	3.289265
	3 h	<	<	<		<	<	<
	6 h	<	<	<		<	<	<
	1 day	<	<	<		<	<	<

Table S2-4. Virus titration data of SARS-CoV-2 for the Cu_2O coating on stainless steel and its control (stainless steel). This data appears in Figure 2-2.

Material	Time	$TCID_{50}$/ml				log ($TCID_{50}$/ml)		
Nil (virus input control)	0	1166925	492917.3	1606690		6.067043	5.692774	6.205932
Glass (5 x disinfection cycle)	0	508079.8	1094625	615552.8		5.705932	6.039265	5.789265
	1 h	745759.2	403582.2	367542		5.872599	5.605932	5.565307
	3 h	419371.2	677535.3	160669		5.622599	5.830932	5.205932
	1 day	50807.98	61555.28	23582.98		4.705932	4.789265	4.372599
Cu_2O on glass (5 x disinfection cycle)	0	162940.7	575810.8	591182.3		5.21203	5.76028	5.771721
	1 h	639.6346	372.6633	677.5353		2.805932	2.571317	2.830932
	3 h	<	117.8465	492.9173		<	2.071317	2.692774
	1 day	<	<	<		<	<	<

Table S2-5. Virus titration data of SARS-CoV-2 on the Cu_2O coating on glass and its control (glass) after exposure to 5 cycles of SARS-CoV-2 plus 5 cycles of disinfection with 70% ethanol. This data appears in Figure 2-3.

Material	Time	$TCID_{50}$/ml				log ($TCID_{50}$/ml)		
Nil (virus input control)	0	692703.4	1606690	472804.9		5.840547	6.205932	5.674682
Glass	0	1606690	745759.2	1391336		6.205932	5.872599	6.143432
	1 h	508079.8	508079.8	235829.8		5.705932	5.705932	5.372599
	3 h	202270.2	372663.3	346150.8		5.305932	5.571317	5.539265
	6 h	434260.3	452826.6	419371.2		5.63775	5.655932	5.622599
	1 day	5911.823	5080.798	7457.592		3.771721	3.705932	3.872599
Polyurethane on glass	0	472804.9	523708.8	508079.8		5.674682	5.71909	5.705932
	1 h	472804.9	160669	591182.3		5.674682	5.205932	5.771721
	3 h	137325.2	194654.9	586721.4		5.13775	5.289265	5.768432
	6 h	74575.92	367542	194654.9		4.872599	5.565307	5.289265
	1 day	508.0798	1495.14	4193.712		2.705932	3.174682	3.622599

Table S2-6. Virus titration data of SARS-CoV-2 for the polyurethane coating on glass and its control (glass).

Material	Time	$TCID_{50}$/ml				log ($TCID_{50}$/ml)		
Nil (virus input control)	0	692703.4	3675420	1606690		5.840547	6.565307	6.205932
Glass (control)	0	615552.8	2221043	508079.8		5.789265	6.346557	5.705932
	0	1204847	508079.8	745759.2		6.080932	5.705932	5.872599
	1 h	508079.8	1094625	472804.9		5.705932	6.039265	5.674682
	1 h	160669	508079.8	439979		5.205932	5.705932	5.643432
	3 h	699553.4	346150.8	372663.3		5.844821	5.539265	5.571317
	6 h	352241.9	50807.98	182087.4		5.546841	4.705932	5.26028
	1 day	23582.98	37266.33	37266.33		4.372599	4.571317	4.571317
Cu_2O on glass	0	1606690	235829.8	615552.8		6.205932	5.372599	5.789265
	0	1094625	1094625	586721.4		6.039265	6.039265	5.768432
	1 h	15587.41	<	<		4.192774	<	<
	1 h	160.669	<	6995.534		2.205932	<	3.844821
	3 h	615.5528	5080.798	6155.528		2.789265	3.705932	3.789265
	6 h	132.6168	160.669	194.6549		2.122599	2.205932	2.289265
	1 day	<	<	<		<	<	<

Table S2-7. Virus titration data of SARS-CoV-2 for the Cu_2O coating on glass and its control (glass). This data appears in Figure S2-8. This batch of solid was more hydrophobic than the solid that was tested for the results in Table S2-3.

Material	Time	$TCID_{50}$/ml				log ($TCID_{50}$/ml)		
Nil (virus input control)	0	692703.4	1606690	472804.9		5.840547	6.205932	5.674682
Glass	0	1606690	745759.2	1391336		6.205932	5.872599	6.143432
	1 h	508079.8	508079.8	235829.8		5.705932	5.705932	5.372599
	3 h	202270.2	372663.3	346150.8		5.305932	5.571317	5.539265
	6 h	434260.3	452826.6	419371.2		5.63775	5.655932	5.622599
	1 day	5911.823	5080.798	7457.592		3.771721	3.705932	3.872599
Cu_2O on glass (stored 13 days under in water)	0	508079.8	508079.8	745759.2		5.705932	5.705932	5.872599
	1 h	<	<	508.0798		<	<	2.705932
	3 h	<	<	<		<	<	<
	6 h	<	<	<		<	<	<
	1 day	<	<	<		<	<	<

Table S2-8. Virus titration data of SARS-CoV-2 for the Cu_2O coating on glass and its control (glass). These samples were stored under water for 13 days prior to the virus tests.

Material	Time	$TCID_{50}$/ml				log ($TCID_{50}$/ml)		
Nil (virus input control)	0	692703.4	3675420	1606690		5.840547	6.565307	6.205932
Glass (control)	0	615552.8	2221043	508079.8		5.789265	6.346557	5.705932
	1 h	508079.8	1094625	472804.9		5.705932	6.039265	5.674682
	3 h	699553.4	346150.8	372663.3		5.844821	5.539265	5.571317
	6 h	194654.9	160669	214255.5		5.289265	5.205932	5.330932
	1 day	23582.98	37266.33	37266.33		4.372599	4.571317	4.571317
	2 days	14951.4	21905.21	15842.89		4.174682	4.340547	4.199834
Polyallyl-amine	0	508079.8	1166925	508079.8		5.705932	6.067043	5.705932
	1 h	1204847	1326168	185537.6		6.080932	6.122599	5.268432
	3 h	194654.9	508079.8	381006.1		5.289265	5.705932	5.580932
	6 h	137325.2	211983.6	160669		5.13775	5.326302	5.205932
	1 day	61555.28	109462.5	50807.98		4.789265	5.039265	4.705932
	2 days	19465.49	21905.21	23582.98		4.289265	4.340547	4.372599

Table S2-9. Virus titration data of SARS-CoV-2 for the PA coating on glass and its control (glass)

Material	Time	$TCID_{50}$/ml				log ($TCID_{50}$/ml)		
Nil (virus input control)	0	692703.4	3675420	1606690		5.840547	6.565307	6.205932
Glass (control)	0	615552.8	2221043	508079.8		5.789265	6.346557	5.705932
	1 h	508079.8	1094625	472804.9		5.705932	6.039265	5.674682
	3 h	699553.4	346150.8	372663.3		5.844821	5.539265	5.571317
	1 day	23582.98	37266.33	37266.33		4.372599	4.571317	4.571317
PDADMAC	0	591182.3	508079.8	615552.8		5.771721	5.705932	5.789265
	1 h	508079.8	508079.8	523708.8		5.705932	5.705932	5.71909
	3 h	615552.8	439979	194654.9		5.789265	5.643432	5.289265
	1 day	41937.12	16066.9	16066.9		4.622599	4.205932	4.205932

Table S2-10. Virus titration data of SARS-CoV-2 for the PDADMAC coating on glass and its control (glass)

2.6.1. Alternative methods for preparing the Cu_2O/PU film.

A. A film with only the Cu_2O particles (no polyurethane) is not robust. We tried the following two procedures:
   1. Coat a glass slide using a suspension of Cu_2O in ethanol.
   2. Roughen the glass slide by placing in 5 M NaOH for 10 min then activate with oxygen plasma then add a suspension of Cu_2O in ethanol.

In both cases, the particles could be easily removed.

B. A film was prepared as described in the manuscript, but instead of being heated in an oven for 2 h at 120ºC, it was left to dry for 24 h. In this case, the outer layer of particles could be removed with tape or light scratching or compressed nitrogen gas or a water droplet. But the remainder of the film was intact.

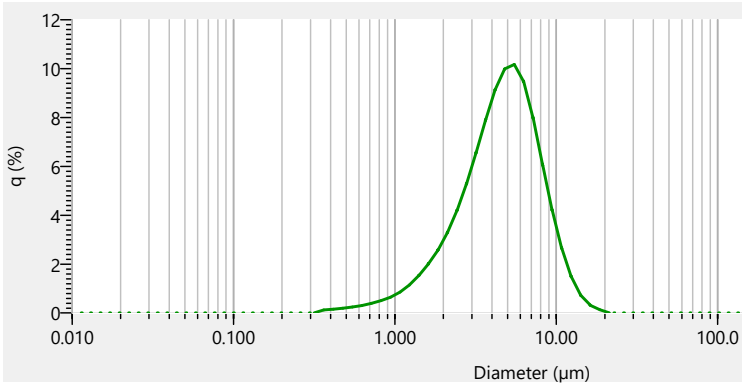


Figure S2-1. Particle Size Distribution of Cu2O particles as measured by a Horiba Laser Scattering Particle Size Distribution Analyser, model LA 960. The mean size is 5.1 µm and the mode is 5.5 µm. This information was provided by American Chemet Corporation.

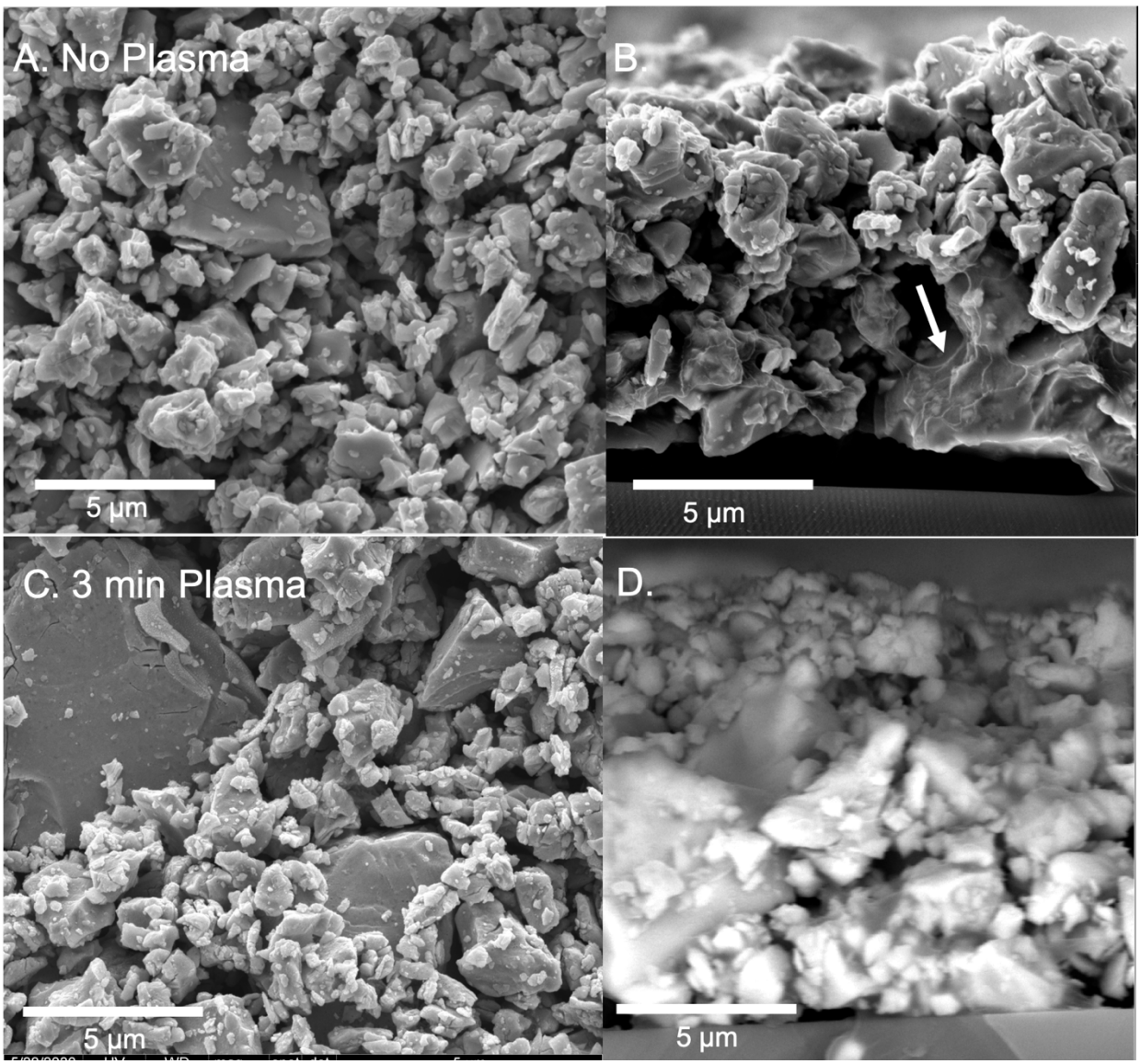


Figure S2-2. SEM Images of the Cu2O/PU coating. A and B. Coating before plasma treatment, C and D Coating after plasma treatment. A and C are plan view and B and D are cross sections. The arrow in B points to a curved meniscus of PU. These features were absent after plasma cleaning. The samples are not the same piece before and after plasma treatment.

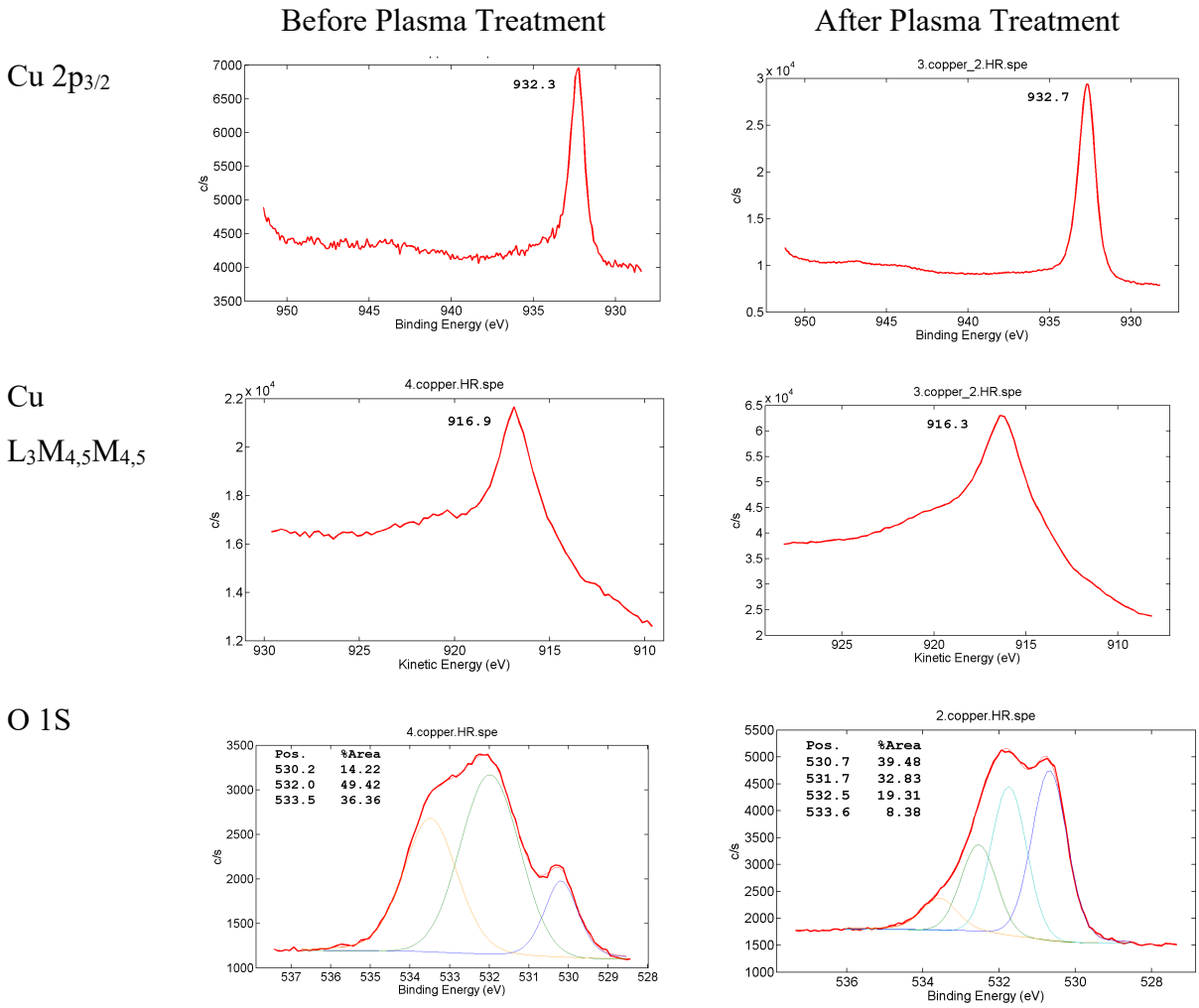
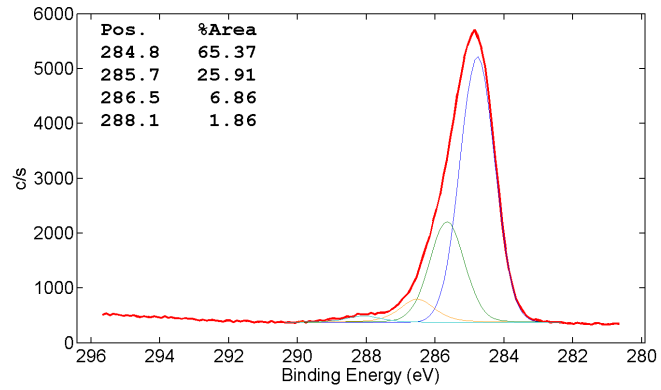


Figure S2-3. XPS data for the Cu_2O/PU film. XPS senses the chemistry of the outer 1 nm of the film. XPS of the Ar plasma-treated surface that was tested for SARS-CoV-2 inactivation shows a Cu $2p_{3/2}$ binding energy peak at 932.7 eV (E_b), which can be assigned to either Cu metal or Cu_2O.[1,2] These two Cu species were distinguished though the Cu $L_3M_{4,5}M_{4,5}$ Auger signal, which had a measured kinetic energy of 916.2 eV (E_k). The resulting Modified Auger Parameter[3,4] of 1849.0 eV (E_b+E_k) is in excellent agreement with the value of Cu_2O[2,4] and differs by 2 eV from the value of Cu metal,[2] indicating that Cu_2O is the primary Cu species on the sample surface. The stoichiometry of the copper oxide can also be determined from the measured ratio of Cu to the metal oxide contribution of the O 1S band (530.7 eV). The measured stoichiometry is 1.8:1, which is a little lower than expected for Cu_2O (2:1). Note that this calculation depends on deconvolution of the various contributions to the O 1s band, which adds uncertainty to the stoichiometry calculation. Results for the film before Ar-plasma-treatment were similar, except

that the measured ratio of Cu:O metal oxide (530.2 eV) is 1:1, which is significantly lower than expected for Cu_2O, despite a Modified Auger Parameter that is consistent with Cu_2O.

A.



B.

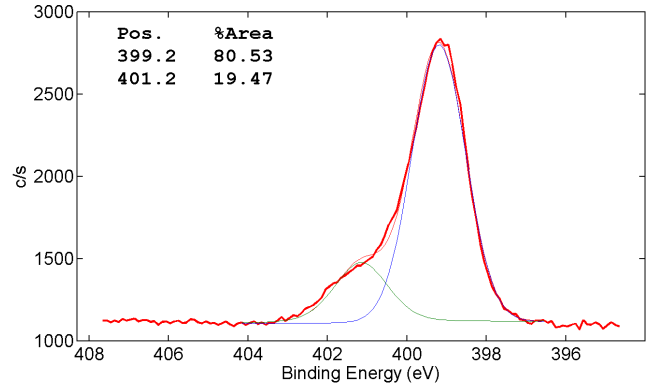
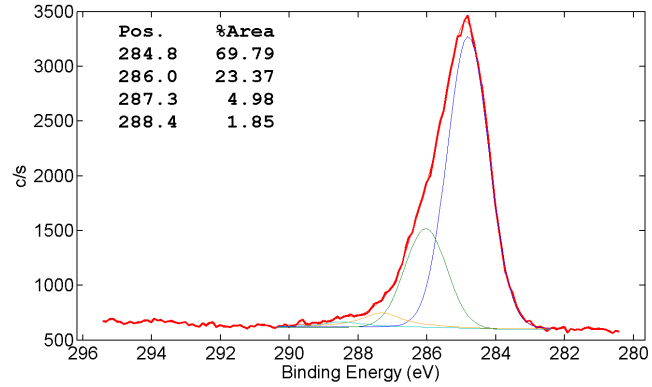


Figure S2-4. XPS results for the PA film. A. C1s peaks and B. N1s peaks for the polyallylamine film. The peak at 399 and the shoulder at 401 eV show the presence of amine groups and are similar to those reported previously for this film.[5]

A.



B.

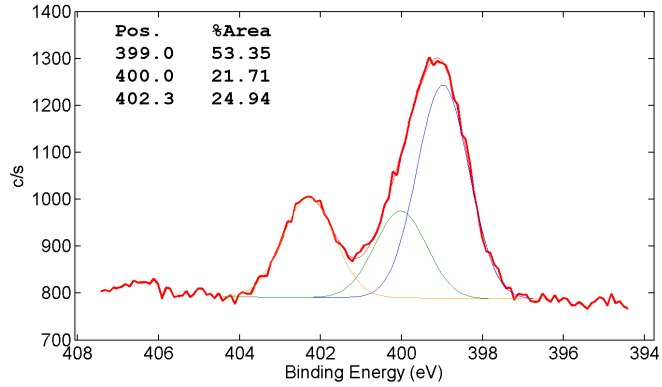


Figure S2-5. XPS results for the PDADMAC film. A. C1s peaks and B. N1s peaks for the PDADMAC film.

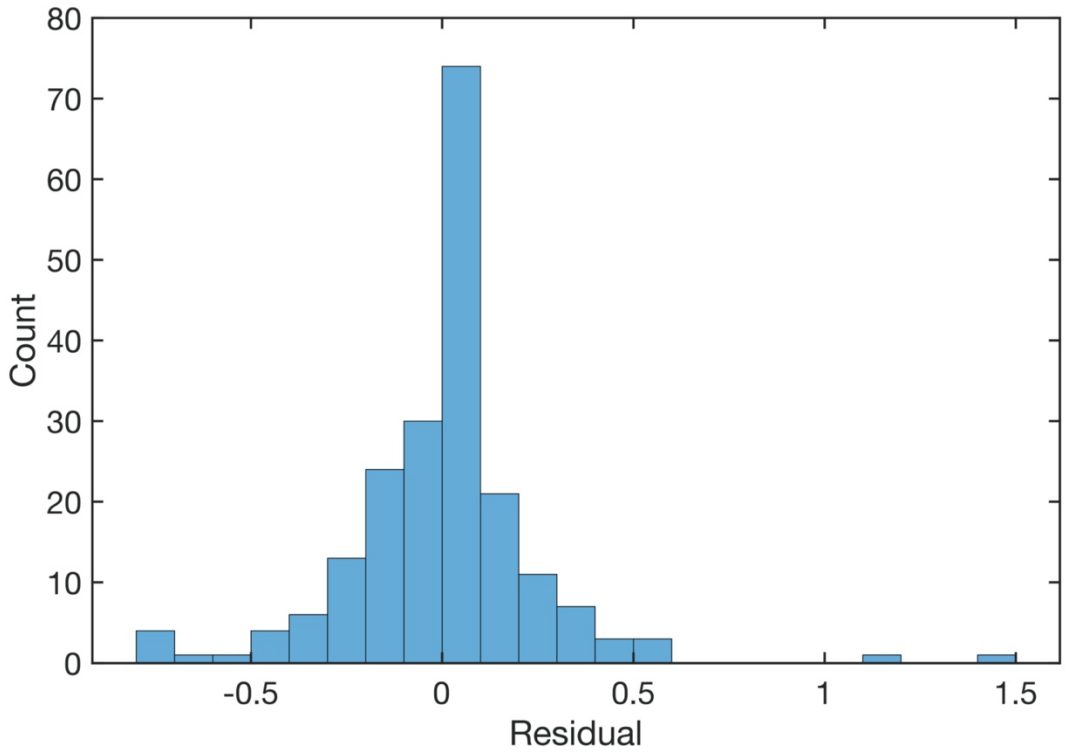


Figure S2-6. Distribution of residuals (log 10(titer/units) minus mean log(titer/units)) for measured virus titers. We include data for all of the samples, with the mean calculated for a particular condition at a particular time. The approximately normal distribution justifies averaging of the log (titer) values rather than the titer values.

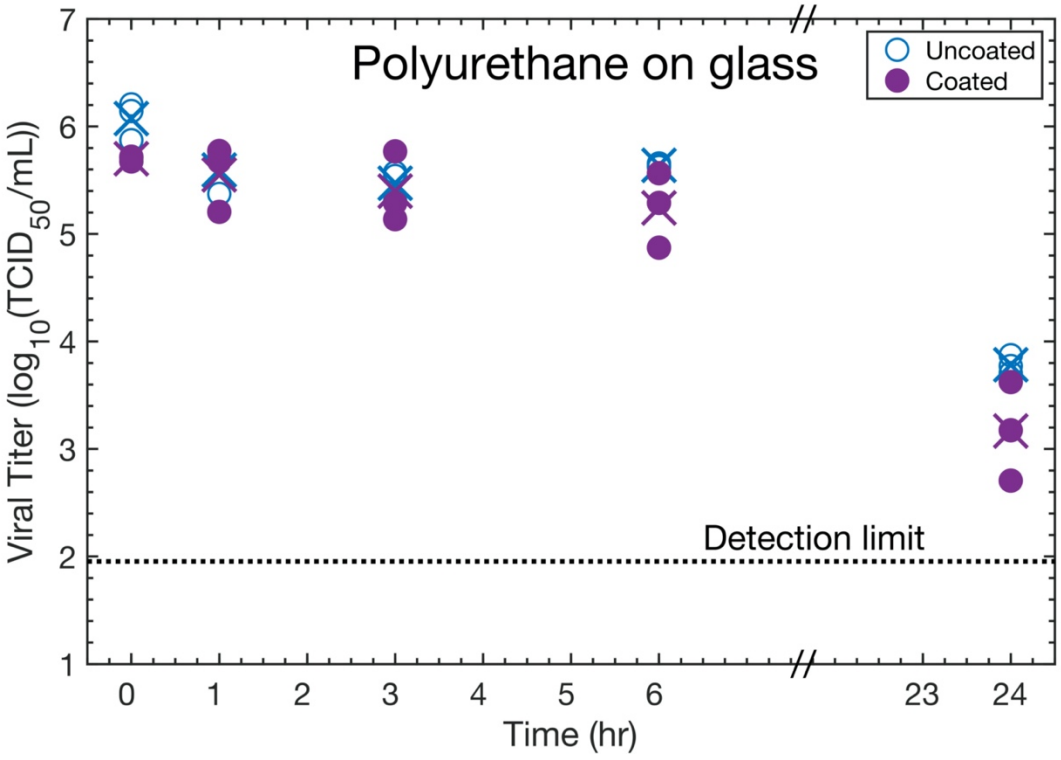


Figure S2-7. SARS-CoV-2 titer on polyurethane-coated glass. Individual circular data points represent each independent measurement and the × symbol represents the mean of the log of independent measurements. There is little effect of the polyurethane coating; $p = 0.2$ at 1 h.

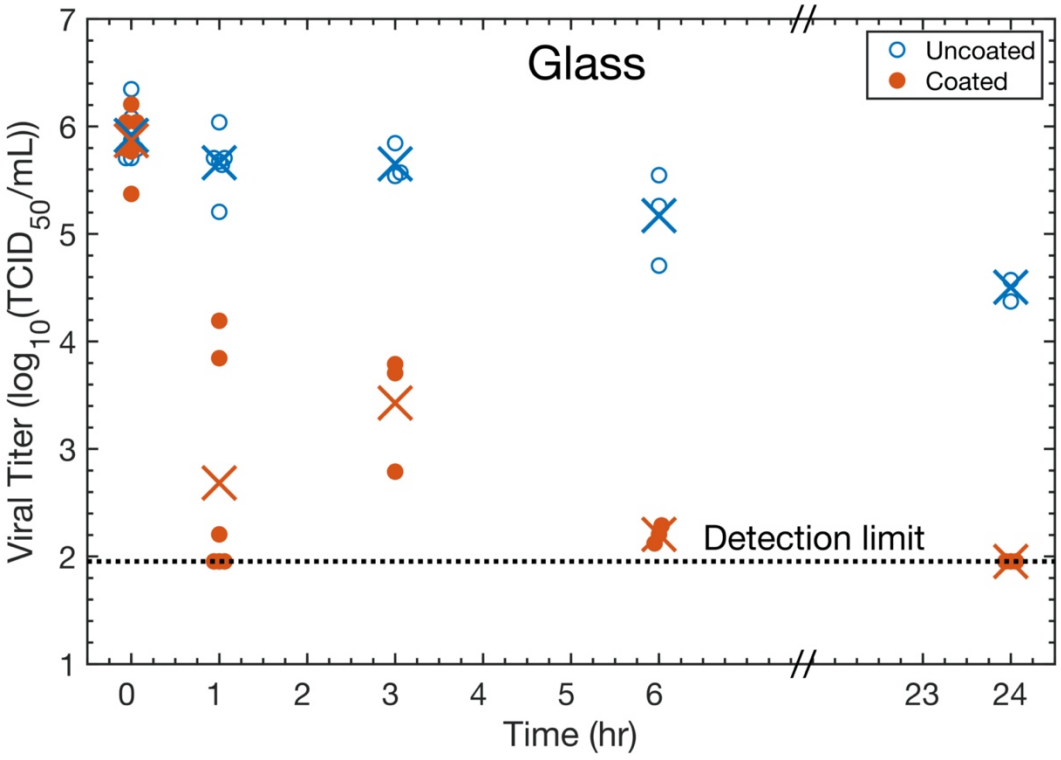
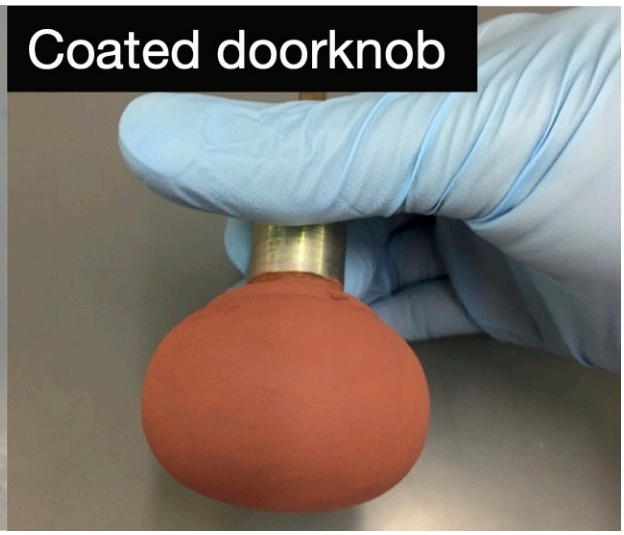


Figure S2-8. SARS-CoV-2 titer on Cu_2O/PU coating. These samples were the first batch that we tested and had a high advancing contact angle, meaning that the droplets did not penetrate into the porous film. The mean fraction inactivated after 1 h on the coating compared to the bare glass was 99.8%, and the 95% confidence interval is between 99.56% and 100% of virus inactivated. This is slightly worse performance than for the more wetting films. Individual circular data points represent each independent measurement and the × symbol represents the mean of the log of independent measurements. SARS-CoV-2 is inactivated much more rapidly on the coated solid than on the bare solid. Where necessary, some noise has been added to the time data for improved visualization.


Regular doorknob


Coated doorknob


Card reader
1 .QZ
2 ABC
3 DEF
Cancel
4 GHI
5 JKL
6 MNO
Clear
7 PRS
8 TUV
9 WXY
Enter
+
0*#,.
−


Card reader – coated ‘enter’ button
1 .QZ
2 ABC
3 DEF
Cancel
4 GHI
5 JKL
6 MNO
Clear
7 PRS
8 TUV
9 WXY
+
0*#,.
−



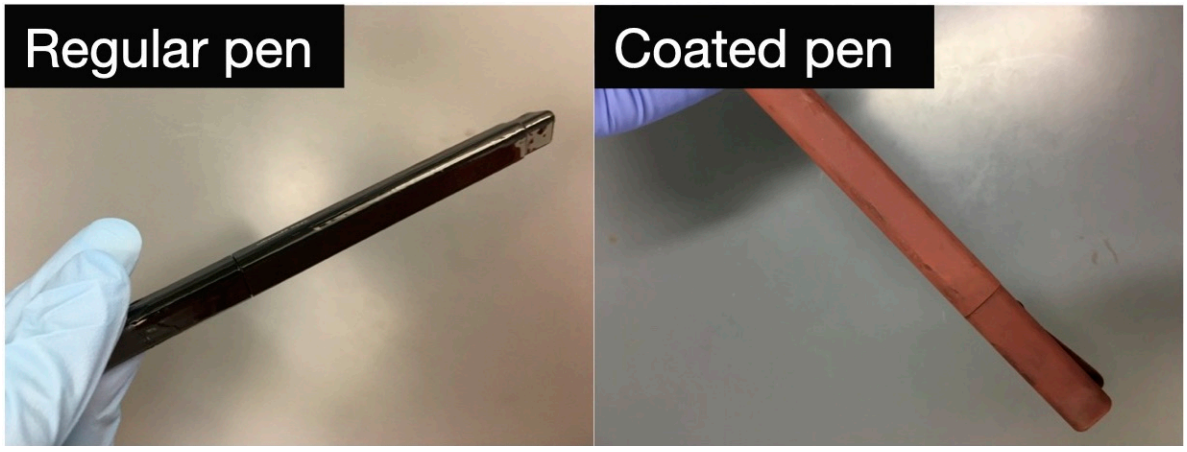


Figure S2-9. Images of various everyday household/commercial items coated with the Cu_2O/PU coating. Although the items were not baked in an oven, the film was very difficult to remove and had to be scraped off with a razor blade.

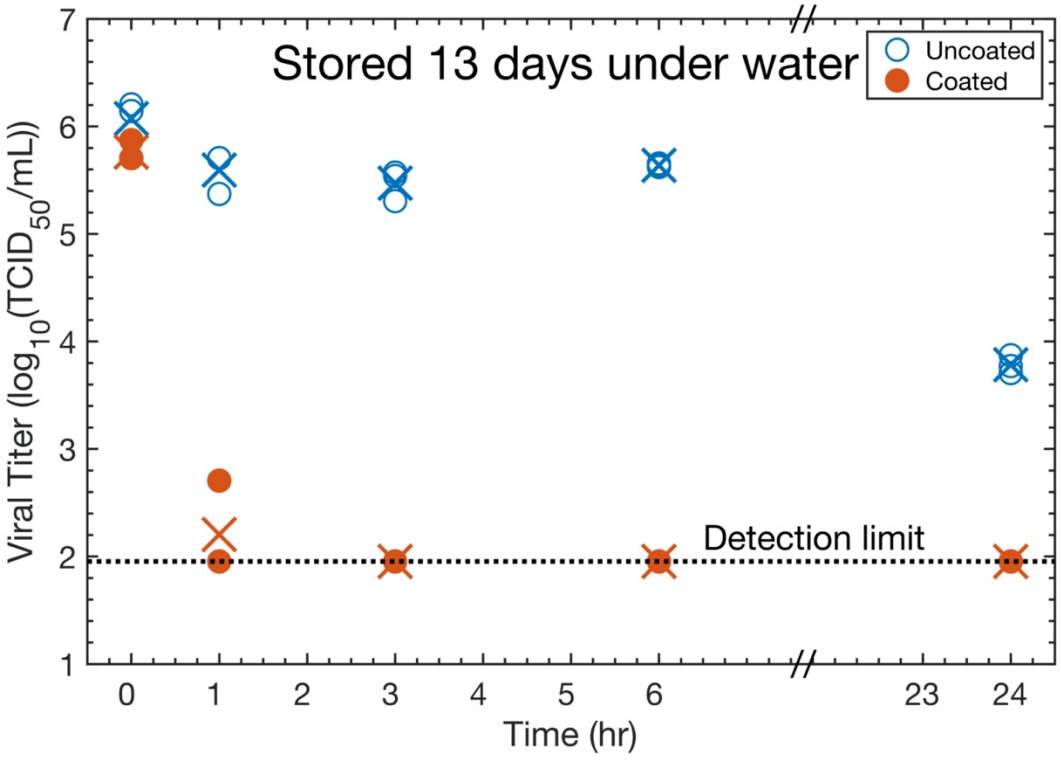


Figure S2-10. Viral titer for samples stored under water for 13 days. Samples were tested 30 minutes after removal from water. Individual circular data points represent each independent measurement and the × symbol represents the mean of the log of independent measurements. Data points where virus was not detected are plotted at or near 90 TCID50/mL (shown with a dotted line) and are included in the average as 90 TCID50/mL. The uncoated surface was not stored under water. SARS-CoV-2 is inactivated much more rapidly on the coated solid than on the bare solid.

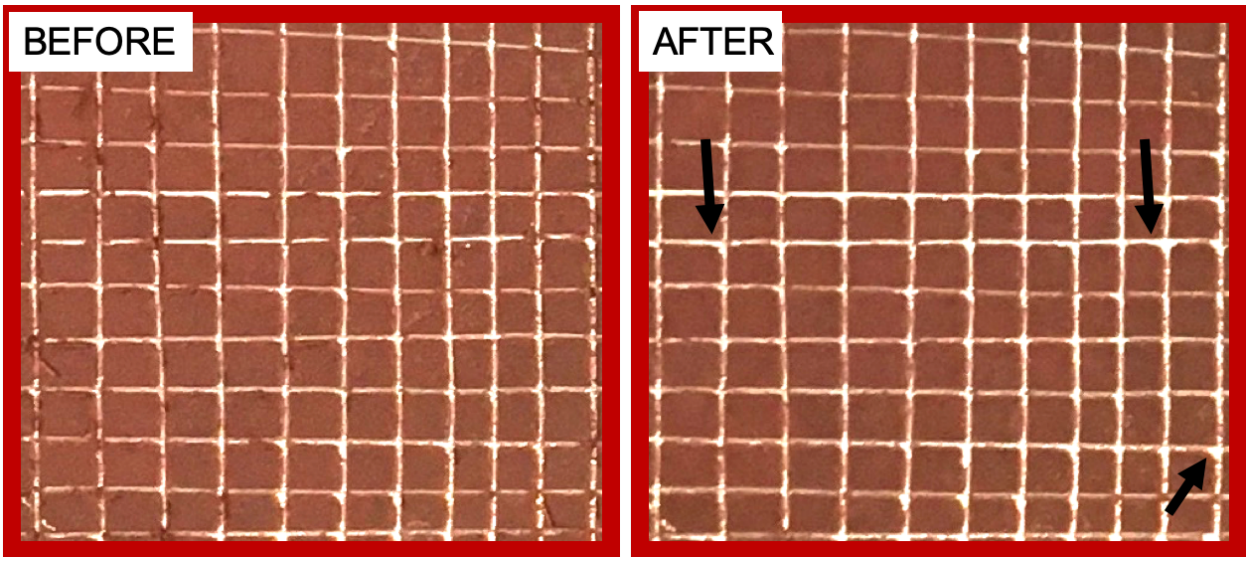


Figure S2-11. Results of Cross-Hatch Test. Image is of the Cu_2O film on stainless steel before and after the tape peel. Arrows indicate where damage was judged to occur. Three independent samples were tested; the average number of affected squares was 2.4 and the standard deviation was 0.8. The stainless steel was type 302 from Precisionbrand.

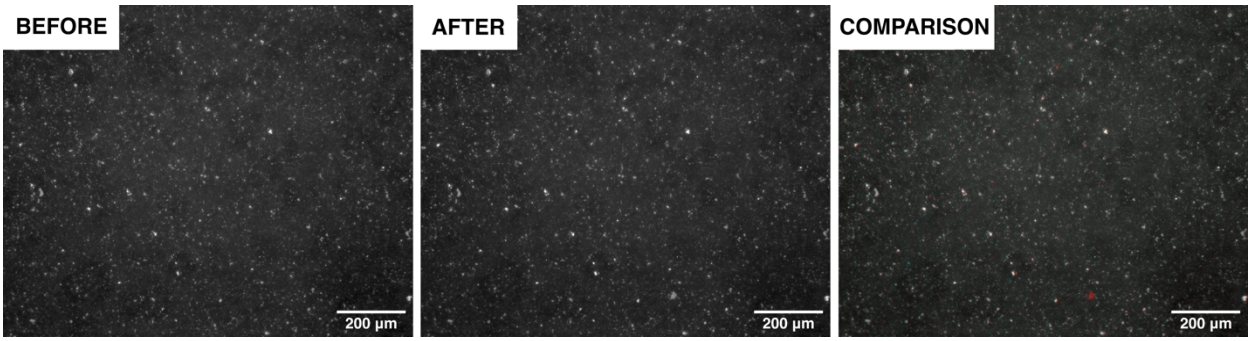


Figure S2-12. Results of Peel Test. Images are of the Cu_2O film on a glass slide before and after the peel test. Voids in the film appear as bright spots. The comparison image shows the new voids colored in red. The areas of red are very minor and quantitative analysis shows that about 99.75% of the surface layer remained intact after peeling for both the glass and stainless steel substrates. Images were captured using a Zeiss Axio Imager M2 microscope. The comparison image was generated by subtraction of the before from the after image, coloring the difference image red and then adding the before image.

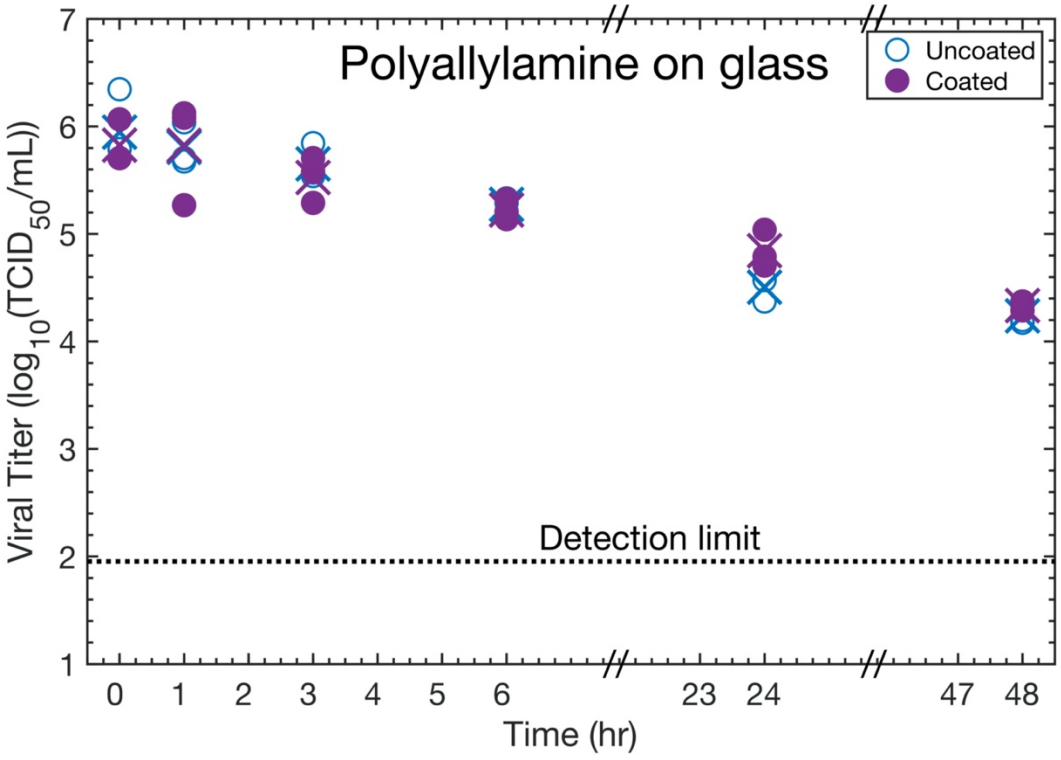


Figure S2-13. Viral titer for polyallylamine (PA) coating on glass solid. Individual circular data points represent each independent measurement and the × symbol represents the mean of the log of independent measurements. There was little effect of the PA coating.

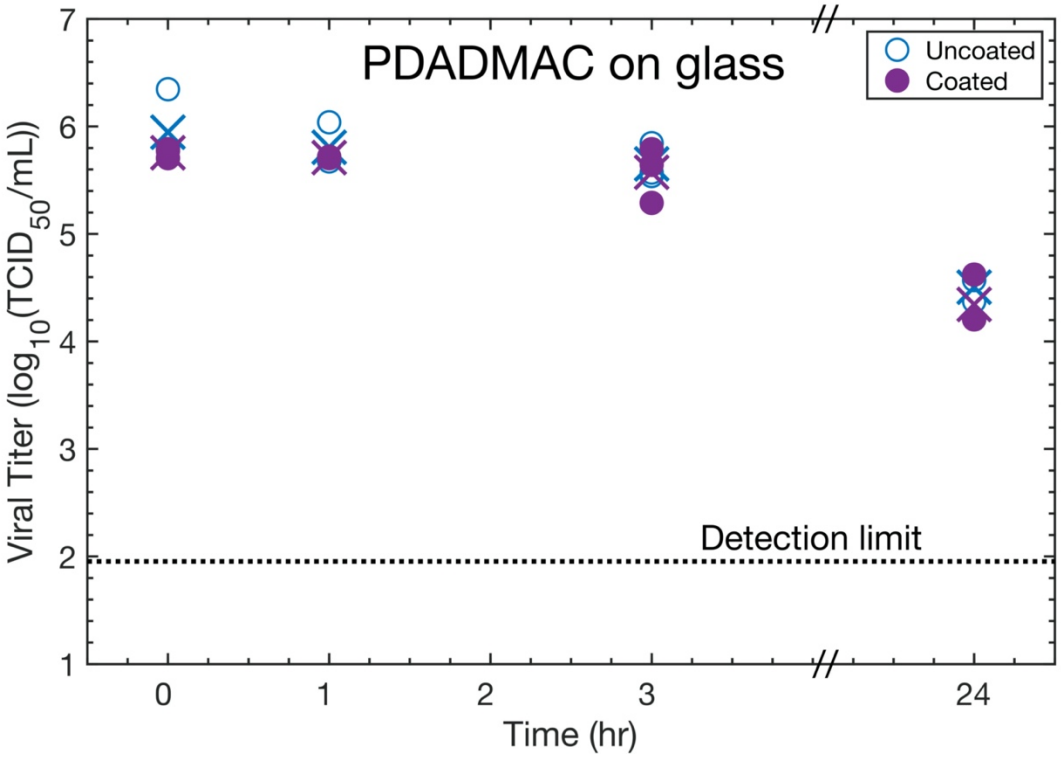


Figure S2-14. Viral titer for PDADMAC coating on glass solids. Individual circular data points represent each independent measurement and the × symbol represents the mean of the log of independent measurements. There was little effect of the PDADMAC coating.

References

(1) Moulder, J. F.; Stickle, W. F.; Sobol, P. E.; Bomben, K. D. *Handbook of X-ray Photoelectron Spectroscopy*; Physical Electronics USA, Inc., 1995.

(2) Biesinger, M. C. Advanced analysis of copper X-ray photoelectron spectra *Surf. Interface Anal.* **2017**, *49*, 1325-1334.

(3) Wagner, C. D. Auger lines in x-ray photoelectron spectrometry *Anal. Chem.* **1972**, *44*, 967-973.

(4) Gaarenstroom, S. W.; Winograd, N. Initial and final state effects in the ESCA spectra of cadmium and silver oxides *J. Chem. Phys.* **1977**, *67*, 3500-3506.

(5) Iarikov, D. D.; Kargar, M.; Sahari, A.; Russel, L.; Gause, K. T.; Behkam, B.; Ducker, W. A. Antimicrobial Surfaces Using Covalently Bound Polyallylamine *Biomacromolecules* **2014**, *15*, 169-176.

Chapter 3. Transparent and Sprayable Surface Coatings that Kill Drug-Resistant Bacteria within Minutes and Inactivate SARS-CoV-2 Virus

Saeed Behzadinasab[1], Myra D. Williams[2], Mohsen Hosseini[1], Leo L. M. Poon[3,4,5], Alex W. H. Chin*[3,4], Joseph O. Falkinham III*[2], and William A. Ducker*[1]

[1]Department of Chemical Engineering and Center for Soft Matter and Biological Physics, Virginia Tech, Blacksburg, Virginia, 24061, USA

[2]Department of Biological Sciences, Virginia Tech, Blacksburg, Virginia, 24061, USA

[3]School of Public Health, LKS Faculty of Medicine, The University of Hong Kong, Hong Kong, China

[4]Centre for Immunity and Infection, Hong Kong Science Park, Hong Kong, China

[5]HKU-Pasteur Research Pole, LKS Faculty of Medicine, The University of Hong Kong, Hong Kong, China

Corresponding Authors' Email: Alex Chin alexchin@hku.hk; Joseph Falkinham jofiii@vt.edu; William Ducker wducker@vt.edu

Keywords: antibacterial, antimicrobial, transparent, coating, drug-resistant bacteria, SARS-CoV-2 virus, COVID-19

ORCIDs:

Saeed Behzadinasab: 0000-0002-6271-2623, Mohsen Hosseini: 0000-0002-9482-0215,

Leo L. M. Poon: 0000-0002-9101-7953, Alex W. H. Chin: 0000-0002-6556-9092,

Joseph O. Falkinham III: 0000-0002-4391-9012, William A. Ducker: 0000-0002-8207-768X

3.1. ABSTRACT

Antimicrobial coatings are one method to reduce the spread of microbial diseases. Transparent coatings preserve the visual properties of surfaces and are strictly necessary for applications such as antimicrobial cell phone screens. This work describes transparent coatings that inactivate microbes within minutes. The coatings are based on polydopamine (PDA) adhesive, which has the useful property that the monomer can be sprayed, and then the monomer polymerizes in a conformal film at room temperature. Two coatings are described: (1) a coating where PDA is deposited first and then a thin layer of copper is grown on the PDA by electroless deposition (PDA/Cu), and (2) a coating where a suspension of Cu_2O particles in a PDA solution is deposited in a single step (PDA/Cu_2O). In the second coating, PDA menisci bind Cu_2O particles to the solid surface. Both coatings are transparent and are highly efficient in inactivating microbes. PDA/Cu kills >99.99% of *Pseudomonas aeruginosa* and 99.18% of methicillin-resistant staphylococcus aureus (MRSA) in only 10 minutes, and inactivates 99.98% of SARS-CoV-2 virus in 1 hr. PDA/Cu_2O kills 99.94% of *Pseudomonas aeruginosa* and 96.82% of MRSA within 10 minutes, and inactivates 99.88% of SARS-CoV-2 in 1 hr.

3.2. Introduction

Many diseases can spread to humans by fomite transmission.[1] Some of these are bacterial and some are viral. Among bacterial diseases, the ones caused by antibiotic-resistant bacteria are particularly problematic. An example of antibiotic-resistant bacteria is methicillin-resistant *Staphylococcus aureus* (MRSA). MRSA, a Gram-positive bacterium, was declared a "Serious Threat" by the United States Center for Disease Control (CDC) in 2019.[2] It has been the cause of both healthcare-associated infections (HAIs)[3] and community-associated infections (CAIs).[4] MRSA causes a wide range of conditions, such as skin infection, pneumonia, and blood infections.[5-6] *Pseudomonas aeruginosa* (*P. aeruginosa*), a Gram-negative bacterium, is another causative agent of HAIs and has also been labelled by the CDC as a "Serious Threat".[7] This is one of the more difficult bacteria to kill because it has both intrinsic and acquired resistance to many antibiotics, and it can adapt to the environment to reduce the effectiveness of antibiotics.[8] *P. aeruginosa* causes many diseases, such as blood, lung, or skin infections.[6, 9]

Both *P. aeruginosa* and MRSA can survive on solids for a prolonged period of time (even up to months),[10] and are known to be transmitted via direct contact, e.g. touching contaminated skins or surfaces.[11-12] To hinder such transmission, it would be desirable to kill the bacteria as soon as they land on surfaces.

The global COVID-19 pandemic has severely impacted life: from early 2020 to July 2021, more than 185 million infections and 4 million deaths have been attributed to COVID-19,[13] and estimates based on excess deaths suggest that the actual number of deaths may be much higher.[14] The financial cost to the U.S. alone is estimated to be $16 trillion.[15] This disease is caused by the virus known as severe acute respiratory syndrome coronavirus 2 (SARS-CoV-2).

The World Health Organization states that "fomite transmission is considered a likely mode of transmission for SARS-CoV-2".[16] Unpublished experimental work shows that a substantial number of SARS-CoV-2 virus can be transferred to skin from contaminated surfaces.[17] A hamster study found that direct inhalation of infectious droplets is the main mechanism of transmission, but that 1/3 of the animals were infected when exposed to fomites only.[18] Mathematical modelling showed that fomite transmission is responsible for up to 25% of COVID-19 transmission during lockdown.[19] SARS-CoV-2 also remains infectious up to 7 days after a droplet of virus-suspension is placed on solid surfaces.[20-21] The SARS-CoV-2 virus remains infective for up to 9 hours (on a dead human skin model[22]) or up to 4 days (on dead pig skin[23]) at room temperature. As a result, there has been significant fear of touching communal objects, and health authorities recommended frequent hand-washing to avoid getting the disease.[24]

The use of common disinfectants, such as 70% ethanol, to decontaminate surfaces is useful for reducing infection, but one significant problem is that contamination can reoccur shortly after the ethanol has evaporated. An alternate approach is to utilize surface coatings that provide an ongoing or continuous kill, and to apply these coatings to everyday solid objects. Some coatings have been developed to meet this objective, both for SARS-CoV-2[25-29] and bacteria,[30-31]and have been reviewed recently.[32-34] In addition, considerable research has investigated the antimicrobial properties of metals and metal oxides,[35-41] textured antimicrobial surfaces,[42-44] and antimicrobial additives to face masks.[45]

An important issue with existing metal and metal oxide coatings is that they are opaque. In some applications this destroys the functionality of the object (e.g., a computer or phone touch screen) and in others it destroys the aesthetic appeal. To this end, we have developed transparent

antimicrobial coatings. To achieve a transparent coating, one needs to avoid both scattering and adsorption of light. Here we are focused on copper and copper oxides because of their known antimicrobial properties. Bulk copper metal is opaque, but we have used a very thin film to achieve transparency[46], and electrodeless deposition for ease of use in applications. Cuprous oxide (Cu_2O) is an excellent antimicrobial agent, but it has a red-brown color. For a transparent coating, we simply use a thin, sparse layer of particles. As one decreases the density of particles to obtain transparency, one expects to ultimately lose antimicrobial properties. In fact, we found that a layer that is sufficiently sparse to obtain transparency maintains antimicrobial activity.

We describe two transparent surface coatings that very rapidly inactivate microbes. The adhesive element in the coatings is polydopamine (PDA),[47-48] which polymerizes from aqueous solution at low temperature (<100 ºC) in a conformal manner, meaning that PDA takes the shape of the surface. This makes the coatings easy to prepare. Our first coating, designated by PDA/Cu, consists of PDA and a very thin layer of copper that was deposited onto PDA by electroless deposition. Our second coating, designated by PDA/Cu_2O, is made by simultaneously polymerizing PDA and depositing Cu_2O particles in a way that the PDA forms menisci between the Cu_2O particles to hold them on a solid and to bind together the particles. PDA/Cu_2O is sprayable in a single step, which makes it easy and rapid to apply to objects with different shape. The coatings are thus easy to prepare and also consist of inexpensive and relatively safe materials.

These coatings have outstanding antimicrobial activity, and are transparent. The PDA/Cu coating reduces the number of viable MRSA by 99.18% and the number of viable *P. aeruginosa* by >99.99% compared to uncoated glass within only 10 minutes. The PDA/Cu_2O coating reduces the number of viable MRSA by 96.82% and the number of viable *P. aeruginosa* by

99.94% compared to uncoated glass within 10 minutes. The PDA/Cu and PDA/Cu_2O coatings inactivate 99.98% and 99.88%, respectively, of SARS-CoV-2 virus within 1 hour, compared to uncoated glass.

3.3. Results and Discussion

3.3.1. The antimicrobial coatings are transparent

The antimicrobial coatings are transparent and allow different colors to be clearly seen when the coatings on glass are held in front of a computer screen. The visible spectra data (Figure 3-1) confirms that there is little variability for transmission of different colors. The PDA, which forms the basis of both coatings, is already somewhat opaque, absorbing 20-40% of the light. The two coatings were made in different ways so have slightly different transmission. Addition of copper to PDA decreases the transmission, with slightly more adsorption at longer wavelength as expected[46], which counteracts the trend for PDA to give a more consistent transmission than PDA alone. The PDA/Cu_2O coating also transmits less light than PDA-alone, presumably because of scattering and absorbance by the particles. (See Figure S3-2 for particle size distribution.)

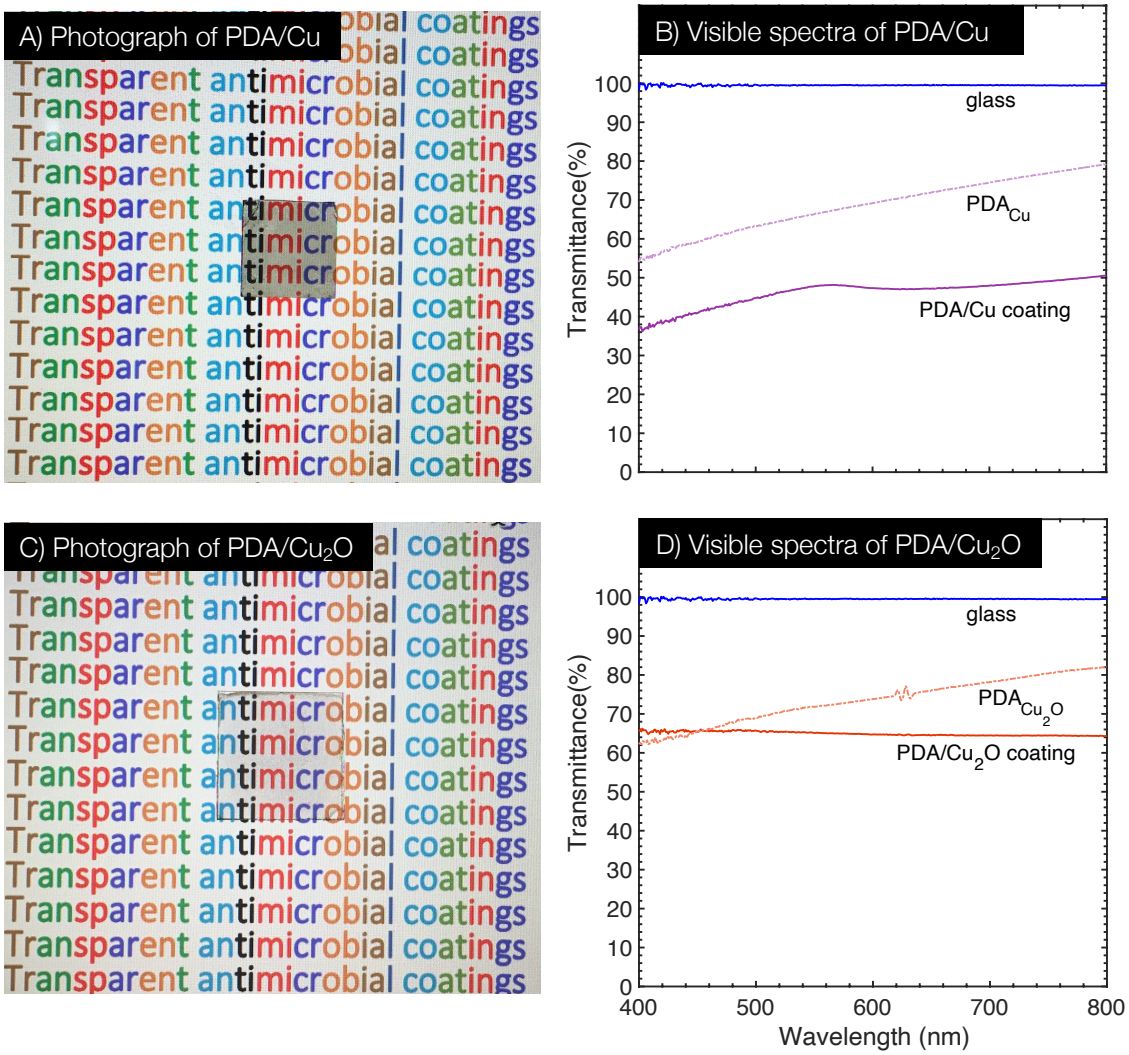


Figure 3-1. A) and C) photographs of PDA/Cu and PDA/Cu_2O coatings, respectively, held in front of a computer monitor. Both coatings are transparent and allow all colors to be seen in transmission. B) and D) visible spectra of the coatings. B) Transmission spectra of PDA, and the PDA/Cu coating. Data for PDA is from the PDA that was prepared in the first step of making the PDA/Cu coating (designated as PDA_{Cu}). D) Transmission spectra of PDA, and the PDA/Cu coating. The PDA was prepared by the same method as the PDA/Cu_2O coating, but without adding the Cu_2O particles (designated as PDA_{Cu2O}). The spectra of the two PDAs (i.e. PDA_{Cu} and PDA_{Cu2O}) are similar. To ensure that coatings formed on one side only for the optical measurements, the PDA_{Cu} and PDA/Cu coatings were prepared with tape covering one side of the glass. The tape was removed prior to spectrometry. The background for the visible spectra is glass.

3.3.2. Other characterization of the coatings

For antimicrobial activity, the active ingredients, i.e., copper or Cu_2O, should be accessible from the surface, and we verified this with SEM imaging and XPS, which is sensitive to the chemistry in the outer few nanometers of a surface. Considering first the PDA/Cu coating, the copper in the PDA/Cu coating was grown from the surface of a PDA coating. That PDA coating is rough (Figure 3-2 A), by design, to present a large surface area on which Cu can form. After deposition of the Cu, some depressions in the PDA coating have been filled in (see Figure 3-2) and additional small-scale roughness is visible (see Figure S3-3 E & F in Supporting Information). SEM images show that the copper layer is approximately 22 nm thick and the PDA is about 55 nm thick (see Figure S3-3 E & F). The presence of Cu in the PDA/Cu coating is also obvious from XPS: the PDA/Cu coating is about 37% copper (See Figure S3-5 in Supporting Information for XPS spectra). High resolution XPS (Figure S3-5) is consistent with an oxidized outer layer consisting of both Cu(I) and Cu(II) species, as observed previously.[49-50] Consistent with existing literature on electroless deposition,[47, 51-54] in this paper we will refer to the coating as copper or Cu, even though the oxidation state of the inner part of the 22 nm layer film is not clear from the XPS spectra (See Figure S3-6).

The PDA/Cu_2O coating utilizes Cu_2O particles that have a mean size of about 5 μm (see Figure S3-2 for Cu_2O particles size distribution), which is a much larger scale than the thickness of the Cu coating in the PDA/Cu coating. In the preparation of PDA/Cu_2O coating, we incorporated a heat treatment step at 80º C for 30 minutes. XPS shows that both Cu(I) and Cu(II) are present on the outer 1 nm or so of the coating (see Figure S3-5). However, The duration and temperature of heat-treatment is not sufficient to oxidize Cu_2O, consistent with our previous work.[25]

The Cu_2O particles clearly protrude from the PDA (Figure 3-2 D). Our goal was a coating with good transparency, so knowing that the Cu_2O particles scatter light, we have deliberately made a sparse layer of Cu2O (Figure 3-2 C&D). XPS data shows that the PDA/Cu_2O coating contains only 5.7% percent copper (see Figure S3-5 in Supporting Information). Closer inspection of the SEM image that was taken on a tilt angle reveals the formation of a PDA meniscus that helps to adhere the Cu_2O particles to the substrate.

Advancing and receding water contact angles for PDA/Cu are 72 ± 22 and 10 ± 7 degrees (the number after "±" sign is the 95% confidence interval from measurements of independent samples). The PDA/Cu_2O is hydrophilic, with both advancing and receding angles being <10°.

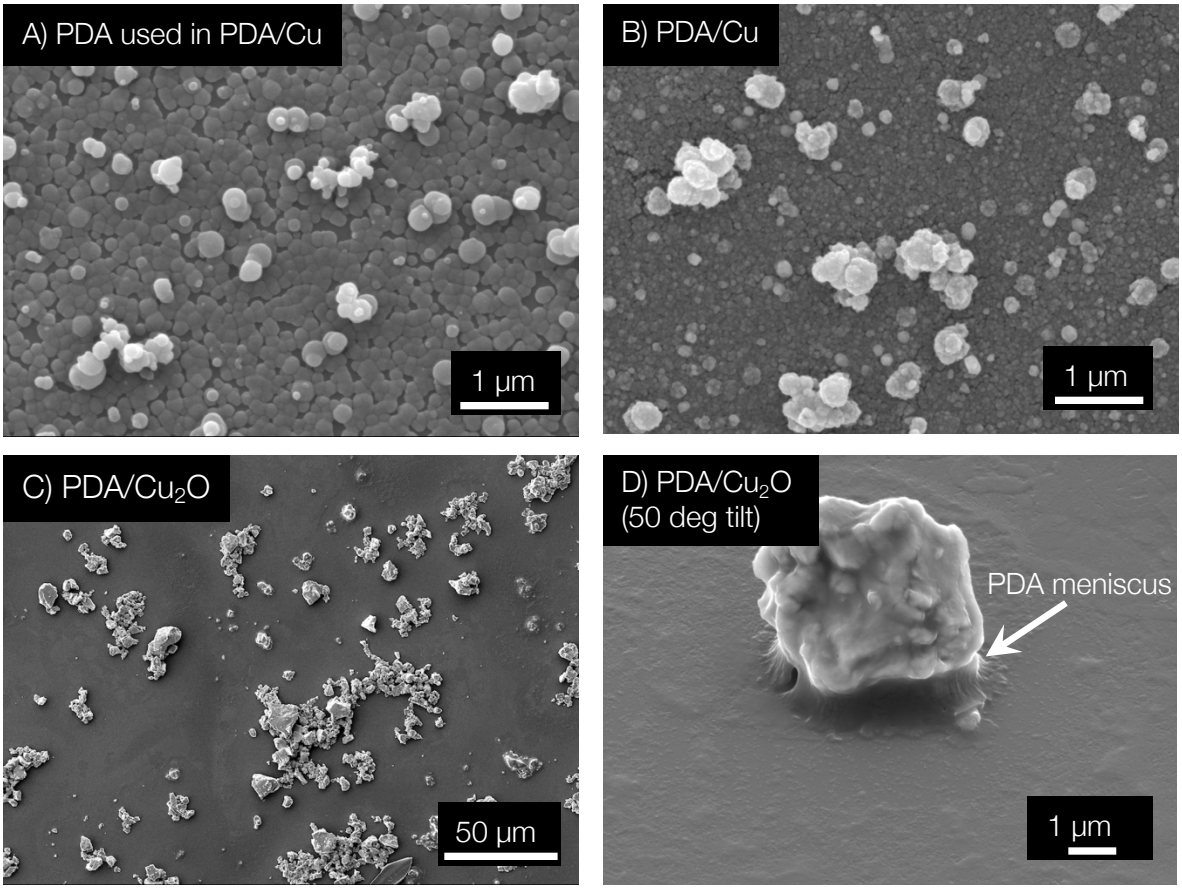


Figure 3-2. Plan view SEM images of the coatings. A) PDA-only from an intermediate step in fabrication of the PDA/Cu coating. B) PDA/Cu coating. The copper coating is apparent from the slight roughening of

the coating as well as the filling of depressions compared to A. C) plan view PDA/Cu_2O coating. D) 50-degree tilt of magnified view of PDA/Cu_2O coating. The PDA meniscus that holds Cu_2O particles is shown with a white arrow. Further images are shown in Supporting Information Figure S3-3 & Figure S3-4.

3.3.3. Inactivation of microbes

3.3.3.1. Both transparent coatings kill bacteria in 10 minutes

Figure 3-3 shows very low survival of *P. aeruginosa* and MRSA on each of the transparent coatings, even after only ten minutes. Survival is a comparison between the input titer and the titer at a later time and is calculated from:

$$\log \text{survival} = \text{mean}\left[\log_{\mathbf{10}}\left(\frac{\text{sample titer}}{\text{units}}\right)\right] - \text{mean}\left[\log_{\mathbf{10}}\left(\frac{\text{input titer}}{\text{units}}\right)\right] \qquad \text{Equation 3-1}$$

$$\%\ \text{survival} = \left[1 - 10^{-\log \text{survival}}\right] \times 100 \qquad \text{Equation 3-2}$$

Microbes can become inactivated with time on inanimate surfaces, and bacteria can die, even without an active ingredient, so we also measured survival of the microbes on the uncoated glass as a control. Figure 3-3 shows that survival is very high on uncoated glass. Our performance metric is “Reduction”, which is a comparison of the titer on the coated and uncoated samples:

$$\log \text{Reduction} = \text{mean}\left[\log_{10}\left(\frac{\text{uncoated glass titer}}{\text{units}}\right)\right] - \text{mean}\left[\log_{10}\left(\frac{\text{sample titer}}{\text{units}}\right)\right] \quad \text{Equation 3-3}$$

$$\%\ \text{Reduction} = \left[1 - 10^{-\log \text{Reduction}}\right] \times 100 \quad \text{Equation 3-4}$$

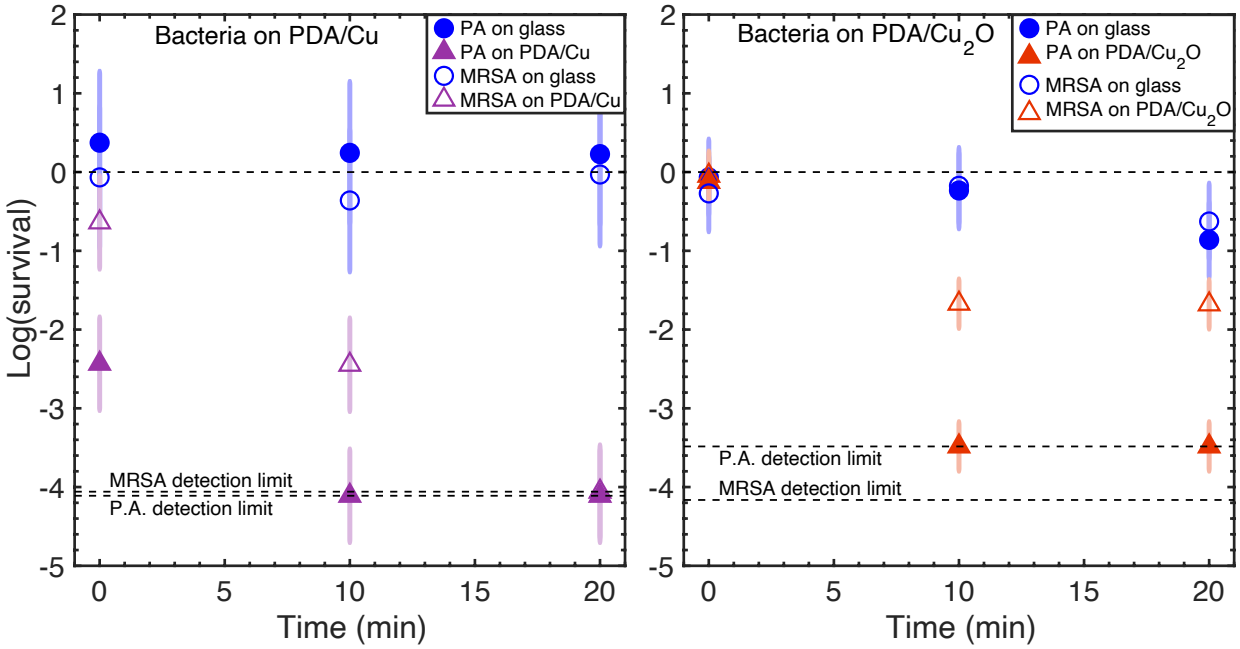


Figure 3-3. Time course of survival of *P. aeruginosa* (PA) and methicillin-resistant staphylococcus aureus (MRSA) on transparent PDA/Cu (left) and PDA/Cu_2O (right) coatings. Survival was calculated with Equation 3-3 so zero represents the CFU in the initial droplet. For the coatings, each symbol represents the average of 3 separate samples, the error bar is the comparison interval from ANOVA, and the detection limit for each bacterium is shown with a dotted line. Compared to glass control, within 10 minutes, the PDA/Cu coating caused a Reduction of more than 99.99% of *P. aeruginosa* and 99.18% of MRSA, and the PDA/Cu_2O caused a Reduction of more than 99.94% of *P. aeruginosa* and 96.82% of MRSA. We performed a 3-way ANOVA with each of the coatings: factor 1 = surface type (glass vs each coating), factor 2 = time, factor 3 = bacteria type (*P. aeruginosa* and MRSA). The *p*-values for surface type were $< 10^{-10}$ for PDA/Cu and $< 10^{-9}$ for PDA/Cu_2O.

The %Reduction by PDA/Cu is 99.99% (4-logs) for *P. aeruginosa* and 99.18% (> 2-logs) for MRSA within only 10 minutes (Figure 3-3). The Reduction on PDA/Cu_2O is 99.94% (> 3-logs) for *P. aeruginosa* and 96.82% (~ 2-logs) for MRSA in 10 minutes. This compares favorably to typical United States Environmental Protection Agency (EPA) standards of 99.9% (3-logs) in 1 hour of exposure.[55]

We also measured antimicrobial properties of PDA alone and found that PDA did not have antimicrobial activity against bacteria or viruses (see Supporting Information, Figure S3-7 and Figure S3-8), confirming that copper and Cu_2O are the active ingredients in the two coatings.

3.3.3.2. Both coatings rapidly inactivate SARS-CoV-2

PDA/Cu and PDA/Cu_2O coatings reduce the infectivity of SARS-CoV-2 virus by 99.98% and 99.88% within 1 hour, respectively compared to a glass control (see Figure 3-4). PDA alone does not inactivate SARS-CoV-2 (see Figure S3-8), demonstrating that the Cu and Cu_2O are the active ingredients.

The PDA/Cu_2O results can be compared to our previous results for Cu_2O in a polyurethane coating.[25] The earlier coating used a much higher loading of Cu_2O particles, such that the coating was completely opaque, and it inactivated ~99.9% of SARS-CoV-2 after one hour. The similarity of the results for the two coatings shows that there is little benefit to the greater solids loading. On the other hand, the lower solids loading confers the significant advantage that the coating is transparent and therefore can be used on touch screens, monitors, etc., and maintains aesthetic appeal of solids. Additionally, the similarity of two results supports

the idea that the killing is a surface effect. The infectivity of SARS-CoV-2 over time was previously measured on a copper sheet. In that work, the virus remained infectious for 4-8 hr[20], while here ~99.9% of it is inactivated within 1 hr. on our coatings. Note that in the work on copper[20], the starting titer was about log(TCID50/ml) of 3.7, which is about 2.5 logs lower that in this work. The coatings therefore work more rapidly than copper, even with a greater initial dose of virus.

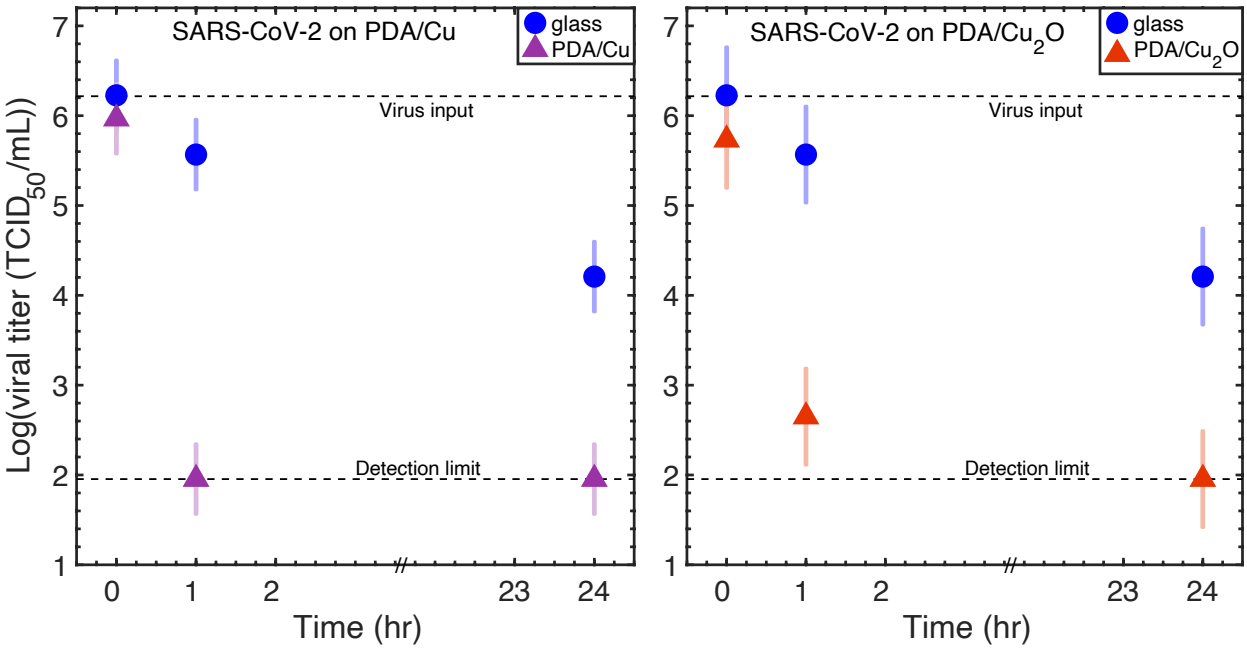


Figure 3-4. Time course of SARS-CoV-2 titer for transparent PDA/Cu (left) and PDA/Cu_2O (right) coatings. Each marker shows the average of 3 independent samples and the error bars are the comparison interval from ANOVA. The detection limit was 90 TCID50/mL (shown with dotted line). When data was below the detection limit, the point was plotted at the detection limit. PDA/Cu reduces the infectivity of SARS-CoV-2 by 99.98% and PDA/Cu_2O reduces the infectivity by 99.88% in 1 hour. We performed a 2-way ANOVA with each of the coatings: factor 1 = surface type (glass vs each coating), factor 2 = time. The *p*-value for coating was $< 10^{-8}$ for PDA/Cu and $< 10^{-6}$ for PDA/Cu_2O.

3.3.4. Mechanism of action

The mechanism of action of copper or Cu_2O against microbes is one or combination of 3 routes: contact killing, ion release, and generation of reactive oxygen species (ROSs).[32, 35, 56] In the contact killing route, the microbe needs to physically make contact with the active ingredient. Ion release from copper can be in the forms of simple ions (Cu^+ and Cu^{2+})[35], and possibly hydroxides and/or oxides of copper ions[57] where the composition of copper species depends on the presence of other ions[58]. These dissolved species are typically cationic and can interact with anionic biomolecules such as DNA[59], RNA, some lipids, parts of proteins etc. For example, copper species may inactivate metalloenzymes by replacing native metal ions.[32] Another mechanism is that Cu_2O is thought to produce ROSs, including superoxide (O_2^-•), hydroxyl radicals (•OH), and hydrogen peroxide (H_2O_2), which can oxidize biological material.[35] Typically this oxidation begins with superoxide and/or hydrogen peroxide, which are produced by bacteria but not viruses. The current literature appears to propose that the generation of ROSs does not play a role in inactivation of viruses.[35, 60]

3.3.5. The PDA/Cu_2O coating is sprayable

It is desirable that a coating is easy to deploy, and spraying is one of the fastest techniques for coating. The microbial results above are for drop-casted coatings. We made a second set of PDA/Cu_2O coatings by spraying glass with a suspension of Cu_2O suspension in aqueous dopamine (see Experimental section), and subsequently dried the coated slides at 80°C in an oven. The sprayed coating was characterized with UV-Vis, SEM, and XPS (see Figure S3-9 in Supporting Information). The results were similar to the drop-cast coating, i.e., the

coating was transparent with wavelength-independent transmission (Figure S3-9D), XPS shows a similar copper composition and SEM shows that the particles protrude from the PDA.

Spraying was typically done within about 4-5 minutes after the suspension was prepared. At this time the particles were still suspended. We found that the particles eventually sedimented, but after sedimentation, the particles could be resuspended simply by shaking and then sprayed.

3.3.6. Other aspects of the coatings

The polymerization of dopamine is achieved in water, which is an environmental-friendly and non-toxic solvent. Likewise polydopamine is non-toxic: polydopamine nanoparticles injected in a mice have a median lethal dose (LD_{50}) in the range 400 – 585 mg/kg.[61] Although copper has some toxicity to aquatic species, the US EPA allows its use in antimicrobial coatings.[62] Also, since ancient times, copper has been in wide circulation as coins that are already frequently handled by the public. The cost of copper in 2021 is about $6 per kg, which is not a substantial factor in a coating that is very thin. In some applications, surfaces are wiped periodically with disinfectant. We tested the antimicrobial efficacy of the coating after it was abraded by a sponge and found that the coating still caused a Reduction of ~99.8% (see Table S3-1). Finally, the process of coating is simple, using spraying or dip coating, with low temperature curing, and no need for expensive equipment.

3.4. Conclusion

Two rapid methods are described for preparing transparent antimicrobial coatings based on PDA using inexpensive and relatively safe materials. These coatings are very effective at killing bacteria and inactivating the SARS-CoV-2 virus. Using a thin layer of copper deposited on a PDA layer, we achieved a Reduction of >99.99% of *P. aeruginosa* and 99.18% of MRSA within 10 minutes compared to a glass control, as well as 99.98% Reduction of SARS-CoV-2 virus infectivity in 1 hr. Using a sparse layer of Cu_2O bound to, but protruding from PDA, we obtained a Reduction of 99.94% of *P. aeruginosa* and 96.82% of MRSA within 10 minutes, as well as 99.88% of SARS-CoV-2 virus in 1 hr. compared to a glass control. The activity against SARS-CoV-2 virus is similar to the activity obtained from much greater solids loading in previous work. The coatings are thus highly effective against important pathogens and should find applications on common-use objects to reduce the spread of microbial diseases. A transparent coating is an essential feature for a coating on touch screens, and also extremely desirable for maintaining the visual appeal of an object while achieving a strong antimicrobial effect.

3.5. Experimental Section

3.5.1. Materials

Glass slides (25 × 75 × 1 mm), 200 Proof ethanol, 70% ethanol, nitric acid (70%, ACS grade), and sodium hydroxide (beads, ACS grade) were purchased from VWR. The following were purchased from Fischer Scientific: dopamine hydrochloride (99%), dimethylamineborane (DMAB, 98%). Cu_2O particles (Chem Copp HP III UltraFine Type -5; mean size = 5.4µm) were purchased from American Chemet Corporation. The following were obtained from Sigma Aldrich: copper(II) chloride (97%), boric acid (ACS reagent), tris(hydroxymethyl)aminomethane (Tris, ACS reagent), and ethylenediaminetetraacetic acid (EDTA, >99%). Tryptic soy broth (TSB) and Tryptic Soy Agar (TSA) were purchased from BD, Sparks, MD. Cell suspensions were diluted in either phosphate-buffered saline (PBS) or DE Broth (BD, Sparks, MD). Water was purified by Milli-Q Reference system. Glass slides were serially cleaned with DI water, 70% ethanol, DI water, nitric acid (6 M), and DI water, and subsequently dried with high pressure nitrogen.

3.5.2. Fabrication of the surface coatings

3.5.2.1. Fabrication of PDA/Cu coating

A two-step procedure was used in which the first step was coating preparation of a thin coating of PDA.[47, 63] Pieces of cleaned glass slides (12 x 12 mm) were immersed in tris solution (10 mM in water) at 60ºC and stirred. Dopamine hydrochloride was added to achieve a final concentration of 5 g dopamine /L and then stirring at 60ºC continued for 4 hours. After cooling

to room temperature, the glass slides were washed with purified water and dried with nitrogen gas. PDA makes conformal coatings on solids, so we assume that the coating forms on both sides of the glass,[47] but we always tested the coating on the side that was not touching the container. Copper was deposited onto a preformed layer of PDA, using a method from the literature,[47, 51-54] but with a thinner layer than in previous work. The copper was electrolessly deposited using an aqueous solution containing EDTA (50 mM), $CuCl_2$ (50 mM), and boric acid (100 mM) with the pH adjusted to 7 using NaOH solution.[47, 51-54] The solution was placed on a heater at 37ºC under stirring. DMAB was added to achieve a final concentration of 100 mM and subsequently, polydopamine-coated glass-slides were immersed in the solution. The reaction was stopped 30 minutes after the solution color changed to dark green. The samples were washed with DI water and dried with high-pressure nitrogen.

3.5.2.2. Fabrication of PDA/Cu_2O coating

A 0.2% w/w suspension of Cu_2O particles in tris solution (10 mM) was sonicated for 1 hr. Dopamine hydrochloride was added to achieve a concentration of 0.05 g dopamine/L. Next, 140 µL of Cu_2O and dopamine suspension was drop cast on 15 x 15 mm pieces of cleaned glass slides, to give a Cu_2O-loading of 1.27×10^{-4} g/cm^2. Two to three minutes after deposition, the samples were heat-treated at 80ºC in an oven for 30 minutes to dry. Subsequently they were forcefully blown with high pressure nitrogen gas. These samples were coated on one side of glass only.

3.5.3. Characterization

SEM (JEOL IT500) was used to characterize the morphology of the coatings (the samples were coated with 5 nm of Pt/Pd prior to SEM measurements). XPS (PHI VersaProbe III with a monochromatic Al Kα source of 1486.6 eV) was utilized for measuring of chemical composition of the samples. UV-Vis transmittance was measured using an Agilent model 8453 UV-VIS spectrometer. Water contact angles were measured using First Ten Angstroms FTA125.

3.5.4. Antibacterial assay

Microbial Strains. The microbial strains employed in this study were *Pseudomonas aeruginosa* strain (DSM-9644) and methicillin-resistant *S. aureus* (MRSA) strain (MA43300, obtained from the Danville Community Hospital, VA).

Growth of Microbial Strains. Each bacterial strain was grown in 5 mL of Tryptic Soy Broth (TSB, BD, Sparks, MD) to mid-exponential phase at 37° C with aeration (60 rpm). Following growth, the purity and identity of the cells in the cultures were verified by streaking bacterial cultures on Tryptic Soy Agar (TSA, BD, Sparks, MD) and incubated at 37° C for 48 hr and examining colonies for species-specific traits (e.g., pigmentation and surface texture).

Preparation of Microbial Strains for Testing. Grown cells were collected by centrifugation (5,000 g for 20 min), the supernatant medium discarded, and the cells were resuspended in 5 mL of sterile phosphate-buffered saline (PBS) by vortexing for 60 sec. Those suspensions were centrifuged (5,000 g for 20 min), the supernatant was discarded, and the washed cells suspended in 5 mL of sterile PBS by vortexing for 60 sec. The number of colony-forming

units (CFU)/mL of each washed suspension was measured by spreading 0.10 mL (in duplicate) of serial dilutions in PBS on TSA plates.

Measurement of Cell Number. The cell number of PBS-suspensions of bacteria were measured as colony-forming units (CFU)/mL of suspension. A 10-fold dilution series was prepared for each suspension in either PBS or DE Broth, 0.1 mL of each dilutions was spread on TSA in triplicate, and colonies were counted after 48 hr. incubation at 37° C. If zero colonies were present for the least dilution, then to enable a log transformation of all data, we designated the zero as one. This is the detection limit, which is an upper bound.

Measurement of Surface-Killing. For each microbial strain, a 5 μL droplet of bacterial cells in PBS was placed on each coated or uncoated glass sample. Immediately and after 10 min and 20 min (or longer where noted), each sample was transferred to a separate sterile 50 mL centrifuge tube containing 5 mL of PBS or DE broth, vortexed at the highest setting for 10 sec and sonicated for 1 min in a Branson Model 12 Ultrasonic Cleaner (Shelton, CT) to detach cells from the solid, and then the CFU/mL of the resulting bacterial suspension measured by removing a sample of the suspension without coming in contact with the glass sample and preparing a dilution series. The process was repeated at each time point, and three different samples were used for each condition, i.e., each surface coating at each time. Note that the bacterial suspension contacts only one side of the glass.

3.5.5. SARS-CoV-2 assay

The viral assay methods were described previously.[25, 27] In summary, the stock virus (BetaCoV/Hong Kong/VM20001061/2020, isolated from a confirmed COVID-19 patient in Hong Kong) was prepared in Vero-E6 cells cultured in Dulbecco's Modified Eagle Medium with 2% fetal bovine serum and 1% v/v penicillin-streptomycin at 37°C with 5% CO_2. Prior to tests with the virus, all of the surfaces were sterilized with 70% ethanol and air-dried. A 5 µL SARS-CoV-2 droplet at 7.8 $\log_{10}$ unit $TCID_{50}$/ml was placed on the test solid (temp=22-23°C and 60–70% relative humidity) and after a prescribed time, the solid was soaked in 300 µL of viral transport medium (Earle's balanced salt solution including 0.5%(w/v) bovine serum albumin and 0.1%(w/v) glucose, pH 7.4) to elute the virus. Subsequently, the eluted virus was titrated by 50% tissue culture infective dose ($TCID_{50}$) assay in Vero E6 cells.[64-65] In brief, confluent Vero E6 cells on 96-well plates were infected with serially diluted virus in quadruplicates. The infected cells were incubated at 37°C with 5% CO_2. On day 5 post-infection, the cells were examined for a cytopathic effect. The $TCID_{50}$/ml is the dilution that caused a cytopathic effect in 50% of treated Vero E6 cell cultures. Three independent samples were tested at each condition.

3.5.6. Calculation of microbe Survival and Reduction

Microbe survival and Reduction are defined in Equation 3-1 to Equation 3-4. We use the word survival for simplicity but acknowledge that the CFU assay measures those cells that can reproduce to form a colony and that the $TCID_{50}$ assay does not measure numbers of virions.

3.5.7. Statistical analysis

The statistical analysis used N-way ANOVA in MATLAB. The error bars were calculated for each figure with Post Hoc multiple comparison using Dunn-Sidák's approach. We chose a significance level of 0.05. Before statistical analysis, each microbial titer was $\log_{10}$ transformed.

Supporting Information

Supporting Information includes additional methods, characterizations, results, and tables of raw data, as follows:

Figure S3-1. Schematic of abrasion tests

Figure S3-2. Particle Size Distribution of Cu_2O particles

Figure S3-3. Additional SEM images of PDA (prior to copper deposition) and PDA/Cu

Figure S3-4. Additional SEM images of coatings

Figure S3-5. XPS results

Figure S3-6. XPS results of Ar^+-etched coatings

Figure S3-7. Bacteria assay for PDA sample

Figure S3-8. SARS-CoV-2 titer for PDA sample

Figure S3-9. Characterization of PDA/Cu_2O coating on glass that was prepared by spray-coating

Table S3-1 to Table S4-7. Data tables

Acknowledgments

This work was supported by the National Science Foundation (NSF) under Grant No. CBET-1902364, the Health and Medical Research Fund (COVID190116), and the National Institute of

Allergy and Infectious Diseases (contract HHSN272201400006C). This work used shared facilities at the Virginia Tech National Center for Earth and Environmental Nanotechnology Infrastructure supported by NSF (ECCS 1542100 and ECCS 2025151). We also thank Dr. Xu Feng, who captured the XPS spectra and provided analysis, and the Surface Analysis Laboratory in the Department of Chemistry at VT, which is supported by the NSF under Grant No. CHE-1531834.

Conflict of Interest

WD declares part ownership in a startup company that intends to produce surface coatings. Other authors declare no conflict of interest.

Data Availability Statement

The raw data that support the findings of this study are available in the Supporting Information file.

REFERENCES

(1) Stephens, B.; Azimi, P.; Thoemmes, M. S.; Heidarinejad, M.; Allen, J. G.; Gilbert, J. A. Microbial Exchange Via Fomites and Implications for Human Health. *Curr. Pollut. Rep.* **2019,** *5* (4), 198-213.

(2) Centers for Disease Control and Prevention Methicillin-Resistant Staphylococcus Aureus (Mrsa). https://www.cdc.gov/drugresistance/pdf/threats-report/mrsa-508.pdf (accessed June 2nd 2021).

(3) Maree, C. L.; Daum, R. S.; Boyle-Vavra, S.; Matayoshi, K.; Miller, L. G. Community-Associated Methicillin-Resistant Staphylococcus Aureus Isolates and Healthcare-Associated Infections. *Emerg. Infect. Dis.* **2007,** *13* (2), 236.

(4) David, M. Z.; Daum, R. S. Community-Associated Methicillin-Resistant Staphylococcus Aureus: Epidemiology and Clinical Consequences of an Emerging Epidemic. *Clin. Microbiol. Rev.* **2010,** *23* (3), 616-687.

(5) Pantosti, A.; Venditti, M. What Is Mrsa? *Eur. Respir. J.* **2009,** *34* (5), 1190-1196.

(6) Williams, B. J.; Dehnbostel, J.; Blackwell, T. S. Pseudomonas Aeruginosa: Host Defence in Lung Diseases. *Respirology* **2010,** *15* (7), 1037-1056.

(7) Centers for Disease Control and Prevention Multidrug-Resistant Pseudomonas Aeruginosa https://www.cdc.gov/drugresistance/pdf/threats-report/pseudomonas-aeruginosa-508.pdf (accessed June 2nd 2021).

(8) Pang, Z.; Raudonis, R.; Glick, B. R.; Lin, T.-J.; Cheng, Z. Antibiotic Resistance in Pseudomonas Aeruginosa: Mechanisms and Alternative Therapeutic Strategies. *Biotechnol. Adv.* **2019,** *37* (1), 177-192.

(9) Campa, M.; Bendinelli, M.; Friedman, H. *Pseudomonas Aeruginosa as an Opportunistic Pathogen*, Springer Science & Business Media: New York, NY, 1993.

(10) Kramer, A.; Schwebke, I.; Kampf, G. How Long Do Nosocomial Pathogens Persist on Inanimate Surfaces? A Systematic Review. *BMC Infect. Dis.* **2006,** *6* (1), 1-8.

(11) Vos, M. C.; Verbrugh, H. A. Mrsa: We Can Overcome, but Who Will Lead the Battle? *Infect. Control Hosp. Epidemiol.* **2005,** *26* (2), 117-120.

(12) de Abreu, P. M.; Farias, P. G.; Paiva, G. S.; Almeida, A. M.; Morais, P. V. Persistence of Microbial Communities Including Pseudomonas Aeruginosa in a Hospital Environment: A Potential Health Hazard. *BMC Microbiol.* **2014,** *14* (1), 1-10.

(13) World Health Organization Who Coronavirus Disease (Covid-19) Dashboard. https://covid19.who.int/ (accessed July 7th, 2021).

(14) IHME Estimation of Total Mortality Due to Covid-19. http://www.healthdata.org/special-analysis/estimation-excess-mortality-due-covid-19-and-scalars-reported-covid-19-deaths (accessed May 13, 2021).

(15) Cutler, D. M.; Summers, L. H. The Covid-19 Pandemic and the $16 Trillion Virus. *JAMA* **2020,** *324* (15), 1495-1496.

(16) World Health Organization Transmission of Sars-Cov-2: Implications for Infection Prevention Precautions. https://www.who.int/news-room/commentaries/detail/transmission-of-sars-cov-2-implications-for-infection-prevention-precautions (accessed Feb 28, 2021).

(17) Behzadinasab, S.; Chin, A. W. H.; Hosseini, M.; Poon, L. L. M.; Ducker, W. A. Sars-Cov-2 Virus Transfers to Skin through Contact with Contaminated Solids. *medRxiv* **2021**, 2021.04.24.21256044, DOI: 10.1101/2021.04.24.21256044.

(18) Sia, S. F.; Yan, L.-M.; Chin, A. W.; Fung, K.; Choy, K.-T.; Wong, A. Y.; Kaewpreedee, P.; Perera, R. A.; Poon, L. L.; Nicholls, J. M. Pathogenesis and Transmission of Sars-Cov-2 in Golden Hamsters. *Nature* **2020,** *583* (7818), 834-838.

(19) Meiksin, A. Dynamics of Covid-19 Transmission Including Indirect Transmission Mechanisms: A Mathematical Analysis. *Epidemiol. Infect.* **2020,** *148*, e257, DOI: 10.1017/S0950268820002563.

(20) Van Doremalen, N.; Bushmaker, T.; Morris, D. H.; Holbrook, M. G.; Gamble, A.; Williamson, B. N.; Tamin, A.; Harcourt, J. L.; Thornburg, N. J.; Gerber, S. I. Aerosol and Surface Stability of Sars-Cov-2 as Compared with Sars-Cov-1. *N. Engl. J. Med.* **2020,** *382* (16), 1564-1567.

(21) Chin, A. W. H.; Chu, J. T. S.; Perera, M. R. A.; Hui, K. P. Y.; Yen, H.-L.; Chan, M. C. W.; Peiris, M.; Poon, L. L. M. Stability of Sars-Cov-2 in Different Environmental Conditions. *The Lancet Microbe* **2020,** *1* (1), e10, DOI: 10.1016/S2666-5247(20)30003-3.

(22) Hirose, R.; Ikegaya, H.; Naito, Y.; Watanabe, N.; Yoshida, T.; Bandou, R.; Daidoji, T.; Itoh, Y.; Nakaya, T. Survival of Severe Acute Respiratory Syndrome Coronavirus 2 (Sars-Cov-2) and

Influenza Virus on Human Skin: Importance of Hand Hygiene in Coronavirus Disease 2019 (Covid-19). *Clin. Infect. Dis.* **2020**, DOI: 10.1093/cid/ciaa1517.

(23) Harbourt, D. E.; Haddow, A. D.; Piper, A. E.; Bloomfield, H.; Kearney, B. J.; Fetterer, D.; Gibson, K.; Minogue, T. Modeling the Stability of Severe Acute Respiratory Syndrome Coronavirus 2 (Sars-Cov-2) on Skin, Currency, and Clothing. *PLoS Negl. Trop. Dis.* **2020,** *14* (11), e0008831.

(24) Alzyood, M.; Jackson, D.; Aveyard, H.; Brooke, J. Covid-19 Reinforces the Importance of Handwashing. *J. Clin. Nurs.* **2020,** *29* (15-16), 2760-2761, DOI: 10.1111/jocn.15313.

(25) Behzadinasab, S.; Chin, A.; Hosseini, M.; Poon, L.; Ducker, W. A. A Surface Coating That Rapidly Inactivates Sars-Cov-2. *ACS Appl. Mater. Interfaces* **2020,** *12* (31), 34723-34727.

(26) Hutasoit, N.; Kennedy, B.; Hamilton, S.; Luttick, A.; Rashid, R. A. R.; Palanisamy, S. Sars-Cov-2 (Covid-19) Inactivation Capability of Copper-Coated Touch Surface Fabricated by Cold-Spray Technology. *Manuf. Lett.* **2020,** *25*, 93-97.

(27) Hosseini, M.; Chin, A. W.; Behzadinasab, S.; Poon, L. L.; Ducker, W. A. Cupric Oxide Coating That Rapidly Reduces Infection by Sars-Cov-2 Via Solids. *ACS Appl. Mater. Interfaces* **2021,** *13* (5), 5919-5928.

(28) Sousa, B. C.; Cote, D. L. Antimicrobial Copper Cold Spray Coatings and Sars-Cov-2 Surface Inactivation. *MRS Adv.* **2020,** *5* (56), 2873-2880.

(29) Hosseini, M.; Behzadinasab, S.; Chin, A. W.; Poon, L. L.; Ducker, W. A. Reduction of Infectivity of Sars-Cov-2 by Zinc Oxide Coatings. *ACS Biomater. Sci. Eng.* **2021**.

(30) Cloutier, M.; Mantovani, D.; Rosei, F. Antibacterial Coatings: Challenges, Perspectives, and Opportunities. *Trends Biotechnol.* **2015,** *33* (11), 637-652.

(31) Salwiczek, M.; Qu, Y.; Gardiner, J.; Strugnell, R. A.; Lithgow, T.; McLean, K. M.; Thissen, H. Emerging Rules for Effective Antimicrobial Coatings. *Trends Biotechnol.* **2014,** *32* (2), 82-90.

(32) Rakowska, P. D.; Tiddia, M.; Faruqui, N.; Bankier, C.; Pei, Y.; Pollard, A. J.; Zhang, J.; Gilmore, I. S. Antiviral Surfaces and Coatings and Their Mechanisms of Action. *Commun. Mat.* **2021,** *2* (1), 1-19.

(33) Hosseini, M.; Behzadinasab, S.; Benmamoun, Z.; Ducker, W. A. The Viability of Sars-Cov-2 on Solid Surfaces. *Curr. Opin. Colloid Interface Sci.* **2021**, 101481.

(34) Singha, P.; Locklin, J.; Handa, H. A Review of the Recent Advances in Antimicrobial Coatings for Urinary Catheters. *Acta Biomater.* **2017,** *50*, 20-40.

(35) Sunada, K.; Minoshima, M.; Hashimoto, K. Highly Efficient Antiviral and Antibacterial Activities of Solid-State Cuprous Compounds. *J. Hazard. Mater.* **2012,** *235*, 265-270.

(36) Aydin Sevinç, B.; Hanley, L. Antibacterial Activity of Dental Composites Containing Zinc Oxide Nanoparticles. *J. Biomed. Mater. Res. B Appl. Biomater.* **2010,** *94* (1), 22-31.

(37) Pasquet, J.; Chevalier, Y.; Pelletier, J.; Couval, E.; Bouvier, D.; Bolzinger, M.-A. The Contribution of Zinc Ions to the Antimicrobial Activity of Zinc Oxide. *Colloids Surf. Physicochem. Eng. Aspects* **2014,** *457*, 263-274.

(38) Young, M.; Ozcan, A.; Myers, M. E.; Johnson, E. G.; Graham, J. H.; Santra, S. Multimodal Generally Recognized as Safe Zno/Nanocopper Composite: A Novel Antimicrobial Material for the Management of Citrus Phytopathogens. *J. Agric. Food Chem.* **2017,** *66* (26), 6604-6608.

(39) El Saeed, A. M.; Abd El-Fattah, M.; Azzam, A. M.; Dardir, M. M.; Bader, M. M. Synthesis of Cuprous Oxide Epoxy Nanocomposite as an Environmentally Antimicrobial Coating. *Int. J. Biol. Macromol.* **2016,** *89*, 190-197.

(40) Akiyama, T.; Miyamoto, H.; Yonekura, Y.; Tsukamoto, M.; Ando, Y.; Noda, I.; Sonohata, M.; Mawatari, M. Silver Oxide-Containing Hydroxyapatite Coating Has in Vivo Antibacterial Activity in the Rat Tibia. *J. Orthop. Res.* **2013,** *31* (8), 1195-1200.

(41) Johnson, J. R.; Roberts, P. L.; Olsen, R. J.; Moyer, K. A.; Stamm, W. E. Prevention of Catheter-Associated Urinary Tract Infection with a Silver Oxide-Coated Urinary Catheter: Clinical and Microbiologic Correlates. *J. Infect. Dis.* **1990,** *162* (5), 1145-1150.

(42) Reddy, S. T.; Chung, K. K.; McDaniel, C. J.; Darouiche, R. O.; Landman, J.; Brennan, A. B. Micropatterned Surfaces for Reducing the Risk of Catheter-Associated Urinary Tract Infection: An in Vitro Study on the Effect of Sharklet Micropatterned Surfaces to Inhibit Bacterial Colonization and Migration of Uropathogenic Escherichia Coli. *J. Endourol.* **2011,** *25* (9), 1547-1552.

(43) Ivanova, E. P.; Hasan, J.; Webb, H. K.; Truong, V. K.; Watson, G. S.; Watson, J. A.; Baulin, V. A.; Pogodin, S.; Wang, J. Y.; Tobin, M. J. Natural Bactericidal Surfaces: Mechanical Rupture of Pseudomonas Aeruginosa Cells by Cicada Wings. *Small* **2012,** *8* (16), 2489-2494.

(44) Hasan, J.; Xu, Y.; Yarlagadda, T.; Schuetz, M.; Spann, K.; Yarlagadda, P. K. Antiviral and Antibacterial Nanostructured Surfaces with Excellent Mechanical Properties for Hospital Applications. *ACS Biomater. Sci. Eng.* **2020,** *6* (6), 3608-3618.

(45) Hewawaduge, C.; Senevirathne, A.; Jawalagatti, V.; Kim, J. W.; Lee, J. H. Copper-Impregnated Three-Layer Mask Efficiently Inactivates Sars-Cov2. *Environ. Res.* **2021,** *196*, 110947.

(46) Babar, S.; Weaver, J. Optical Constants of Cu, Ag, and Au Revisited. *Appl. Opt.* **2015,** *54* (3), 477-481.

(47) Lee, H.; Dellatore, S. M.; Miller, W. M.; Messersmith, P. B. Mussel-Inspired Surface Chemistry for Multifunctional Coatings. *Science* **2007,** *318* (5849), 426-430.

(48) Ryu, J. H.; Messersmith, P. B.; Lee, H. Polydopamine Surface Chemistry: A Decade of Discovery. *ACS Appl. Mater. Interfaces* **2018,** *10* (9), 7523-7540.

(49) Platzman, I.; Brener, R.; Haick, H.; Tannenbaum, R. Oxidation of Polycrystalline Copper Thin Films at Ambient Conditions. *J. Phys. Chem. C* **2008,** *112* (4), 1101-1108.

(50) Park, J.-H.; Natesan, K. Oxidation of Copper and Electronic Transport in Copper Oxides. *Oxid. Met.* **1993,** *39* (5), 411-435.

(51) Zhao, L.; Chen, D.; Hu, W. Patterning of Metal Films on Arbitrary Substrates by Using Polydopamine as a Uv-Sensitive Catalytic Layer for Electroless Deposition. *Langmuir* **2016,** *32* (21), 5285-5290.

(52) Wang, K.; Dong, Y.; Zhang, W.; Zhang, S.; Li, J. Preparation of Stable Superhydrophobic Coatings on Wood Substrate Surfaces Via Mussel-Inspired Polydopamine and Electroless Deposition Methods. *Polymers* **2017,** *9* (6), 218.

(53) Frick, C. P.; Merkel, D. R.; Laursen, C. M.; Brinckmann, S. A.; Yakacki, C. M. Copper-Coated Liquid-Crystalline Elastomer Via Bioinspired Polydopamine Adhesion and Electroless Deposition. *Macromol. Rapid Commun.* **2016,** *37* (23), 1912-1917.

(54) Gonzalez-Martinez, E.; Saem, S.; Beganovic, N. E.; Moran-Mirabal, J. Fabrication of Microstructured Electrodes Via Electroless Metal Deposition onto Polydopamine-Coated Polystyrene Substrates and Thermal Shrinking. *Nano Select* **2021**.

(55) Environmental Protection Agency Protocol for the Evaluation of Bactericidal Activity of Hard, Non-Porous Copper Containing Surface Products. https://www.epa.gov/sites/production/files/2016-02/documents/copper_and_copper-alloy_surface_protocol_revised_012916.pdf (accessed June 2nd 2021).

(56) Bleichert, P.; Santo, C. E.; Hanczaruk, M.; Meyer, H.; Grass, G. Inactivation of Bacterial and Viral Biothreat Agents on Metallic Copper Surfaces. *Biometals* **2014,** *27* (6), 1179-1189.

(57) Palmer, D. A.; Bénézeth, P.; Simonson, J. In *Solubility of Copper Oxides in Water and Steam*, 14th International Conference on the Properties of Water and Steam in Kyoto, 2004; pp 491-496.

(58) Edwards, M.; Powers, K.; Hidmi, L.; Schock, M. The Role of Pipe Ageing in Copper Corrosion by-Product Release. *Water Sci. Technol. Water Supply* **2001,** *1* (3), 25-32.

(59) Rifkind, J. M.; Shin, Y. A.; Heim, J. M.; Eichhorn, G. L. Cooperative Disordering of Single-Stranded Polynucleotides through Copper Crosslinking. *Biopolymers* **1976,** *15* (10), 1879-1902.

(60) Warnes, S. L.; Keevil, C. W. Inactivation of Norovirus on Dry Copper Alloy Surfaces. *PLoS One* **2013,** *8* (9), e75017.

(61) Liu, Y.; Ai, K.; Liu, J.; Deng, M.; He, Y.; Lu, L. Dopamine-Melanin Colloidal Nanospheres: An Efficient near-Infrared Photothermal Therapeutic Agent for in Vivo Cancer Therapy. *Adv. Mater.* **2013,** *25* (9), 1353-1359.

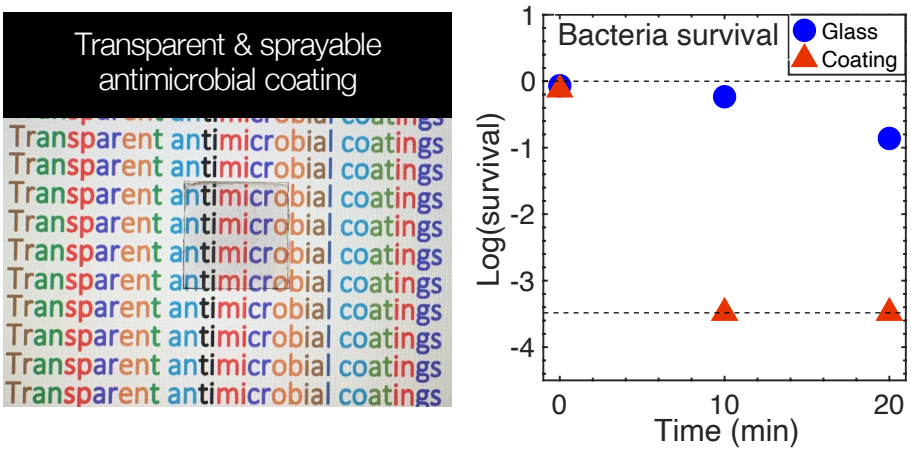
(62) Environmental Protection Agency Reregistration Eligibility Decision (Red) for Coppers. https://www3.epa.gov/pesticides/chem_search/reg_actions/reregistration/red_G-26_26-May-09.pdf (accessed June 2nd 2021).

(63) Zhou, P.; Deng, Y.; Lyu, B.; Zhang, R.; Zhang, H.; Ma, H.; Lyu, Y.; Wei, S. Rapidly-Deposited Polydopamine Coating Via High Temperature and Vigorous Stirring: Formation, Characterization and Biofunctional Evaluation. *PLoS One* **2014,** *9* (11), e113087.

(64) Chan, K.; Lai, S.; Poon, L.; Guan, Y.; Yuen, K.; Peiris, J. Analytical Sensitivity of Rapid Influenza Antigen Detection Tests for Swine-Origin Influenza Virus (H1n1). *J. Clin. Virol.* **2009,** *45* (3), 205-207.

(65) Malenovska, H. Virus Quantitation by Transmission Electron Microscopy, Tcid50, and the Role of Timing Virus Harvesting: A Case Study of Hree Animal Viruses. *J. Virol. Methods* **2013,** *191* (2), 136-140.

For Table of Contents Only



3.6. SUPPORTING INFORMATION

Transparent and Sprayable Surface Coatings that Kill Drug-Resistant Bacteria within Minutes and Inactivate SARS-CoV-2 Virus

Saeed Behzadinasab[1], Myra D. Williams[2], Mohsen Hosseini[1], Leo L. M. Poon[3,4,5], Alex W. H. Chin*[3,4], Joseph O. Falkinham III*[2], and William A. Ducker*[1]

[1]Department of Chemical Engineering and Center for Soft Matter and Biological Physics, Virginia Tech, Blacksburg, Virginia, 24061, USA

[2]Department of Biological Sciences, Virginia Tech, Blacksburg, Virginia, 24061, USA

[3]School of Public Health, LKS Faculty of Medicine, The University of Hong Kong, Hong Kong, China

[4]Centre for Immunity and Infection, Hong Kong Science Park, Hong Kong, China

[5]HKU-Pasteur Research Pole, LKS Faculty of Medicine, The University of Hong Kong, Hong Kong, China

Corresponding Authors' Email: Alex Chin alexchin@hku.hk; Joseph Falkinham jofiii@vt.edu;

William Ducker wducker@vt.edu

Keywords: antibacterial, antimicrobial, transparent, coating, drug-resistant bacteria, SARS-CoV-2 virus, COVID-19

3.6.1. Additional materials and methods:

3.6.1.1. Antibacterial assay

Confirmation of Surface Killing. To rule out the possibility that microbial cells remained adherent to the coupons, after the vortexing and sonication steps, coupons were placed coating-side-down on TSA plates for 10 min. The inverted coupons were removed and the plates were incubated at 37° C to determine whether any adherent, viable cells were present on the coupons and able to form colonies. For the experiments reported here, no colonies were formed, which indicates that no viable cells remained adhering to the coupons.

Surface Killing Not Influenced by Post Exposure to Particulate Copper or Copper Oxide. During the vortexing and sonication steps, it was possible that particulate copper or copper oxide was released, which may kill suspended cells; thereby increasing the extent of killing of bacteria. To rule out this possibility, in separate experiments, coupons were suspended in PBS as well as DE-buffer (BD, Sparks, MD). DE buffer contains agents that are able to block or inhibit killing by a wide variety of antimicrobial agents, including metals.[1] For the experiments reported here, there was no reduction in killing when coupons were vortexed and sonicated in DE buffer, compared to PBS. Thus, there was no killing of suspended cells by copper (oxide) released from coupons.

3.6.1.2. Abrasion tests

The PDA/Cu and PDA/Cu_2O coatings were abraded using a sponge mounted on a Gardco D10V abrasion tester. We based the test on the EPA protocol[2] which is used to evaluate

antimicrobial coatings for approval. The protocol has abrasion with a sponge that is wetted with an antimicrobial agent. One important application of transparent coatings is to touch screens, which are often cleaned with ethanolic solution, so we used 70% alcohol in water as our antimicrobial agent. The tester translates a sponge parallel but in contact with the active surface of the sample with a load of 0.45 kg, an amplitude of ~26 cm, and a period of ~5 s. The sponge was wetted with 20 mL of 70% ethanol in water solution prior to the abrasion tests. One abrasion cycle was performed as follows: the sponge was translated across the sample 8 times, then 70% ethanol was sprayed on the abrasion platform and the sample with a subsequent 30 minutes waiting period. 10 cycles (= 80 passes in total) were applied to the sample. A single sponge was used for the first 5 cycles and this was replaced with a second sponge for the second 5 cycles. The abraded samples were sent to quantify their antibacterial properties by the methods in Section 4.4. Tabulated values are the average of results from three independent samples.

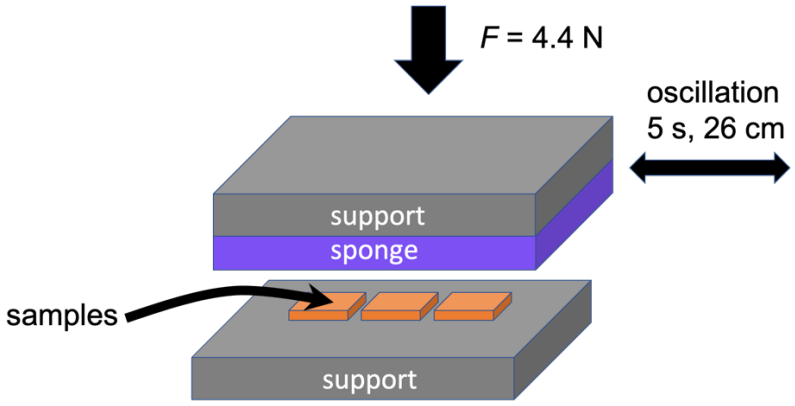


Figure S3-1. Schematic of abrasion tests on our coatings. A load of 0.45 kg (4.4. N) was applied to a sponge and then the sponge was passed back and forth on the samples. The sponge was in contact with the samples during the test; the schematic has a gap so that the samples can be seen.

3.6.2. Additional characterizations

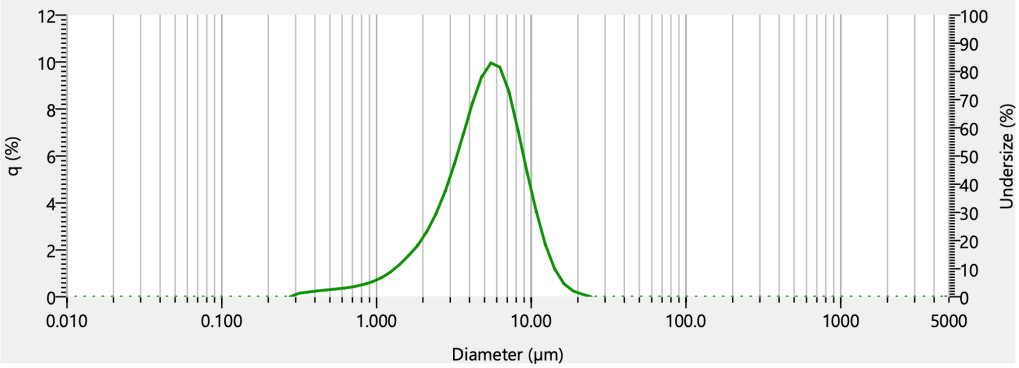


Figure S3-2. Particle Size Distribution of Cu_2O particles used in PDA/Cu_2O coating. The distribution was measured by a Horiba Laser Scattering Particles Size Distribution Analyzer LA-960. The mean size is 5.5 µm, and the median size is 5.0 µm, and the mode size is 5.5 µm. This information was provided by the vendor (American Chemet Corporation).

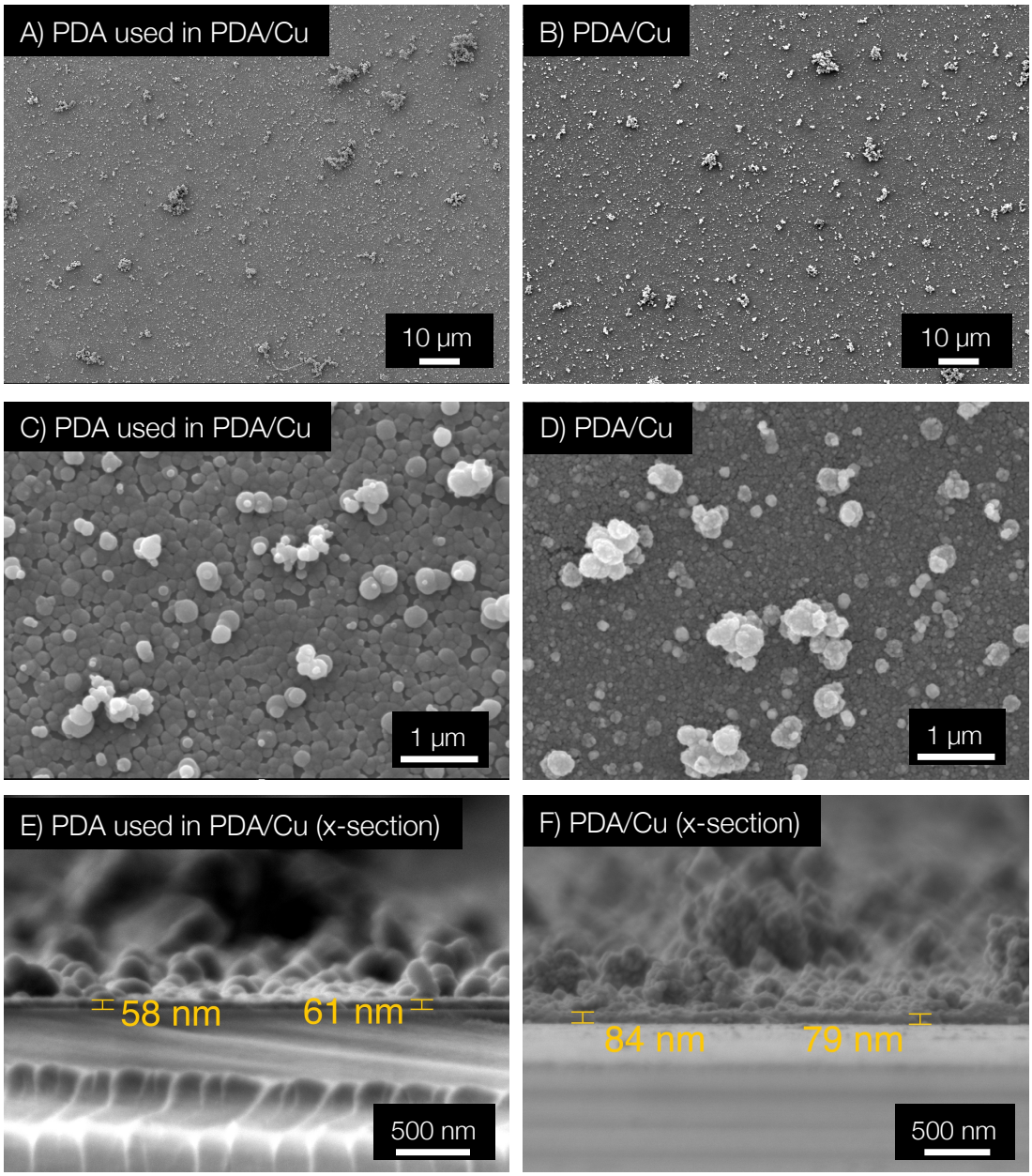


Figure S3-3. Additional SEM images of PDA (prior to copper deposition) and PDA/Cu. A, C, E, show PDA prior to copper deposition, and B, D, and F show the PDA/Cu coating. Comparing high magnification images of PDA and PDA/Cu (i.e. C and D images), the copper coating is apparent from the slight roughening of the coating as well as the filling of depressions compared to C. Also, no individual copper particles are visible on the PDA/Cu. E and F show cross section images of PDA and PDA/Cu, respectively. The orange text shows the thickness of each coating. The difference of thickness between PDA and PDA/Cu shows that the copper layer has a thickness of approximately 22 nm. Note that the samples were coated with 5 nm of Pt/Pd prior to SEM imaging, thus the actual thickness of PDA and PDA/Cu are ~55 and ~77 nm. The coatings are on glass, the same substrate as all other tests.

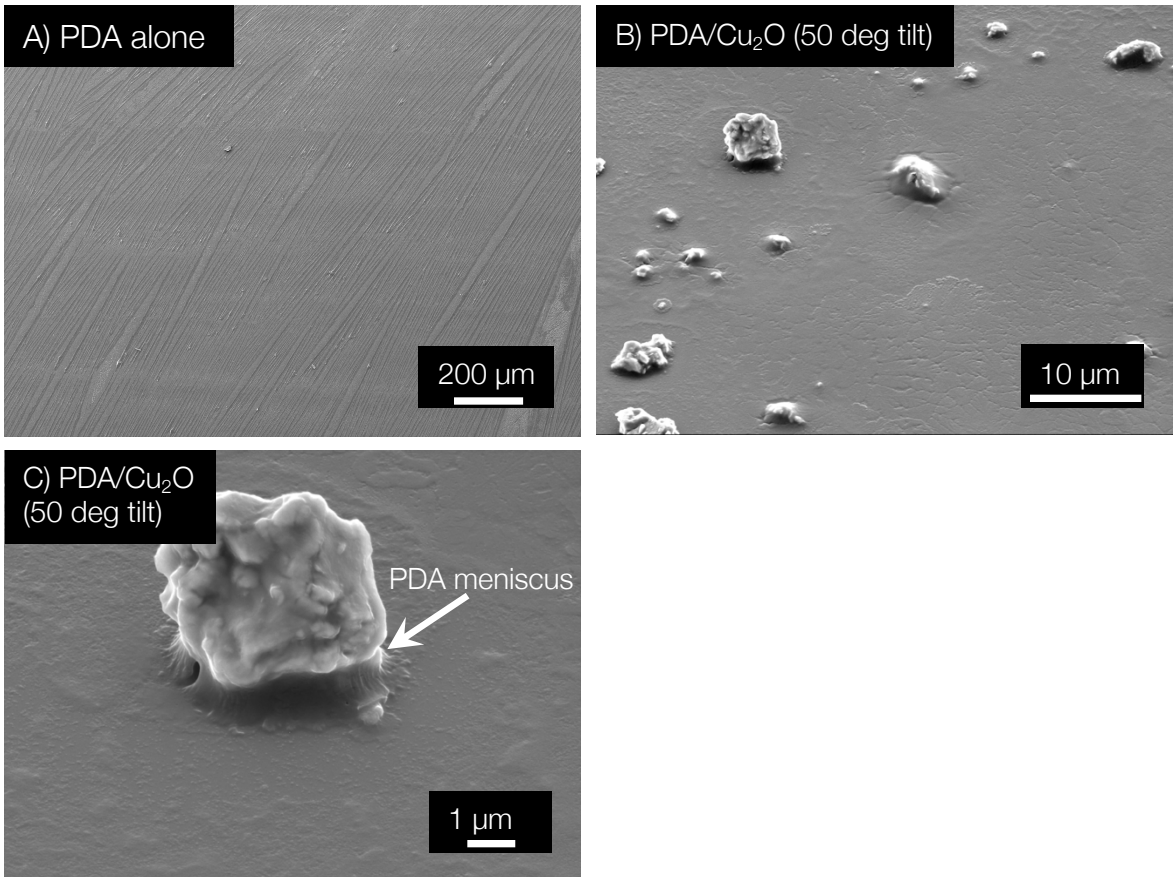
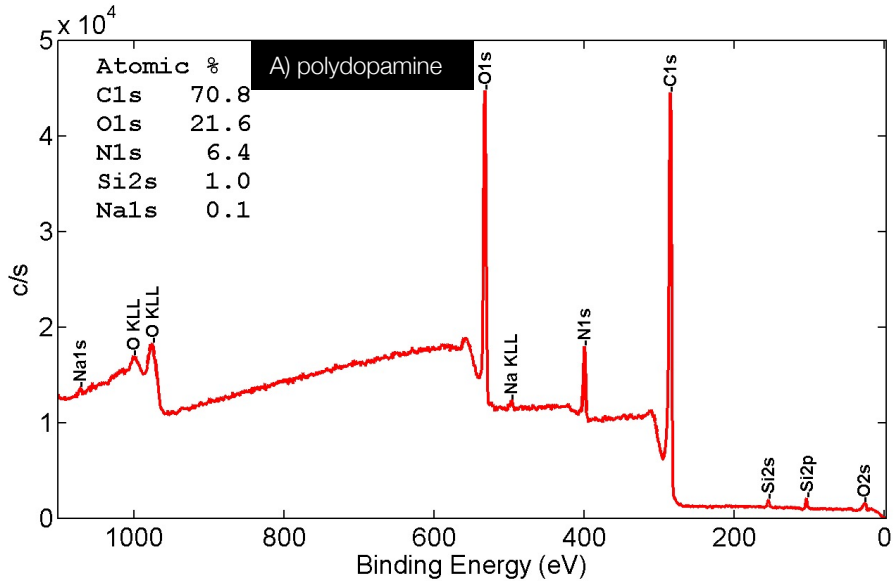
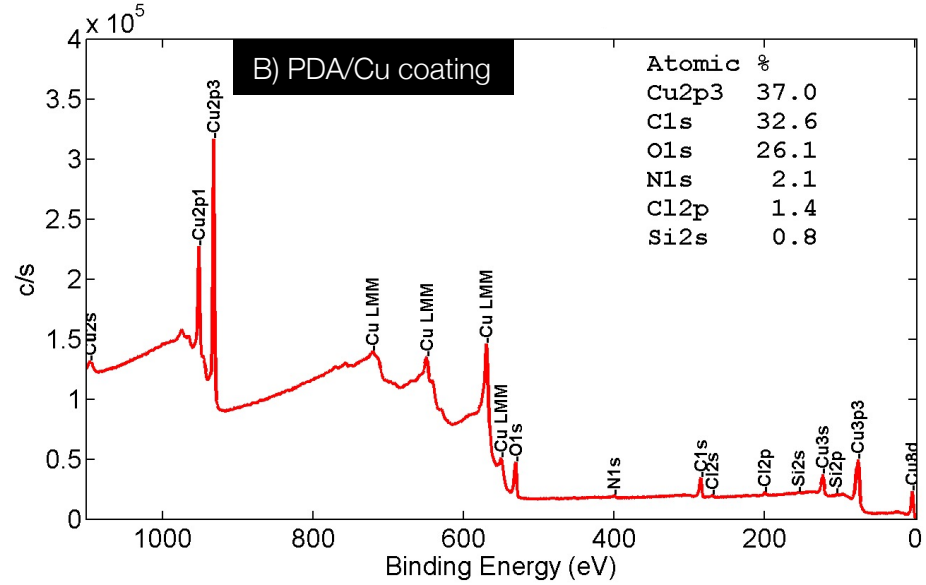
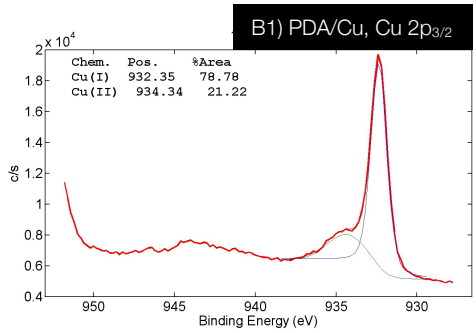
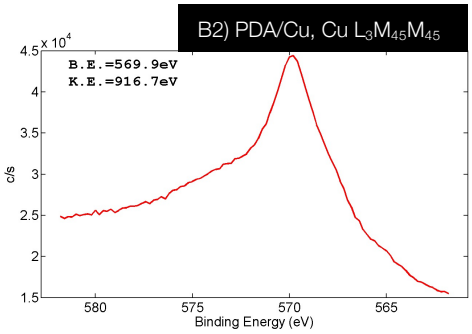


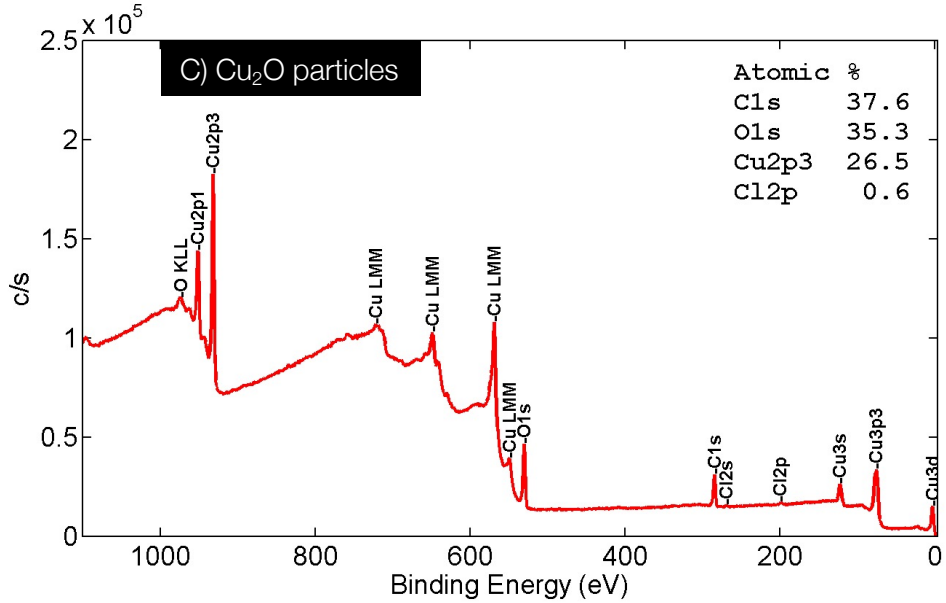
Figure S3-4. Additional SEM images of coatings. A) Plan view image of PDA was made was prepared by the same method as the PDA/Cu_2O coating. B) 50 degrees tilt image of PDA/Cu_2O. C) 50 degrees tilt image of PDA/Cu_2O at higher magnification. Cu_2O is clearly protruding from the PDA and the PDA meniscus is shown with white arrow.

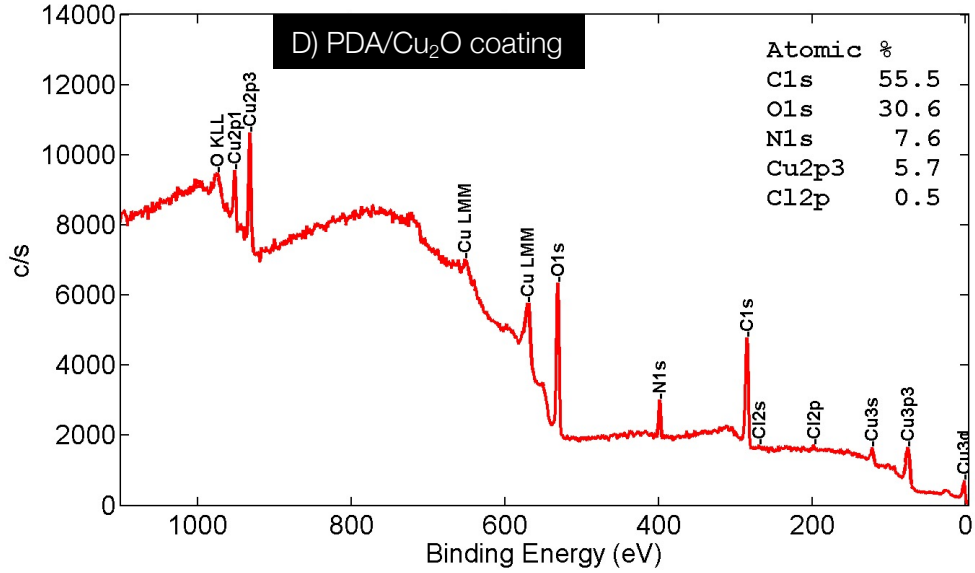

x 10^4
A) polydopamine
Atomic %
C1s 70.8
O1s 21.6
N1s 6.4
Si2s 1.0
Na1s 0.1
c/s
Binding Energy (eV)
Na1s
O KLL
O KLL
O1s
Na KLL
N1s
C1s
Si2s
Si2p
O2s

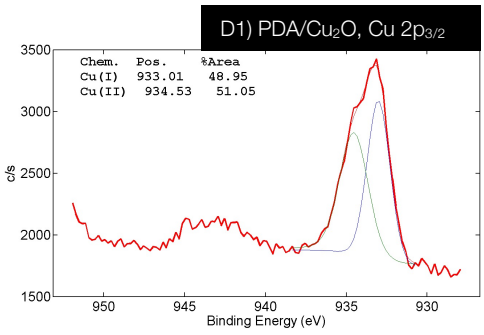

x 10^5
B) PDA/Cu coating
Atomic %
Cu2p3 37.0
C1s 32.6
O1s 26.1
N1s 2.1
Cl2p 1.4
Si2s 0.8
c/s
Binding Energy (eV)
Cu2s
Cu2p3
Cu2p1
Cu LMM
Cu LMM
Cu LMM
Cu LMM
O1s
N1s
C1s
Cl2s
Cl2p
Si2s
Cu3s
Si2p
Cu3p3
Cu8d


B1) PDA/Cu, Cu 2p3/2
x 10^4
Chem. Pos. %Area
Cu(I) 932.35 78.78
Cu(II) 934.34 21.22
c/s
Binding Energy (eV)


B2) PDA/Cu, Cu L3M45M45
x 10^4
B.E.=569.9eV
K.E.=916.7eV
c/s
Binding Energy (eV)


C) Cu2O particles
x 10^5
Atomic %
C1s 37.6
O1s 35.3
Cu2p3 26.5
Cl2p 0.6
c/s
Binding Energy (eV)
O KLL
Cu2p1
Cu2p3
Cu LMM
Cu LMM
Cu LMM
Cu LMM
O1s
C1s
Cl2s
Cl2p
Cu3s
Cu3p3
Cu3d


D) PDA/Cu2O coating
Atomic %
C1s 55.5
O1s 30.6
N1s 7.6
Cu2p3 5.7
Cl2p 0.5
c/s
Binding Energy (eV)
O KLL
Cu2p1
Cu2p3
Cu LMM
Cu LMM
O1s
N1s
C1s
Cl2s
Cl2p
Cu3s
Cu3p3
Cu3d


D1) PDA/Cu2O, Cu 2p3/2
Chem. Pos. %Area
Cu(I) 933.01 48.95
Cu(II) 934.53 51.05
c/s
Binding Energy (eV)

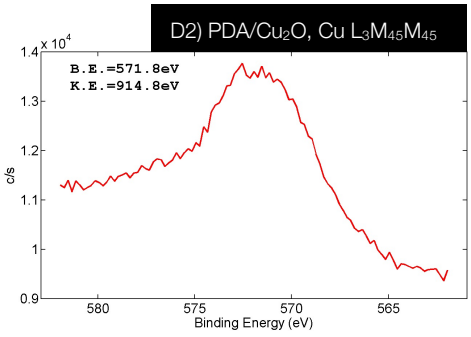

D2) PDA/Cu2O, Cu L3M45M45
x 10^4
B.E.=571.8eV
K.E.=914.8eV
c/s
Binding Energy (eV)

Figure S3-5. XPS characterization of coatings. XPS survey data of A) Polydopamine, B) PDA/Cu coating, C) commercial Cu_2O particles that were used in PDA/Cu_2O, and D) PDA/Cu_2O coating. For the XPS survey data, the elemental composition is shown in the inset. The PDA/Cu coating has 37 % copper and the PDA/Cu_2O coating has 5.7% copper on the surface.

More detailed information for the PDA/Cu coating is shown in B1 and B2. The high-resolution Cu $2p_{3/2}$ (B1) shows a major peak at 932.4 eV and a minor peak at 934.4 eV (E_b), as well as a characteristic satellite feature of Cu(II) at 940-945 eV. The peak at 932.4 eV can be assigned to either Cu(0) or Cu(I),[3-4] while the peak at 934.4 eV is attributed to Cu(II). The Cu $L_3M_{45}M_{45}$ Auger (B2) feature exhibits a single peak with a kinetic energy of 916.7 eV (E_k). The Modified Auger Parameter[4] of 1849.1 eV (E_b+E_k) for the 932.4 eV peak is in excellent agreement with the value for Cu_2O (1849.2 eV).[5-6] This shows that Cu(I) is the major Cu species on the surface of the PDA/Cu coating.

More detailed information for the PDA/Cu_2O coating is shown in D1 and D2. The high-resolution Cu $2p_{3/2}$ (D1) shows two peaks at 933.0 eV and 934.5 eV (E_b), as well as a characteristic satellite feature of Cu(II) at 940-945 eV. We attribute the peak at 933.0 eV to Cu(I) The peak at 934.5 eV is attributed to Cu(II). The Cu $L_3M_{45}M_{45}$ Auger feature (D2) exhibits a single peak with a kinetic energy of 914.8 eV (E_k). The Modified Auger Parameter[4] of 1847.8 eV (E_b+E_k) for the 933.0 eV peak is in agreement with the value of Cu(I)Cl (1847.8 eV)[4]. Survey data shows only 1.4% chlorine, so the amount of CuCl must be very low. A small amount of Cl is not surprising since chlorine is already present on the outer surface of the commercial Cu_2O particles (See sub figure C) that we have used for preparation of this coating. In summary, both Cu(I) and Cu(II) species are present on the outer 1 nm or so of the PDA/Cu_2O coating.

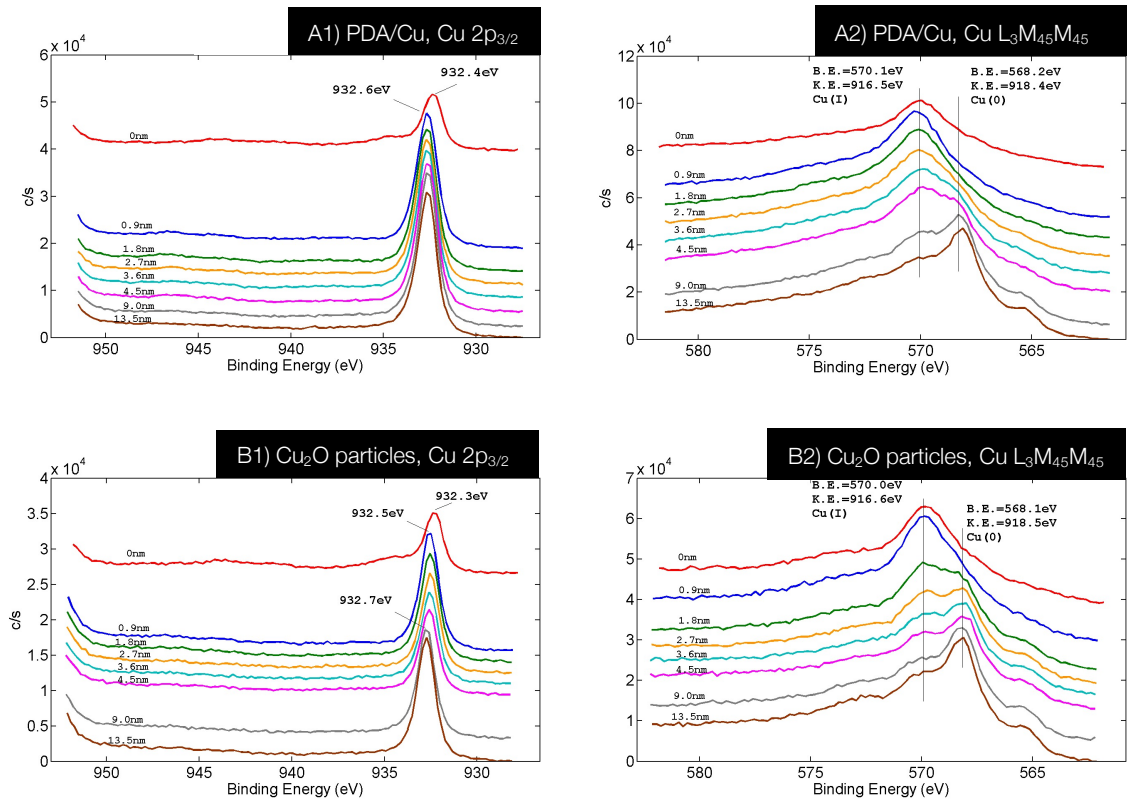


Figure S3-6. High resolution XPS characterization of Cu_2O particles and PDA/Cu coating as a function of depth of etching with Ar^+. Each curve is labelled with the depth of etching in nanometers. Both the Cu $2p_{3/2}$ and the Auger peak are shown. XPS of the air-exposed surface showed that the surface of the PDA/Cu coating was predominantly oxidized, as expected, and the objective here was to determine the identity of subsurface copper material. As described for Figure S3-5, the Cu $2p_{3/2}$ peak does not allow good discrimination of Cu(0) from Cu(I) but the empirical Modified Auger Parameter does allow discrimination. During etching of the PDA/Cu layer, there is a gradual shift in the Auger peak from the characteristic binding energy for Cu(0) (570.1 ev) to the binding energy for Cu(0) (568.2 eV) which is suggestive of underlying metallic copper. However, a control experiment where we etched Cu_2O shows a similar shift, which demonstrates that the Ar^+ etching leads to reduction of the Cu(I) species. Therefore the experiment on the PDA/Cu does not provide unambiguous evidence of Cu(0). In fact, the PDA/Cu required deeper etching than the Cu_2O particles to produce a similar peak shift, and there was no sudden shift to a pure Cu(0) Auger spectrum, which is suggestive that the 22 nm layer may not be Cu(0).

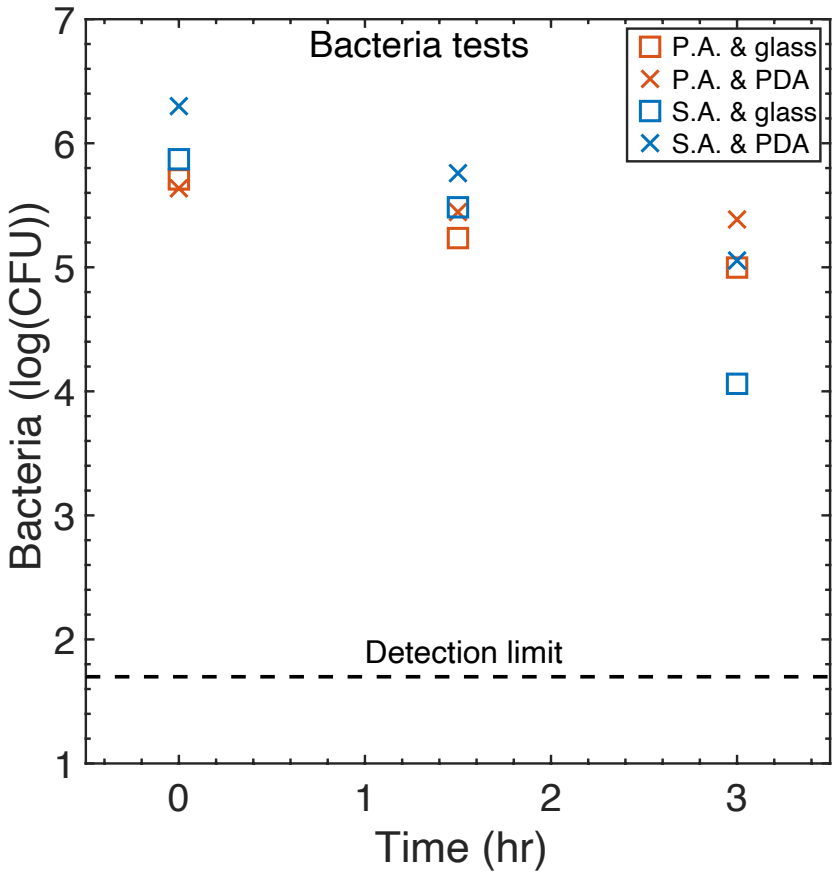


Figure S3-7. Bacteria assay for PDA sample, that was prepared in the first step of the PDA/Cu coating. There is no reduction compared to glass against P. aeruginosa (P.A) or staphylococcus aureus (S.A.). This proves that copper or cuprous oxide are the active ingredients against bacteria. Bacteria on PDA and on glass are shown with "x" and square markers, respectively.

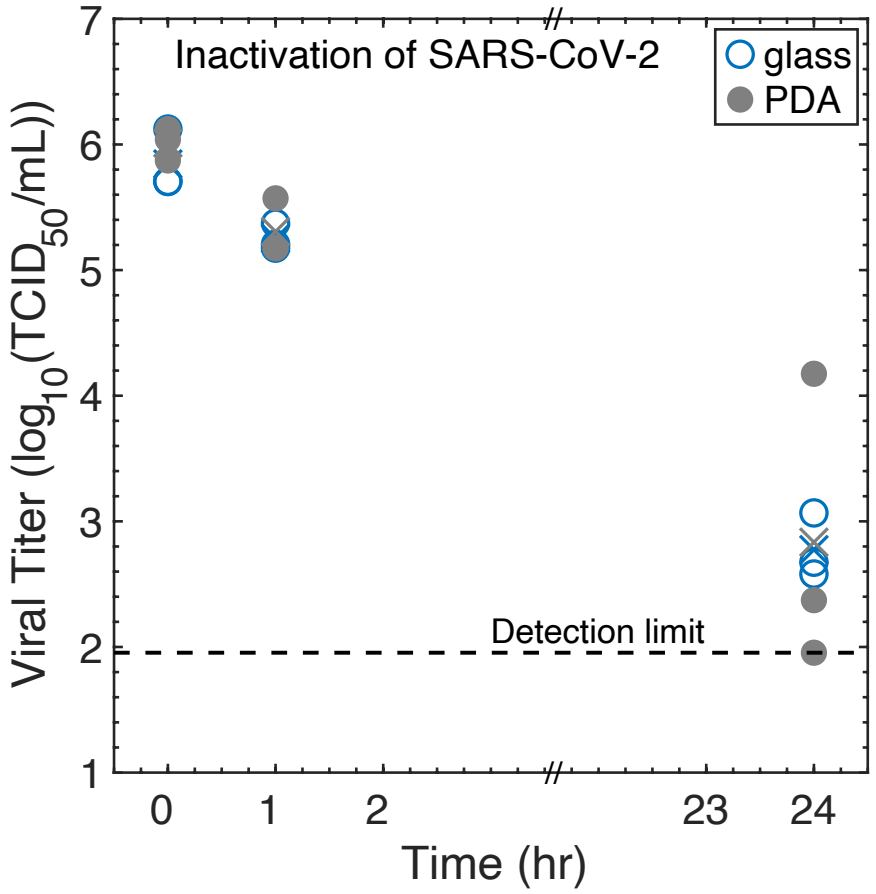


Figure S3-8. SARS-CoV-2 titer for PDA sample, that was used in PDA/Cu coating, and control (i.e. glass). PDA (shown with grey) does not have antimicrobial effects against SARS-CoV-2 virus (two sample t-test, two tailed, unequal variance, at 1 hr, $p = 0.72$). This proves that copper or cuprous oxide are the active ingredients against SARS-CoV-2. Individual data points are shown with circles and averages are shown with "x" sign.

3.6.3. Characterization of PDA/Cu2O coating that was prepared by spray-coating

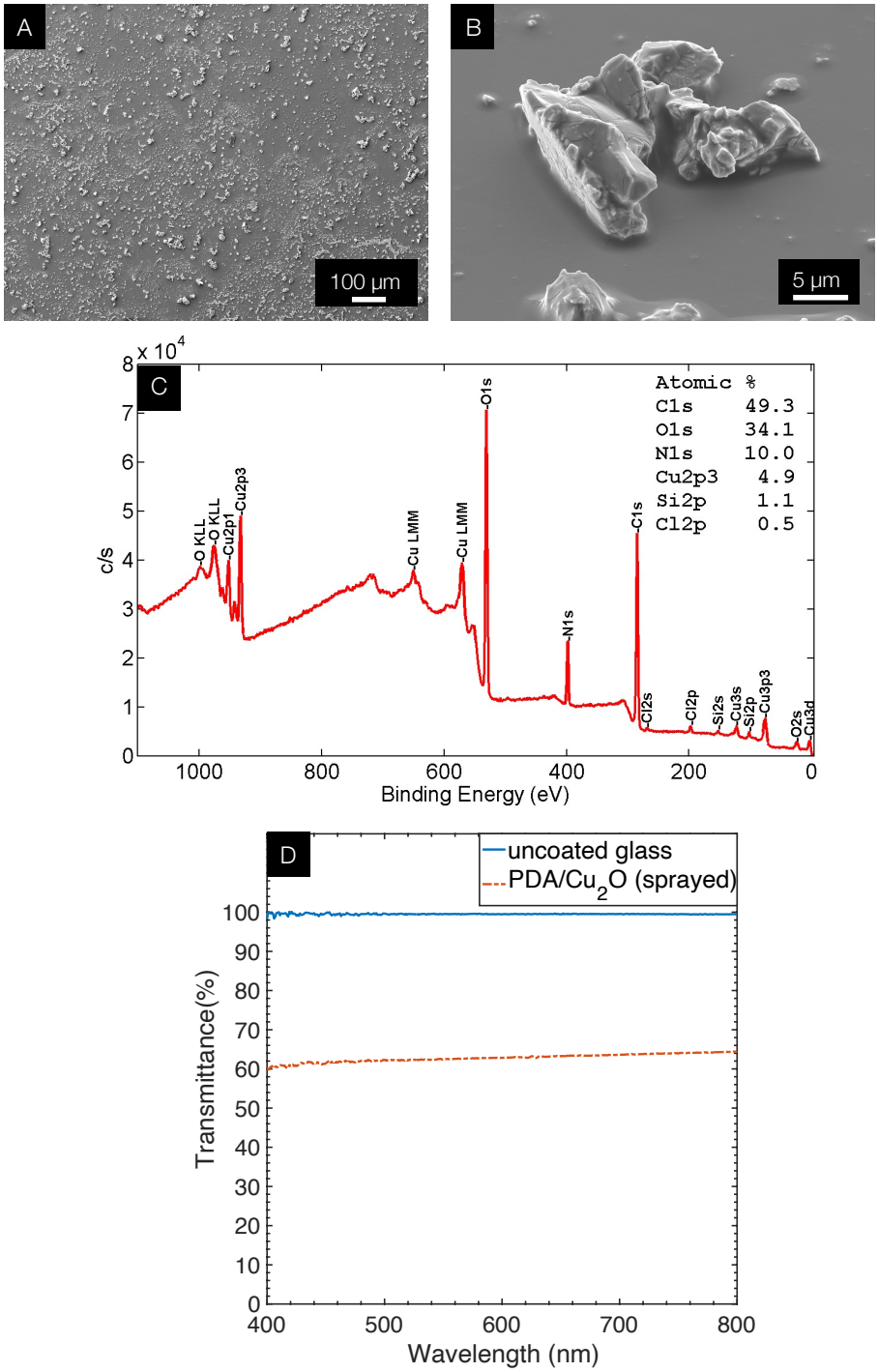


Figure S3-9. Characterization of PDA/Cu_2O coating on glass that was prepared by spray-coating. A) Plan view SEM image, B) 50-degree tilted SEM image. C) XPS survey spectra of the surface. XPS shows there are 4.9% copper on the surface of the coating. D) Visible spectra of the coating. The background for capturing visible spectra is glass. The sprayed coating is similar to PDA/Cu_2O by drop casting method.

3.6.4. Data tables of bacterial and viral tests

	log (CFU) at 0 hr	log (CFU) at 1 hr	Reduction compared to glass (at 1hr)
Glass	5.5377	5.011	---
PDA/Cu coating	5.5585	2.350	99.78%
PDA/Cu_2O coating	5.5327	2.394	99.76%

Table S3-1. Log CFU of Pseudomonas aeruginosa after antimicrobial coatings were abraded using the method described previously. The first and second columns show average log CFU of bacteria 0 and 1 hr after the droplet was placed on the sample. The third column show the Reduction of bacteria for each abraded coating compared to glass at 1 hr. The PDA/Cu2O coating was noticeably worn after the abrasion but the PDA/Cu coating was not. Both coatings retained a strong ability to kill bacteria after abrasion.

Material	Time	CFU				log (CFU)		
MRSA Bacteria input	---	517500	698000	502500		5.7139	5.8439	5.7011
Glass	0	490000				5.6902		
	10 min	249500				5.3971		
	20 min	533000				5.7267		
PDA/Cu coating	0	388500	76500	76500		5.5894	4.8837	4.8837
	10 min	1550	1700	3250		3.1903	3.2304	3.5119
	20 min	<	<	<		<	<	<

Table S3-2. MRSA bacteria tests with PDA/Cu data. With the coating samples, each time point was repeated 3 times. The symbol "<" shows the detection limit (i.e. all bacteria were dead). The detection limit is 50 CFU.

Material	Time	CFU				log (CFU)		
MRSA Bacteria input	---	878000	726000	584000		5.9434	5.8609	5.7664
Glass	0	391000				5.5922		
	10 min	488000				5.6884		
	20 min	172000				5.2355		
PDA/Cu_2O coating	0	586000	698500	687500		5.7679	5.8442	5.8373
	10 min	15850	23000	10300		4.2000	4.3617	4.0128
	20 min	13950	14500	17500		4.1446	4.1614	4.2430

Table S3-3. MRSA bacteria tests with PDA/Cu_2O coating data. With the coating samples, each time point was repeated 3 times. The symbol "<" shows the detection limit (i.e. all bacteria were dead). The detection limit is 50 CFU.

Material	Time	CFU				log (CFU)		
Pseudomonas aeruginosa Bacteria input	---	706000	579500	650000		5.8488	5.7630	5.8129
Glass	0	1522500				6.1826		
	10 min	1131000				6.0535		
	20 min	1090500				6.0376		
PDA/Cu coating	0	9300	1200	1200		3.9685	3.0792	3.0792
	10 min	<	<	<		<	<	<
	20 min	<	<	<		<	<	<

Table S3-4. Pseudomonas aeruginosa bacteria tests with PDA/Cu coating data. With the coating samples, each time point was repeated 3 times. The symbol "<" shows the detection limit (i.e. all bacteria were dead). The detection limit is 50 CFU.

Material	Time	CFU				log (CFU)		
Pseudomonas aeruginosa Bacteria input	---	145500	161000	151500		5.1629	5.2068	5.1804
Glass	0	130500				5.1156		
	10 min	89000				4.9494		
	20 min	21000				4.3222		
PDA/Cu_2O coating	0	92500	133500	121500		4.9661	5.1255	5.0846
	10 min	<	<	<		<	<	<
	20 min	<	<	<		<	<	<

Table S3-5. Pseudomonas aeruginosa bacteria tests with data. With PDA/Cu_2O coating the coating samples, each time point was repeated 3 times. The symbol "<" shows the detection limit (i.e. all bacteria were dead). The detection limit is 50 CFU.

Material	Time	$TCID_{50}$/ml				log ($TCID_{50}$/ml)		
Nil (virus input control)	---	1.178×10^{6}	2.35×10^{6}	1.607×10^{6}		6.071	6.373	6.206
Glass	0	5.081×10^{6}	5.08079×10^{5}	1.855×10^{6}		6.706	5.706	6.268
	1 h	6.927×10^{5}	1.946×10^{5}	3.727×10^{5}		5.841	5.289	5.571
	24 h	7.824×10^{3}	3.461×10^{4}	1.559×10^{4}		3.893	4.539	4.193
PDA/Cu coating	0	1.178×10^{6}	6.155×10^{5}	1.095×10^{6}		6.071	5.789	6.039
	1 h	<	<	<		<	<	<
	24 h	<	<	<		<	<	<
PDA/Cu_2O coating	0	5.080×10^{5}	6.155×10^{5}	5.010×10^{5}		5.706	5.789	5.700
	1 h	6.155×10^{2}	<	1.606×10^{3}		2.789	<	3.206
	24 h	<	<	<		<	<	<

Table S3-6. SARS-CoV-2 test $TCID_{50}$/mL data. Each time point was repeated 3 times. The "Nil" is the virus input is the initial quantity of the virus place on the coating. The symbol "<" shows the detection limit (i.e. no infectious virus was detected). The detection limit is 90 $TCID_{50}$/ml.

Material	Time	CFU				log (CFU)		
Pseudomonas aeruginosa Bacteria input	---	379000	420500	351000		5.5786	5.6238	5.5453
Glass	0 min	441000	214400	434000		5.6444	5.3312	5.6375
	1 hr	139500	97000	80000		5.1446	4.9868	4.9031
PDA/Cu coating	0 min	315000	411000	366000		5.4983	5.6138	5.5635
	1 hr	4500	<	<		3.6532	<	<
PDA/Cu_2O coating	0 min	366000	339500	319000		5.5635	5.5308	5.5038
	1 hr	6100	<	<		3.7853	<	<

Table S3-7. Pseudomonas aeruginosa bacteria tests with abraded PDA/Cu and PDA/Cu_2O coatings data. The symbol "<" shows the detection limit (i.e. all bacteria were dead). The detection limit is 50 CFU.

References

(1) Dey, B.; Engley Jr, F. Methodology for Recovery of Chemically Treated Staphylococcus Aureus with Neutralizing Medium. *Appl. Environ. Microbiol.* **1983,** *45* (5), 1533-1537.

(2) Environmental Protection Agency *Antimicrobial Testing Methods & Procedures: Interim Method for Evaluating the Efficacy of Antimicrobial Surface Coatings* *Https://Www.Epa.Gov/Pesticide-Analytical-Methods/Antimicrobial-Testing-Methods-Procedures-Interim-Method-Evaluating*; 2020.

(3) Moulder, J. F.; Stickle, W. F.; Sobol, P. E.; Bomben, K. D. *Handbook of X-Ray Photoelectron Spectroscopy*, Physical Electronics USA, Inc.: 1995.

(4) Biesinger, M. C. Advanced Analysis of Copper X-Ray Photoelectron Spectra. *Surf. Interface Anal.* **2017,** *49* (13), 1325-1334, DOI: 10.1002/sia.6239.

(5) Wagner, C. Auger Lines in X-Ray Photoelectron Spectrometry. *Anal. Chem.* **1972,** *44* (6), 967-973.

(6) Gaarenstroom, S.; Winograd, N. Initial and Final State Effects in the Esca Spectra of Cadmium and Silver Oxides. *J. Chem. Phys.* **1977,** *67* (8), 3500-3506.

Chapter 4. Porous Antimicrobial Coatings for Killing Microbes within Minutes

Saeed Behzadinasab[1,2,3], Myra D. Williams[4], Mete Aktuglu[1], Joseph O. Falkinham III*[4], and William A. Ducker*[1,2,3]

[1]Department of Chemical Engineering, Virginia Tech, Blacksburg, Virginia, 24061, USA

[2]Center for Soft Matter and Biological Physics, Virginia Tech, Blacksburg, Virginia, 24061, USA

[3]Macromolecules Innovation Institute, Virginia Tech, Blacksburg, Virginia, 24061, USA

[4]Department of Biological Sciences, Virginia Tech, Blacksburg, Virginia, 24061, USA

Corresponding Authors' Email: Joseph Falkinham jofiii@vt.edu; William Ducker wducker@vt.edu

Keywords: porous, polydopamine, copper, antibacterial, antimicrobial, coating, bacteria

ORCIDs:

Saeed Behzadinasab: 0000-0002-6271-2623

Joseph O. Falkinham III: 0000-0002-4391-9012

William A. Ducker: 0000-0002-8207-768X

4.1. ABSTRACT

Antimicrobial coatings can be used to reduce the transmission of infectious agents that are spread by contact. An effective coating should kill microbes in the time between users, which is sometimes minutes or less. Fast killing requires fast transport, and our proposed method of fast transport is a porous coating where the contaminated liquid imbibes (infiltrates) into the pores to achieve rapid contact with active material inside the pores. We test the hypothesis that a porous antimicrobial coating will enable faster inactivation of microorganisms than a planar coating of the same material. We use hydrophilic pores of dimensions 5-100 μm such that liquid droplets imbibe in seconds, and from there transport distances and times are short, defined by the pore size, rather than the droplet size. Our coating has two levels of structure: (A) a porous scaffold and (B) an antimicrobial coating within the pore structure containing the active ingredient. Two scaffolds are studied: stainless steel and poly(methylmethacrylate) (PMMA). The active ingredient is electrolessly-deposited copper. To enhance adhesion and growth of copper, a layer of polydopamine (PDA) is deposited on the scaffold prior to deposition of the copper. This porous copper coating kills 99.84% of *Pseudomonas aeruginosa* within three minutes, which is equivalent to a half-life of 27 s. In contrast, the same layer of PDA/copper on a non-porous coating kills 79.65% in the same time frame, consistent with the hypothesis that the killing rate is increased by the addition of porosity. Using the porous PMMA scaffold, the porous antimicrobial coating kills >99.99% *Pseudomonas aeruginosa* in 5 min, which is equivalent to a half-life of 21 s. The higher rate of kill on the porous antimicrobial solid is appropriate for hindering the spread of infectious agents on common use objects.

4.2. Introduction

Microbial diseases kill millions of people annually, and cause immense economic damage.[1-5] One method of transmitting infectious agents (e.g., bacteria and viruses) is via solid surfaces ("fomite transmission").[6-7] By addition of antimicrobial coatings, we expect to reduce transmission and therefore to reduce both the incidence of morbidity and mortality and the need for antibiotic treatments. Antibiotic-resistant pathogens[8-10] are the most troublesome because treatment options are more limited. A recent report indicated that 1.2 million people die annually due to antibiotic-resistant bacteria.[10] Antibiotic-resistance is sometimes called the "silent pandemic" as it causes a very high level of mortality and morbidity while receiving little attention by the media.[11] A Special Report[12-13] from the US Centers for Disease Control and Prevention (CDC) recently discussed that drug-resistant infections and deaths increased during the COVID-19 pandemic. Such infections occur in both hospitals,[14] and in the wider community.

Multidrug resistant *Pseudomonas aeruginosa* (*P. aeruginosa*) is a well-known bacterium that is categorized in both Healthcare-Acquired Infections and Community-Acquired Infection, and therefore is considered a "Serious Threat" by the CDC.[15-17] Infections caused by *P. aeruginosa* are difficult to treat due to the intrinsic capability of the bacterium to adapt to new environments and acquire resistance to new antibiotics.[18]

P. aeruginosa bacterial cells can survive and remain infectious on solids for very long periods of time, from a few days to months.[19] Also, the bacterium can be transferred to humans from contaminated surfaces.[20-21] Therefore *P. aeruginosa* is a good target for restricting infection through killing bacteria on common-use surfaces, and is the test organism in this study. The traditional method for disinfecting surfaces is to use disinfectants such as 70% ethanol or bleach.

A major problem with that approach is that contamination can reoccur soon after the ethanol evaporates. Another major problem is that some disinfectants are hazardous, including bleach.[22]

Antimicrobial surface coatings provide an alternative to traditional disinfectants such as bleach. A recent study showed that healthcare units that employ antimicrobial coatings have significant improvement in patient outcomes as well as reductions in environmental contamination.[23] Unlike traditional disinfectants, antimicrobial coatings have the potential to provide an ongoing kill for days, months, or even years without human intervention, although they likely still require cleaning to prevent fouling of the surface. To be effective, the coating should also provide a quick kill. The time to killing should ideally be less than the time between users of the same object, which could be minutes or even seconds. Although many existing coatings are effective,[24-34] they would be more effective at reducing transmission if they could kill microbes more quickly. Therefore, a major research objective is to obtain both a fast kill and an ongoing kill. A typical standard for killing is 99.9%, and our objective is to achieve this in only a few minutes. For comparison, the typical standard for the US Environmental Protection Agency (EPA) is reduction of 99.9% of microbes compared to an uncoated solid in an hour.[35-36]

Our hypothesis is that a porous hydrophilic coating will provide a faster kill than a flat coating of the same material. Killing requires contact between the microbe and the antimicrobial, so the transport time for the bacterium or the antimicrobial is part of the overall killing time. When a droplet lands on an impermeable solid, one component must diffuse through the droplet, which is typically of the order of 100 μm to several mm in size. If instead the droplet is immediately imbibed (infiltrated) into a porous coating, the relevant length scale for transport is the pore size, which is controllable and can be made smaller than the drop size. For example, it is simple to make materials with pore sizes of 100 μm, 10 μm, or 1 μm. Diffusion times depend on

pore geometry but typically scale faster than diffusion lengths so a reduction in diffusion length from 1000 μm to 10 μm will result in a greater than 100-fold reduction in diffusion time. A porous antiviral coating was previously explored for a very mild antimicrobial CuO material,[29] but the antiviral activity was not compared to a non-porous coating.

To rationally speed the killing of bacteria, we need to examine all the relevant time scales. The relevant time scales in this problem are: the time between users of the coated item, the transport time within the droplet, the droplet imbibition time, the droplet evaporation time, and the "intrinsic" killing time for the bacterium when the active ingredient is already present at the surface of the bacteria. Our goal is to minimize the other times so that killing can approach the intrinsic killing time. The diffusion time within a droplet depends on what is diffusing: small molecules will take minutes to an hour to diffuse one millimeter across a droplet, and a non-motile bacterium will take even longer. This is too long for our desired total killing time. Evaporation will speed the contact between the antimicrobial and the bacterium in two ways: by reducing the drop volume and by introducing convection. But reliance on evaporation is challenging because it depends on environmental factors. In our lab (approximately 22 ˚C and 32% humidity), 5 μL and 10 μL droplets take 44 and 73 minutes, respectively, to dry on the bench, which is too long. In more humid environments, we expect longer evaporation times.

Once the bacterial suspension has imbibed into a porous coating, diffusion will be fast because of the smaller distance. However, the imbibition time also needs to be faster than our target time of a few minutes to realize an advantage from the more rapid imbibition. Imbibition times can be estimated from the Washburn Equation, which applies to a single straight pore:[37]

$$t_I = \frac{2\eta}{\gamma r_{\mathrm{p}} \cos\theta} L^2 \qquad \text{Equation 4-1}$$

where η is the liquid viscosity, γ is the vapor–liquid interfacial tension, r_{p} is the radius of the pore, θ is the contact angle of liquid on the non-porous solid, and L is the distance travelled. Imbibition times of less than one minute are easily achievable if we use a hydrophilic solid with large pores (> few micrometers). Therefore, we expect to have the droplet imbibition, diffusion, and intrinsic killing times all below the target of a few minutes.

In addition to exhibiting more rapid killing, we expect that porous coatings will have the following benefits compared to flat surfaces:[31] 1) increased surface area for more active material 2) protection of the active ingredient from loss due to abrasion, and 3) less microbial transfer from surface to fingers.[7]

Here we used a modular approach to the preparation of porous antimicrobial coatings in which we purchased or prepared a porous coating and then coated the interior pore space with an antimicrobial. We investigated two porous structures: stainless steel and poly(methyl methacrylate) (PMMA). For the antimicrobial coating we used copper on polydopamine (PDA), which is already known to kill both Gram positive (*Staphylococcus aureus*) and Gram negative (*Pseudomonas aeruginosa*) bacteria and to inactivate Severe Acute Respiratory Syndrome Coronavirus 2 (SARS-CoV-2).[27] Copper usually occurs with an oxidized surface, and copper and its oxides are very broad spectrum antimicrobials, and therefore useful for inhibiting transmission of a broad spectrum of microbes.[26, 38]. A simple two-step procedure was followed:[27] first a thin, conformal adhesion layer of PDA was deposited on all the interior of the porous structure, then copper was deposited on this layer. PDA has many advantages[39,40] for example, it

is a naturally-derived and safe material, it only requires water as its polymerization solvent, it polymerizes on virtually any solid, and it is hydrophilic which allows penetration of microbial droplets (if the pore space is not covered by the antimicrobial). Being a thin layer, we expect PDA to cause minimal blockage of pores. Metals and metal oxides are commonly used in antimicrobial coatings,[41-45] and here we use copper,[46] which was deposited on the PDA by electroless deposition, and created an even and conformal layer of copper. Prior work shows an outer oxidation layer on the surface of the copper, consistent with some Cu^{+}.[27]

The porous coatings had excellent antimicrobial properties: within 3 minutes, they reduced the number of colony forming units (CFUs) of bacteria by 99.83% on porous antimicrobial stainless steel, which is superior to the 77.82% achieved on the non-porous antimicrobial steel and very close to our target kill rate.

4.3. Results and Discussion

4.3.1. The pore structure is retained after addition of the PDA/Cu layer

The original stainless steel (SS) scaffold porosity is heterogeneous but even the small pores have dimensions >10 μm, which is enough for passage of almost all typical microbes (Figure 4-1A, further images in Figure S4-2 in Supporting Information). The porous antimicrobial SS was prepared by first depositing a layer of polydopamine via solution and then copper via electroless deposition onto an SS scaffold. The presence of the copper layer on the interior porosity was confirmed by EDS, as shown in Table S4-1. The amount of copper on porous SS is smaller than on the flat sample as measured by EDS (see Table S4-1), but the surface

composition as measured by XPS is similar (see Table S4-2). The antimicrobial layer is mainly conformal as demonstrated in Figure 4-1 and Figure S4-3. The porosity is thus retained after the antimicrobial coating is added. Some additional roughness can be seen on the coated structure, but the SEM images show that the effect is minor, and therefore is not enough to impede passage of bacteria. Antimicrobial coatings were also prepared on flat SS surfaces to act as non-porous controls. SEM images for these flat surfaces are shown in Figure S4-4. The small additional roughness from the antimicrobial coating is also evident on the flat control surface.

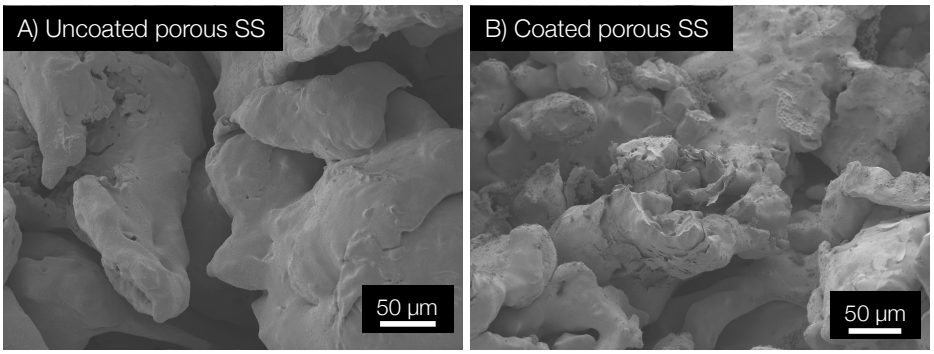


Figure 4-1. Cross-section SEM images of the porous stainless steel A) without and B) with the PDA/Cu coating.

4.3.2. The porous PDA/Cu coating allows for very rapid imbibition and drying of droplets

The porous PDA/Cu coating is hydrophilic; on the flat PDA/Cu surface the advancing angle is 71 ± 7º (standard deviation) and the receding angle is 9 ± 4º, which is suitable for imbibition of aqueous solutions. When a droplet (10 µL) is placed on the porous material, imbibition occurs within <0.5 sec, a much smaller time than our target time for killing, so imbibition will not be the limiting process (Figure 4-2).

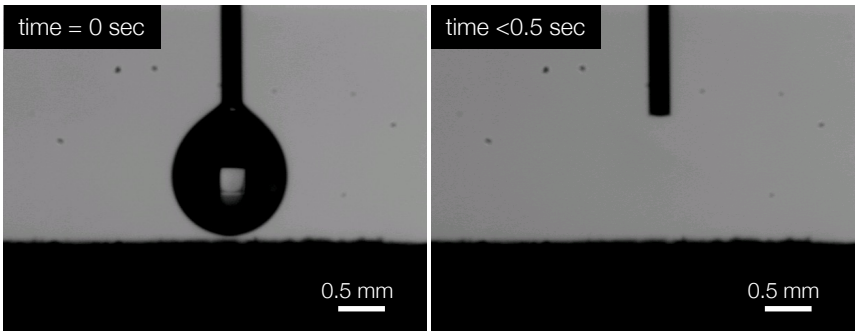


Figure 4-2. Photographs showing the time for a 10 µL water droplet to imbibe into the PDA/Cu-coated porous stainless steel structure.

We also measured the drying of droplets of the porous coating. A 5 µL droplet typically dried in about 11 minutes on the porous SS surface, which is much faster than the 45 min for drying on the flat coating under the same conditions. Faster drying on thin porous coatings has been noted previously,[47] and this is a significant advantage of a porous coating. A layer of water on the solid provides an additional diffusion distance for suspended bacteria in an incoming contaminated droplet, so it is better if the solid naturally evaporates water more quickly. The "reload time" on the porous surface is thus shorter than for an impermeable solid.

4.3.3. Porous PDA/Cu stainless steel is highly antimicrobial

We measured the colony-forming units (CFU) of *P. aeruginosa* that were extracted from the porous PDA/Cu stainless steel as a function of time since the bacterial suspension droplet was placed on the solid, and results are shown in Figure 4-3. Over the very short time period of 3–5 minutes, the CFU level dropped by about 3 orders of magnitude, and therefore the porous PDA/Cu is a very effective antimicrobial material

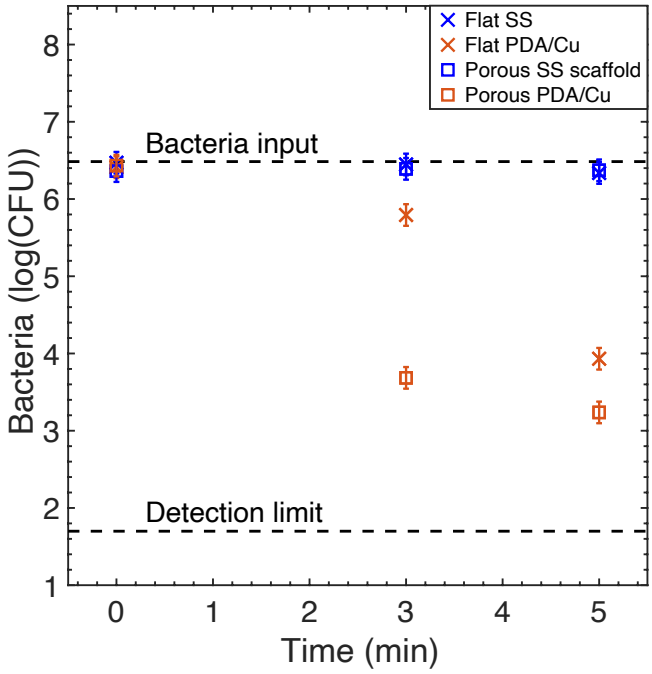


Figure 4-3. Time course of *P. aeruginosa* on flat PDA/Cu and porous PDA/Cu coatings. Compared to the control SS, the porous PDA/Cu coating causes a reduction of 99.83% of P. aeruginosa within only 3 minutes, while the same coating in a flat configuration causes a 77.82% reduction (see Equation 4-3 in the Experimental Section for the equation for reduction). The bacteria input on the coatings and the detection limit for the bacterium is shown with dotted lines. Each symbol represents the average of two independent samples. A 3-way ANOVA gave the following p values: porosity (porous vs flat), $p = 0.008$; surface type (uncoated vs coated sample), $p < 10^{-6}$; and time, $p < 10^{-4}$. The 2-way interactions are as follows: $p_{\text{surface type and time}} < 10^{-4}$, $p_{\text{surface type and porosity}} = 0.0135$, $p_{\text{time and porosity}} = 0.0436$. The 3-way interaction p-value between all three factors is 0.038, which indicates that over time, the porosity makes a difference if the antimicrobial coating is present.

The effectiveness of the surface treatment is usually considered by comparison of the surface treatment to some standard. Two different standards are frequently considered: (1) the input level of bacteria or (2) a control surface at the same time. Comparison to the input level gives us the metric of "Killing" defined in Equation 4-4 of the Experimental Section.

Comparison to a control surface is important because bacteria may slowly die on their own without an antimicrobial, and we use the term "Reduction" as defined in Equation 4-6 in the Experimental section.

The porous PDA/Cu kills 99.84% of *P. aeruginosa* within 3 minutes. The effective half-life is 27 s (95% confidence:17–73 s), calculated by assuming exponential decay for the first 5 minutes. We now compare this result to various controls. The flat PDA/Cu surface kills 79.65% of *P. aeruginosa* within 3 minutes, so the number of surviving bacteria at this time point was reduced by a factor of 127 by introducing the porosity. Our statistical evidence is a 3-way ANOVA (factors time, porosity and antimicrobial) where we assess whether the addition of porosity gives an increased kill over time with a 3-factor interaction term. The 3-factor interaction has $p = 0.038$, so we consider this interaction significant, and this is consistent with the hypothesis that a porous antimicrobial coating kills faster than a flat surface. We attribute the additional killing to the increased interfacial area of the antimicrobial component (i.e., copper) and the shorter diffusion transport distance.

Antimicrobial coatings are usually assessed by the % reduction compared to a control (uncoated surface) as shown in Equation 4-6, and such a comparison is required by the EPA.[35-36] In this case, we use the flat SS as the comparison, and Figure 4-3 indicates that flat SS kills few bacteria. The porous PDA/Cu coating causes a reduction of 99.83% of *P. aeruginosa* within only 3 minutes, while the same coating in a flat configuration causes a 77.82% reduction. The 95% confidence interval for the log reduction compared to the flat SS is 2.76 in three minutes. To be registered by the EPA, a coating needs a 3-log reduction in 1 hour, whereas the porous material achieves a similar level in only a few minutes.

From Figure 4-3, it is clear the number of viable bacteria that survive exposure to the porous material depends strongly on the presence of the antimicrobial. For example, after 5 minutes only 0.05% of the original inoculum is viable on the porous coating containing the antimicrobial whereas 80.5% was viable on the porous material without the antimicrobial. Comparing these two results we know that the low CFUs observed for the porous antimicrobial coatings are not simply due to trapping of the bacteria on the solid.

4.3.4. Our assay is effective at extracting bacteria from the porous coating

A question naturally arises as to whether bacteria can be extracted from the porosity. If bacteria were to be trapped, then they would not show up in our colony forming unit (CFU) assay and there may be ambiguity as to whether our porous antimicrobial layer traps or kills bacteria. We do note that if bacteria were trapped, then such trapped bacteria would not be available for transfer to humans and being trapped on an antimicrobial surface is not an ideal location for a bacterium to replicate.

We have deliberately selected large pores to limit trapping of microbes, but we investigated the extent of trapping. It is difficult to test trapping separately from killing on antimicrobial surface, so we tested trapping on the same microstructure but with two different chemistries, stainless steel and PDA, both of which have no antimicrobial coating. Clearly both the chemistry and time in contact could in principle affect the extraction. A suspension of bacteria was placed on the porous coating and then the bacteria were extracted by the same procedures later used for killing (sonication and vortexing). Five minutes inside the coating was used as the test period because this was our approximate target time for killing by the active

material. Figure 4-4 compares the measured CFU after extraction to the CFU obtained from the test droplet: almost all bacteria inside the pores of the porous scaffolds were successfully extracted. Comparing the PDA and SS chemistries there is no effect of the surface chemistry on trapping (p = 0.192). The lack of killing also shows that the bare PDA or SS are not good antimicrobial surfaces. The ability to extract bacteria from planar surfaces was also high (**Figure S*4-5***). We also tested the trapping effect on a variety of drop sizes. Bacteria were successfully extracted from the porous scaffold when 10, 30, and 50 µL volumes of suspension were used (see Figure S4-6 in Supporting Information).

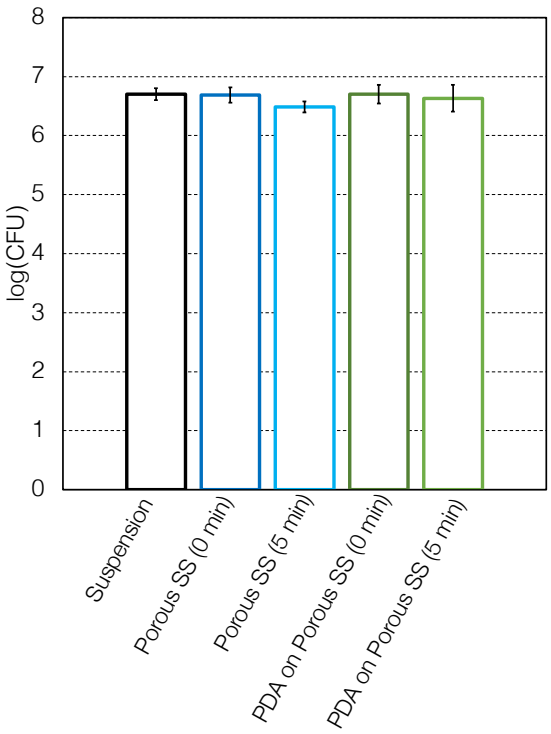


Figure 4-4. CFUs of *P. aeruginosa* extracted from solids compared to the CFUs input on the solid. A very high percentage of bacteria is extracted from the porous coating. The detection limit is 50 CFU. There is a small, but not significant (p = 0.071) decrease in the CFU for porous stainless steel compared to the input, but this also occurs for flat stainless steel (see Figure 4-3 and Figure S4-5). After the porous structure was coated with PDA, the bacteria were still extracted (p = 0.44 comparing input and extracted).

4.3.5. Porous antimicrobial polymer coating

Polymer coatings can easily be added to surfaces, the most obvious example of which is latex paint, in which polymer particles are applied to a solid and then chain migration ripens the particles into a continuous film. Here we make a 110 μm thick porous antimicrobial coating by a similar method, except that we choose a polymer with a glass transition temperature, T_g, above room temperature. With this feature we can control a period of elevated temperature such that ripening is halted when the polymer film is continuous, but the porosity is still present. We chose PMMA particles because PMMA has a relatively low T_g,[48] and heated the particles at 125 ˚C for 2 h. We chose 1–40 μm particle size range so that large pores could form for passage of bacteria and rapid imbibition. PMMA also has high compressive and tensile strengths,[49] making it an attractive material for a coating. Figure 4-5 and **Figure S*4-7*** (in Supporting Information) show SEM images of the fabricated porous PMMA scaffold. High magnification images (Figure 4-5B) show the formation of necks after heat treatment, which indicate that polymer migration has occurred to form connections between the particles, and therefore a continuous coating, but the porosity has not been lost.

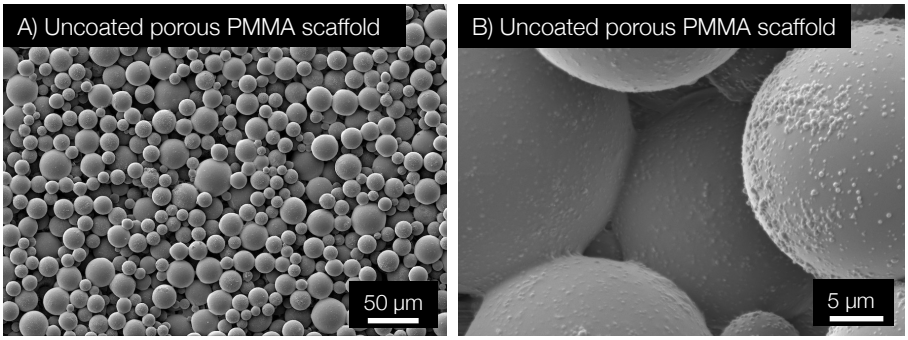


Figure 4-5. SEM images of porous PMMA scaffold fabricated by partial sintering of PMMA particles through 2 h of heat treatment at 125ºC (above T_g). (A) Image showing the retained porosity and (B) Image showing the formation of polymer "necks" or frozen mensci. Further images are in Figure S4-7.

Water does not penetrate uncoated porous PMMA – the advancing and receding angles of flat 111 ± 4° (std dev), and 16 ± 2° respectively. After deposition of a PDA layer, the coating becomes hydrophilic and imbibes (infiltrates) water droplets in seconds. CFU measurements (Figure S4-8 in Supporting Information) shows neither the flat nor porous PMMA scaffolds are good antimicrobial coatings.

The antimicrobial PDA/Cu layer was prepared within the pores of the porous PMMA. SEM images confirmed that porosity was retained (see Figure 4-6); EDS confirmed the presence of the copper in the coating (see Table S4-3); and imbibition was achieved in <0.5 sec (see Figure S4-9 in Supporting Information), which together make this coating suitable for examining killing in a porous antimicrobial coating. A control experiment showed that PDA is not the active ingredient (Figure S4-10). Additionally, a 5 μL water droplet dries in about 5 min. on PDA/Cu coated porous PMMA, whereas the same volume takes about 45 min. to dry on a flat surface.

Figure 4-7 shows the time course of *P. aeruginosa* CFU on the porous PDA/Cu, which was made using the porous PMMA scaffold. The coating is highly antimicrobial; it kills 99.27% and >99.99% of *P. aeruginosa* in 3 and 5 min, respectively. To compare the coating to the uncoated control, the coating causes a reduction of 99.02% and >99.99% of the bacterium in 3 and 5 minutes ($p < 0.01$), respectively. The log reduction in five minutes is 4.5 ± 0.6 (95% confidence interval). The effective half-life is 21 sec (95% confidence: 18 to 26 s); calculated over 5 minutes). Our hypothesis was that adding porosity would improve killing speed, and when we compare the porous coating to the flat coating, we see the killing is increased from 79.65% to 99.02% in 3 min and from 99.71% to >99.99% in 5 minutes, which is consistent with the hypothesis (p <0.001 for coating-time interaction in a 2-way ANOVA), Again, we attribute the fast killing to the short diffusion distances, and the high surface area of the antimicrobial layer.

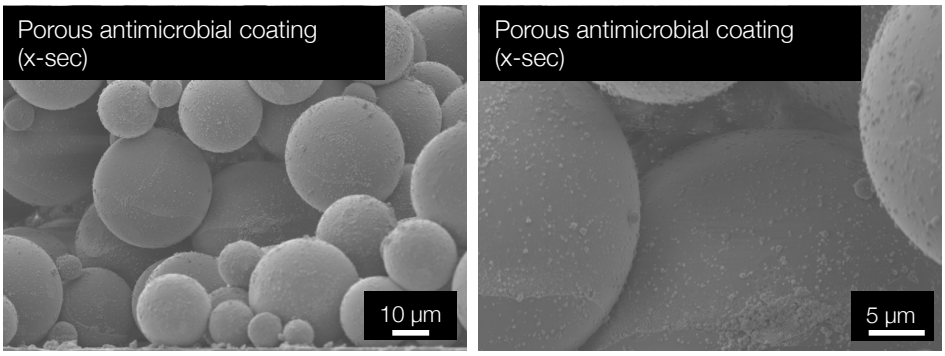


Figure 4-6. SEM images of porous antimicrobial coating (scaffold = PMMA). The antimicrobial layer (PDA/Cu) was successfully prepared inside the pores of the porous PMMA scaffold.

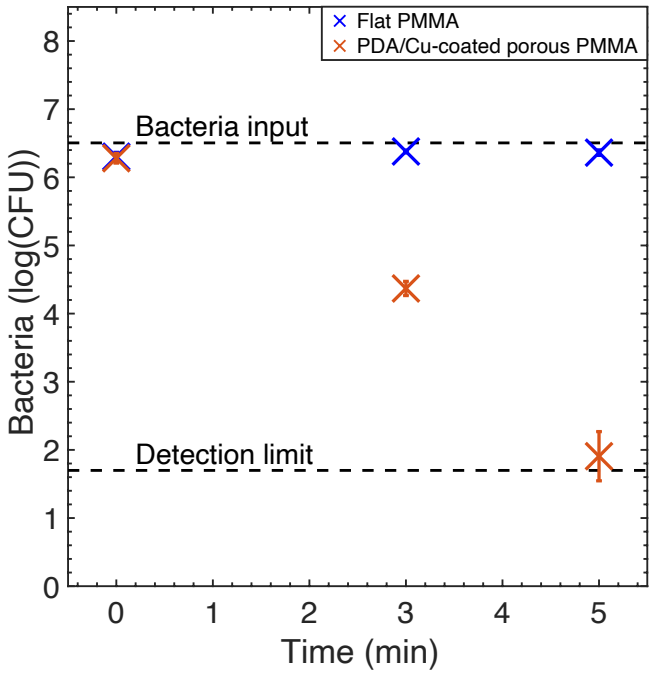


Figure 4-7. Time course of bacteria on uncoated flat PMMA (control) and PDA/Cu-coated porous PMMA. Porous PDA/Cu coating is highly effective. The porous PDA/Cu causes a reduction of >99.99% of *P. aeruginosa* in 5 minutes compared to the uncoated sample ($p = 0.009$). Each symbol represents the average of two separate samples, and the error bars are standard deviation. The bacteria input on the coatings and the detection limit for the bacterium is shown with dotted lines. To determine the effect of porosity, we compared the PDA/Cu-coated porous material to the flat PDA/Cu material on

SS, assuming that the underlying support was not important. For a 2-way ANOVA with factors of sample (p <0.001), time (p <0.001), and the sample-time (p <0.001), were significant, providing additional support for the hypothesis that porosity speeds the killing of *P. aeruginosa*.

4.3.6. Abrasion Resistance

In principle, a huge advantage of a porous antimicrobial coating should be improved resistance to abrasion. This abrasion resistance can arise from two avenues. First, one can choose the scaffold independently from the antimicrobial, so that an abrasion-resistant scaffold can protect the antimicrobial material. Second, abrasion affects only the outer layer, so even when the outer layer is abraded, the inner layer is retained. To test this idea, we abraded the SS antimicrobial coating with a sponge using a modified EPA test[35] and the results are shown in Figure 4-8. After abrasion, the antimicrobial properties were retained and 99.9% of the bacteria were killed. This is not surprising as one would not expect a sponge to abrade the inner layer.

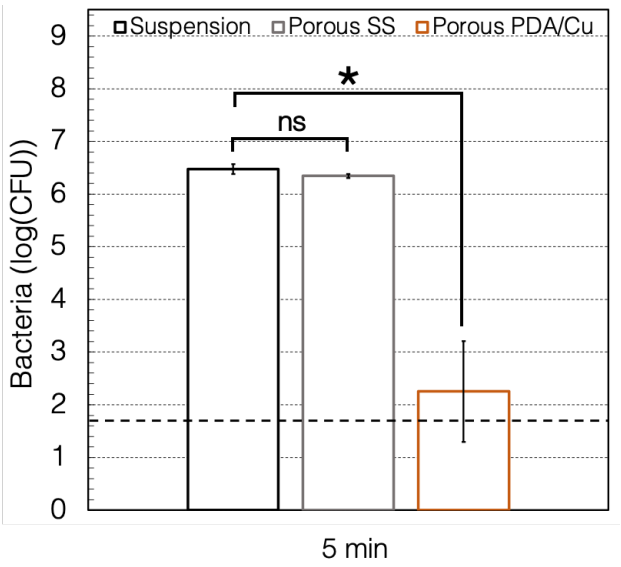


Figure 4-8. Bacteria tests with abraded porous PDA/Cu coating. The abraded coatings kill 99.9% of bacteria within 5 minutes. The detection limit (i.e., all bacteria were dead) is 50 CFU. (* represents $p < 0.05$; ns represents $p > 0.05$)

4.3.7. Other Characteristics of the PMMA Coating

We have used convenient conditions and low toxicity materials. Creation of the PMMA scaffold occurs at low temperature and a short duration (125 ˚C for 2 h). In principle, a lower T_g material could be used, providing it was above room temperature. Dopamine polymerization is completed in water, and therefore no harmful organic solvents are required. Throughout the process, there is no specialized equipment. In addition, PDA has a high Median Lethal Dose (LD_{50}).[50] Copper and PMMA are inexpensive materials and only a very thin layer of PDA is used. One can imagine other antimicrobial materials being added to a scaffold, such as Cu_2O or Ag_2O particles, providing that the particles do not completely block the porosity. Thus, the porous scaffold plus active agent is modular where each one can be optimized separately.

4.4. Conclusion

For maximum effectiveness, an antimicrobial coating should kill microbes between users. Common use objects, such as doorknobs, are sometimes touched by different individuals within a period of minutes or even less, so the kill needs to be swift. We hypothesized that the rate of kill of an antimicrobial coating was transport limited due to millimeter transport distances within droplets, and that a faster kill could be obtained with shorter transport distances. To achieve shorter transport distances, we devised the idea of porous hydrophilic antimicrobial coatings, where a droplet contaminated with microbes that lands on the solid would quickly penetrate into the porosity and then the transport distance would be the pore size. We fabricated two examples of porous antimicrobial surfaces using PDA/Cu as the active material and found very rapid killing. For a porous SS scaffold, 99.84% of *P. aeruginosa* were killed in 3 minutes. The effective half-life of *P aeruginosa* in the liquid within the porosity was 27 sec. For porous PMMA, >99.99 of *P. aeruginosa* was killed within 5 min and the effective half-life of the bacterium was 21 sec. We demonstrated that the antimicrobial material was more effective on a porous scaffold than on a flat impermeable solid ($p = 0.038$ for the 3-way interaction on stainless steel and $p < 0.001$ for the 2-way interaction on PMMA), consistent with our hypothesis of transport limited inactivation on the flat antimicrobial surface. The larger surface area of active material per volume of liquid within the porous material may have also contributed to the kill, and this is an additional advantage of the porous geometry.

A further advantage is the that the inner active layers can be protected from abrasion by the outer layers. We tested the latter idea by doing a standard abrasion test on the porous coating, and found that the coating was still active after abrasion. The use of a modular scaffold plus

active ingredient system allows an independent choice of the porous scaffold from the antimicrobial material. We demonstrated this with the use of two scaffolds: stainless steel and PMMA. Both scaffolds had similar, excellent, antimicrobial activity when used with the same antimicrobial coating layer.

A critical aspect of the porous layer is that the microbial droplet should absorb into the solid quickly. This is simple to achieve providing that the porosity is large (> few micrometers) and the pore space is hydrophilic. It is not necessary for the structural component of the scaffold to be hydrophilic providing that the antimicrobial coating is sufficiently hydrophilic. This was demonstrated with PDA/Cu-coated porous PMMA.

Specific advantages of our choice of materials are that we used common, inexpensive, and relatively non-toxic materials (Cu, PDA, PMMA, stainless steel) and the procedures were simple and required no specialized equipment.

4.5. Experimental Section

4.5.1. Materials

70% ethanol and sodium hydroxide beads (ACS grade) were purchased from VWR. Dopamine hydrochloride (99%) and dimethylamineborane (DMAB, 98%) were obtained from Fischer Scientific. Flat stainless steel (SS), porous SS (Catalog No. = 9446T32, diameter = 12.7 mm, thickness = 1.6 mm), and flat acrylic (PMMA; Catalog No. = 4615T61) were obtained from McMaster-Carr. The following were purchased from Sigma Aldrich: copper(II) chloride (97%), boric acid (ACS grade), tris(hydroxymethyl)aminomethane (Tris, ACS reagent), ethylenediaminetetraacetic acid (EDTA, >99%), and sodium dodecyl sulfate (SDS, >99%). PMMA particles (PMMA Microspheres, 1-40 µm) were purchased from Cosphere. Water was purified by a Milli-Q Reference water purification system. Flat SS or porous stainless steel were cleaned using soapy water, DI water, (70%) ethanol, and final rinsing with DI water. After preparation of antimicrobial coating, the coated porous SS was fixed on a flat SS using double sided tape. Bacterial cell suspensions were diluted in either phosphate-buffered saline (PBS) or DE Broth (BD, Sparks, MD). Tryptic Soy Agar (TSA) and Tryptic soy broth (TSB) were obtained from BD (Sparks, MD).

4.5.2. Fabrication of porous PMMA scaffold test samples

80 µL of PMMA particle suspension (15% w/w in water with 8 mM SDS) was drop cast on flat acrylic (size = 12x12 mm). The samples were left at room temperature to dry. Then, the samples were placed in furnace at room temperature, and the temperature was increased to 125

˚C at a rate of 2 ˚C/min. After 2 h at 125 ˚C, the furnace was turned off and the samples were cooled to room temperature. The samples were washed three times with DI water (6 min each) to remove residual SDS. The thickness of the porous PMMA scaffold was about 110 µm.

4.5.3. Deposition of antimicrobial PDA/Cu surface coating

The PDA and Cu deposition both use dissolved molecular reagents so are not affected by the rection being in confinement in >µm-sized pores. However, it is necessary for the water solvent to penetrate the porosity, and this requires that the interior surfaces are hydrophilic. Steel is sufficiently hydrophilic to allow imbibition, but PMMA is hydrophobic, so the interior pores of the PMMA samples were rendered hydrophilic by plasma treatment with oxygen for 3 minutes at 100 W. Preparation of antimicrobial coating had two steps:[27] deposition of the adhesive layer (polydopamine; PDA), followed by deposition of copper via electroless deposition. PDA[39, 51] was deposited as follows: on a stirring hot plate, tris buffer (10 mM) was heated to 60ºC, after which dopamine hydrochloride was added (final conc = 5 g/L). The samples were then submerged in this aqueous liquid for 4 hours while stirring. After deposition, the container was subsequently removed from the hot plate and allowed to cool to room temperature. The samples were washed with DI water and dried with N_2 gas.

For electroless deposition of copper on the PDA,[27, 39, 52-55] an aqueous solution of EDTA (50 mM), $CuCl_2$ (50 mM), and boric acid (100 mM) (pH = 7 using NaOH) was stirred at 38 ºC while DMAB was added (final conc. = 100 mM). The PDA-coated samples were submerged in this solution and kept for 160 min after the solution color changed to dark green. The porous solids were hydrophilic, so the coating solution is rapidly imbibed into the porosity and the

copper deposition can occur on the interior and exterior of the surfaces. The samples were removed and then washed with DI water and dried with N_2 gas.

4.5.4. Characterization

Characterization of the morphology of the coatings was achieved by SEM images using a JEOL IT500 SEM. Samples for SEM imaging (only) were treated with a 5 nm layer of Pt/Pd. Advancing and receding water contact angles were measured with a First Ten Angstroms FTA125. Void volume % of the porous SS and porous PMMA scaffolds are 33 ± 3% (standard deviation) and 53 ± 1% respectively.

4.5.5. Antibacterial Assay

4.5.5.1. Choice of Microbial Strain.

Following the guidance of the US EPA[35-36] *Pseudomonas aeruginosa* strain DSM-9644 was chosen for the experiments.

4.5.5.2. Growth of Microbial Strains.

Pseudomonas aeruginosa strain (DSM-9644) was grown in TSB (5 mL) to mid-exponential phase at 37° C with aeration (at 60 rpm). The purity and identity of the cells were verified by streaking bacterial from these liquid cultures on TSA plates, incubating at 37° C for 48 hr, and then examining these colonies for species-specific traits (such as surface texture and pigmentation).

4.5.5.3. Preparation of Microbial Strains for Testing.

Bacterial cells from the cultures were collected by centrifugation for 20 min at 5,000 g. The supernatant was then discarded, and the bacterial cells were re-suspended in sterile PBS (5 mL) using vortexing for 60 sec. The said suspensions were centrifuged for 20 min at 5,000 g, the supernatant was discarded, and the washed cells re-suspended in sterile PBS (5 mL) using vortexing for 60 sec.

4.5.5.4. Measurement of Viable Cell Number.

The viable number of cells in the PBS-suspensions of the bacterium was measured as colony-forming units per mL (CFU)/mL) of suspension as follows: A 10-fold dilution series was prepared for each suspension in either PBS or DE Broth, 0.1 mL of each dilution was spread on TSA plates (in triplicate), and colonies were counted after 48 hr of incubation at 37° C for the dilution that produced a convenient number to resolve (typically 20–200 colonies). If no colonies were present for the lowest dilution, then to enable a $\log_{10}$ transformation of all data, we designated the zero as one. This is our detection limit for measurement on a particular plate.

4.5.5.5. Measurement of Surface-Killing.

For each named bacterial strain, a droplet of bacterial cells in PBS was placed on individual coated or uncoated sample. The droplet size was 10 µL for flat or porous SS samples, and 5 µL for flat or porous PMMA samples. Immediately, after specific timepoints, each sample was placed in a separate sterile 50 mL centrifuge tube containing 5 mL of DE broth (or PBS where noted), vortexed for 10 sec at the highest setting, and sonicated for 1 min (Branson Model 12 Ultrasonic Cleaner, Shelton, CT) to detach cells from the solid. DE was chosen because it is known to

neutralize metals[56]. The CFU/mL of the resulting bacterial suspension was measured by removing a 0.1 mL sample of the suspension without coming in contact with the coated or uncoated sample, preparing a dilution series, plating on TSA plates, and incubating at 37°C for 48 hr at 37 C. This process was repeated at each specific time point, and independent samples were used for each condition, i.e., each coated or uncoated sample at each time point. Note that the test droplet contacts only one side of the samples. The detection limit and resolution of plate counting is 1 colony, but because the original bacterial sample droplet of 10 µL or 5 µL was diluted to 5 mL in the centrifuge tube and from this only 0.1 mL was sampled, the detection limit of bacteria from the original test droplet was 50 CFU.

4.5.6. Abrasion tests

The porous coatings were abraded by an abrasion tester (model: Gardco D10V) using a mounted sponge. This was based on the EPA protocol[35] which is utilized to evaluate antimicrobial coatings for EPA approval. This protocol has abrasion with a sponge wetted with an antimicrobial agent (70% ethanol). The tester machine moves back and forth a sponge that is in contact with the samples with an amplitude of ~26 cm and a period of approximately 5 sec. The sponge was loaded with load of 0.45 kg during the tests, and it was wetted with 20 mL of 70% ethanol before the abrasion cycles. An abrasion cycle was done as following: the sponge was moved across the sample 8 times, subsequently 70% ethanol was sprayed on the abrasion platform and the samples with a subsequent waiting period (30 minutes). A total of 10 cycles (equal to 80 passes) were performed on the samples. A single sponge was used for the first 5 abrasion cycles, and it was replaced with a separate sponge for the second 5 abrasion cycles.

4.5.7. Statistical Analysis

We carried out bacterial assays in a randomized manner (with randomized factors), and our statistical power was at least 80% for each factor at the significance level of 0.05. All statistics were calculated from log CFU, and Student's t-tests were two-tailed and heteroscedastic. Error bars are standard deviation unless otherwise noted.

4.5.8. Calculation of Microbial Reduction

The word "killing" in results is used for simplicity; we recognize that the CFU counting assay actually measures those cells that can reproduce to form a colony but we refer to any cell that does not produce a colony as having been killed. Killing is defined as:

$$\log \text{survival} = \text{mean}\left[\log_{10}\left(\frac{\text{sample titer}}{\text{units}}\right)\right] - \text{mean}\left[\log_{10}\left(\frac{\text{input titer}}{\text{units}}\right)\right] \qquad \text{Equation 4-2}$$

$$\%\ \text{survival} = \left[1 - 10^{-\log \text{survival}}\right] \times 100 \qquad \text{Equation 4-3}$$

$$\%\ \text{killing} = 1 - \%\ \text{survival} \qquad \text{Equation 4-4}$$

The term "Reduction" compares CFU measurement for two surfaces, an uncoated and a coated surface, at the same time.

$$\log \text{Reduction} = \text{mean}\left[\log_{\mathbf{10}}\left(\frac{\text{uncoated surface titer}}{\text{units}}\right)\right] - \text{mean}\left[\log_{\mathbf{10}}\left(\frac{\text{sample titer}}{\text{units}}\right)\right] \quad \text{Equation 4-5}$$

$$\% \text{ Reduction} = \left[1 - 10^{-\log \text{Reduction}}\right] \times 100 \quad \text{Equation 4-6}$$

Half-life was calculated from a linear fit of the slope of all log (CFU)–time data for a particular condition. The half-life is:

$$t_{1/2} = -\frac{0.30}{\text{slope}} \quad \text{Equation 4-7}$$

Supporting Information

Supporting Information includes additional methods, characterizations, and results, as follows:

Schematic of abrasion tests on the coatings.

SEM images of porous SS scaffold.

Elemental characterization (EDS) of x-section of porous PDA/Cu.

Plan-view and cross-section SEM images of coated porous SS.

Plan-view SEM images of PDA/Cu-coated flat SS surfaces.

Bacterial CFUs extracted from flat and porous scaffolds.

Extraction of P. aeruginosa from porous SS as a function of droplet volume.

SEM images of porous PMMA scaffold.

Time course of bacteria CFU on flat and porous PMMA scaffolds

Photographs showing the time for a water droplet to imbibe into the PDA/Cu-coated porous PMMA.

Time course of P. aeruginosa CFU on PDA-coated porous PMMA.

Acknowledgments

This work was supported by the National Science Foundation (NSF) under Grant No. CBET-1902364, by Virginia Tech's Proof of Concept program under Grant No. 238079, and by Virginia Tech GRDP program under grant number 118965. This work used shared facilities at the Virginia Tech National Center for Earth and Environmental Nanotechnology Infrastructure, which is supported by NSF (ECCS 1542100 and ECCS 2025151). We thank Dr. Kristin Knight, who captured the XPS spectra, and the Surface Analysis Laboratory in the Department of Chemistry at VT, which is supported by the NSF under Grant No. CHE-1531834. We also thank Christopher Stoll who helped with preparing some of the porous PMMA scaffolds.

Conflict of Interest

WAD declares part ownership in a startup company that intends to produce surface coatings. Other authors declare no conflict of interest.

REFERENCES

(1) Piret, J.; Boivin, G. Pandemics Throughout History. *Front. Microbiol.* **2021,** *11*, 631736.

(2) Cutler, D. M.; Summers, L. H. The Covid-19 Pandemic and the $16 Trillion Virus. *JAMA* **2020,** *324* (15), 1495-1496.

(3) Fonkwo, P. N. Pricing Infectious Disease: The Economic and Health Implications of Infectious Diseases. *EMBO reports* **2008,** *9* (S1), S13-S17.

(4) Hoffmann, S.; Ahn, J.-W. Economic Cost of Major Foodborne Illnesses Increased $2 Billion from 2013 to 2018. https://www.ers.usda.gov/amber-waves/2021/april/economic-cost-of-major-foodborne-illnesses-increased-2-billion-from-2013-to-2018/ (accessed 02/20/2023).

(5) Benedict, K.; Whitham, H. K.; Jackson, B. R. Economic Burden of Fungal Diseases in the United States. *Open Forum Infectious Diseases* **2022,** *9* (4), ofac097.

(6) Stephens, B.; Azimi, P.; Thoemmes, M. S.; Heidarinejad, M.; Allen, J. G.; Gilbert, J. A. Microbial Exchange Via Fomites and Implications for Human Health. *Curr. Pollut. Rep.* **2019,** *5* (4), 198-213.

(7) Behzadinasab, S.; Chin, A. W. H.; Hosseini, M.; Poon, L. L. M.; Ducker, W. A. Sars-Cov-2 Virus Transfers to Skin through Contact with Contaminated Solids. *Sci. Rep.* **2021,** *11* (1), 22868.

(8) Jit, M.; Ng, D. H. L.; Luangasanatip, N.; Sandmann, F.; Atkins, K. E.; Robotham, J. V.; Pouwels, K. B. Quantifying the Economic Cost of Antibiotic Resistance and the Impact of

Related Interventions: Rapid Methodological Review, Conceptual Framework and Recommendations for Future Studies. *BMC Med.* **2020,** *18* (1), 1-14.

(9) ECDPC 33000 People Die Every Year Due to Infections with Antibiotic-Resistant Bacteria. https://www.ecdc.europa.eu/en/news-events/33000-people-die-every-year-due-infections-antibiotic-resistant-bacteria (accessed Sep 20, 2022).

(10) Murray, C. J.; Ikuta, K. S.; Sharara, F.; Swetschinski, L.; Aguilar, G. R.; Gray, A.; Han, C.; Bisignano, C.; Rao, P.; Wool, E. Global Burden of Bacterial Antimicrobial Resistance in 2019: A Systematic Analysis. *The Lancet* **2022,** *399* (10325), 629-655.

(11) Mahoney, A. R.; Safaee, M. M.; Wuest, W. M.; Furst, A. L. The Silent Pandemic: Emergent Antibiotic Resistances Following the Global Response to Sars-Cov-2. *Iscience* **2021,** *24* (4), 102304.

(12) Centers for Disease Control and Prevention Covid-19: U.S. Impact on Antimicrobial Resistance, Special Report 2022. https://www.cdc.gov/drugresistance/pdf/covid19-impact-report-508.pdf (accessed Sep 29, 2022).

(13) Centers for Disease Control and Prevention Covid-19 & Antibiotic Resistance. https://www.cdc.gov/drugresistance/covid19.html (accessed Sep 28, 2022).

(14) Centers for Disease Control and Prevention Hai and Antibiotic Use Prevalence Survey. https://www.cdc.gov/hai/eip/antibiotic-use.html (accessed Sep 28, 2022).

(15) Centers for Disease Control and Prevention Multidrug-Resistant Pseudomonas Aeruginosa https://www.cdc.gov/drugresistance/pdf/threats-report/pseudomonas-aeruginosa-508.pdf (accessed Sep 20, 2022).

(16) Restrepo, M. I.; Babu, B. L.; Reyes, L. F.; Chalmers, J. D.; Soni, N. J.; Sibila, O.; Faverio, P.; Cilloniz, C.; Rodriguez-Cintron, W.; Aliberti, S. Burden and Risk Factors for Pseudomonas Aeruginosa Community-Acquired Pneumonia: A Multinational Point Prevalence Study of Hospitalised Patients. *Eur. Respir. J.* **2018,** *52* (2), 1701190,

(17) Chatzinikolaou, I.; Abi-Said, D.; Bodey, G. P.; Rolston, K. V.; Tarrand, J. J.; Samonis, G. Recent Experience with Pseudomonas Aeruginosa Bacteremia in Patients with Cancer: Retrospective Analysis of 245 Episodes. *Arch. Intern. Med.* **2000,** *160* (4), 501-509.

(18) Pang, Z.; Raudonis, R.; Glick, B. R.; Lin, T.-J.; Cheng, Z. Antibiotic Resistance in Pseudomonas Aeruginosa: Mechanisms and Alternative Therapeutic Strategies. *Biotechnol. Adv.* **2019,** *37* (1), 177-192.

(19) Kramer, A.; Schwebke, I.; Kampf, G. How Long Do Nosocomial Pathogens Persist on Inanimate Surfaces? A Systematic Review. *BMC Infect. Dis.* **2006,** *6* (1), 1-8.

(20) Vos, M. C.; Verbrugh, H. A. Mrsa: We Can Overcome, but Who Will Lead the Battle? *Infect. Control Hosp. Epidemiol.* **2005,** *26* (2), 117-120.

(21) de Abreu, P. M.; Farias, P. G.; Paiva, G. S.; Almeida, A. M.; Morais, P. V. Persistence of Microbial Communities Including Pseudomonas Aeruginosa in a Hospital Environment: A Potential Health Hazard. *BMC Microbiol.* **2014,** *14* (1), 1-10.

(22) Rutala, W. A.; Weber, D. J. Uses of Inorganic Hypochlorite (Bleach) in Health-Care Facilities. *Clin. Microbiol. Rev.* **1997,** *10* (4), 597-610.

(23) Ellingson, K. D.; Pogreba-Brown, K.; Gerba, C. P.; Elliott, S. P. Impact of a Novel Antimicrobial Surface Coating on Health Care–Associated Infections and Environmental Bioburden at 2 Urban Hospitals. *Clin. Infect. Dis.* **2020,** *71* (8), 1807-1813.

(24) Cloutier, M.; Mantovani, D.; Rosei, F. Antibacterial Coatings: Challenges, Perspectives, and Opportunities. *Trends Biotechnol.* **2015,** *33* (11), 637-652.

(25) Salwiczek, M.; Qu, Y.; Gardiner, J.; Strugnell, R. A.; Lithgow, T.; McLean, K. M.; Thissen, H. Emerging Rules for Effective Antimicrobial Coatings. *Trends Biotechnol.* **2014,** *32* (2), 82-90.

(26) Behzadinasab, S.; Hosseini, M.; Williams, M.; Ivester, H.; Allen, I.; Falkinham III, J.; Ducker, W. Antimicrobial Activity of Cuprous Oxide-Coated and Cupric Oxide-Coated Surfaces. *J. Hosp. Infect.* **2022,** *129*, 58-64.

(27) Behzadinasab, S.; Williams, M. D.; Hosseini, M.; Poon, L. L.; Chin, A. W.; Falkinham III, J. O.; Ducker, W. A. Transparent and Sprayable Surface Coatings That Kill Drug-Resistant Bacteria within Minutes and Inactivate Sars-Cov-2 Virus. *ACS Appl. Mater. Interfaces* **2021,** *13* (46), 54706-54714.

(28) Behzadinasab, S.; Chin, A.; Hosseini, M.; Poon, L.; Ducker, W. A. A Surface Coating That Rapidly Inactivates Sars-Cov-2. *ACS Appl. Mater. Interfaces* **2020,** *12* (31), 34723-34727.

(29) Hosseini, M.; Chin, A. W.; Behzadinasab, S.; Poon, L. L.; Ducker, W. A. Cupric Oxide Coating That Rapidly Reduces Infection by Sars-Cov-2 Via Solids. *ACS Appl. Mater. Interfaces* **2021,** *13* (5), 5919-5928.

(30) Rakowska, P. D.; Tiddia, M.; Faruqui, N.; Bankier, C.; Pei, Y.; Pollard, A. J.; Zhang, J.; Gilmore, I. S. Antiviral Surfaces and Coatings and Their Mechanisms of Action. *Commun. Mat.* **2021,** *2* (1), 1-19.

(31) Hosseini, M.; Behzadinasab, S.; Benmamoun, Z.; Ducker, W. A. The Viability of Sars-Cov-2 on Solid Surfaces. *Curr. Opin. Colloid Interface Sci.* **2021**, 101481.

(32) Singha, P.; Locklin, J.; Handa, H. A Review of the Recent Advances in Antimicrobial Coatings for Urinary Catheters. *Acta Biomater.* **2017,** *50*, 20-40.

(33) Liu, G.; Li, K.; Wang, H.; Ma, L.; Yu, L.; Nie, Y. Stable Fabrication of Zwitterionic Coating Based on Copper-Phenolic Networks on Contact Lens with Improved Surface Wettability and Broad-Spectrum Antimicrobial Activity. *ACS Appl. Mater. Interfaces* **2020,** *12* (14), 16125-16136.

(34) Bergemann, C.; Zaatreh, S.; Wegner, K.; Arndt, K.; Podbielski, A.; Bader, R.; Prinz, C.; Lembke, U.; Nebe, J. B. Copper as an Alternative Antimicrobial Coating for Implants-an in Vitro Study. *World J. Transplant* **2017,** *7* (3), 193-202.

(35) Environmental Protection Agency Antimicrobial Testing Methods & Procedures: Interim Method for Evaluating the Efficacy of Antimicrobial Surface Coatings https://www.epa.gov/pesticide-analytical-methods/antimicrobial-testing-methods-procedures-interim-method-evaluating (accessed Sep 2, 2022).

(36) Environmental Protection Agency Protocol for the Evaluation of Bactericidal Activity of Hard, Non-Porous Copper Containing Surface Products. https://www.epa.gov/sites/production/files/2016-02/documents/copper_and_copper-alloy_surface_protocol_revised_012916.pdf (accessed Sep 2, 2022).

(37) Washburn, E. W. The Dynamics of Capillary Flow. *Phys. Rev.* **1921,** *17* (3), 273.

(38) Borkow, G.; Gabbay, J. Copper, an Ancient Remedy Returning to Fight Microbial, Fungal and Viral Infections. *Curr. Chem. Biol.* **2009,** *3* (3), 272-278.

(39) Lee, H.; Dellatore, S. M.; Miller, W. M.; Messersmith, P. B. Mussel-Inspired Surface Chemistry for Multifunctional Coatings. *Science* **2007,** *318* (5849), 426-430.

(40) Ryu, J. H.; Messersmith, P. B.; Lee, H. Polydopamine Surface Chemistry: A Decade of Discovery. *ACS Appl. Mater. Interfaces* **2018,** *10* (9), 7523-7540.

(41) Sunada, K.; Minoshima, M.; Hashimoto, K. Highly Efficient Antiviral and Antibacterial Activities of Solid-State Cuprous Compounds. *J. Hazard. Mater.* **2012,** *235*, 265-270.

(42) Aydin Sevinç, B.; Hanley, L. Antibacterial Activity of Dental Composites Containing Zinc Oxide Nanoparticles. *J. Biomed. Mater. Res. B Appl. Biomater.* **2010,** *94* (1), 22-31.

(43) El Saeed, A. M.; Abd El-Fattah, M.; Azzam, A. M.; Dardir, M. M.; Bader, M. M. Synthesis of Cuprous Oxide Epoxy Nanocomposite as an Environmentally Antimicrobial Coating. *Int. J. Biol. Macromol.* **2016,** *89*, 190-197.

(44) Akiyama, T.; Miyamoto, H.; Yonekura, Y.; Tsukamoto, M.; Ando, Y.; Noda, I.; Sonohata, M.; Mawatari, M. Silver Oxide-Containing Hydroxyapatite Coating Has in Vivo Antibacterial Activity in the Rat Tibia. *J. Orthop. Res.* **2013,** *31* (8), 1195-1200.

(45) Johnson, J. R.; Roberts, P. L.; Olsen, R. J.; Moyer, K. A.; Stamm, W. E. Prevention of Catheter-Associated Urinary Tract Infection with a Silver Oxide-Coated Urinary Catheter: Clinical and Microbiologic Correlates. *J. Infect. Dis.* **1990,** *162* (5), 1145-1150.

(46) Grass, G.; Rensing, C.; Solioz, M. Metallic Copper as an Antimicrobial Surface. *Appl. Environ. Microbiol.* **2011,** *77* (5), 1541-1547.

(47) Hosseini, M.; Rodriguez, A.; Ducker, W. A. Super-Enhanced Evaporation of Droplets from Porous Coatings. *J. Colloid Interface Sci.* **2023,** *633*, 132-141.

(48) Roth, C. B.; Dutcher, J. Glass Transition Temperature of Freely-Standing Films of Atactic Poly (Methyl Methacrylate). *Eur Phys J E* **2003,** *12* (1), 103-107.

(49) Jaeblon, T. Polymethylmethacrylate: Properties and Contemporary Uses in Orthopaedics. *J. Am. Acad. Orthop. Surg.* **2010,** *18* (5), 297-305.

(50) Liu, Y.; Ai, K.; Liu, J.; Deng, M.; He, Y.; Lu, L. Dopamine-Melanin Colloidal Nanospheres: An Efficient near-Infrared Photothermal Therapeutic Agent for in Vivo Cancer Therapy. *Adv. Mater.* **2013,** *25* (9), 1353-1359.

(51) Zhou, P.; Deng, Y.; Lyu, B.; Zhang, R.; Zhang, H.; Ma, H.; Lyu, Y.; Wei, S. Rapidly-Deposited Polydopamine Coating Via High Temperature and Vigorous Stirring: Formation, Characterization and Biofunctional Evaluation. *PLoS One* **2014,** *9* (11), e113087.

(52) Zhao, L.; Chen, D.; Hu, W. Patterning of Metal Films on Arbitrary Substrates by Using Polydopamine as a Uv-Sensitive Catalytic Layer for Electroless Deposition. *Langmuir* **2016,** *32* (21), 5285-5290.

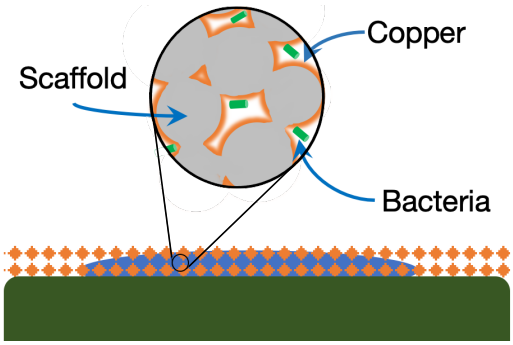
(53) Wang, K.; Dong, Y.; Zhang, W.; Zhang, S.; Li, J. Preparation of Stable Superhydrophobic Coatings on Wood Substrate Surfaces Via Mussel-Inspired Polydopamine and Electroless Deposition Methods. *Polymers* **2017,** *9* (6), 218.

(54) Frick, C. P.; Merkel, D. R.; Laursen, C. M.; Brinckmann, S. A.; Yakacki, C. M. Copper-Coated Liquid-Crystalline Elastomer Via Bioinspired Polydopamine Adhesion and Electroless Deposition. *Macromol. Rapid Commun.* **2016,** *37* (23), 1912-1917.

(55) Gonzalez-Martinez, E.; Saem, S.; Beganovic, N. E.; Moran-Mirabal, J. Fabrication of Microstructured Electrodes Via Electroless Metal Deposition onto Polydopamine-Coated Polystyrene Substrates and Thermal Shrinking. *Nano Select* **2021,** *2* (10), 1926-1940.

(56) Dey, B.; Engley Jr, F. Methodology for Recovery of Chemically Treated Staphylococcus Aureus with Neutralizing Medium. *Appl. Environ. Microbiol.* **1983,** *45* (5), 1533-1537.

Figure For Table of Contents Only



4.6. SUPPORTING INFORMATION

Porous Antimicrobial Coatings for Killing Microbes within Minutes

Saeed Behzadinasab[1,2,3], Myra D. Williams[4], Mete Aktuglu[1], Joseph O. Falkinham III*[4], and William A. Ducker*[1,2,3]

[1]Department of Chemical Engineering, Virginia Tech, Blacksburg, Virginia, 24061, USA

[2]Center for Soft Matter and Biological Physics, Virginia Tech, Blacksburg, Virginia, 24061, USA

[3]Macromolecules Innovation Institute, Virginia Tech, Blacksburg, Virginia, 24061, USA

[4]Department of Biological Sciences, Virginia Tech, Blacksburg, Virginia, 24061, USA

Corresponding Authors' Email: Joseph Falkinham jofiii@vt.edu; William Ducker wducker@vt.edu

Keywords: porous, polydopamine, copper, antibacterial, antimicrobial, coating, bacteria

ORCIDs:

Saeed Behzadinasab: 0000-0002-6271-2623

Joseph O. Falkinham III: 0000-0002-4391-9012

William A. Ducker: 0000-0002-8207-768X

4.6.1. Supplementary methods

4.6.1.1. Abrasion tests

The porous coatings were abraded by an abrasion tester (model: Gardco D10V) using a mounted sponge. This was based on the EPA protocol[1] which is utilized to evaluate antimicrobial coatings for EPA approval. This protocol has abrasion with a sponge wetted with an antimicrobial agent (70% ethanol). The tester machine moves back and forth a sponge that is in contact with the samples with an amplitude of ~26 cm and a period of approximately 5 sec. The sponge was loaded with load of 0.45 kg during the tests, and it was wetted with 20 mL of 70% ethanol before the abrasion cycles. An abrasion cycle was done as following: the sponge was moved across the sample 8 times, subsequently 70% ethanol was sprayed on the abrasion platform and the samples with a subsequent waiting period (30 minutes). A total of 10 cycles (equal to 80 passes) were performed on the samples. A single sponge was used for the first 5 abrasion cycles, and it was replaced with a separate sponge for the second 5 abrasion cycles. Did you rinse the coating before doing the CFU test? I imagine that there were bits of sponge on it because ss would rip it up.

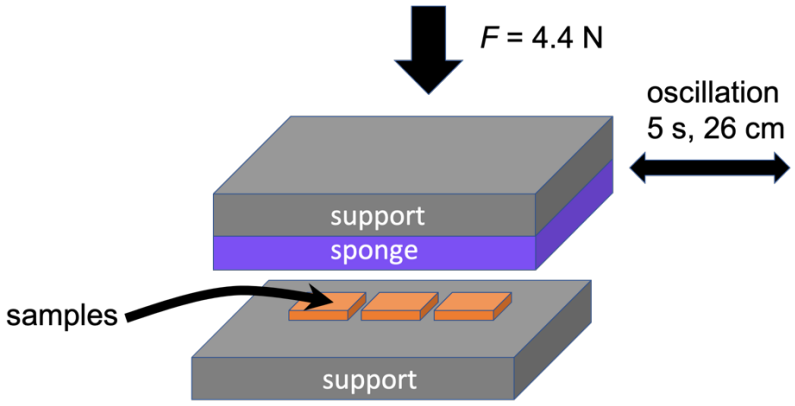


Figure S4-1. Schematic of abrasion tests on the coatings. The sponge was loaded with a load of 0.45 kg (4.4. N), while it was moved back and forth by the abrasion tester on the samples. Schematic is not to scale; there is a gap in the schematic so the samples can be seen. During the tests, the sponge was in

contact with the samples. The figure is reused with permission from Reference[2], © 2021 American Chemical Society.

4.6.2. Supplementary Results

4.6.2.1. SEM images of uncoated porous SS scaffold

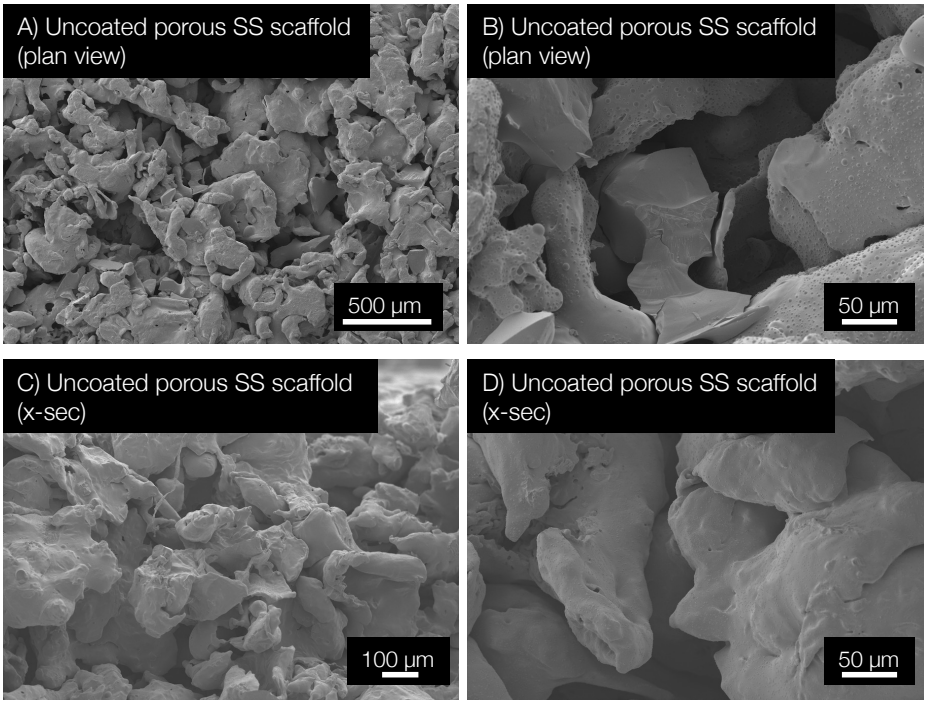


Figure S4-2. SEM images of porous SS scaffold. A & B show plan view images, and C & D are cross-section SEM images. The porous scaffold has large pores which easily allows for penetration of droplets and microbial cells with all sizes.

4.6.2.2. XPS, EDS, and SEM images of coated porous SS

Element	Mol% (EDS)		
	Plan-view		X-section
	Flat SS	Porous SS	Porous SS
Fe	24.5	28.9	32.8
Cu	24.8	11.8	12.8
Cr	7.1	9.0	10.1
C	33.7	29.0	33.0
Ni	2.2	5.1	5.6
O	7.6	11.5	5.0
Si	---	2.0	0.7
Mo	---	0.6	---
Al	---	2.0	---

Table S4-1. Chemical composition (mol%) of surface of PDA/Cu-coated flat and porous SS measured by EDS.

Element	Atomic% (XPS) Plan-view		
	Flat SS	**Porous SS**	**Porous PMMA**
O	**41.0**	**40.3**	**30.3**
C	**31.7**	**38.0**	**32.5**
Cu	**26.7**	**21.1**	**33.9**
Cl	**0.6**	**0.6**	**1.1**
N	**---**	**---**	**2.2**

Table S4-2. Chemical composition (atomic%) of surface of PDA/Cu-coated flat and porous scaffolds as measured by XPS.

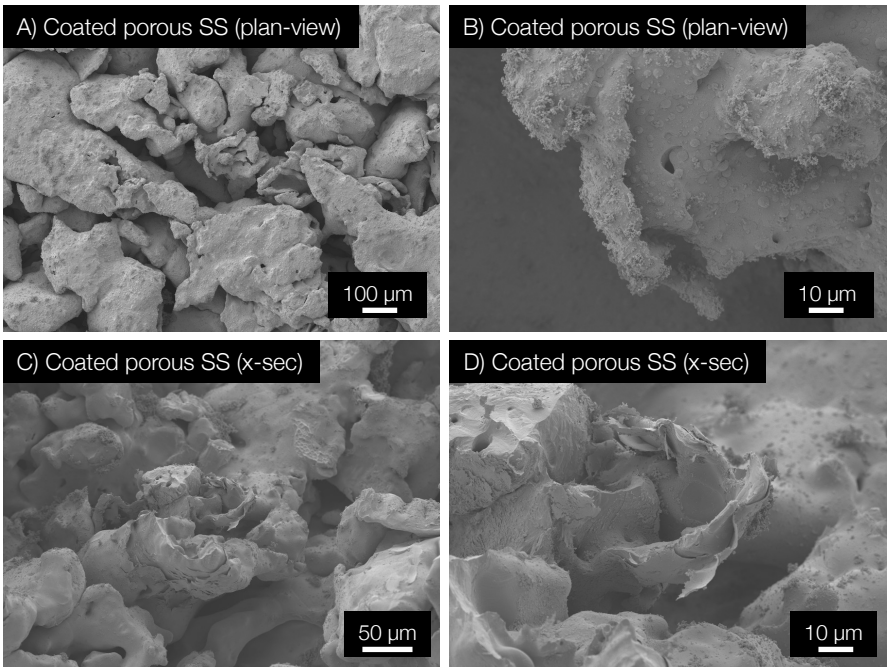


Figure S4-3. Plan-view and cross-section SEM images of coated porous SS. The PDA/Cu layer is successfully made within the pores of the porous SS coating.

4.6.2.3. SEM image of flat SS surfaces

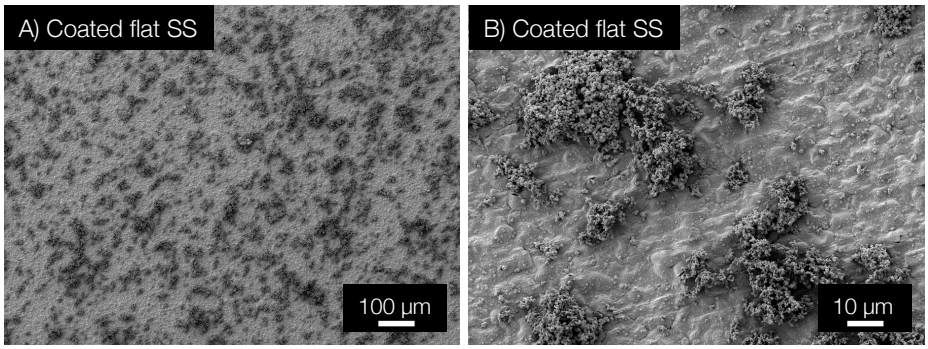


Figure S4-4. Plan-view SEM images of PDA/Cu-coated flat SS surfaces.

4.6.2.4. Extraction of bacteria from porous and non-porous solids

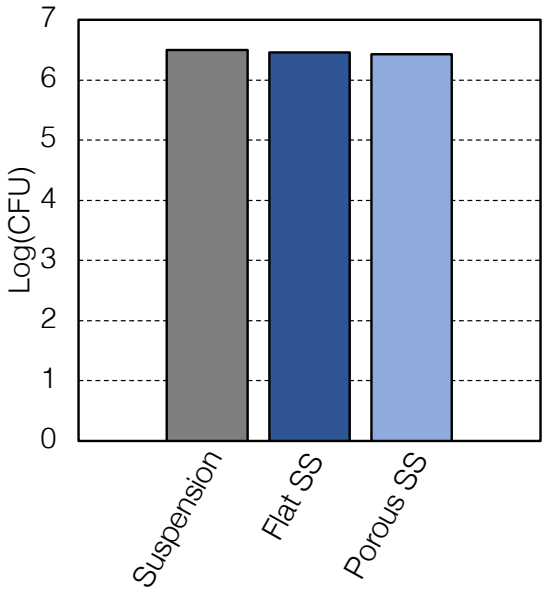


Figure S4-5. Bacterial CFUs extracted from flat and porous scaffolds. The droplet size used in this experiment was 10 µL and the detection limit is 50 CFU.

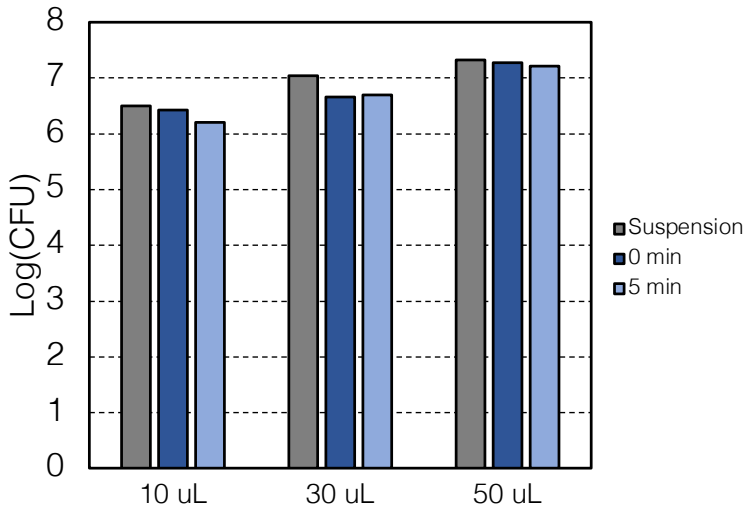


Figure S4-6. Extraction of P. aeruginosa from porous SS as a function of droplet volume. Three droplet sizes were tested (10, 30, and 50 µL). The detection limit is 50 CFU. In each case a high percentage of bacteria are extracted.

4.6.2.5. SEM images of porous PMMA scaffold

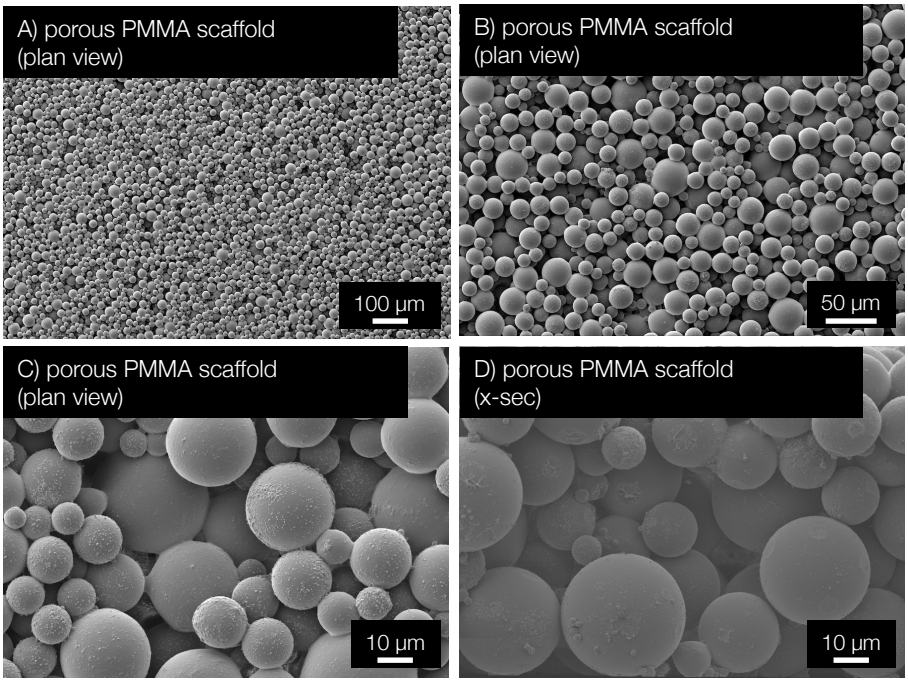


Figure S4-7. SEM images of porous PMMA scaffold. PMMA particles were partially sintered (Ostwald ripening) to produce a porous scaffold. A, B, and C are the plan view SEM images and D shows the cross-section image.

Element	mol%
C	75.4
Cu	9.1
O	15.5

Table S4-3. Chemical composition of x-section of porous PDA/Cu-coated PMMA measured by EDS.

4.6.2.6. CFU measurements for flat or porous PMMA scaffolds

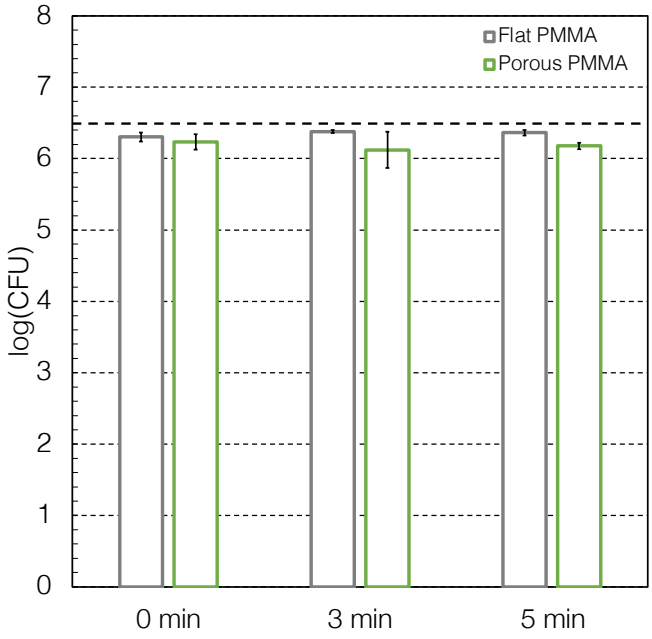


Figure S4-8. Time course of bacteria CFU on flat and porous PMMA scaffolds. Neither of these coatings kill bacteria. The *p*-value = 0.088 for flat vs porous PMMA scaffolds (Student's t-test). The detection limit is 50 CFU.

4.6.2.7. Photographs of water droplet absorbing into PDA/Cu-coated porous PMMA.

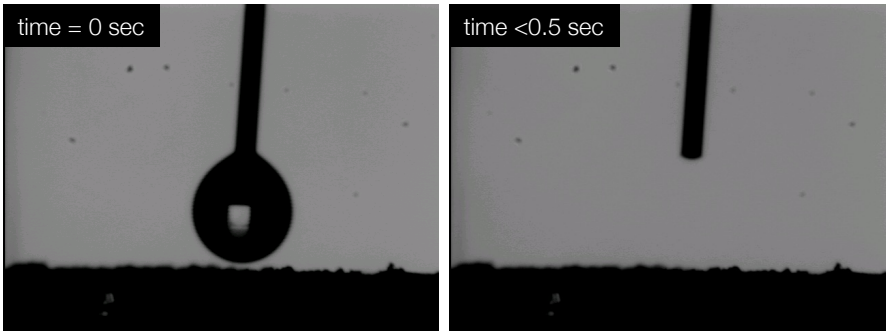


Figure S4-9. Photographs showing the time for a water droplet to imbibe into the PDA/Cu-coated porous PMMA.

4.6.2.8. Porous PMMA scaffold does not possess antimicrobial properties.

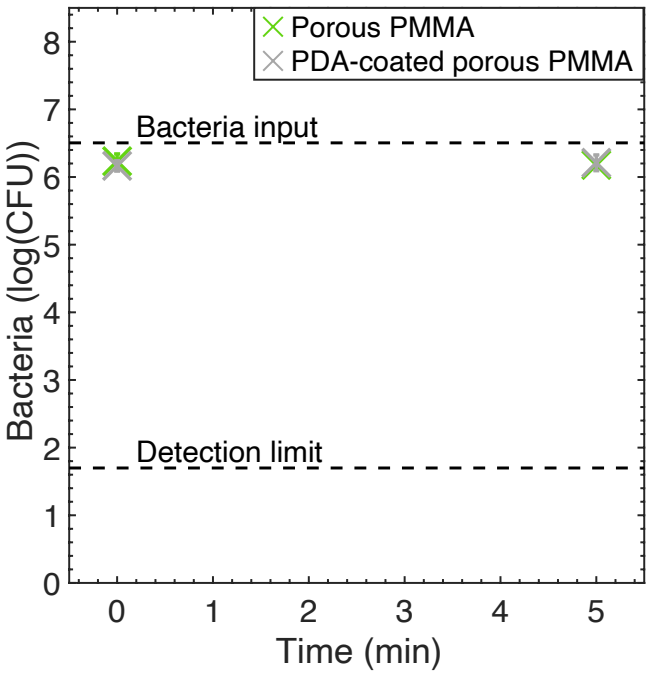


Figure S4-10. Time course of *P. aeruginosa* CFU on PDA-coated porous PMMA. PDA does not have antimicrobial properties. The p-value = 0.711 for porous PMMA vs PDA-coated porous PMMA scaffold.

References

(1) Environmental Protection Agency Antimicrobial Testing Methods & Procedures: Interim Method for Evaluating the Efficacy of Antimicrobial Surface Coatings https://www.epa.gov/pesticide-analytical-methods/antimicrobial-testing-methods-procedures-interim-method-evaluating (accessed Sep 2, 2022).

(2) Behzadinasab, S.; Williams, M. D.; Hosseini, M.; Poon, L. L.; Chin, A. W.; Falkinham III, J. O.; Ducker, W. A. Transparent and Sprayable Surface Coatings That Kill Drug-Resistant Bacteria within Minutes and Inactivate Sars-Cov-2 Virus. *ACS Appl. Mater. Interfaces* **2021,** *13* (46), 54706-54714, DOI: https://doi.org/10.1021/acsami.1c15505.

Chapter 5. Antimicrobial Activity of Cuprous Oxide and Cupric Oxide-Coated Surfaces

Saeed Behzadinasab[†1], Mohsen Hosseini[†1], Myra D. Williams[2], Hannah M. Ivester[3], Irving C. Allen[3,4,5], Joseph O. Falkinham III[2], and William A. Ducker*[1]

*Corresponding Authors' Email: wducker@vt.edu

[1]Department of Chemical Engineering and Center for Soft Matter and Biological Physics, Virginia Tech, Blacksburg, Virginia, 24061, USA

[2]Department of Biological Sciences, Virginia Tech, Blacksburg, Virginia, 24061, USA

[3]Graduate Program in Translational Biology, Medicine and Health, Virginia Tech, Roanoke, Virginia, 24016, USA

[4]Department of Biomedical Sciences and Pathobiology, Virginia-Maryland College of Veterinary Medicine, Blacksburg, Virginia, 24061, USA

[5]Department of Basic Science Education, Virginia Tech Carilion School of Medicine, Roanoke, Virginia, 24016, USA

[†] These authors contributed equally

5.1. STRUCTURE SUMMARY

5.1.1. Background

Disease can be spread through contact with contaminated surfaces (fomites). For example, fomites have been implicated in the spread of methicillin-resistant *Staphylococcus aureus* (MRSA) and *Pseudomonas aeruginosa*. Antimicrobial surface treatments are a potential method of reducing disease transmission from fomites, and broad-spectrum activity is desirable.

5.1.2. Aims

Test cuprous oxide (Cu_2O) and cupric oxide (CuO) coatings for antimicrobial activity against 12 microorganisms including bacteria and fungi.

5.1.3. Methods

We fabricated two surface coatings. The Cu_2O coating was fabricated in a simple two-step process using polyurethane to bind the active copper oxide particles; CuO was prepared by heat treatment of Cu_2O particles in air to produce cupric oxide (CuO) and to cause early-stage sintering to form a continuous coating. The antimicrobial activity was examined with 10 μL of microbial suspension droplets followed by counting cells as colony-forming units (CFUs).

5.1.4. FINDINGS

The coatings rapidly killed 9 different microorganisms, including Gram-negative and Gram-positive bacteria, mycobacteria, yeast and another fungus. For example, the Cu_2O/PU coating killed 99.9997% of *P. aeruginosa* and 99.9993% of *S. aureus* after 1 hour. The efficacy was not reduced after weekly cleanings. The antimicrobial activity of the Cu_2O coating was unchanged after abrasion treatment, and the coatings were not cytotoxic to human cells.

5.1.5. Conclusion

The combination of broad-spectrum antimicrobial activity, abrasion resistance, and low toxicity of the Cu_2O coating suggests potential use in healthcare settings.

Keywords:

Antimicrobial, Antibacterial, Surface, Coatings, Cuprous oxide, Durable

5.2. Introduction

Microorganisms infect millions of people throughout the world and cost billions of dollars to treat [1-3]. Serious infections are treated with antibiotics and thus antibiotic-resistant microorganisms present particular problems. The United States (US) Center for Disease Control and Prevention (CDC) has listed the most serious microbial threats [4] and these include the yeast *Candida auris* (an Urgent Threat) and the bacteria, methicillin-resistant *Staphylococcus aureus* (MRSA) and *Pseudomonas aeruginosa* (Serious Threats) [5, 6].

Infection from microorganisms occurs via several routes [7]. Microbes from the air, water, solids and food enter the body through inhalation, ingestion and skin contact. In this work we focus on disease transmission via contaminated solids (fomites) onto skin [8-11]. A variety of studies have shown that microorganisms are present on readily assessable public surfaces [12-15], including hospital surfaces [16, 17] and that these bacteria can survive for a long time [18], up to months [12, 15]. Transmission of bacterial pathogens from surfaces in hospitals is well established [19]. Specifically, hospital-acquired infections have been reported due to transfer from surface-adherent *S. aureus*, [20] vancomycin-resistant and vancomycin-sensitive Enterococci (VRE), [21, 22] and *P.* aeruginosa [19]. The US CDC estimates reports that there were 323,700 MRSA infections in the US in 2017 and 10,600 fatalities [4].

Methods to reduce transmission from fomites are currently based on treating contaminated surfaces with a disinfectant. However, that approach is limited by the fact that the surface can be immediately re-contaminated by contact with the pathogen. Frequent decontamination is labor-intensive and, therefore, expensive, and the more time spent on decontamination, the less time the surface is available for use.

One alternative to frequent disinfection would be a surface coating that can kill pathogens on contact. Such a coating would need to kill quickly, last for an extended period of time, and be able to kill pathogens after cleaning. Such coatings have been produced, specifically to target various organisms, including bacteria [23-26], and viruses such as COVID-19 virus (SARS-CoV-2) [25, 27-32]. Metals and metal oxides, including copper, copper oxides, silver, silver oxide, zinc oxide [33-40], have been used as the active ingredients. A few surfaces have been studied that are not coatings but are modifications to the topology of the surface [41-44].

Here we describe the antimicrobial efficacy of coatings containing either cuprous oxide (Cu_2O) or cupric oxide (CuO) as the active microbicide. These two copper oxides have broad antimicrobial properties, so are promising candidates for antimicrobial coatings [45-48]. During the COVID-19 pandemic, we described two coatings that rapidly reduced the ability of the virus SARS-CoV-2 on surfaces to infect human cells [27, 29]: (1) Cu_2O/PU, which consisted of a layer of cuprous oxide particles bound to a solid surface by commercial polyurethane (PU) [27], which reduced the infectivity of SARS-CoV-2 by ~99.9%in 1 h; and (2) porous CuO that was made by heat treatment of Cu_2O[29]. In this work, we show that both these coatings have strong (e.g., > 3-log killing) antimicrobial activity against a broad spectrum of pathogenic microorganisms (See Table 5-1), including methicillin-resistant *S. aureus* (MRSA), *P. aeruginosa*, and *Candida albicans*.

The central idea in this manuscript is that the lifetime of pathogenic bacteria can be reduced by a coating. Therefore, it is necessary to compare results for a coated surface to the uncoated surface at the same time after inoculation. We chose stainless steel (SS) as our uncoated surfaces because of its widespread in hospitals. Our performance metric is relative

survival percentage, which is a comparison of colony forming units (CFU) on stainless steel to CFU on the coated surface after the same time since the surface was first contaminated:

$$\%\ \text{relative survival} = \frac{\text{mean}(\text{CFU}_{\text{coated}})}{\text{mean}(\text{CFU}_{\text{uncoated}})} \times 100\% \qquad \text{Equation 5-1}$$

When there were no survivors, we rounded the CFU up to 1 and prefixed the result with the "< "sign.

5.3. Materials and Methods

5.3.1. Materials

5.3.1.1. Materials for Preparation of Antimicrobial Copper Surfaces

Cu_2O particles (Chem Copp HP III Type UltraFine -5) were obtained from American Chemet Corporation. Polyurethane (brand: Miniwax, Fast-Drying Polyurethane, clear satin) was purchased from Lowes Home Improvement Store. Stainless steel 301 (SS 301) shim (0.015" thick) was purchased from McMaster Carr. SS 301 was thoroughly washed with soap and water and rinsed with water. 200 PROOF ethanol and glass slides (25 × 75 × 1 mm) were obtained from VWR. For sample (coupon) preparation, deionized water was further purified by Milli-Q Reference system.

5.3.1.2. Fabrication of Cu_2O/PU coating[27]

A thin layer of polyurethane was applied to stainless steel 301 using a sponge; it was allowed to partially dry for a few min, then a suspension of Cu_2O in ethanol (10% w/w) was added dropwise, and it was left to partially dry for a few minutes at room temperature. Subsequently, the sample was heat treated at about 80º, blown with nitrogen gas, and washed thoroughly with DI water. The coated stainless steel was cut into ≈ 12×12 mm pieces, and each piece was cleaned with argon plasma. The films were stored under water, unless otherwise stated. Scanning Electron Microscopy (SEM) showed that the coating was 10–16 µm in thickness. Optical images of the coatings and SEM images are in Supplementary Material, Figure S5-1 and Figure S5-2 respectively and the elemental composition is in Table S5-1.

5.3.1.3. Fabrication of partially-sintered CuO coating[29]

A suspension of Cu_2O in ethanol (10% w/w) was deposited on SS 301 (≈ 12×12 mm), left to partially dry, and then heat-treated in a furnace at 700 °C for 2 hours, followed by natural cooling to room temperature overnight. SEM showed that the thickness was about 32 ± 1 µm.

5.3.2. Measurement of Antimicrobial Activity

5.3.2.1. Growth of Microbial Strains

With the exception of the mycobacterial strains that were grown in 5 mL Middlebrook 7H9 Broth at 37° C with aeration (60 rpm), all other bacterial strains were grown 5 mL in

Tryptic Soy Broth (TSB) at 37° C with aeration (60 rpm). Yeast strains were grown in Potato Dextrose Broth (PDB) at 37° C with aeration (60 rpm). The *Bacillus anthracis* strain was grown in TSB at 37° C with aeration (60 rpm) until the culture contained greater than 95 % spores as measured by microscopic examination. The *Aspergillus niger* strain was grown on PDA agar plates at 30° C until the plate was covered with black-pigmented spores. Spores of both *B. anthracis* and *A. niger* were harvested by suspension in 5 mL sterile water and collected by centrifugation (5,000 x G for 20 min) and suspended in water. Following growth, the purity and identity of the cells in the cultures were verified by streaking bacterial cultures on agar plates (mycobacteria on M7H10 agar for up to 14 days, other bacteria on Tryptic Soy Agar (TSA), and yeast and fungal cultures on Potato Dextrose Agar (PDA) at 37° C for 2 days.

5.3.2.2. Preparation of Microbial Cells for Surface Killing Measurements

Cells were separated from the growth media and suspended in phosphate buffered saline (PBS) by the following method. The cells were centrifuged (5,000 x g for 20 min), the supernatant medium discarded and the cells resuspended in 5 mL of sterile PBS by vortexing 60 s. Those suspensions were centrifuged (5,000 x g for 20 min), the supernatant wash discarded, and the washed cells suspended in 5 mL of sterile PBS by vortexing for 60 s. The cell density of suspension was adjusted by dilution to Equal that of a McFarland No. 1 Standard and the number of colony-forming units (CFU)/mL of each washed suspension was measured by spreading 0.1 mL (in duplicate) of serial dilutions on agar as above. Typical cell were 3.2×10^5–$1.3\text{x}10^6$ CFU/ mL.

5.3.2.3. Measurement of Surface-Killing

A 10 µL test droplet of the cell suspension in PBS was placed on the test solid. Immediately afterwards, one surface of each type (i.e., control, Cu_2O/PU, Sintered CuO) was transferred to a sterile 50 mL centrifuge tube containing 5 mL of sterile PBS, vortexed for 30 sec. and sonicated for 5 min, and the CFU/mL of the suspension measured as described above. This was the zero time control that indicated our ability to recover bacteria. At later times (e.g. 1 h, 2 h, etc), one sample of each material type was processed in the same way. Following 48 h incubation of the plates (14 days for *Mycobacterium* spp.), colonies were counted, the number of surviving cells expressed as CFU/mL of suspension calculated, and the survival calculated via Equation 5-1. One coupon was measured for each time point, and results show the average of duplicate CFU measurements from the same bacterial suspension that was recovered from the coupon.

5.3.3. Cytotoxicity study

The cytotoxicity was assessed in human monocyte cells (white blood cells, Thp1, ATCC®TIB 202™) that form part of the immune system and in connective tissue cells (murine fibroblasts, L929 ATCC®CCL-1™) using a lactate dehydrogenase (LDH) assay as described in Supplementary Material 1.3.

5.4. Results

5.4.1. Controls and Validation

The following validation experiments are described in more detail in Supplementary Material, Section 2.2. (1) We tested whether viable bacteria remained on the stainless steel after our extraction procedure, in which case we would overcount killing. Results showed no significant difference between the number of viable cells plated onto the steel and the number extracted from stainless steel. (2) We tested whether there was carry over of antimicrobial liquid into the CFU assay. Such antimicrobial material could have provided an ongoing kill during the incubation for the CFU assay, thereby undermining our claim that killing was occurring on the coupon in 1 h. We did not find ongoing kill during the CFU incubation (See SI, 2.2.3, Table S5-5).

5.4.2. Both Cu_2O/PU and Sintered CuO Coatings have broad-spectrum antimicrobial activity

Measurements were made against 12 microbial species, including bacteria, mycobacteria, fungi, and yeast (Table 5-1). The Cu_2O/PU coating was strongly antimicrobial: specifically, there were no surviving colonies (with the exception of *Mycobacterium* cells and *Bacillus anthracis* spores) after 2 h. exposure to the surface. Strong *antiviral* activity of the same coating has been reported previously [27]. It is possible that the killing of the *A. niger* spores (Table 5-1) was a consequence of their germination. The sintered CuO coating was also effective, but less so than the Cu_2O/PU coating. The survival after 1 h exposure of cells of the two *Mycobacterium* spp. strains was substantial. For example, survival on sintered CuO was 43% for *M. avium* and 29%

for *M. abscessus*. *Mycobacterium* spp. is difficult to kill,[49, 50] likely due to the thick, lipid-rich outer membrane[51]. Anthrax spores are typically even more difficult to kill,[50] and CuO was ineffective. The Cu_2O/PU coating showed a mild effect against *Bacillus anthracis* after two hours.

Survival was so low in some cases that our initial experiment did not resolve the full killing ability of the Cu_2O coating. To obtain improved resolution, we tested the survival for higher cell densities of *P. aeruginosa* (7.28×10^6 CFU/coupon) and *S. aureus* (3.76×10^6 CFU/coupon).

Survival after one hour exposure was 0.0003% for *P. aeruginosa* and 0.0007% for S. aureus (See Table S5-7 for more times). A full study of the killing as a function of cell density is described in Supplementary Material (Section 2.4 and Figure S5-3), and indicates that killing is at the detection limit at all but the very highest cell densities. This indicates both a high kill and the ability to kill different densities of cells. Killing at short times, 5 min. and 10 min., is reported in Table S5-8 in the SM. Killing is rapid, particularly for *P. aeruginosa.*

Strain	**Time* (h)**	**% Relative Survival‡**	
		Cu_2O/PU	**Sintered CuO**
Staphylococcus aureus ATCC® 6538	0	0.16	51.0†
	1	0.3	0.3
	2	< 0.1	< 0.1
Staphylococcus aureus (MRSA) ATCC® 43330	0	0.1	3.0†
	1	< 0.1	< 0.1
	2	< 0.1	< 0.1
Escherichia coli ATCC® 13706 DX	0	7.0	34.0
	1	< 1.4	< 1.4

	2	< 1.4	< 1.4
Pseudomonas aeruginosa ATCC® BAA-2111	0	< 0.2	105.
	1	< 0.2	< 0.2
	2	< 0.2	< 0.2
Stenotrophomonas maltophilia ATCC® 17666	0	173.	158.
	1	< 2.0	< 2.0
	2	< 2.0	< 2.0
Acinetobacter baumannii ATCC® 2802	0	14.	172.
	1	< 1.4	22.
	2	< 1.4	< 1.4
Bacillus anthracis Spores Sterne Strain 34F2 (LLNL A0517)	0	79.1	79.4
	1	78.2	100.1
	2	57.4	82.8
Mycobacterium avium ATCC® 25291	0	108.	98.
	1	14.	43.
	2	14.	29.
Mycobacterium abscessus ATCC® 23045	0	23	44.
	1	1.4	29.
	2	< 0.5	17.
Candida albicans ATCC® 10231	0	23.	110.
	1	20.	0.4
	2	< 0.4	< 0.4
Candida auris CDC & FDA AR Bank # 0386	0	14	105.
	1	< 0.3	< 0.3
	2	< 0.3	< 0.3
Aspergillus niger Spores ATCC® 10535	0	67.	78.
	1	19.	33.
	2	< 1.4	< 1.4

Table 5-1. Relative Survival of microbes on cuprous oxide/polyurethane (Cu2O/PU) or sintered cupric oxide (CuO) coatings compared to on stainless steel.

*Time since contact of the droplet with the sample; in practice, time = zero is actually a few minutes processing time. "<" indicates that no colonies were formed on the coated sample and the number following is the % if 1 colony were formed on the agar plate.

†The difference in results for the two S. aureus strains for CuO at zero time was large. To test whether the difference was significant, we performed a second round of experiments, described in Supporting Materials, 2.5, and concluded that there was not a significant difference.

‡Data for stainless steel in Table S5-10.

5.4.3. Repeated Disinfection/Cleaning of the Cu_2O/PU Coating with ethanol over 20-weeks Did Not Reduce Killing

We determined whether the copper surfaces retained antimicrobial activity after repeated, cleaning/disinfection (see Table S5-3 for more details) over a period of 20 weeks. The results (Table 5-2) demonstrate that killing was maintained at high levels throughout regular contamination and disinfection.

WEEK	Percent of bacteria surviving after 60 min exposure to Cu_2O/PU coating ($CFU_{coated, 1h}/CFU_{coated, 0h}$)	
	S. aureus	***P. aeruginosa***
0	0.07	0.5
1	0.07	< 0.02
2	0.65	< 0.02
3	< 0.003	< 0.03
4	< 0.04	< 0.17
5	< 0.0067	< 0.035
7	< 0.009	< 0.01
9	< 0.008	< 0.009
10	0.017	< 0.002
20 (time = 1.5 h)	0.065	< 0.0047

Table 5-2. Repeated killing of S. aureus and P. aeruginosa on rinsed and disinfected Cu2O/PU coating. The contact time between bacteria and the coating was 1 h, except in week 20, when it was 1.5 h

5.4.4. The PU/Cu2O and Sintered CuO coatings are Not Cytotoxic Against Human Monocytes and Murine Fibroblasts

The cytotoxicity of the two coatings were assessed in human monocyte cells (white blood cells, Thp1) that form part of the immune system and in connective tissue cells (murine fibroblasts, L929) using a lactate dehydrogenase (LDH) assay as described in Supplementary Material**.** Results in Figure 5-1 show that the lysis in the presence each of the coatings was negligible in comparison to full lysis.

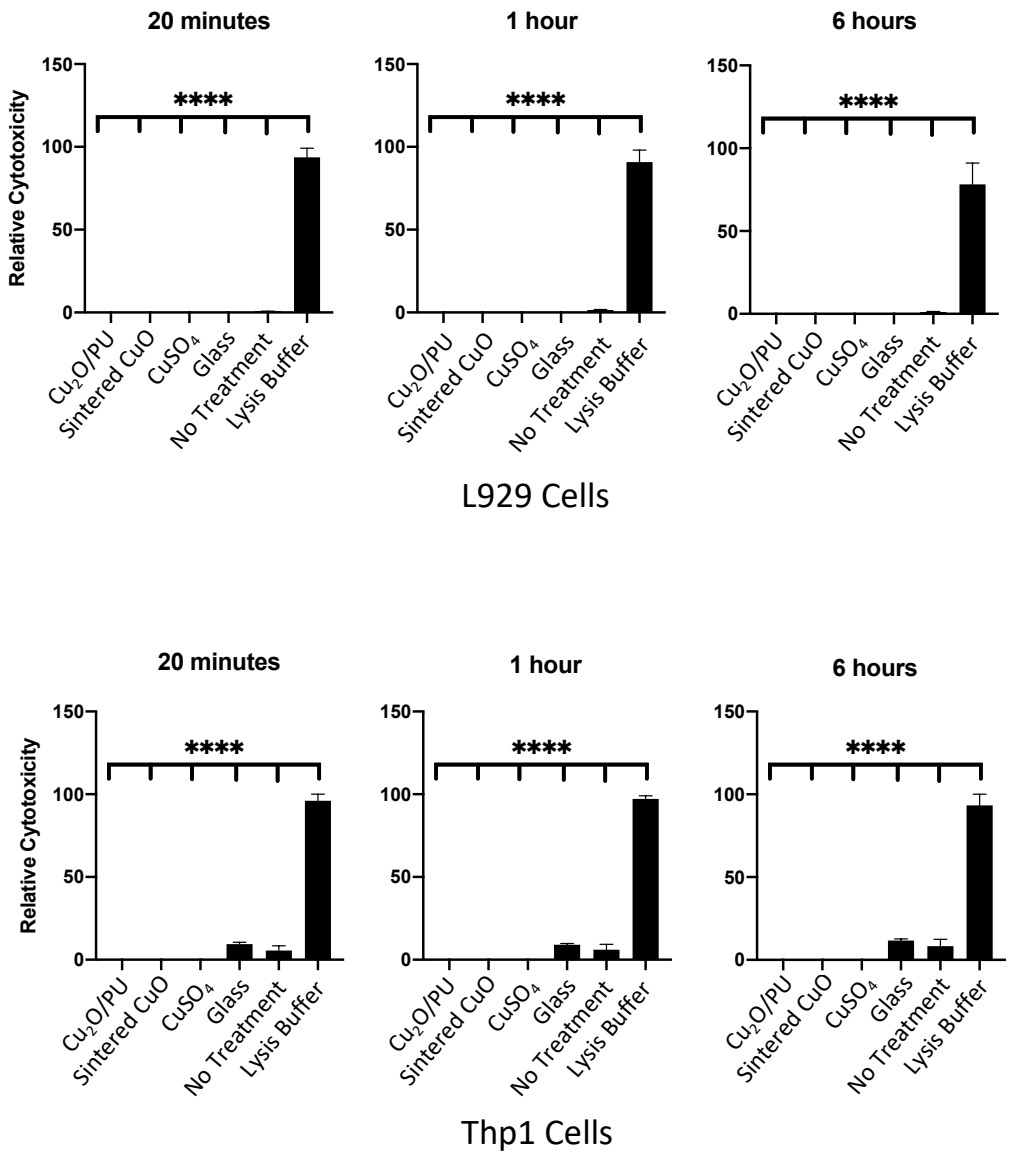


Figure 5-1. Cytotoxicity study of the coatings. Cell lysis caused by Cu2O/PU or sintered CuO coatings was negligible compared to full lysis.

5.4.5. Antimicrobial Activity of Cu_2O/PU Coating Survive Abrasion

In our previous publication, we demonstrated the resistance of the Cu_2O/PU coating to scratching using a cross-hatch test [27]. Here we extend the durability testing using an abrasion

test that we modified from the standard US EPA test[52] (See SI 1.1). The essence of the test is to compare the microbiocidal activity on a sample that is mechanically rubbed with a sponge to a non-rubbed sample. Here we used coatings on glass that were stored in air. The results (Table 5-3) show that Cu_2O/PU coating is as effective against *P. aeruginosa* as the original coating.

	Time* (h)	**Fresh coating % Survival**	**Abraded % Survival**
Repeat 1	0	99.3	84.5
	1	< 0.6	< 0.6
Repeat 2	0	84.6	97.1
	1	< 0.4	< 0.4
Repeat 3	0	78.5	78.5
	1	< 0.5	< 0.5

Table 5-3. Survival of P. aeruginosa on fresh and abraded Cu_2O/PU coatings. Abraded coupons are as effective as the fresh ones. Two-tailed heteroscedastic P-value for $\log(CFU_{coated})$ of fresh vs abraded coatings is 0.42, i.e., we found no significant effect of the rubbing.

5.5. Discussion

5.5.1. Are Cells Killed or Are They Simply Trapped in the Matrix?

Our antimicrobial coatings are porous (See Supplementary Material Figure S5-2) and water permeable. The lack of viable bacteria that we detected in our CFU assay at zero time for *P. aeruginosa* and *S. aureus* (Table 5-1) raises the question of whether these bacteria are simply trapped in the porosity rather than killed, despite our vigorous efforts to shake them loose with 30 s of vortexing and 5 min of sonication. Here we discuss two lines of evidence for the hypothesis that these two bacterial strains were simply trapped in porosity rather than killed.

(1) We fabricated porous samples from glass, a material with no antimicrobial properties, and examined the recovery of *P. aeruginosa* from these samples. Recovery was defined as:

$$\%\ \text{recovery} = \frac{\text{mean}(\text{CFU}_{\text{coupon}})}{\text{mean}(\text{CFU}_{\text{suspension}})} \times 100\% \qquad \text{Equation 5-2}$$

where $\text{CFU}_{\text{suspension}}$ is from a 2 µL suspension droplet diluted and placed on agar, whereas $\text{CFU}_{\text{coupon}}$ is from an identical droplet that was placed on the glass coupon for 1 min. and then eluted with the same dilution volume. The average recovery was 27% (Data in Supplementary Material Table S5-4). This demonstrates that *P. aeruginosa* can be recovered from a porous sample. The 27% is much greater than the $<4.5\times10^{-4}$ % that were recovered from the Cu_2O/PU coating, which is consistent with the idea that the bacteria were not trapped in Cu_2O/PU. Glass is clearly a different material than Cu_2O so the trapping may be different.

(2) If viable bacteria are simply trapped and not killed, then we should be able to form colonies from these trapped bacteria. To detect residual viable bacteria within a (porous)

Cu_2O/PU coupon *after our extraction procedure*, we placed the coated side of the coupon on TSB agar and incubated in contact for 48 h. After 48 h, we peeled of the coupon and looked for colony formations upon further incubation. We found only at most one or two colonies on the plate compared to thousands of colonies that would need to be trapped to account for the results.

The Cu_2O/PU coating is only about ~15 μm thick, and so water and nutrient can easily be wicked or diffused over this distance. *P. aeruginosa* is motile so could migrate the ~15 μm [53]. Alternatively, viable, embedded cells could grow in diffused nutrients from the agar medium and progeny could reach the nutrient agar in time to grow a visible colony on the agar. This experiment shows that, given ideal growth conditions, trapped bacteria do not present an infection risk. Additionally, it suggests that viable bacteria are not present at all.

We also examined a Cu_2O/PU sample with no access to porosity to see its capability to kill *P. aeruginosa.* This experiment is simple to arrange, because, with time, our samples become hydrophobic due to a change in the PU that is used as the matrix. This hydrophobicity of the aged sample prevents access to the porosity. The samples used for the abrasion testing were aged, and the measured zero-time survival was 87%. Without the evidence in (1) and (2) above, this might be considered evidence for trapping in the regular samples. But given the above evidence, we have a different interpretation. When the bacteria penetrate into the porosity, there is a tremendous contact area with the active ingredient, and short diffusion distances that allows a very rapid kill compared to an impermeable material.

Considering the evidence in these experiments, we think that the bacteria is not trapped in the porosity, but that the porosity does contribute to killing of the bacteria in a shorter period of time.

5.5.2. Widespread application of the Cu_2O/PU coating

Given the microbiological success of the coating, we investigated the different types of materials that could be coated. In addition to stainless steel and glass reported previously [27], we found that the coating could be easily applied on polypropylene plastic, ABS plastic, granite, and wood. While we focused on 1 h time point throughout this work, commensurate with the US EPA standard [52], our Cu_2O/PU kills bacteria much more rapidly than in 1 h. After 10 minutes, for example, the relative survival of *P. aeruginosa* on the coating is <0.2% and that of MRSA is 14% (See Table S5-8 in Supplementary Material).

5.6. Conclusion

A Cu_2O and a CuO coating that are each highly effective against 9 pathogens, including bacteria, fungi, and yeast. The Cu_2O/PU coating was superior, leaving no survivors after 1 h for 8 of 12 organisms. The kill% was over 99.999% in 1 hour in high resolution experiments for *P. aeruginosa* and *S. aureus*. Survival was poor over a large range of cell densities, as high as 10^9 CFU per mL for *P. aeruginosa* and 10^8 CFU per mL for *S. aureus*. The efficacy of the Cu_2O/PU coating was unaffected by 10 repeat exposure/disinfection/rinse cycles over 20 weeks or by cycles of abrasion. The coating was less effective against mycobacteria and anthrax spores but these are typically difficult organisms to kill. The ability to pass durability testing and lack of cytotoxicity for human cells suggest that the Cu_2O/PU coating may be useful in hospital settings to reduce the transfer of microorganisms that are spread by contact.

Acknowledgement

This work used shared facilities at the Virginia Tech National Center for Earth and Environmental Nanotechnology Infrastructure supported by NSF (ECCS 1542100 and ECCS 2025151). We also thank Dr. Xu Feng, who captured the XPS spectra and the Surface Analysis Laboratory in the Department of Chemistry at VT, which is supported by the NSF under Grant No. CHE-1531834. We also thank Saurabh Sharma, who performed the abrasion testing, and Jared Arkfeld who helped prepare the substrate for Cu_2O/PU coating.

Conflict of Interest statement

WAD declares part ownership in a startup company that intends to produce surface coatings. Other authors declare no conflict of interest.

Funding Statement

This work was supported by the National Science Foundation (NSF) (Grant No. CBET-1902364), and by Virginia Tech's Proof of Concept program (grant number 238079), the Virginia Tech Institute for Critical Technology and Applied Science Center for Engineered Health, and the Virginia Tech Center for Emerging, Zoonotic, and Arthropod-Borne Pathogens.

REFERENCES

[1] Fonkwo PN. Pricing infectious disease: The economic and health implications of infectious diseases. EMBO reports 2008;9(S1):S13-S7.

[2] Buzby JC, Roberts T, Lin C-TJ, MacDonald JM. Bacterial foodborne disease: medical costs and productivity losses. 1996.

[3] Fauci AS, Touchette NA, Folkers GK. Emerging infectious diseases: a 10-year perspective from the National Institute of Allergy and Infectious Diseases. Int J Risk Saf Med 2005;17(3, 4):157-67.

[4] CDC. Antibiotic Resistance Threats in the United States, https://www.cdc.gov/drugresistance/pdf/threats-report/2019-ar-threats-report-508.pdf.

[5] Centers for Disease Control and Prevention. METHICILLIN-RESISTANT STAPHYLOCOCCUS AUREUS (MRSA), https://www.cdc.gov/drugresistance/pdf/threats-report/mrsa-508.pdf; [accessed June 2nd 2021.

[6] Centers for Disease Control and Prevention. MULTIDRUG-RESISTANT PSEUDOMONAS AERUGINOSA https://www.cdc.gov/drugresistance/pdf/threats-report/pseudomonas-aeruginosa-508.pdf; [accessed June 2nd 2021.

[7] Doron S, Gorbach S. Bacterial infections: overview. International Encyclopedia of Public Health 2008:273.

[8] Stephens B, Azimi P, Thoemmes MS, Heidarinejad M, Allen JG, Gilbert JA. Microbial exchange via fomites and implications for human health. Curr Pollut Rep 2019;5(4):198-213.

[9] Vos MC, Verbrugh HA. MRSA: we can overcome, but who will lead the battle? Infect Control Hosp Epidemiol 2005;26(2):117-20.

[10] de Abreu PM, Farias PG, Paiva GS, Almeida AM, Morais PV. Persistence of microbial communities including Pseudomonas aeruginosa in a hospital environment: a potential health hazard. BMC Microbiol 2014;14(1):1-10.

[11] Behzadinasab S, Chin AWH, Hosseini M, Poon LLM, Ducker WA. SARS-CoV-2 virus transfers to skin through contact with contaminated solids. Sci Rep 2021;11(1):22868. https://doi.org/10.1038/s41598-021-00843-0.

[12] Kramer A, Schwebke I, Kampf G. How long do nosocomial pathogens persist on inanimate surfaces? A systematic review. BMC Infect Dis 2006;6(1):1-8.

[13] Ross AA, Neufeld JD. Microbial biogeography of a university campus. Microbiome 2015;3(1):1-12.

[14] Wang H-P, Zhang H-J, Liu J, Dong Q, Duan S, Ge J-Q, et al. Antimicrobial resistance of 3 types of gram-negative bacteria isolated from hospital surfaces and the hands of health care workers. Am J Infect Control 2017;45(11):e143-e7.

[15] Kampf G, Todt D, Pfaender S, Steinmann E. Persistence of coronaviruses on inanimate surfaces and their inactivation with biocidal agents. J Hosp Infect 2020;104(3):246-51.

[16] Ledwoch K, Dancer S, Otter J, Kerr K, Roposte D, Maillard J. How dirty is your QWERTY? The risk of healthcare pathogen transmission from computer keyboards. J Hosp Infect 2021;112:31-6.

[17] Wang Y, Chen W, Chen Y, Tseng S, Chien L, Wu H, et al. Bacterial contamination on surfaces of public areas in hospitals. J Hosp Infect 2010;74(2):195-6.

[18] Otter JA, French GL. Survival of nosocomial bacteria and spores on surfaces and inactivation by hydrogen peroxide vapor. J Clin Microbiol 2009;47(1):205-7.

[19] Russotto V, Cortegiani A, Raineri SM, Giarratano A. Bacterial contamination of inanimate surfaces and equipment in the intensive care unit. J Intensive Care 2015;3(1):1-8.

[20] Fritz SA, Hogan PG, Singh LN, Thompson RM, Wallace MA, Whitney K, et al. Staphylococcus aureus contamination of environmental surfaces in households with children infected with methicillin-resistant S. aureus. JAMA Pediatr 2014;168(11):1030.

[21] Wendt C, Wiesenthal B, Dietz E, Rüden H. Survival of vancomycin-resistant and vancomycin-susceptible enterococci on dry surfaces. J Clin Microbiol 1998;36(12):3734-6.

[22] Noskin GA, Stosor V, Cooper I, Peterson LR. Recovery of vancomycin-resistant enterococci on fingertips and environmental surfaces. Infect Control Hosp Epidemiol 1995;16:577-.

[23] Cloutier M, Mantovani D, Rosei F. Antibacterial coatings: challenges, perspectives, and opportunities. Trends Biotechnol 2015;33(11):637-52.

[24] Salwiczek M, Qu Y, Gardiner J, Strugnell RA, Lithgow T, McLean KM, et al. Emerging rules for effective antimicrobial coatings. Trends Biotechnol 2014;32(2):82-90.

[25] Behzadinasab S, Williams MD, Hosseini M, Poon LL, Chin AW, Falkinham III JO, et al. Transparent and Sprayable Surface Coatings that Kill Drug-Resistant Bacteria Within Minutes and Inactivate SARS-CoV-2 Virus. ACS Appl Mater Interfaces 2021;13(46):54706-14.

[26] Adlhart C, Verran J, Azevedo NF, Olmez H, Keinänen-Toivola MM, Gouveia I, et al. Surface modifications for antimicrobial effects in the healthcare setting: A critical overview. J Hosp Infect 2018;99(3):239-49.

[27] Behzadinasab S, Chin A, Hosseini M, Poon L, Ducker WA. A surface coating that rapidly inactivates SARS-CoV-2. ACS Appl Mater Interfaces 2020;12(31):34723-7.

[28] Hutasoit N, Kennedy B, Hamilton S, Luttick A, Rashid RAR, Palanisamy S. Sars-CoV-2 (COVID-19) inactivation capability of copper-coated touch surface fabricated by cold-spray technology. Manuf Lett 2020;25:93-7.

[29] Hosseini M, Chin AW, Behzadinasab S, Poon LL, Ducker WA. Cupric oxide coating that rapidly reduces infection by SARS-CoV-2 via solids. ACS Appl Mater Interfaces 2021;13(5):5919-28.

[30] Sousa BC, Cote DL. Antimicrobial Copper Cold Spray Coatings and SARS-CoV-2 Surface Inactivation. MRS Adv 2020;5(56):2873-80.

[31] Hosseini M, Behzadinasab S, Chin AW, Poon LL, Ducker WA. Reduction of infectivity of SARS-CoV-2 by zinc oxide coatings. ACS Biomater Sci Eng 2021;7(11):5022-7.

[32] Hosseini M, Behzadinasab S, Benmamoun Z, Ducker WA. The Viability of SARS-COV-2 on Solid Surfaces. Curr Opin Colloid Interface Sci 2021:101481.

[33] Sunada K, Minoshima M, Hashimoto K. Highly Efficient Antiviral and Antibacterial Activities of Solid-State Cuprous Compounds. J Hazard Mater 2012;235:265-70.

[34] Aydin Sevinç B, Hanley L. Antibacterial activity of dental composites containing zinc oxide nanoparticles. J Biomed Mater Res B Appl Biomater 2010;94(1):22-31.

[35] Pasquet J, Chevalier Y, Pelletier J, Couval E, Bouvier D, Bolzinger M-A. The contribution of zinc ions to the antimicrobial activity of zinc oxide. Colloids Surf Physicochem Eng Aspects 2014;457:263-74.

[36] Young M, Ozcan A, Myers ME, Johnson EG, Graham JH, Santra S. Multimodal generally recognized as safe ZnO/nanocopper composite: A novel antimicrobial material for the management of citrus phytopathogens. J Agric Food Chem 2017;66(26):6604-8.

[37] El Saeed AM, Abd El-Fattah M, Azzam AM, Dardir MM, Bader MM. Synthesis of cuprous oxide epoxy nanocomposite as an environmentally antimicrobial coating. Int J Biol Macromol 2016;89:190-7.

[38] Akiyama T, Miyamoto H, Yonekura Y, Tsukamoto M, Ando Y, Noda I, et al. Silver oxide-containing hydroxyapatite coating has in vivo antibacterial activity in the rat tibia. J Orthop Res 2013;31(8):1195-200.

[39] Johnson JR, Roberts PL, Olsen RJ, Moyer KA, Stamm WE. Prevention of catheter-associated urinary tract infection with a silver oxide-coated urinary catheter: clinical and microbiologic correlates. J Infect Dis 1990;162(5):1145-50.

[40] Gopal V, Nilsson-Payant BE, French H, Siegers JY, Yung W-s, Hardwick M, et al. Zinc-Embedded Polyamide Fabrics Inactivate SARS-CoV-2 and Influenza A Virus. ACS Appl Mater Interfaces 2021;13(26):30317-25.

[41] Reddy ST, Chung KK, McDaniel CJ, Darouiche RO, Landman J, Brennan AB. Micropatterned surfaces for reducing the risk of catheter-associated urinary tract infection: an in vitro study on the effect of sharklet micropatterned surfaces to inhibit bacterial colonization and migration of uropathogenic Escherichia coli. J Endourol 2011;25(9):1547-52.

[42] Ivanova EP, Hasan J, Webb HK, Truong VK, Watson GS, Watson JA, et al. Natural bactericidal surfaces: mechanical rupture of Pseudomonas aeruginosa cells by cicada wings. Small 2012;8(16):2489-94.

[43] Hasan J, Xu Y, Yarlagadda T, Schuetz M, Spann K, Yarlagadda PK. Antiviral and antibacterial nanostructured surfaces with excellent mechanical properties for hospital applications. ACS Biomater Sci Eng 2020;6(6):3608-18.

[44] Gentili V, Pazzi D, Rizzo S, Schiuma G, Marchini E, Papadia S, et al. Transparent Polymeric Formulations Effective against SARS-CoV-2 Infection. ACS Appl Mater Interfaces 2021.

[45] Meghana S, Kabra P, Chakraborty S, Padmavathy N. Understanding the pathway of antibacterial activity of copper oxide nanoparticles. RSC Adv 2015;5(16):12293-9.

[46] Ren G, Hu D, Cheng EW, Vargas-Reus MA, Reip P, Allaker RP. Characterisation of copper oxide nanoparticles for antimicrobial applications. International journal of antimicrobial agents 2009;33(6):587-90.

[47] Pang H, Gao F, Lu Q. Morphology effect on antibacterial activity of cuprous oxide. Chem Commun 2009(9):1076-8.

[48] Li B, Li Y, Zhao Y, Sun L. Shape-controlled synthesis of Cu2O nano/microcrystals and their antibacterial activity. J Phys Chem Solids 2013;74(12):1842-7.

[49] Falkinham 3rd J, George K, Parker B, Gruft H. In vitro susceptibility of human and environmental isolates of Mycobacterium avium, M. intracellulare, and M. scrofulaceum to heavy-metal salts and oxyanions. Antimicrobial agents and chemotherapy 1984;25(1):137-9.

[50] Taylor RH, Falkinham III JO, Norton CD, LeChevallier MW. Chlorine, chloramine, chlorine dioxide, and ozone susceptibility of Mycobacterium avium. Applied and Environmental Microbiology 2000;66(4):1702-5.

[51] Brennan PJ, Nikaido H. The envelope of mycobacteria. Annu Rev Biochem 1995;64(1):29-63.

[52] Environmental Protection Agency. Antimicrobial Testing Methods & Procedures: Interim Method for Evaluating the Efficacy of Antimicrobial Surface Coatings https://www.epa.gov/pesticide-analytical-methods/antimicrobial-testing-methods-procedures-interim-method-evaluating. 2020.

[53] Chang Y-R, Weeks ER, Barton D, Dobnikar J, Ducker WA. Effect of topographical steps on the surface motility of the bacterium pseudomonas aeruginosa. ACS Biomater Sci Eng 2019;5(12):6436-45.

5.7. SUPPLEMENTARY MATERIAL

Antimicrobial Activity of Cuprous Oxide and Cupric Oxide-Coated Surfaces

Saeed Behzadinasab[†1], Mohsen Hosseini[†1], Myra D. Williams[2], Hannah M. Ivester[3], Irving C. Allen[3,4,5], Joseph O. Falkinham III[2], and William A. Ducker*[1]

*Corresponding Authors' Email: William Ducker wducker@vt.edu

[1]Department of Chemical Engineering and Center for Soft Matter and Biological Physics, Virginia Tech, Blacksburg, Virginia, 24061, USA

[2]Department of Biological Sciences, Virginia Tech, Blacksburg, Virginia, 24061, USA

[3]Graduate Program in Translational Biology, Medicine and Health, Virginia Tech, Roanoke, Virginia, 24016, USA

[4]Department of Biomedical Sciences and Pathobiology, Virginia-Maryland College of Veterinary Medicine, Blacksburg, Virginia, 24061, USA

[5]Department of Basic Science Education, Virginia Tech Carilion School of Medicine, Roanoke, Virginia, 24016, USA

[†] These authors contributed equally

5.7.1. Supplementary Materials and Methods

5.7.1.1. Abrasion Tests

Fresh Cu_2O/PU coating were abraded by a sponge (9.5 cm x 8 cm x 2.3 cm) mounted on an abrasion tester (Gardco D10V). The abrasion tester translates a sponge on the surface of the test sample (coupon) with a load of 0.45 kg, an amplitude of ~26 cm, and a period of ~5 s. The test was based on an United States (US) Environmental Protection Agency (EPA) protocol[1], which is employed to evaluate antimicrobial coatings for EPA registration for antimicrobial products to be distributed in the USA. Hospital surfaces are often cleaned with ethanolic solution, so our procedure diverged from the official EPA test by exposing the surface and sponge to 70% ethanol. Prior to conducting the tests, the sponge was wetted with 20 mL of 70% ethanol. An abrasion cycle was conducted as follows: the sponge was translated across the sample 8 times, then 70% ethanol was sprayed on the abrasion tester platform and the sample with a subsequent 30 minutes waiting period. 10 cycles (= 80 passes in total) were applied to the sample. A single sponge was used for the first 5 cycles and the sponge was replaced with a second sponge for the second 5 cycles.

5.7.1.2. Statistical Analysis

Hypothesis testing was done with Student t-tests, where *p*-values less than about 0.05 were indicative of significant differences from the null hypothesis. In some instances, colony counts of the copper coupons were below the limit of detection. In statistical tests these were

calculated at the detection limit (<1 CFU/plate), which overestimates the mean and underestimates the standard deviation.

5.7.1.3. Cytotoxicity Experiments

Lactate Dehydrogenase (LDH) is an enzyme naturally present in the cytosol of many cells. When cells die, the plasma membrane degrades, allowing LDH to be found outside of the cell membrane. For cell culture, this means that LDH is released into the media. The colorimetric assay used utilizes a two-step enzymatic reaction to produce a red formazan product that can then be read spectrophotometrically at 490nm[2]. Importantly, the level of the produced formazan byproduct is directly proportional to the level of LDH in the sample media, which can be inferred as a measure of cytotoxicity. In this assay, the use of a 10x Lysis buffer provides a positive control by disrupting the plasma membrane, allowing the release of cytosolic LDH into the media. By lysing a high percentage of cells, it provides a maximum baseline of LDH in the media which can be compared to treatment groups to determine the relative level of cytotoxicity induced by each treatment. These studies were performed in two cell lines- Thp1 cells and L929 cells. Thp1 cells (ATCC®TIB 202™) are human monocyte (white blood) cells that form part of the immune system, and generally do not adhere to solids. To perform a valid cytotoxicity experiment, we needed to obtain contact between the cell and the test solid. To force contact, a test solid (coupon) and a cell suspension were placed in a centrifuge tube and the tube was centrifuged in order to force contact with the test solid. The copper compounds did result in a visual color change in the media. In order to correct for this, we measured the absorbance of leachate from the cuprous oxide and cupric oxide as well as the copper sulfate in media in the

absence of cells, and we subtracted the appropriate baseline absorbance from the absorbance in the presence of cells.

5.7.2. Supplementary Results and Discussion

5.7.2.1. Characterization of Coatings

Figure S5-2 shows cross section scanning electron microscope (SEM) image of each coating. Both coatings were uniform in thickness, even though they were made by hand. The thickness of the Cu_2O/PU coating was 10-16 µm and the sintered CuO coating was ~32 µm. The expected stochiometric ratio for the coatings was observed as shown by X-ray photoelectron spectroscopy (XPS) data in Table S5-1. XPS samples only the outer few nanometers of the coating.

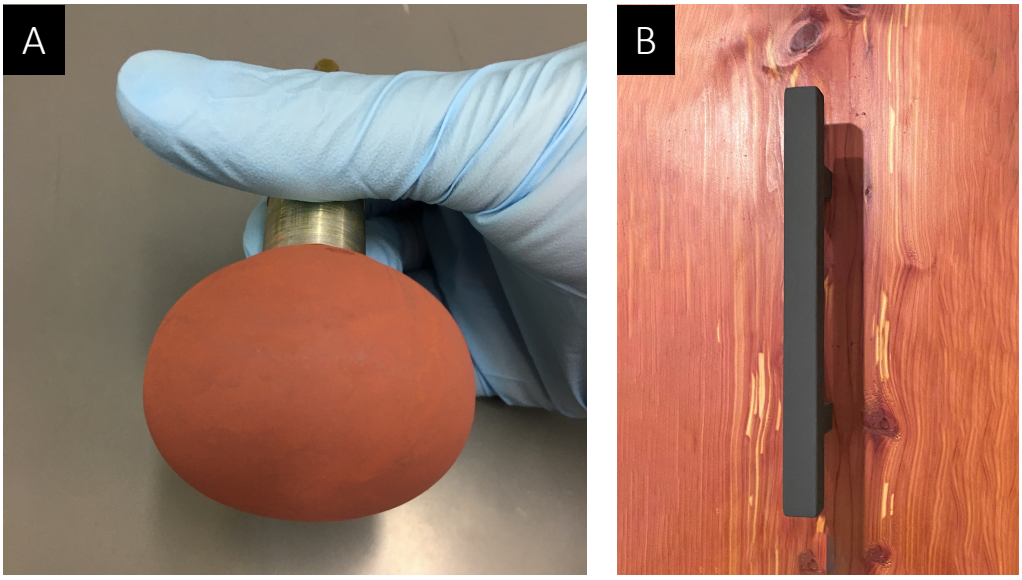


Figure S5-1. A) Optical images of the coatings. A) Cu_2O/PU that was made on a doorknob B) Sintered CuO that was made on a door handle.

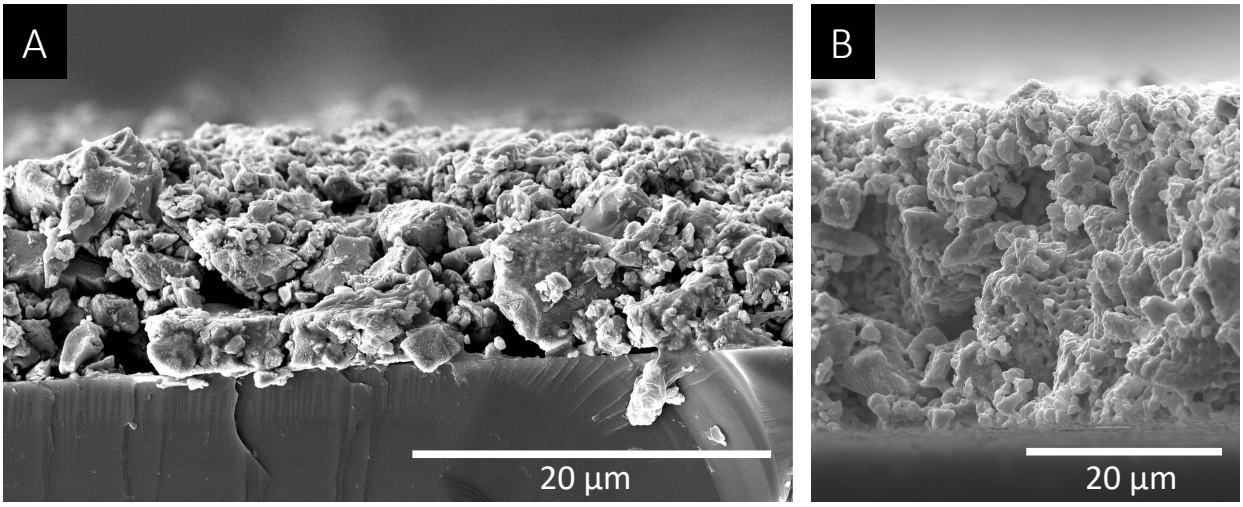


Figure S5-2. Cross section SEM images of the coatings. A) Cu_2O/PU and B) Sintered CuO.

Element	Cu_2O/PU	Sintered CuO
Copper	1.8	0.99
Oxygen	1	1

Table S5-1. XPS data of coatings. Both stoichiometric ratio are similar to theoretical ratios.

5.7.2.2. Tests of Microbial Survival on Surfaces

There Is a High Rate of Recovery of Microbial Cells from Stainless Steel Samples

We examined the hypothesis that we failed to recover all viable, colony-forming microbial cells from the stainless-steel samples. This hypothesis was tested by comparing the number of CFUs that were recovered from stainless steel to the number when a bacterial suspension was plated directly on agar. The number of CFUs from stainless steel were measured in the normal way, i.e., a bacterial suspension droplet was first placed on stainless steel and then the stainless-steel coupon was immediately transferred to 5 mL PBS, vortexed 30 secs and sonicated for 5 min and then 0.1 mL samples of the suspension spread on the agar medium surface. For all organisms (Table S5-2), the CFUs are similar: we performed a Student's t-test to check whether there was a significant difference between the recovered and the original CFU count and the p-value was > 0.05. For the two cases where the *p*-value was low, *C. albicans* and *M. abscessus,* the number of bacteria extracted from the stainless steel was *greater* than the input (rather than lesser), so the hypothesis of "failure to extract" should still be rejected.

Microbe strain	Colony-Forming Units/Plate (%)		Paired t-test
	Suspension	Stainless	p-value
S. aureus	582 ± 62 (100)	531 ± 47 (91)	0.6286
MRSA	33 ± 13 (100)	68 ± 4 (206)	0.2103
E. coli	45 ± 14 (100)	43 ± 8 (96)	0.9208
P. aeruginosa	1278 ± 25 (100)	1494 ± 71 (117)	0.2157
A. baumannii	157 ± 23 (100)	110 ± 11 (70)	0.3193
S. maltophilia	33 ± 7 (100)	31 ± 11 (94)	0.8743
C. albicans	55 ± 13 (100)	73 ± 8 (133)	0.1190
C. auris	165 ± 29 (100)	163 ± 0.7 (99)	0.8834
M. abscessus	79 ± 0.7 (100)	110 ± 11 (139)	0.1414
M. avium	1917 ± 86 (100)	1656 ± 223 (86)	0.4444

Table S5-2. Recovery of different microorganisms from stainless steel coupons.

Week	Cleaning/disinfection Treatment
1	The coupon was rinsed 3 times in DI water, then immersed in 70% ethanol for 30 mins. After which the coupon was left in air to dry.
2	Same as Week 1
3	Same as Week 2
4	The coupon was immersed in 3% Lysol for 30 mins, then rinsed 3 times in DI water.
5	Same as Week 4
7	Same as Week 4
8	The coupon was rinsed with H_2O; vortexed in H_2O; vortexed in ethanol, rinsed with H_2O, vortexed in H_2O.
9	The coupon was immersed in 3% lysol for 30 mins, then it was immersed in 70% ethanol for 1 min (3 times). After which it was rinsed 3 times in DI water (each for 1 min).
10	Same as Week 9
20	Same as Week 9

Table S5-3. Details of cleaning/disinfection cycles for each week. Note that in each case, the disinfectant was removed by either rinsing with water or for ethanol by air drying before subsequent testing of the antimicrobial

There Is a High Rate of Recovery of Microbial Cells from an Inactive Porous Medium

We examined the possibility that we achieved poor recovery from the porous materials. We examined this hypothesis by measuring recovery from an inert porous material, porous glass (size = ~12x12mm), to help to distinguish the role of porosity from an active surface. 2µL of *P. aeruginosa* was placed on the porous glass sample, and after 1-2 minutes, the sample was vortexed (for 1 min), sonicated (for 1 min), and again vortexed. Then the suspension was plated as mentioned in Materials & Methods section. The experiment was repeated 3 times, and the data is shown in Table S5-4. We found that 27% of the bacteria is recovered from an inert sample.

		CFU/plate
Porous glass	Repeat 1	197
	Repeat 2	388
	Repeat 3	198
Suspension	**---**	1494

Table S5-4. Recovery data of porous glass and the suspension used.

Microbial-killing is Not Affected by Carryover of Antimicrobials from the Coupon to the CFU Assay

Our reported killing times indicate the time period during which droplets of bacterial suspension remained on the antimicrobial test solid. It was possible, however, that dissolved ions or particles from the copper oxide surface that are shaken loose by sonication and vortexing could be carried over into our CFU assay and there inhibit colony formation. Colony formation occurs over 48 h, which is much longer than the 1-2 h of contact with the test solid, and this large difference in time-scales means that subtle carry-over effects may influence our results. In a test of an antimicrobial *solid* almost all of the antimicrobial is removed by physical removal of the antimicrobial solid before the CFU assay is performed. This is very different to a test of an antimicrobial *liquid* where the antimicrobial liquid is much more difficult to extract. However, even for a solid, there remains that possibility of some antimicrobial carryover.

To determine the possibility of carryover, we utilized Dey-Engley (DE) buffer, which is specifically formulated to contain compounds that are able to block or inhibit killing by a wide variety of antimicrobial agents, including metals [3]. This type of buffer is sometimes referred to as a neutralizer. We compared CFU counts when elution from the solid was done with PBS and DE buffers. Two bacteria, *P. aeruginosa* and MRSA were examined; all statistics were calculated in Microsoft Excel.

In contrast to PBS, DE buffer contains nutrients and other species that may aid the survival of the bacterial, so we first compared bacterial survival in the buffer (i.e., no coupon used). Our results, shown in Table S5-5A, show that that there is greater survival in DE buffer for both organisms, and that the effect is larger for MRSA (linear regression using two factors,

buffer (p = 0.0035) and bacterium (p = 0.0066)). To control for this increased survivability, in further statistical results in section 2.2.3, we normalized results by the average survivability for the particular bacterium and buffer combination.

To test for the effect of "neutralizing" antimicrobials from the solid, the bacteria were initially suspended in PBS and then a 10 μL droplet was placed on the solid for a specified time. For elution, the coupon was transferred to either 5 mL of PBS or 5 mL of DE Broth, vortexed for 10 sec and then sonicated for 1 minute before spreading 0.1 mL samples on Tryptic Soy Agar plates. Those manipulations took about 3 min. Samples were incubated at 37° C overnight and then colonies were counted. The results, shown in Table S5-5B, demonstrate that both bacteria are killed by Cu_2O, even when the DE buffer was used.

We performed a regression analysis (Table S5-6) with the following variables: bacterium (*P. aeruginosa* vs MRSA), surface type (stainless steel vs Cu_2O/PU), buffer type (PBS vs DE), and time (0 vs 60 min). The p-value of 0.95 for buffer is consistent with no effect of the buffer and therefore no effect of carryover.

The resolution of the effect of buffer on the 60 minute samples was, however, diminished by the very poor survival in both buffers. In the above analysis, results at the detection limit were analyzed as if they were at the detection limit, which inflates the p-value for buffer. When we excluded the 60 min samples from the analysis and repeated the regression, the p-value for the buffer dropped to 0.87 but remained high. This is consistent with the idea that extraction of species during the sonication and vortexing of the copper coupons did not cause a carry-over effect.

Strain	Buffer	Log(CFU)
P. aeruginosa	PBS	6.36
		6.33
		6.34
	DE	6.53
		6.49
		6.49
MRSA	PBS	5.28
		5.19
		5.30
	DE	6.46
		6.35
		6.43

Table S5-5A. Effect of buffer on CFU counts with no coupon present.

Bacterium	Surface	Time* (min)	Repeat	Log(CFU)	
				PBS	DE broth
Pseudomonas aeruginosa	Cu_2O/PU	0	1	6.47	6.51
			2	6.30	6.56
			3	6.29	6.51
		60	1	<	<
			2	<	<
			3	<	<
Pseudomonas aeruginosa	Stainless steel	0	1	6.43	6.54
			2	6.27	6.53
			3	6.35	6.48
		60	1	5.09	6.08
			2	5.016	5.95
			3	5.07	6.15
MRSA	Cu_2O/PU	0	1	5.21	6.30
			2	4.94	6.39
			3	5.53	6.43
		60	1	<	3.32
			2	<	<
			3	<	<
MRSA	Stainless steel	0	1	5.50	6.36
			2	5.18	6.42
			3	5.44	6.37
		60	1	5.13	6.31
			2	5.33	6.31
			3	5.35	6.37

Table S4-5B. Effect of buffer on Cu_2O coupon experiments. Bacteria were inoculated on stainless steel or Cu_2O/PU coupons, and extracted into PBS or DE broth. < indicates below the detection limit, which

was 1.70 in this experiment. Regression analysis of this data (Table S5-6) found that effect of buffer is not significant.

Variable	Coefficients	P-value	note
Bacterium	-0.378	0.232	not significant
Surface	-1.98	1.087E-07	significant
Buffer	-0.0212	0.946	not significant
Time	-0.0397	1.50E-09	significant

Table S5-6. Regression analysis results for data in Table S5-5.

5.7.2.3. Survival of P. aeruginosa and S. aureus at Higher Cell Densities

To obtain a clear resolution, we repeated the experiment in 3.3. with two bacteria (*P. aeruginosa and S. aureus)* that had much higher cell densities. The results are shown in Table S5-7 and they clearly show that the Cu_2O/PU coating is very effective. Only 0.0003% of *P. aeruginosa* and 0.0007% of *S. aureus* survived After one hour of contact with the coating.

Strain	**Time* (hr)**	**% Survival**	
		Cu_2O/PU	**Sintered CuO**
Pseudomonas aeruginosa (Density = 7,280,000 CFU/coupon)	0	57.1 ± 0.02	71.4 ± 0.01
	1	< 0.0003	34.3 ± 0.01
	2	< 0.0008	73.6 ± 0.03
	3	< 0.0007	55.0 ± 0.04
Staphylococcus aureus (Density = 3,760,000 CFU/coupon)	0	94.1 ± 0.02	133.0 ± 0.04
	1	< 0.0007	37.3 ± 0.02
	2	< 0.0007	6.5 ± 0.02
	3	< 0.001	30.7 ± 0.03

Table S5-7. Survival of *P. aeruginosa* or *S. aureus* on cuprous oxide/polyurethane (Cu_2O/PU) or sintered cupric oxide (CuO) coatings with high initial loading of bacteria. The initial density of *P. aeruginosa* was 7,280,000 CFU/coupon and for *S. aureus* 3,760,000 CFU/coupon**.** Even at this high load, no colonies grew for Cu_2O/PU.

5.7.2.4. Bacterial Killing as a Function of Cell Density

It is advantageous for a coating to kill bacteria in suspensions with a range of bacterial densities. To measure whether cell killing was reduced at higher cell densities, the survival of a 10-fold dilution series of *P. aeruginosa* and MRSA cells was prepared. 60 min after a 10 μL droplet was placed on the Cu_2O/PU coating, the survival of cells was measured by colony-formation. Results (Figure S5-3) show that survival was reduced by 3 logs for all the dilutions where we had resolution. For very dilute suspensions, there were insufficient survivors to resolve 3 logs. The coating killed all of the *S. aureus* in 60 minutes except for the highest cell density (10^7 CFU/10 μL). Likewise, all of the *P. aeruginosa* was killed in 60 min except at the highest concentration (10^7 CFU/10 μL) and after 180 minutes there were no survivors.

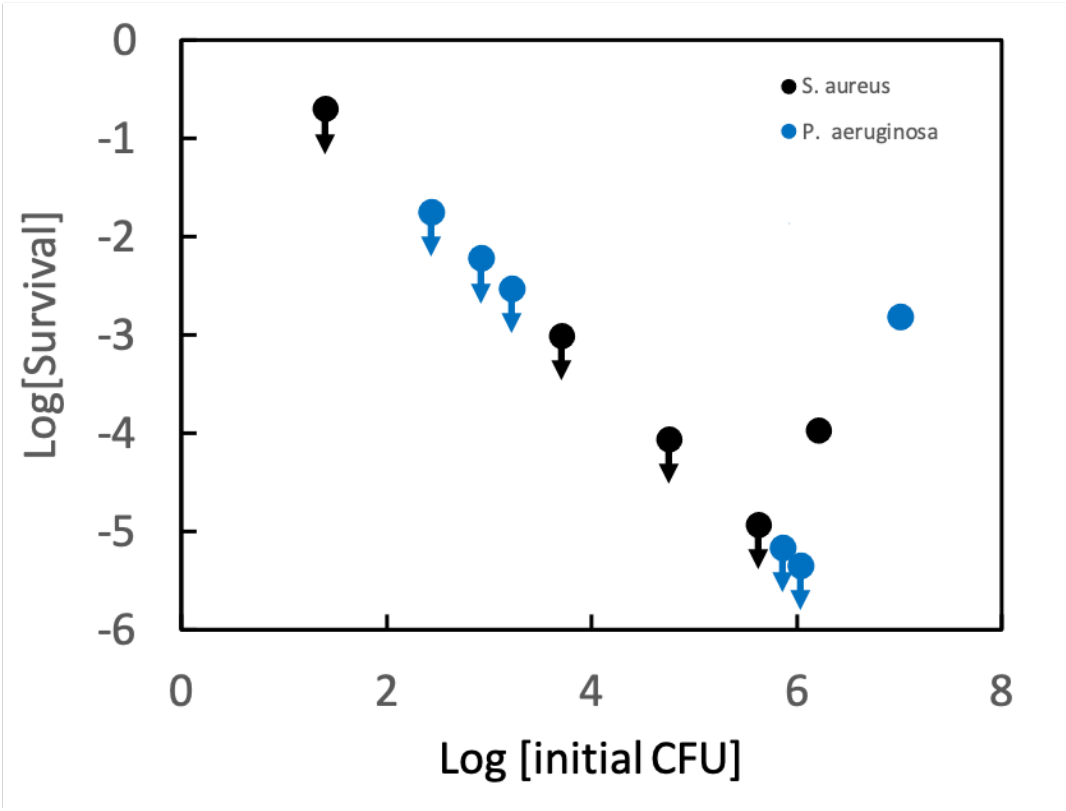


Figure S5-3. Effect of initial bacterial concentration on survival of *S. aureus* or *P. Aeruginosa* on the Cu_2O/PU coating after 60 minutes. The horizontal axis shows the measured CFU from a series dilution of bacteria, starting at 1.9 x 10^6 and diluted by 1/10 for each data point going from right to left. The vertical axis shows the survival, measured by CFU count of the bacteria on the coating. Fewer than 5 bacteria were found for all but the most concentrated bacterial suspension, so the data shows an upper bound as indicated by an arrow. Many upper bounds fall on a line because the dilution changes by a factor of 10 while the resolution of colonies remains constant. Results are the same if the bacteria are on the coating for 180 min., except that for *P. Aeruginosa* in the most concentrated suspension, no cells survived.

5.7.2.5. Cu_2O/PU Coating Kills Bacteria Rapidly

The EPA standard period for 3 logs (99.9%) killing of bacteria is1 hr [1]. We tested our Cu_2O/PU coating at shorter timepoints, and found that it kills bacteria very rapidly (See the Table below). As a reminder, relative survival compares the survival on the coated and uncoated samples:

$$\%\ \text{relative survival} = \frac{\text{mean}(\text{CFU}_{\text{coated}})}{\text{mean}(\text{CFU}_{\text{uncoated}})} \times 100\%$$

Bacterium	Time* (min)	Repeat	Relative survival (%)	Average Relative survival (%)
Pseudomonas aeruginosa	0	1	7.92	7.6
		2	7.37	
		3	7.42	
	5	1	0.07	0.04
		2	0.01	
		3	0.06	
	10	1	<0.01	0.20
		2	0.52	
		3	0.07	
MRSA	0	1	31.87	29
		2	29.94	
		3	26.16	
	5	1	20.11	17
		2	14.60	
		3	15.08	
	10	1	17.27	14
		2	8.57	
		3	16.23	

Table S5-8. Relative Survival of bacteria on Cu_2O/PU coating. Within 10 minutes, relative survival of *P. aeruginosa* and *MRSA* are <0.2% and 14%, respectively.

5.7.2.6. Comparison of killing of S. aureus and Methicillin-resistant S. aureus by Sintered CuO Coating at 0 Time Point

In our survey of multiple organisms, there was a large, unexpected, difference in results for the two *S. aureus* strains on CuO at zero time. We followed initial experiments with further experiments to examine the null hypothesis that these the results for the two strains at this specific condition were the same. The results for the repeat test are shown in Table S5-9, and the result for the Student's t-test was $p = 0.77$, so we were unable to reject the hypothesis that the two stains have the same killing rates.

Strain	**Time (min)**	**Repeat**	**Relative survival (%)**
Non-resistant	0	1	118.3
		2	62.7
		3	142.5
		average	108
Resistant	0	1	118.6
		2	167.2
		3	71.0
		average	119

Table S5-9. Zero-time survival of *S. aureus* by Sintered CuO for two strains.

5.7.2.7. Survival of bacteria on uncoated stainless-steel control

Bacteria can die on their own on uncoated surfaces at a slow rate. Table S5-10 reports the data for survival of bacteria on uncoated stainless steel control.

Bacterium	**Time* (min)**	**Average (Colony-Forming Units/Plate)**
Pseudomonas aeruginosa	suspension	547
	0	669
	5	631
	10	658
	suspension	878
	0	594
	60	686
MRSA	suspension	287
	0	244
	5	269
	10	271
	suspension	1075
	0	1196
	60	870

Table S5-10. Survival of bacteria on uncoated stainless-steel control

References

[1] Environmental Protection Agency. Antimicrobial Testing Methods & Procedures: Interim Method for Evaluating the Efficacy of Antimicrobial Surface Coatings https://www.epa.gov/pesticide-analytical-methods/antimicrobial-testing-methods-procedures-interim-method-evaluating. 2020.

[2] Willingham SB, Allen IC, Bergstralh DT, Brickey WJ, Huang MT-H, Taxman DJ, et al. NLRP3 (NALP3, Cryopyrin) facilitates in vivo caspase-1 activation, necrosis, and HMGB1 release via inflammasome-dependent and-independent pathways. J Immunol 2009;183(3):2008-15.

[3] Dey B, Engley Jr F. Methodology for recovery of chemically treated Staphylococcus aureus with neutralizing medium. Appl Environ Microbiol 1983;45(5):1533-7.

Chapter 6. Facile Implementation of Antimicrobial Coatings through Adhesive Films (Wraps) Demonstrated with Cuprous Oxide Coatings

Saeed Behzadinasab[1,2,3], Myra D. Williams[4], Joseph O. Falkinham III[4], and William A. Ducker*[1,2,3]

[1]Department of Chemical Engineering, Virginia Tech, Blacksburg, Virginia, 24061, USA

[2]Center for Soft Matter and Biological Physics, Virginia Tech, Blacksburg, Virginia, 24061, USA

[3]Macromolecules Innovation Institute, Virginia Tech, Blacksburg, Virginia, 24061, USA

[4]Department of Biological Sciences, Virginia Tech, Blacksburg, Virginia, 24061, USA

Keywords: antimicrobial, antibacterial, wrap, copper, cuprous oxide, Cu2O, coating, bacteria, polydopamine, polyurethane

ORCIDs:

Saeed Behzadinasab: 0000-0002-6271-2623

Joseph O. Falkinham III: 0000-0002-4391-9012

William A. Ducker: 0000-0002-8207-768X

6.1. Abstract

Antimicrobial coatings have a finite lifetime because of wear, depletion of the active ingredient, or surface contamination that produces a barrier between the pathogen and the active ingredient. The limited lifetime means that facile replacement is important. Here, we describe a generic method for rapidly applying and reapplying antimicrobial coatings to common-touch surfaces. The method is to deposit an antimicrobial coating on a generic adhesive film (wrap), and then to attach that modified wrap to the common-touch surface. In this scenario, the adhesion of the wrap and antimicrobial efficacy are separated and can be optimized independently. We demonstrate the fabrication of two antimicrobial wraps, both using cuprous oxide (Cu_2O) as the active ingredient. The first uses polyurethane (PU) as the polymeric binder and the second uses polydopamine (PDA). Our antimicrobial PU/Cu_2O and PDA/Cu_2O wraps, respectively, kill >99.98% and >99.82% of the human pathogen, *P. aeruginosa,* in only 10 min, and each of them kill >99.99% of the bacterium in 20 min. These antimicrobial wraps can be removed and replaced on the same object in <1 min with no tools. Wraps are already frequently used by consumers to coat drawers or cars for aesthetic or protective purposes.

6.2. Introduction

The human and economic burdens of infectious disease are vast [1–5]. Reducing the frequency of infections reduces this burden and reduces the demand for antibiotics and the concomitant danger of selection for antibiotic resistance in microorganisms [6–8]. Antibiotic resistance has worsened recently [9–11], and sadly, more than one million people die every year from antibiotic-resistant bacterial infections [8]. These infections occur both in healthcare settings [12] and in the general public domain. Infections occur via a number of routes, and here, we focus on transmission via contaminated solids, also known as fomite transmission [13,14].

The most common strategy to inhibit disease transmission via fomites is to disinfect solid surfaces by wiping them with bleach or 70% ethanol, but it is time-consuming to wipe many surfaces, and some disinfectants (e.g., bleach) are hazardous [15]. Perhaps most importantly, there is no protection subsequent to disinfection: the surface can be re-contaminated within minutes. An alternate approach is to provide ongoing protection with a surface coating that inactivates, or kills, pathogens for an extended period (e.g., weeks) after the coating is applied. Such coatings have shown effectiveness against a variety of pathogens [16–27]. Important aspects of antimicrobial coatings are that they do not use antibiotics and therefore are less likely to contribute to antibiotic resistance, and they operate outside the body. They provide an additional approach rather than an alternative measure against infection. Work by Ellingson et al. [28] has demonstrated the efficacy of antimicrobial surface coatings in a hospital setting; the coating caused significant reductions in both the number of bacteria detected on surfaces and the number of healthcare-acquired infections (HAI). Furthermore, Marik et al. showed that the use of copper oxide coatings on hard surfaces in a hospital was correlated with a reduction in infections [29].

Antimicrobial coatings can be either incorporated during the manufacture of an object or applied to the finished object. Application to existing facilities is particularly important for a rapid response to evolving situations such as the COVID-19 pandemic: it is expensive and time-consuming to replace many common-touch items (e.g., bed railings) in a short period of time. Ideally, the installation of antimicrobial coatings in existing facilities should be rapid and should not require sophisticated technical skills or equipment so that it can be carried out by non-experts on site.

In this manuscript, we describe a method for rapidly applying an antimicrobial coating to common-use objects. The method is simple. We prepare an antimicrobial coating with an adhesive backing layer that can be simply applied to a solid by removal of the backing paper, application to the solid, and sometimes followed by moderate pressure onto the solid. This type of coating is common for cars, where it is called a wrap, or for lining drawers, where it is called contact paper, and is available in sheets with dimensions of meters. The primary criteria for the preparation of the antimicrobial wrap are that application of the antimicrobial layer does not degrade the integrity of the wrap and does not reduce its ability to adhere to surfaces. The use of a wrap also solves an important problem with antimicrobial coatings. Antimicrobial coatings have a finite lifetime because of wear, depletion of the active ingredient, or surface contamination (e.g., oils from skin) that produces a barrier between the pathogen and the active ingredient. When the coating is no longer functional, the coating must be cleaned (to remove contamination) or removed and replaced with a functional coating. The removal step can be time-consuming as is well-known for repainting houses, etc. For situations where the coating must be replaced frequently, the time for replacement is a significant cost, whether or not the old coating must be removed. In situations such as these, a wrap is very efficient. When the old

coating is compromised, the wrap is peeled off, and a new wrap is applied. The adhesive properties of the wrap can be optimized for easy removal or longevity, depending on the application. In general, the adhesion and the antimicrobial layer can be optimized independently.

This work describes two antimicrobial wraps that allow the very easy conversion of a common-touch surface into an antimicrobial common-touch surface. Both wraps utilize a potent antimicrobial material: cuprous oxide (Cu_2O) [30,31]. Cu_2O has broad antimicrobial activity against many pathogens, for example, against *Pseudomonas aeruginosa, Escherichia coli, Staphylococcus aureus,* and *Enterococcus hirae* [18,32,33], and methicillin-resistant *S. aureus* (MRSA) [18,19]. The wraps were coated with Cu_2O using previously developed coatings [18–20] that were shown to rapidly inactivate a variety of pathogens and were robust to abrasion [19]. The other ingredients in these coatings were shown to be inactive.

We provide measurements of the bactericidal activity of the Cu_2O wraps against *P. aeruginosa. P. aeruginosa* is labeled by the United States (US) Center for Disease Control (CDC) as a serious threat [34] because *P. aeruginosa* has developed antibiotic resistance to many antimicrobials [35,36]. Of particular relevance to this study, it remains viable [37] and forms biofilms on surfaces [38].

To illustrate the versatility, we prepared two antimicrobial coatings on the same commercial wrap, which was adhesive-backed polyethylene (PE). The first wrap was prepared using polyurethane (PU/Cu_2O wrap), which caused a 99.97% reduction in *P. aeruginosa* colony-forming units (CFUs) in 10 min and >99.99% in 20 min. The second used polydopamine (PDA/Cu_2O wrap) which caused a reduction of 99.80% in 10 min and >99.99% in 20 min. Polydopamine (PDA) has numerous advantages: it is derived from natural sources, uses water as

the polymerization medium, has a high LD_{50} (~500 mg/kg), and polymerizes on most solid materials [39,40].

6.3. Results

6.3.1. Preparation and Characterization of the Antimicrobial Wraps

The fabrication of both wraps is uncomplicated. The PU/Cu_2O wrap was prepared in a two-step procedure where a PE wrap was first coated with polyurethane (PU), and then, a suspension of Cu_2O in ethanol was cast on the tacky PU layer. The sample was heated for 2 h to accelerate the cure of PU. Scanning electron microscopy (SEM) images of the coating are presented in Figure 6-1. The PU/Cu_2O coating only had a thickness of 10–20 µm, and the loading of particles in the PU/Cu_2O wrap was 4.5×10^{-3} g/cm^2. Because the coating is thin, only a very small amount of copper is used per area, which reduces the cost of implementation.

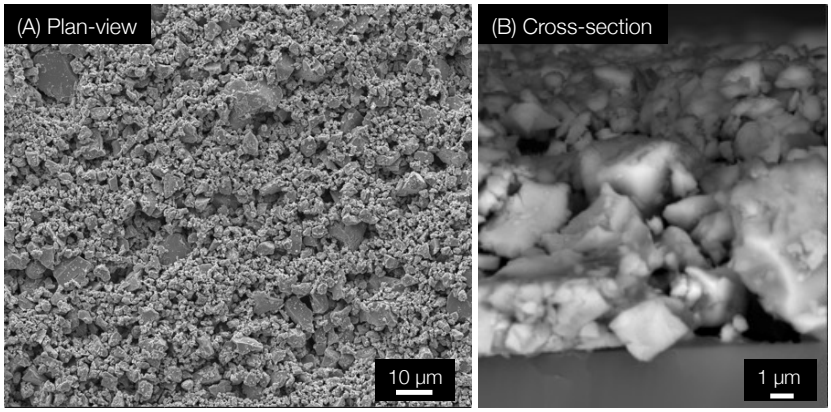


Figure 6-1. (**A**) Plan-view and (**B**) cross-section SEM images of PU/Cu_2O wrap. The thickness of the coating was approximately 12 µm. For SEM imaging, the coating was prepared on glass.

The PDA/Cu_2O wrap was prepared by applying a suspension of Cu_2O in dopamine to the uncoated wrap, and then, it was heat-treated to complete the polymer cure. Figure 6-2 shows

SEM images of the PDA/Cu_2O wrap. As shown in Figure 6-2B, the Cu_2O particle morphology is visible, indicating that the particles protrude from the coating and therefore are accessible to solutions and bacterial suspensions. The particles form a much sparser layer on the solid compared to the PU/Cu_2O wrap. The PDA/Cu_2O wrap has a loading of 0.13×10^{-3} g/cm^2 of Cu_2O particles, which is about 1/35th of the loading of PU/Cu_2O wrap, thereby enabling even lower costs of the active ingredient.

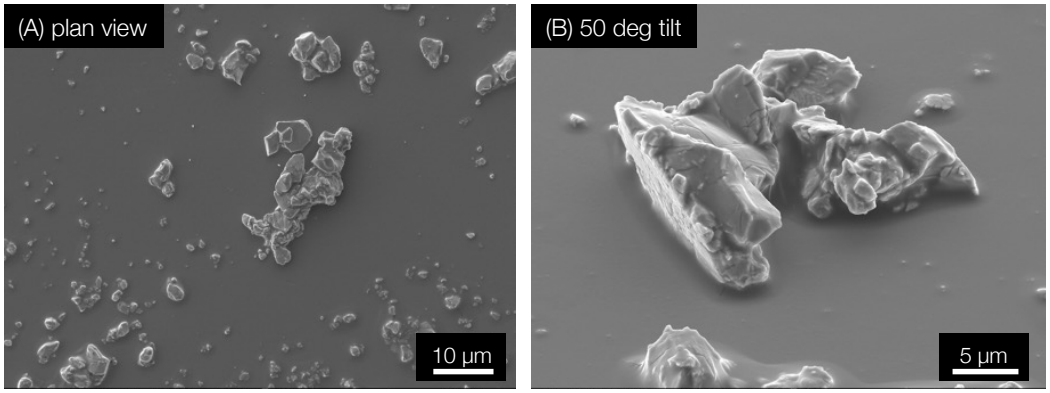


Figure 6-2. SEM images of PDA/Cu2O wrap. (A) Plan-view SEM image and (B) 50 degree tilt image. The coating was prepared on glass.

6.3.2. The Wraps are Highly Antimicrobial

The antimicrobial activities of the wraps were tested by placing a 5 µL droplet of approximately 1.6×10^7 CFU/mL *P. aeruginosa* on each wrap, waiting for a preset interval (0, 10, or 20 min), and extracting the bacteria from the solid, followed by counting the colonies formed by bacteria that remained viable (CFUs). The resulting CFUs were compared to the input CFUs to obtain the log survival, as defined by the following equation:

$$\log \text{survival} = \text{mean}[\log_{10}(\text{sample CFU})] - \text{mean}[\log_{10}(\text{input CFU})] \quad \text{Equation 6-1}$$

Both wraps caused a large decrease in the bacterial viability in a short period of time.

For the PU/Cu2O wrap, as shown in Figure 6-3, the log (CFU) decreased by 3.8 log units (99.984% killing) within 10 min, and no colonies were detected after 20 min (>99.998% killing), demonstrating excellent antimicrobial properties. The fitted half-life was 1.3 min (95% CI of 0.88–2.69 min). The half-life was calculated using Equation 6-2 in the Section 4. Bacteria can die on surfaces that do not have active ingredients, and for this reason, the US Environmental Protection Agency (EPA) [41,42] uses as its metric a comparison to the uncoated solid. For this reason, we also calculated "reduction" (see Equation 6-5) in the Section 4) to compare the coated and uncoated wrap. The PU/Cu2O wrap caused a reduction of 99.97% of *P. aeruginosa* in 10 min, and >99.99% (4 log reduction) in 20 min. For registration, the EPA requires an antimicrobial coating to cause a minimum 3-log (99.9%) reduction in 1 h; the wrap achieved a greater reduction in only 10 min. Using the 99.9% reduction from the control as our metric, we performed Student's *t*-tests separately on the 10 min and 20 min data, comparing 1/1000th of the control CFUs to the wrap CFUs to show that the antimicrobial wrap caused a reduction of >99.9% ($p < 0.001$) compared to the uncoated wrap after 20 min, but that this target was not achieved in 10 min ($p = 0.22$).

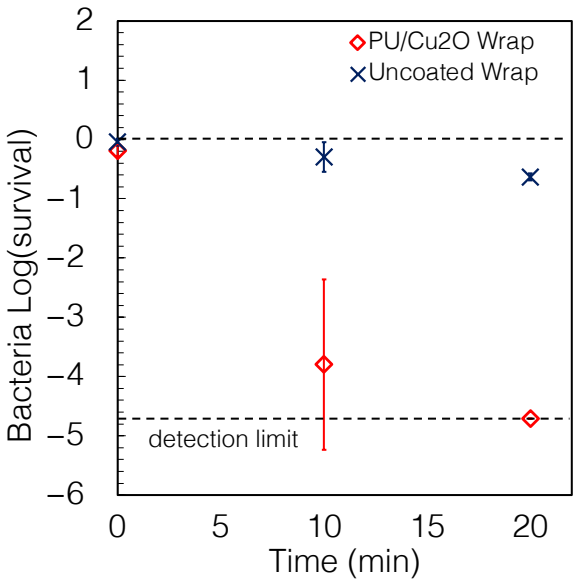


Figure 6-3. Survival of *P. aeruginosa* on PU/Cu_2O wrap. The PU/Cu_2O wrap caused a reduction of 99.97% and >99.99% of *P. aeruginosa* in 10 and 20 min, respectively, compared to the uncoated wrap. Survival was calculated using Equation 6-1. Each point in this and subsequent figures of survival represents the average of three independent measurements, and the error bars represent the standard deviation. Some error bars are smaller than the size of the symbols.

The preparation of the PU/Cu_2O coating described above included heat and plasma treatments, whereas for simplicity, it would be beneficial to prepare a coating that does not require these steps. We prepared a second set of PU/Cu_2O coatings with no heat or plasma treatment. As shown in Figure 6-4, these wraps killed 95.177% of bacteria in 10 min and >99.996% in 20 min, i.e., a slightly reduced performance than the wrap with the extra treatments at 10 min but no resolved difference at 20 min. The reduction compared to the uncoated control was again >99.9% (p = 0.003) for 20 min of exposure.

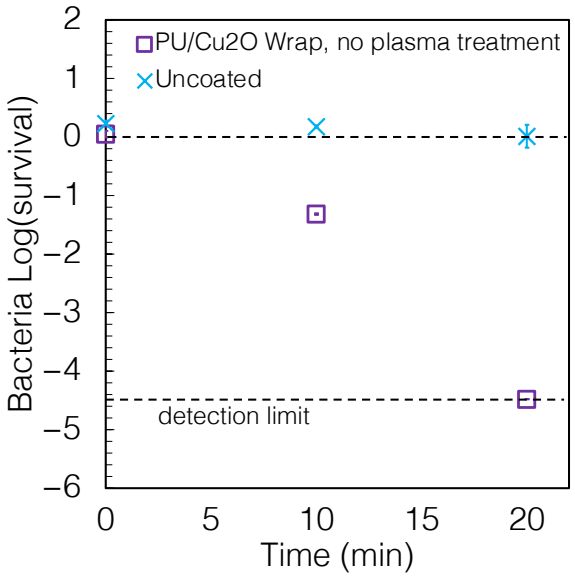


Figure 6-4. Survival of *P. aeruginosa* on PU/Cu_2O wrap that was not heat-treated or plasma-treated. The wrap caused a reduction of 96.81% and >99.99% of *P. aeruginosa* in 10 and 20 min, respectively. Some error bars are smaller than the size of the symbols.

The PDA/Cu_2O wrap was also extremely effective against *P. aeruginosa*, as shown in Figure 6-5. The wrap killed 99.826% in 10 min and >99.995% in 20 min and had a half-life of 1.38 min (95% CI of 1.10–1.85 min). It caused a reduction of 99.80% and >99.99% of the bacterium in 10 and 20 min, respectively. It is important to note that this very similar level of performance was achieved with about 1/35th of the loading of the PU/Cu_2O wrap. This shows that the Cu_2O is a very potent antimicrobial, and it is unnecessary to provide the high loading of the PU/Cu_2O wrap to achieve a good performance in these tests.

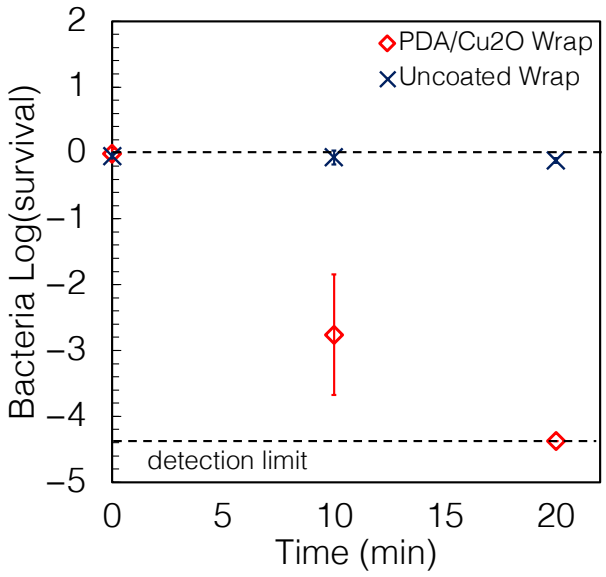


Figure 6-5. Survival of *P. aeruginosa* on PDA/Cu_2O wrap. The PDA/Cu_2O wrap caused a reduction of 99.80% and >99.99% of *P. aeruginosa* in 10 and 20 min, respectively. The reduction compared to the uncoated wrap was >99.9% ($p < 0.001$) again for 20 min exposure.

6.3.3. The Antimicrobial Wraps is Easy to Replace

Recall that the motivation for this work is the simple replacement of an antimicrobial coating to overcome the problems of wear and contamination. Both the PU/Cu_2O and PDA/Cu_2O wraps were designed for rapid replacement. Figure 6-6 is a series of photographs where a PU/Cu_2O wrap was added and then replaced. The replacement of the coating took less than 1 min and was achieved without tools.

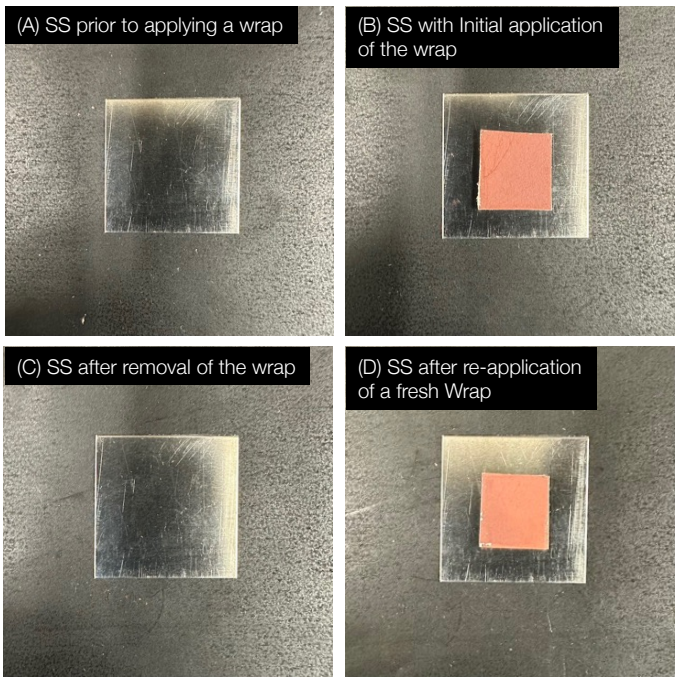


Figure 6-6. Series of photographs demonstrating the ability to apply, remove, and reapply an antimicrobial wrap to stainless steel (SS). (**A**) Bare SS. (**B**) Initial application of antimicrobial wrap to SS. (**C**) After removal of wrap. (**D**) After application of a new antimicrobial wrap to the same SS. Removal and replacement of the wraps took less than one minute.

6.3.4. Other Characteristics of the Coating

Here, we discuss characteristics of the specific coatings that we used on the wraps. The PU/Cu_2O coating used ethanol, which is a relatively safe solvent. The polymerization of dopamine only requires water as the solvent. Both coatings require a low temperature to complete the cure (80 or 120 °C), and we found that heating was not even required for the PU coating. In any case, this heat treatment is not required on site but is only used for manufacturing. Paintable PU formulations have some toxicity due to the evaporation of solvents, but this need only be carried out during the manufacture of the wrap, not at the implementation site. The Median Lethal Dose (LD_{50}) of polydopamine is high, about 500 mg/kg [43]. Cuprous

oxide is an abundant material made from recycled copper and costs only a few dollars per kg. Additionally, other materials used in this study are inexpensive, which is beneficial for implementation. Furthermore, the coatings remain potent after a long time. For example, as seen in Figure 6-7, 3.5-month-old PU/Cu_2O wrap (no plasma or heat-treatment) that was tested against *P. aeruginosa* remained active against the bacterium. Finally, the processes used to prepare both antimicrobial wraps do not require complex equipment.

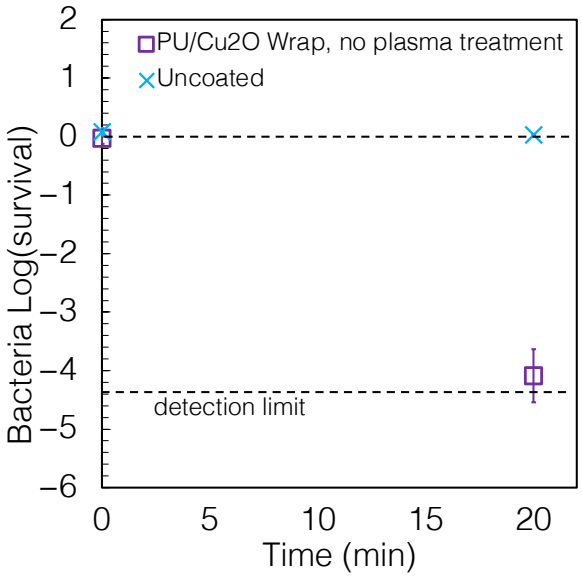


Figure 6-7. Survival of *P. aeruginosa* on an aged PU/Cu_2O wrap (no heat or plasma treatments). The antimicrobial wrap was 3.5 months old at the time it was tested. The aged wrap caused a reduction of >99.99% of *P. aeruginosa* in 20 min. Some error bars are smaller than the size of the symbols.

6.4. Conclusion

The utilization of antimicrobial coatings has been shown to correlate with a lower number of infections [28,29]. However, it can be a significant challenge for an untrained person to install antimicrobial coatings in their desired location. Here, we show that a simple adhesive-

backed version of an antimicrobial coating could be fabricated and that it retained antimicrobial efficacy for 3.5 months. This antimicrobial coating can be applied in the field in seconds, as demonstrated on stainless steel. This is a very important feature for antimicrobial coatings that can become fouled or worn or whose active material can become depleted. Large area wraps have already been used on cars, and antimicrobial coatings can be sprayed or painted, so large- or small-scale objects can be made antimicrobial.

For the highest effectiveness, an antimicrobial wrap needs to kill microbes rapidly. We prepared two different antimicrobial wraps based on the active ingredient Cu_2O. One utilized polyurethane and the other polydopamine as the binding polymer. Both coatings killed >99.995% of *P. aeruginosa* in 20 min, and the bacteria had half-lives of <1.4 min. By demonstrating the preparation of two antimicrobial coatings on the same base wrap, we showed that the wrap concept is modular, which allows the independent optimization of the adhesive coating and the antimicrobial surface.

6.5. Materials and Methods

6.5.1. Materials

In this study, 70% ethanol was purchased from VWR (Radnor, PA, USA). Dopamine hydrochloride (99%) was obtained from Fisher Scientific (Waltham, Massachusetts, USA). In-house DI water was further purified using a Milli-Q Reference system. Tris(hydroxymethyl)aminomethane (Tris, ACS reagent) was obtained from Sigma Aldrich. Adhesive-backed polyethylene sheets (catalog number: 8722K23) and stainless steel 301 were

purchased from McMaster-Carr (Elmhurst, Illinois, USA), washed with (70%) ethanol, rinsed with DI water, and dried with nitrogen gas. Cu_2O particles (Chem Copp HP III UltraFine Type-5; mean size = 5.4 µm) were obtained from American Chemet Corporation, Deerfield, Illinois, USA. Polyurethane (PU; Miniwax, Fast-Drying Polyurethane, clear satin) was obtained from Lowes Home Improvement departmental store, VA, USA. TSA (Tryptic Soy Agar) and TSB (Tryptic soy broth) were purchased from BD, Sparks, MD, USA.

6.5.2. Fabrication of antimicrobial PU/Cu2O Wrap

A PU/Cu_2O coating was applied as described previously [20]. In brief, a thin layer of PU was cast onto the uncoated wrap and air-dried for a few minutes. A suspension of 10% Cu_2O in ethanol was subsequently applied on the PU film, and it was left to partially dry for a few min. The coated wrap was then heat-treated in an oven (120 °C for 2 h) to speed up the formation of the PU coating, washed using DI water, and cut into smaller pieces (12 × 12 mm). In some cases, where indicated, the wrap was plasma-treated with Argon (3 min, at 100 W, and <200 mTorr). The antimicrobial wrap was applied to stainless steel.

6.5.3. Fabrication of Antimicrobial PDA/Cu2O Wrap

The PDA/Cu_2O wrap was prepared using the method in reference [19]. A suspension of Cu_2O particles (0.2% *w*/*w*) in 10 mm tris solution was sonicated, and dopamine hydrochloride was added to the suspension to yield a final concentration of 0.05 g dopamine/L. Subsequently, 140 µL of the prepared suspension was applied to the uncoated wrap (15 × 15 mm in size). The

sample was heat-treated in an oven (80 °C for 30 min). The antimicrobial wrap was applied to stainless steel.

6.5.4. Characterization of Test Solids

The morphology of the coatings was characterized via scanning electron microscopy (SEM) using either a JEOL IT500 SEM (manufactured in Japan) or a FEI Quanta 600 FE-ESEM (manufactured in the Czech Republic). Samples for SEM were treated with a 5 nm layer of Pt/Pd to enhance electrical conductivity.

6.5.5. Antibacterial Assay

6.5.5.1. Choice of Microbial Strain

According to the United States Environmental Protection Agency [41,42] guidance, *P. aeruginosa* (strain DSM-9644) was chosen to test the antimicrobial properties of the samples.

6.5.5.2. Growth of Microbial Strains

Bacteria were grown to the mid-exponential phase at 37 °C in 5 mL of Tryptic Soy Broth (TSB) with aeration (rpm = 60). For the visual verification of the identity and purity of the bacterium, cells were streaked from the liquid culture on Tryptic Soy Agar (TSA) plates and then incubated (37 °C for 48 h). The specific color and morphology traits of *P. aeruginosa* were confirmed before using the batch to test the antimicrobial coatings.

6.5.5.3. Preparation of Microbial Strains for Testing

Bacterial cells were extracted from liquid cultures via centrifugation (20 min at 5000× *g*), followed by the removal of the supernatant and then re-suspension in 5 mL of Phosphate-Buffered Saline (PBS), followed by vortexing (60 s). Two rounds of centrifugation and resuspension in PBS were carried out.

6.5.5.4. Measurement of Viable Cell Number

Viable cell number was determined from colony forming units (CFUs). CFU/mL of the suspension was measured by spreading 0.1 mL of a suspension on a TSA plate (in triplicate), and colonies were counted after incubation for 48 h at 37 °C. Because of the large range of CFU, each test suspension was used to create a 10-fold dilution series, and each of these dilutions were measured to obtain the optimum number of CFUs for counting (20–200). The suspensions had a CFU/mL of approximately 1.6×10^7. If zero colonies were present for the lowest dilution, that number was counted as one colony to enable a $\log_{10}$ transformation of all the data. This was our detection limit for measurement on a particular plate.

6.5.5.5. Measurement of Surface-Killing

A 5 µL droplet of *P. aeruginosa* cells in PBS was placed on solid test samples six days after the antimicrobial wraps were prepared. An uncoated wrap was used as the control. After a known time interval (e.g., 0, 10, or 20 min), an individual sample was placed in a 50 mL centrifuge tube containing 5 mL of PBS. The sample was then vortexed (10 s and at the highest setting) and sonicated (1 min; model: Branson Model 12 Ultrasonic Cleaner, Shelton, CT, USA) to detach all cells from the solid. Assuming the resulting suspension of cells was homogeneous, the total number of surviving cells could be measured by obtaining the CFU/mL of this bacterial suspension. In total, 0.1 mL of the suspension was removed without contacting the sample, and

the CFUs were measured as described above. In addition, the CFU/mL for input bacterial suspension was measured for the calculation of survival. Three independent solid samples were tested in each condition (i.e., coated or uncoated at each time point), and three repeats were carried out for each of these independent measurements. The detection limit and resolution on the agar plate was 1 colony, but because only 0.1 mL of the 5 mL volume was sampled, the detection limit of bacteria was 50 CFU or log (CFU) = 1.7.

6.5.6. Statistical Analysis

All statistics were calculated from log CFUs, and Student's *t*-tests were two-tailed and heteroscedastic. A significance level of 0.05 was employed for statistical analysis. The half-life was calculated from a linear fit of the slope of all log (CFU)–time data at the three time points. The half-life is:

$$t_{1/2} = -\frac{0.30}{\text{slope}} \qquad \text{Equation 6-2}$$

All data from 0 to 20 min were used to calculate $t_{1/2}$, and the uncertainty was the 95% confidence interval (CI). Because the CFUs at 20 min were all below the detection limit, the calculated half-life was an upper bound.

6.5.7. Calculation of Microbial Survival and Reduction

The CFU counting technique counts cells that can reproduce enough times to form a visible bacterial colony. We use the term "kill" as a shorthand for cells that cannot form a

colony. Percentage kill is a comparison of the CFUs measured after a specific time to the CFUs of the input suspension:

$$\log \text{kill} = \text{mean}[\log_{10}(\text{input CFU})] - \text{mean}[\log_{10}(\text{sample CFU})] \quad \text{Equation 6-3}$$

$$\% \text{ kill} = \left[1 - 10^{-\log \text{kill}}\right] \times 100 \quad \text{Equation 6-4}$$

For calculations, the measured sample CFUs were adjusted for dilutions that took place during extraction of bacteria from the solid. When compared to a standard at the same time, we used reduction, defined as:

$$\log \text{Reduction} = \text{mean}[\log_{10}(\text{uncoated sample CFU})] - \text{mean}[\log_{10}(\text{antimicrobial sample CFU})] \quad \text{Equation 6-5}$$

$$\% \text{ Reduction} = \left[1 - 10^{-\log \text{Reduction}}\right] \times 100 \quad \text{Equation 6-6}$$

where the same volume and concentration of bacterial suspension was added to the coated and uncoated sample. In this paper, the uncoated sample was always the uncoated commercial wrap.

We began the statistical treatment with a log transformation because we found that the residuals were approximately normally distributed after a log transformation. Each CFU measurement in Equation 6-3 and Equation 6-5 is the mean of three repeat counts of a different agar plate from the liquid sample; each mean in Equation 6-3 and Equation 6-5 is the mean from three measurements on three independent samples. *p*-values for 99.9% reduction were obtained by the following method: for each of the three independent measurements, we calculated:

$$[\log_{10}(\text{uncoated sample CFU})] - 3$$

and then performed a one-sided *t*-test to determine whether those values were different to the three independent values of $[\log_{10}(\text{antimicrobial sample CFU})]$ for the same time condition. The resulting *p*-value indicated the confidence that the antimicrobial coating decreased the cell numbers by more than 99.9%.

Author Contributions: Conceptualization and design, S.B.; methodology, S.B. and W.A.D.; validation, S.B., W.A.D., J.O.F.III, and M.D.W.; formal analysis, S.B. and W.A.D.; investigation, S.B., W.A.D., J.O.F.III, and M.D.W.; writing—original draft preparation, S.B.; writing—review and editing, S.B., W.A.D., J.O.F.III, and W.A.D.; supervision, W.A.D. and J.O.F.III; project administration, W.A.D.; funding acquisition, W.A.D. and J.O.F.III. All authors have read and agreed to the published version of the manuscript.

Funding: This work was supported by Virginia Tech's Proof of Concept program under Grant No. 238079. This work used shared facilities at the Virginia Tech National Center for Earth and Environmental Nanotechnology Infrastructure, which is supported by NSF (ECCS 1542100 and ECCS 2025151).

Institutional Review Board Statement: Not applicable.

Informed Consent Statement: Not applicable.

Data Availability Statement: Data will be provided on request.

Conflicts of Interest: W.A.D. declares part ownership in a startup company that intends to produce surface coatings. The other authors declare no conflicts of interest. W.A.D. and S.B. are the authors of a patent related to this work.

REFERENCES

1. Piret, J.; Boivin, G. Pandemics throughout history. *Front. Microbiol.* **2021**, *11*, 631736.

2. Cutler, D.M.; Summers, L.H. The COVID-19 pandemic and the $16 trillion virus. *JAMA* **2020**, *324*, 1495–1496.

3. Fonkwo, P.N. Pricing infectious disease: The economic and health implications of infectious diseases. *EMBO Rep.* **2008**, *9*, S13–S17.

4. Hoffmann, S.; Ahn, J.-W. Economic cost of major foodborne illnesses increased $2 billion from 2013 to 2018. In *Amber Waves: The Economics of Food, Farming, Natural Resources, and Rural America*; United States Department of Agriculture: Washington, DC, USA, 2021; Volume 2021.

5. Benedict, K.; Whitham, H.K.; Jackson, B.R. Economic Burden of Fungal Diseases in the United States. *Open Forum. Infect. Dis.* **2022**, *9*, ofac097.

6. Jit, M.; Ng, D.H.L.; Luangasanatip, N.; Sandmann, F.; Atkins, K.E.; Robotham, J.V.; Pouwels, K.B. Quantifying the economic cost of antibiotic resistance and the impact of related interventions: Rapid methodological review, conceptual framework and recommendations for future studies. *BMC Med.* **2020**, *18*, 38.

7. ECDPC. 33000 People Die Every Year Due to Infections with Antibiotic-Resistant Bacteria. Availabe online: https://www.ecdc.europa.eu/en/news-events/33000-people-die-every-year-due-infections-antibiotic-resistant-bacteria (accessed on 20 January 2023).

8. Murray, C.J.; Ikuta, K.S.; Sharara, F.; Swetschinski, L.; Aguilar, G.R.; Gray, A.; Han, C.; Bisignano, C.; Rao, P.; Wool, E. Global burden of bacterial antimicrobial resistance in 2019: A systematic analysis. *Lancet* **2022**, *399*, 629–655.

9. Mahoney, A.R.; Safaee, M.M.; Wuest, W.M.; Furst, A.L. The silent pandemic: Emergent antibiotic resistances following the global response to SARS-CoV-2. *Iscience* **2021**, *24*, 102304.

10. Centers for Disease Control and Prevention. COVID-19: U.S. Impact on Antimicrobial Resistance, Special Report 2022. Availabe online: https://www.cdc.gov/drugresistance/pdf/covid19-impact-report-508.pdf (accessed on 25 March 2023).

11. Centers for Disease Control and Prevention. COVID-19 & Antibiotic Resistance. Availabe online: https://www.cdc.gov/drugresistance/covid19.html (accessed on 28 March 2023).

12. Centers for Disease Control and Prevention. HAI and Antibiotic Use Prevalence Survey. Availabe online: https://www.cdc.gov/hai/eip/antibiotic-use.html (accessed on 24 March 2023).

13. Stephens, B.; Azimi, P.; Thoemmes, M.S.; Heidarinejad, M.; Allen, J.G.; Gilbert, J.A. Microbial exchange via fomites and implications for human health. *Curr. Pollut. Rep.* **2019**, *5*, 198–213.

14. Behzadinasab, S.; Chin, A.W.H.; Hosseini, M.; Poon, L.L.M.; Ducker, W.A. SARS-CoV-2 virus transfers to skin through contact with contaminated solids. *Sci. Rep.* **2021**, *11*, 22868. https://doi.org/10.1038/s41598-021-00843-0.

15. Rutala, W.A.; Weber, D.J. Uses of inorganic hypochlorite (bleach) in health-care facilities. *Clin. Microbiol. Rev.* **1997**, *10*, 597–610.

16. Cloutier, M.; Mantovani, D.; Rosei, F. Antibacterial coatings: Challenges, perspectives, and opportunities. *Trends Biotechnol.* **2015**, *33*, 637–652.

17. Salwiczek, M.; Qu, Y.; Gardiner, J.; Strugnell, R.A.; Lithgow, T.; McLean, K.M.; Thissen, H. Emerging rules for effective antimicrobial coatings. *Trends Biotechnol.* **2014**, *32*, 82–90.

18. Behzadinasab, S.; Hosseini, M.; Williams, M.; Ivester, H.; Allen, I.; Falkinham, J., III; Ducker, W. Antimicrobial activity of cuprous oxide-coated and cupric oxide-coated surfaces. *J. Hosp. Infect.* **2022**, *129*, 58–64. https://doi.org/10.1016/j.jhin.2022.07.022.

19. Behzadinasab, S.; Williams, M.D.; Hosseini, M.; Poon, L.L.; Chin, A.W.; Falkinham, J.O., III; Ducker, W.A. Transparent and Sprayable Surface Coatings that Kill Drug-Resistant Bacteria Within Minutes and Inactivate SARS-CoV-2 Virus. *ACS Appl. Mater. Interfaces* **2021**, *13*, 54706–54714. https://doi.org/10.1021/acsami.1c15505.

20. Behzadinasab, S.; Chin, A.; Hosseini, M.; Poon, L.; Ducker, W.A. A surface coating that rapidly inactivates SARS-CoV-2. *ACS Appl. Mater. Interfaces* **2020**, *12*, 34723–34727. https://doi.org/10.1021/acsami.0c11425.

21. Rakowska, P.D.; Tiddia, M.; Faruqui, N.; Bankier, C.; Pei, Y.; Pollard, A.J.; Zhang, J.; Gilmore, I.S. Antiviral surfaces and coatings and their mechanisms of action. *Commun. Mat.* **2021**, *2*, 1–19.

22. Bharadishettar, N.; Bhat, K.U.; Bhat Panemangalore, D. Coating technologies for copper based antimicrobial active surfaces: A perspective review. *Metals* **2021**, *11*, 711.

23. Singha, P.; Locklin, J.; Handa, H. A review of the recent advances in antimicrobial coatings for urinary catheters. *Acta Biomater.* **2017**, *50*, 20–40.

24. Liu, G.; Li, K.; Wang, H.; Ma, L.; Yu, L.; Nie, Y. Stable fabrication of zwitterionic coating based on copper-phenolic networks on contact lens with improved surface wettability and broad-spectrum antimicrobial activity. *ACS Appl. Mater. Interfaces* **2020**, *12*, 16125–16136.

25. Adlhart, C.; Verran, J.; Azevedo, N.F.; Olmez, H.; Keinänen-Toivola, M.M.; Gouveia, I.; Melo, L.F.; Crijns, F. Surface modifications for antimicrobial effects in the healthcare setting: A critical overview. *J. Hosp. Infect.* **2018**, *99*, 239–249.

26. Iarikov, D.D.; Kargar, M.; Sahari, A.; Russel, L.; Gause, K.T.; Behkam, B.; Ducker, W.A. Antimicrobial surfaces using covalently bound polyallylamine. *Biomacromolecules* **2014**, *15*, 169–176.

27. Behzadinasab, S.; Williams, M.D.; Aktuglu, M.; Falkinham, J.O., III; Ducker, W.A. Porous Antimicrobial Coatings for Killing Microbes within Minutes. *ACS Appl. Mater. Interfaces* **2023**, *15*, 15120–15128. https://doi.org/10.1021/acsami.2c22240.

28. Ellingson, K.D.; Pogreba-Brown, K.; Gerba, C.P.; Elliott, S.P. Impact of a novel antimicrobial surface coating on health care–associated infections and environmental bioburden at 2 urban hospitals. *Clin. Infect. Dis.* **2020**, *71*, 1807–1813.

29. Marik, P.; Shankaran, S.; King, L. The effect of copper-oxide-treated soft and hard surfaces on the incidence of healthcare-associated infections: A two-phase study. *J. Hosp. Infect.* **2020**, *105*, 265–271.

30. Minoshima, M.; Lu, Y.; Kimura, T.; Nakano, R.; Ishiguro, H.; Kubota, Y.; Hashimoto, K.; Sunada, K. Comparison of the antiviral effect of solid-state copper and silver compounds. *J. Hazard. Mater.* **2016**, *312*, 1–7.

31. Sunada, K.; Minoshima, M.; Hashimoto, K. Highly Efficient Antiviral and Antibacterial Activities of Solid-State Cuprous Compounds. *J. Hazard. Mater.* **2012**, *235*, 265–270.

32. Hans, M.; Erbe, A.; Mathews, S.; Chen, Y.; Solioz, M.; Mücklich, F. Role of copper oxides in contact killing of bacteria. *Langmuir* **2013**, *29*, 16160–16166.

33. Javadhesari, S.M.; Alipour, S.; Mohammadnejad, S.; Akbarpour, M. Antibacterial activity of ultra-small copper oxide (II) nanoparticles synthesized by mechanochemical processing against *S. aureus* and *E. coli*. *Mater. Sci. Eng. C* **2019**, *105*, 110011.

34. Centers for Disease Control and Prevention. Multidrug-Resistant Pseudomonas Aeruginosa. Availabe online: https://www.cdc.gov/drugresistance/pdf/threats-report/pseudomonas-aeruginosa-508.pdf (accessed on 20 March 2023).

35. Kerr, K.G.; Snelling, A.M. Pseudomonas aeruginosa: A formidable and ever-present adversary. *J. Hosp. Infect.* **2009**, *73*, 338–344.

36. Pang, Z.; Raudonis, R.; Glick, B.R.; Lin, T.-J.; Cheng, Z. Antibiotic resistance in Pseudomonas aeruginosa: Mechanisms and alternative therapeutic strategies. *Biotechnol. Adv.* **2019**, *37*, 177–192.

37. Kramer, A.; Schwebke, I.; Kampf, G. How long do nosocomial pathogens persist on inanimate surfaces? A systematic review. *BMC Infect. Dis.* **2006**, *6*, 130.

38. Mulcahy, L.R.; Isabella, V.M.; Lewis, K. Pseudomonas aeruginosa biofilms in disease. *Microb. Ecol.* **2014**, *68*, 1–12.

39. Lee, H.; Dellatore, S.M.; Miller, W.M.; Messersmith, P.B. Mussel-inspired surface chemistry for multifunctional coatings. *Science* **2007**, *318*, 426–430.

40. Ryu, J.H.; Messersmith, P.B.; Lee, H. Polydopamine surface chemistry: A decade of discovery. *ACS Appl. Mater. Interfaces* **2018**, *10*, 7523–7540.

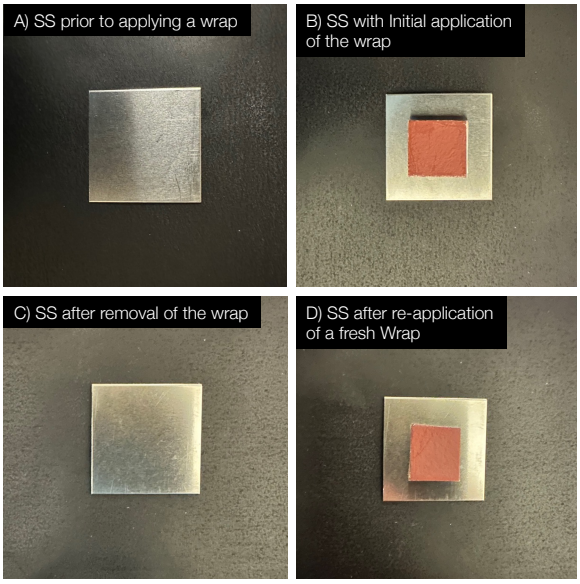
41. Environmental Protection Agency. Antimicrobial Testing Methods & Procedures: Interim Method for Evaluating the Efficacy of Antimicrobial Surface Coatings. Availabe online: https://www.epa.gov/pesticide-analytical-methods/antimicrobial-testing-methods-procedures-interim-method-evaluating (accessed on 2 September 2022).

42. Environmental Protection Agency. Protocol for the Evaluation of Bactericidal Activity of Hard, Non-porous Copper Containing Surface Products. Availabe online: https://www.epa.gov/sites/production/files/2016-02/documents/copper_and_copper-alloy_surface_protocol_revised_012916.pdf (accessed on 2 September 2022).

43. Liu, Y.; Ai, K.; Liu, J.; Deng, M.; He, Y.; Lu, L. Dopamine-melanin colloidal nanospheres: An efficient near-infrared photothermal therapeutic agent for in vivo cancer therapy. *Adv. Mater.* **2013**, *25*, 1353–1359.

Disclaimer/Publisher's Note: The statements, opinions and data contained in all publications are solely those of the individual author(s) and contributor(s) and not of MDPI and/or the editor(s). MDPI and/or the editor(s) disclaim responsibility for any injury to people or property resulting from any ideas, methods, instructions or products referred to in the content.

Table of content's figure:



Chapter 7. Reduction of Infectivity of SARS-CoV-2 by Zinc Oxide Coatings

Mohsen Hosseini[1†], Saeed Behzadinasab[1†], Alex W.H. Chin[2,3†], Leo L.M. Poon[*2,3,4], and William A. Ducker[*1]

† These authors contributed equally

*Corresponding Authors

[1] Dept. of Chemical Engineering and Center for Soft Matter and Biological Physics, Virginia Tech, VA, 24061, USA

[2]School of Public Health, LKS Faculty of Medicine, The University of Hong Kong, Hong Kong Special Administrative Region, China.

[3] Centre for Immunity and Infection, Hong Kong Science Park, Hong Kong, China

[4] HKU-Pasteur Research Pole, LKS Faculty of Medicine, The University of Hong Kong, Hong Kong, China

KEYWORDS: SARS-CoV-2, zinc oxide, zinc oxide tetrapod, coating, coronavirus, antiviral, COVID-19

7.1. Abstract

We developed antimicrobial coatings from ZnO particles that reduce the infectivity of SARS-CoV-2 suspensions by > 99.9% in one hour. The advantage of a coating is that it can be applied to a variety of objects, e.g., hand rails and door knobs, to hinder the spread of disease. Two porous coatings were prepared: one from sub-micron zinc oxide particles bound with silica menisci, and the other from zinc oxide tetrapods bound with polyurethane. Experiments on glass coatings show that infectivity depends on porosity for hydrophilic materials, where aqueous droplets imbibe into the porosity.

7.2. Introduction

Coronavirus disease 2019 (COVID-19) created many negative economic, health, and psychological impacts on human life. During the period January 2020 to May 2021, more than 150 million positive COVID-19 cases were reported worldwide and more than 3.5 million people died as a result of the disease.[1] The causative virus, severe acute respiratory syndrome coronavirus-2, abbreviated as SARS-CoV-2, is believed to be transmitted through two routes. The primary mode of the transmission is through the inhalation of respiratory droplets generated by infected people as a result of breathing, speaking, coughing, sneezing, etc.[2] Small droplets remain suspended in air for up to 30 hours[3] and a healthy individual can become infected simply by inhaling them. Another route of SARS-CoV-2 transfer is through fomites.[4-5] Larger respiratory droplets can land on objects and infected people may transfer contaminated liquid directly to objects by touching their face and then an inanimate object. Such solids contaminated with virus are known as fomites. Examples of fomites are everyday objects such as door handles, railings, elevator buttons, check-out facilities contaminated by respiratory droplets or dried residue of viable virus. SARS-CoV-2 can remain viable up to 7 days on non-porous solid surfaces,[6-7] so there is a significant window of opportunity for infection via this route.

An animal study showed that although inhalation of contaminated droplets is the main route of infection, fomite transmission also occurred[4] and a modeling study showed fomite transmission was responsible 25% of infections.[8] The mechanism for human infection is simple, SARS-CoV-2 can be transferred by touching a contaminated solid and then, when the hand touches the nose, mouth or eyes, the virus may enter the mucus and find its way to the epithelial

cells.[9-10] Recent unpublished work has shown that the virus can transfer from a contaminated surface to skin.[5]

A significant difficulty with the decontamination of solids is that most disinfectants only kill microbes that were present before the disinfectants were used. Almost immediately after the surface is treated with disinfectant, an infected person can again contaminate the solid.[11] Effective control by this method therefore requires very frequent disinfection, which is labor intensive, expensive, and may cause loss of productivity. For example, a train or bus may need to be temporarily out of service during disinfection.

An alternative approach is to use coatings that are designed to provide an ongoing reduction of infectivity. That means they inactivate or kill microbes long after the coating is applied. Copper-based coatings have already been reported to inactivate SARS-CoV-2.[12-15] The virus has also been reported to be less stable on nanostructured aluminum surfaces[16] and light-activated titanium dioxide.[17] Here, we use zinc oxide as an alternative ingredient that has the ability to inactivate SARS-CoV-2. ZnO has a different color (white) compared to copper compounds and has different stability and toxicity. Zn^{2+} and ZnO nanoparticles have recently been shown to have activity against SARS-CoV-2.[18-19]

Zinc oxide (ZnO) particles have been shown to be antibacterial[20-21] and antiviral.[22-23] Prior coatings of ZnO particles on surfaces focused on simply depositing the particles on a surface using ultrasonic irradiation,[24] flame spray pyrolysis,[25] or thin film coater machine.[26] Without immobilized particles this approach may not have a long-lasting effect. Several ZnO nanocomposites have previously been developed and tested against bacteria and have been found to kill *Escherichia coli*.[27-28]

Here, we describe ZnO coatings that were designed such that the coating adhered to the solid without encapsulating the particles within an adhesive. If the active ingredient is a small ion or molecule that elutes from the coating, then the coating should at least be permeable to that ion or small molecule or to the microbe. Coatings can obviously not achieve "contact killing" (where the microbe is inactivated or killed by physical contact) if the solid particle is encapsulated in an impermeable matrix.

Two coatings are described, the first of which consists of crystalline 300 nm ZnO particles that are held together by solid glass menisci produced by a modified version of the Stöber process using tetraethyl orthosilicate (TEOS).[29-30] The menisci form adhesive junctions between the particles but the menisci are sufficiently small that there remains a large exposed surface area of ZnO for inactivation of microbes. First, the liquid menisci were created, and then the menisci were solidified using a gas phase catalyst. The solids loading was 38 g/m^2. The second coating was fabricated from crystalline ZnO with a tetrapodal morphology (ZnO-T). Because the legs avoid close packing, ZnO-T is a low density material with large pores.[31] In this work, we adhered the ZnO tetrapod particles with polyurethane (PU), similarly to prior work with Cu_2O,[12] but with much less PU, thereby allowing imbibition of the droplet. The solids loading was 56 g/m^2. We refer to the coatings as ZnO/Silica and ZnO-T/PU coatings. Our results show that both these coatings were very successful at reducing infection by SARS-CoV-2.

In addition, the porosity of an antiviral coating is important for several reasons: it may affect the drying time,[13, 32] the surface area of active material, the transport time, and perhaps the ability to recover virus that may become adsorbed or otherwise trapped in the porosity.[10] We directly investigate the trapping/adsorption hypothesis by comparing a porous glass coating to a non-porous glass surface.

7.3. Results

7.3.1. Characterization

The active part of the coating is where contact occurs between the droplet of virus suspension and the solid. Therefore, the wetting and imbibition are critical aspects of coating performance. The zinc oxide particles are intrinsically hydrophilic; they immediately fall through the air-water interface. The contact angle of water droplet on ZnO/Silica was 72°±3° (droplet size = 5µL, error shows 95% confidence interval from 5 independent measurements, see Figure S7-1), and the droplet partially and slowly imbibes into the coating (Figure S7-2). The advancing water contact angle of ZnO-T/PU was 13°±23° (1 day after plasma treatment; droplet size = ~10µL). For the ZnO-T/PU sample, the error reflects that angles were as high as 40°. For the low contact angles, the droplet immediately imbibed into the sample (Figure S7-3) In contrast to the earlier coatings fabricated from Cu_2O and PU where the contact angle increased with time, the contact angle of ZnO-T/PU was only 17°±22° after 11 days. The lack of "recovery" of the angle is probably because there is very little PU on the surface. The maintenance of wettability is important for achieving contact between the active ingredient and virus in a droplet.

The microstructure of the coatings is shown in scanning electron microscope images (SEM) images (Figure 7-1). The shapes of individual particles are visible, which demonstrate the that they were not engulfed in silica or PU, and the porosity is also evident. Figure 7-1E and F show the cross-sectional images that enable measurement of the thicknesses of the ZnO/Silica and ZnO-T-PU, which were 30 ± 2 µm and 220 ± 50 µm, respectively (thickness ± 95% confidence interval). The cross-sections also demonstrate that the porosity is throughout the

coatings, and shows the uniform thickness. High magnification images of the ZnO/Silica (Figure 7-1) indicate necks between the particles which were created by the Stöber process.

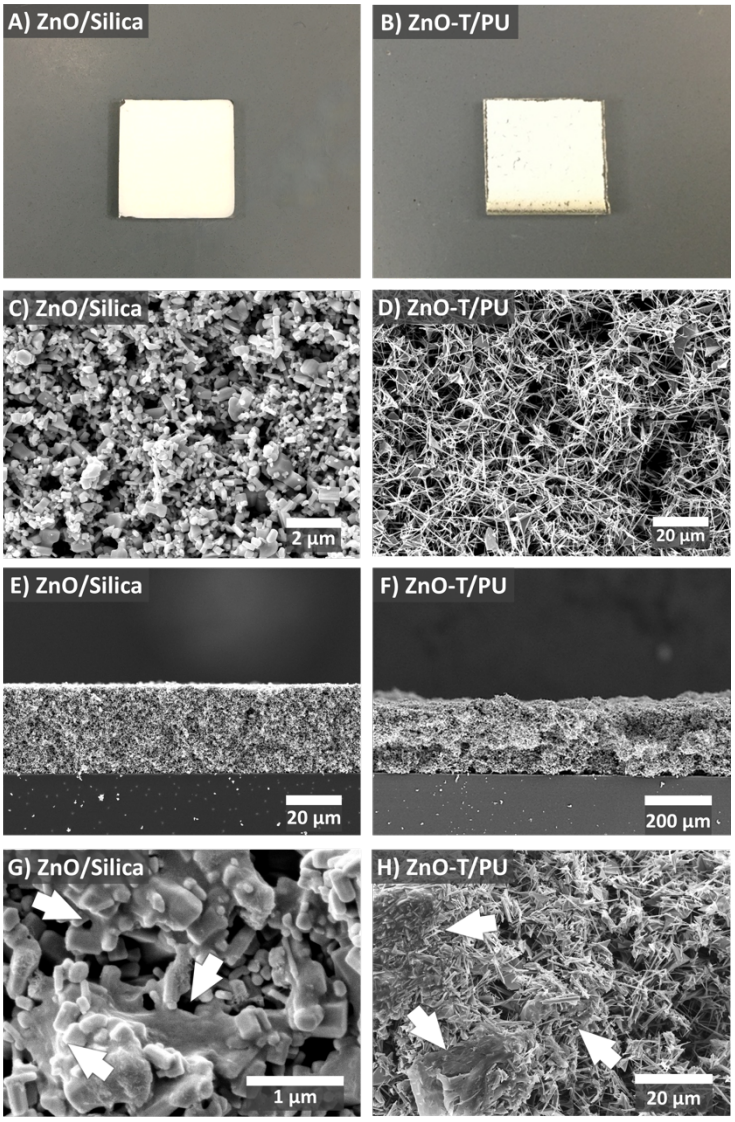


Figure 7-1. Photograph of A) ZnO/Silica coating and B) ZnO-T/PU coating. SEM images of C) the surface ZnO/Silica, D) the surface ZnO-T/PU, E) Cross-section of ZnO/Silica coating, F) Cross-section of ZnO-T/PU coating, G) Silica menisci (necks) between ZnO particles in ZnO/Silica coating and H) Higher resolution cross-sectional image of ZnO-T/PU sample. Arrows point to regions where the coating is amorphous and therefore there is a large volume fraction of PU. Other regions have a lower volume fraction of PU and hence greater porosity. Note scale difference for ZnO/Silica compared to ZnO-T/PU SEM images.

The outer few nanometers of each coating was selectively probed by X-ray photoelectron spectroscopy (XPS). The XPS spectrum of the ZnO/Silica coating (Figure S7-4) shows that 36% of the surface is Zn, which given the stoichiometry of ZnO, is consistent with 73% of the surface being ZnO. There is negligible silicon, which shows that the silica produced by the Stöber process does not cover the ZnO particles, but is confined to menisci, as planned. This was confirmed by the Energy Dispersive X-Ray Spectroscopy (EDS) analysis of the top micrometer of the coating that showed a zinc to oxygen ratio of 0.99±0.04:1, again consistent with only a small amount of silica (SiO_2) in the coating. The silica menisci were too small to resolve their chemistry by EDS imaging. The zinc oxide tetrapod is known to pack with a low mass to volume ratio because the tetrapod has arms that inhibit packing,[31] and the very high void fraction is clearly shown in Figure 7-1: the tetrapods in the coating are not engulfed in PU. XPS reveals that the ZnO-T/PU coating has twice the fraction of carbon (20%) as the ZnO/Silica, which is consistent with the presence of PU in the coating. We also measured the composition of the surface with EDS and the ratio of Zinc to Oxygen was 1.1:1.0, which is consistent with the stoichiometric value of 1:1.

X-ray diffraction (XRD, Figure S7-5) showed that both coatings were predominantly crystalline ZnO with the wurtzite structure.

7.3.2. ZnO Coatings Reduce Infectivity of SARS-CoV-2

We tested the reduction of SARS-CoV-2 suspensions after 5 µL droplets were placed on ZnO/Silica or ZnO-T/PU coatings. The droplet remained on each coating for a predefined period of time, then the virus was eluted from the solid, and then the eluant was used to infect VERO

E6 cells using a $TCID_{50}$ assay (See SI methods). SARS-CoV-2 spontaneously loses its ability to infect cells over time, so in each case, we compare the outcome on the coating to the outcome on an uncoated surface. The coating is on glass, so the uncoated sample is plain glass. We use the word *Reduction* to compare the results on the coating to results on the uncoated glass at the same time point:

$$\log \text{Reduction} = \text{mean}\left[\log_{10}(\text{glass control titer})\right] - \text{mean}\left[\log_{10}(\text{sample titer})\right] \quad \text{Equation 7-1}$$

$$\%\ \text{reduction} = (1 - 10^{-\log \text{Reduction}}) \times 100\% \quad \text{Equation 7-2}$$

Both ZnO coatings caused a dramatic decrease in the infectivity (Figure 7-2): the infectivity of the SARS-CoV-2 dropped by 99.99% in one hour (i.e., more than a 4-logs), while only a 0.7 log drop in infectivity was observed on the uncoated glass within the same period of time. The central idea of this work is that a coating can decrease the activity of SARS-CoV-2 on a coated solid more rapidly than the uncoated solid, so we compared the results on each ZnO coating to results on the uncoated glass. The ZnO/Silica coating caused a >99.98% *Reduction* (>3-log *Reduction*) and ZnO-T/PU caused a 99.97% *Reduction* in 1 hour. The reason for the "greater than symbol" is that all the ZnO/silica titers were below the lower limit of detection. For the ZnO-T/PU coating, two of three measurements were below the detection limit, and the average was calculated as if these measurements were at the detection limit. The one-tailed 95% confidence intervals demonstrate more than 99.92% and more than 99.89% SARS-CoV-2 titer *Reduction* after one hour on ZnO/Silica and ZnO-T/PU coatings respectively.

We tested the adhesion of our coatings according to ASTM D3359 standard. Figure S7-8 shows that both coating demonstrated a satisfactory adhesion, where the adhesion for ZnO/Silica and ZnO-T/PU were rated at least 3B and 3A respectively.

7.4. Discussion

We used zinc oxide particles as the active anti-pathogenic ingredient of our coatings. A key advantage of ZnO is the low level of toxicity to humans. The United States Food and Drug Administration (FDA) has designated ZnO as "generally recognized as safe" (GRAS).[33]

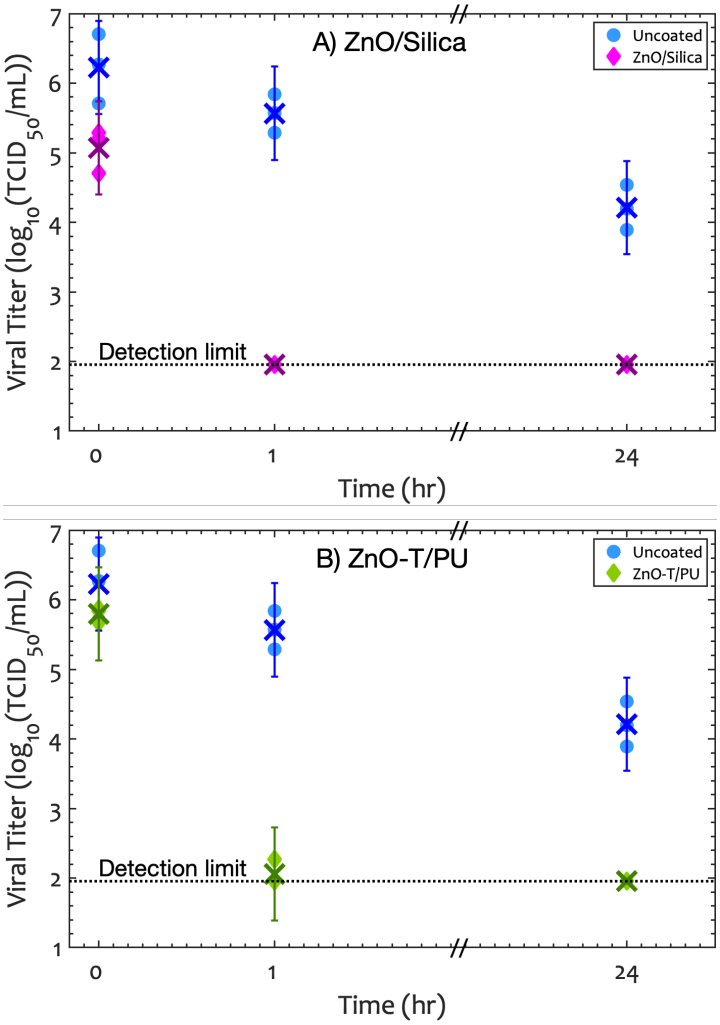


Figure 7-2. Decay of SARS-CoV-2 TCID50 titer on A) ZnO/Silica and B) ZnO-T/PU coatings on glass. Diamonds and circles show independent titer measurements, × represents the average of the log titer at each time, and the dashed line shows the detection limit of the assay (90 TCID50/mL). The error bars are the 95% confidence interval. In comparison to uncoated glass, the virus titer has a 99.98% Reduction on ZnO/Silica ($p = 10\text{-}3$, one tail, unpaired) and 99.97% Reduction on ZnO-T/PU after one hour ($p = 7\times10\text{-}5$, one tail, unpaired).

SARS-CoV-2 is a novel pathogen, so the mechanism of action of ZnO particularly against SARS-CoV-2 is unknown, but here we describe the mechanisms against other organisms, which we consider to be likely mechanisms against SARS-CoV-2. Zinc oxide is known to demonstrate its anti-pathogenic properties through two main mechanisms:[34-37] Zn^{2+} ion release and by creation of reactive oxygen species (ROS). ZnO particles release Zn^{2+} ions in aqueous solutions. These ions would mediate the attachment of negatively charged cell membrane to Zinc oxide particles, causing a localized increase in Zn^{2+} ion concentration which eventually leads to membrane leakage and cell death accordingly.[38-39] It has been reported that $OH^{\bullet}$, $O_2^{\bullet}$ and H_2O_2 are generated on ZnO surface.[37] H_2O_2 is an active agent and when enters cells, exerts oxidative stress that yields to damage or killing of the bacteria.[40] It has also been reported that the trapped oxygen within the porosity of ZnO particles further reinforce the generation of ROS.[40] It is possible that the action against a virus might be different. Despite the potent antimicrobial activity, ZnO has a very low level of cytotoxicity on L929 cells,[41] making it highly biocompatible that can be used for a variety of applications.[42]

As described in the introduction, the use of porous coatings is a substantial advantage because the porosity may affect the drying time, the surface area of active material, the transport time, and the ability to recover virus that may become adsorbed or otherwise trapped in the porosity.[10] To date there has been no direct check of whether porosity affects the infectivity because there are no results on porous and non-porous surfaces of the same material. In order to understand how infectivity is lost due to porosity, we have compared titers obtained from glass and porous glass that have very similar chemistry (See Figure S7-9 for XPS results), so the effect of chemistry is removed from the comparison. Glass has no active material and the decay of SARS-CoV-2 on glass is very slow, so there is no effect of changing the amount of active

material or transport to or of the active material[7, 43]. The comparison thus directly tests the effect of porosity.

Figure 7-3 compares the infectivity of SARS-CoV-2 recovered from droplets on porous and non-porous glass. It is immediately apparent that the infectivity is much lower from the porous glass, so we have shown unambiguously that the introduction of porosity reduces infectivity as measured by elution and $TCID_{50}$ measurement.

Results at time zero are instructive. Aqueous droplets are immediately imbibed into the porous hydrophilic glass: imbibition occurs before elution, which in practice is <1 minute after the droplet is placed on the solid. Therefore, the "zero" time point assays recovery from within the porosity. The majority of the infectivity is lost immediately on the porous glass, with the porous glass titer 2.9 logs below the non-porous glass. This compares sharply with the ZnO results where the viral titers were much greater at time zero. For ZnO-T/PU the imbibition also occurs before elution so time zero titer also assays liquid from the porosity, but in this case the *Reduction* is only 0.4 logs. In summary, the vast majority of infectivity on the porous glass is lost immediately in the porosity but little is lost in the porous ZnO-T/PU. The ZnO/Silica has a much higher contact angle (72°±3°), which prevents immediate imbibition. Student's t-tests showed that the viral titer at 0 hr on porous glass is significantly smaller than ZnO/Silica ($p=6\times10^{-3}$) and ZnO-T/PU ($p=3\times10^{-5}$) coatings.

It is also instructive to compare the 1 h and 0 h time points *for the same material* using the following equation:

$$\log 1\text{h Reduction} = \text{mean}\,[\log_{10}(0\text{ h titer})] - \text{mean}\,[\log_{10}(1\text{ h titer})] \qquad \text{Equation 7-3}$$

The log 1h Reduction on glass is 0.4 and on porous glass is 0.6, which are not significantly different ($p = 0.33$). So, the glass is an inactive material because even by increasing the porosity to make more surface area and a faster transport time, there is no additional loss of infectivity over time. The main effect of porosity is simply to reduce recovery. The porosity could also affect drying time,[13] which has been hypothesized as a parameter for inactivation.[44]

For the ZnO materials, by comparison, there is significant loss of infectivity ($p < 4\times10^{-3}$) over time. The log 1h Reduction is at least 3.1 on ZnO/Silica and at least 3.7 on ZnO-T/PU. This is consistent with an active material. So, in summary, the ZnO coatings reduce infectivity in two ways: (1) some of the virus becomes trapped in the porosity and (2) once the droplet goes into the pores or dries onto the surface, there is an ongoing loss of infectivity that we attribute to the antimicrobial properties of ZnO. The active antimicrobial activity of ZnO is superior to an inactive porous material because the active material has the potential to kill bacteria that may linger in the porosity.

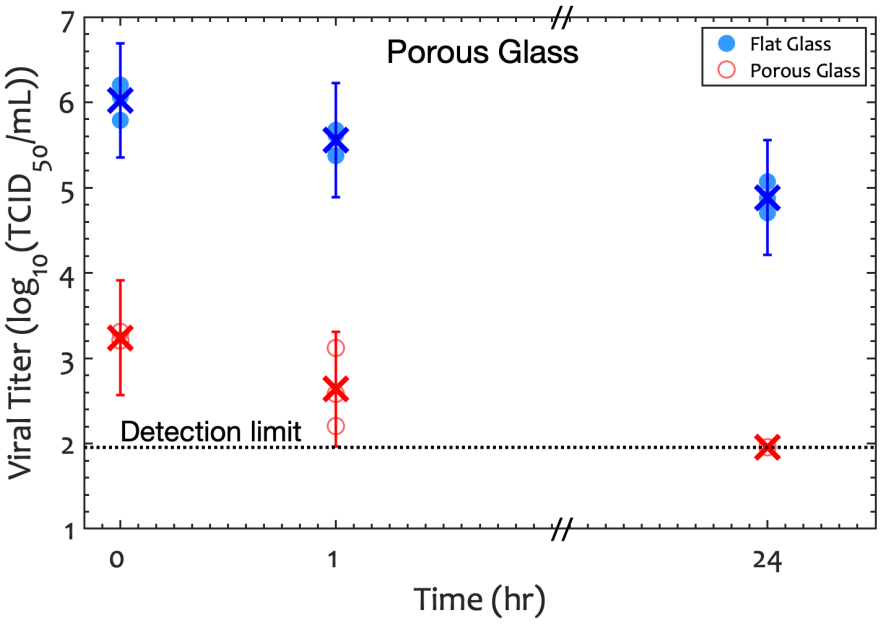


Figure 7-3. Decay of SARS-CoV-2 TCID50 titer on porous glass compared to flat glass. The two glass surfaces are soda-lime glass, and have similar chemistry (See XPS in Figure S7-9). Diamonds and circles show independent titer measurements, × represents the average of the log titer at each time, the dashed line shows the detection limit of the assay (90 TCID50/mL), and the error bars are the 95% confidence interval. The virus titer on porous glass at 0 and 1 hr time points are not statistically different ($p = 0.33$, one tail, unpaired) confirming its inactive nature against SARS-CoV-2.

Recent work has also shown activity of Zn products against SARS-CoV-2. Gopal et al[19] demonstrated a reduction of SARS-CoV-2 of about 90% by coating fibers with Zn^{2+} ions and El-Megharbel et al[18] showed that a ZnO particle spray disinfectant caused a 40% reduction. These results are consistent with our results but show lower reductions. In contrast Merkl et al[25] did not measure activity for ZnO particles deposited on a surface.

7.5. Conclusions

In summary, we have introduced two new porous anti-SARS-CoV-2 coatings. One method used a variant of Stöber sol-gel method to create a coating from sub-micron-sized zinc oxide particles, while the other method used polyurethane to immobilize zinc oxide tetrapod particles. They each reduce infectivity of the virus within one hour: the viral titer of SARS-CoV-2 was decreased by 4 logs (>99.99%), which is a *Reduction* of at least 99.9 % compared to uncoated glass. These coatings can be applied to everyday objects and therefore have potential to reduce infection from solids and limit the spread of COVID-19 disease.

The time course of inactivation on the ZnO coatings is consistent with two actions that reduce infectivity. First, when the viral suspension droplet is imbibed into a hydrophilic porous solid, there is an immediate loss of infectivity due to the inability to recover virus from within the porous material or from the surface of the porous material. Second, over time there is a large (>3 logs) loss of infectivity, which is consistent with an active material. For glass, by contrast, there is only a small loss of infectivity over time, which is insignificant over the first hour. The comparison of results on porous glass and non-porous glass show definitively that loss of infectivity can occur as a result of imbibition into a porous hydrophilic material.

ASSOCIATED CONTENT

See Supporting Information for Materials and Methods section, Time lapse of imbibition of a droplet in ZnO/TEOS film (see Figure S7-1). The disc pattern imbibition of a droplet in ZnO/TEOS film (Figure S7-2), Advancing contact angles measurement of ZnO-T/PU coating (Figure S7-3), XPS spectra and the elemental analysis of the outer surface of the coatings (Figure S7-4), XRD pattern of the coatings (Figure S7-5), The effect of a 3-minute Argon plasma cleaning in the preparation of ZnO-T/PU coating (Figure S7-6) and Size distribution histogram of sub-micron ZnO particles (Figure S7-7), ASTM D3359 adhesion test result for ZnO coatings (Figure S7-8), Table of XPS results for glass and SEM image of porous glass surface (Figure S7-9), Decay of SARS-CoV-2 TCID50 titer on silica and polyurethane coatings and its comparison to glass (Figure S10), $TCID_{50}$ assay data for Figure 7-2 (Table S1), $TCID_{50}$ assay data for Figure 7-3 (Table S2).

The Supporting Information is available free of charge on the ACS Publications website.

Supporting information is a PDF file.

AUTHOR INFORMATION

Corresponding Authors

Leo L. M. Poon - School of Public Health, LKS Faculty of Medicine, The University of Hong Kong, Hong Kong Special Administrative Region, China. Centre for Immunity and Infection, Hong Kong Science Park, Hong Kong, China. HKU-Pasteur Research Pole, LKS Faculty of Medicine, The University of Hong Kong, Hong Kong, China.

Email: llmpoon@hku.hk

William A. Ducker - Dept. of Chemical Engineering and Center for Soft Matter and Biological Physics, Virginia Tech, VA, 24061, USA

Email: wducker@vt.edu

Authors

Mohsen Hosseini - Dept. of Chemical Engineering and Center for Soft Matter and Biological Physics, Virginia Tech, VA, 24061, USA

Saeed Behzadinasab - Dept. of Chemical Engineering and Center for Soft Matter and Biological Physics, Virginia Tech, VA, 24061, USA

Alex W. H. Chin - School of Public Health, LKS Faculty of Medicine, The University of Hong Kong, Hong Kong Special Administrative Region, China. Centre for Immunity and Infection, Hong Kong Science Park, Hong Kong, China.

ACKNOWLEDGMENT

The authors acknowledge use of Microscopy facilities and the use X-ray diffraction machine within the NCFL and MCL at Virginia Tech. We also thank Xu Feng for capturing the XPS spectra and acknowledge the use of Surface Analysis Laboratory in Department of Chemistry at

Virginia Tech, which is supported by the National Science Foundation under Grant No. CHE-1531834. This work was supported by the National Science Foundation under Grant No. CBET-1902364, the Health and Medical Research Fund (COVID190116), and the National Institute of Allergy and Infectious Diseases (contract HHSN272201400006C).

CONFLICT OF INTEREST

WD declares part ownership in a startup company that intends to produce surface coatings. Other authors declare no conflict of interest.

REFERENCES

1. (JHU), J. H. U. COVID-19 Dashboard by the Center for Systems Science and Engineering (CSSE) at Johns Hopkins University (JHU). https://coronavirus.jhu.edu/map.html (accessed April 25, 2021).

2. Prather, K. A.; Wang, C. C.; Schooley, R. T., Reducing Transmission of SARS-CoV-2. *Science* **2020,** *368* (6498), 1422-1424.

3. Duguid, J., The size and the duration of air-carriage of respiratory droplets and droplet-nuclei. *Epidemiol. Infect.* **1946,** *44* (6), 471-479.

4. Sia, S. F.; Yan, L.-M.; Chin, A. W.; Fung, K.; Choy, K.-T.; Wong, A. Y.; Kaewpreedee, P.; Perera, R. A.; Poon, L. L.; Nicholls, J. M., Pathogenesis and transmission of SARS-CoV-2 in golden hamsters. *Nature* **2020,** *583* (7818), 834-838.

5. Behzadinasab, S.; Chin, A. W. H.; Hosseini, M.; Poon, L. L. M.; Ducker, W. A., SARS-CoV-2 virus transfers to skin through contact with contaminated solids. *medRxiv* **2021**, 2021.04.24.21256044. DOI: 10.1101/2021.04.24.21256044.

6. Van Doremalen, N.; Bushmaker, T.; Morris, D. H.; Holbrook, M. G.; Gamble, A.; Williamson, B. N.; Tamin, A.; Harcourt, J. L.; Thornburg, N. J.; Gerber, S. I., Aerosol and surface stability of SARS-CoV-2 as compared with SARS-CoV-1. *N. Engl. J. Med.* **2020,** *382* (16), 1564-1567.

7. Chin, A. W. H.; Chu, J. T. S.; Perera, M. R. A.; Hui, K. P. Y.; Yen, H.-L.; Chan, M. C. W.; Peiris, M.; Poon, L. L. M., Stability of SARS-CoV-2 in different environmental conditions. *Lancet Microbe* **2020,** *1* (1), e10. DOI: 10.1016/S2666-5247(20)30003-3.

8. Meiksin, A., Dynamics of COVID-19 transmission including indirect transmission mechanisms: a mathematical analysis. *Epidemiol. Infect.* **2020,** *148*, e257. DOI: 10.1017/S0950268820002563.

9. (CDC), C. f. D. C. a. P. Centers for Disease Control and Prevention (CDC). https://www.cdc.gov/coronavirus/2019-ncov/hcp/faq.html#:~:text=Surfaces%20can%20become%20contaminated%20with,one's%20face%20or%20mouth. (accessed May 26, 2020).

10. Hosseini, M.; Behzadinasab, S.; Benmamoun, Z.; Ducker, W. A., The Viability of SARS-CoV-2 on Solid Surfaces. *Curr. Opin. Colloid Interface Sci.* **2021**, 101481.

11. Bhalla, A.; Pultz, N. J.; Gries, D. M.; Ray, A. J.; Eckstein, E. C.; Aron, D. C.; Donskey, C. J., Acquisition of Nosocomial Pathogens on Hands After Contact with Environmental Surfaces Near Hospitalized Patients. *Infect. Control Hosp. Epidemiol.* **2004,** *25* (2), 164-167.

12. Behzadinasab, S.; Chin, A.; Hosseini, M.; Poon, L.; Ducker, W. A., A surface coating that rapidly inactivates SARS-CoV-2. *ACS Appl. Mater. Interfaces* **2020,** *12* (31), 34723-34727.

13. Hosseini, M.; Chin, A. W.; Behzadinasab, S.; Poon, L. L.; Ducker, W. A., Cupric oxide coating that rapidly reduces infection by SARS-CoV-2 via solids. *ACS Appl. Mater. Interfaces* **2021,** *13* (5), 5919-5928.

14. Hutasoit, N.; Kennedy, B.; Hamilton, S.; Luttick, A.; Rashid, R. A. R.; Palanisamy, S., SARS-CoV-2 (COVID-19) Inactivation Capability of Copper-Coated Touch Surface Fabricated by Cold-Spray Technology. *Manuf. Lett.* **2020,** *25*, 93-97.

15. Hewawaduge, C.; Senevirathne, A.; Jawalagatti, V.; Kim, J. W.; Lee, J. H., Copper-impregnated three-layer mask efficiently inactivates SARS-CoV2. *Environ. Res.* **2021,** *196*, 110947.

16. Hasan, J.; Pyke, A.; Nair, N.; Yarlagadda, T.; Will, G.; Spann, K.; Yarlagadda, P. K., Antiviral nanostructured surfaces reduce the viability of SARS-CoV-2. *ACS Biomater. Sci. Eng.* **2020,** *6* (9), 4858-4861.

17. Micochova, P.; Chadha, A.; Hesseloj, T.; Fraternali, F.; Ramsden, J. J.; Gupta, R. K., Rapid inactivation of SARS-CoV-2 by titanium dioxide surface coating. *Wellcome Open Res.* **2021,** *6* (56), 56.

18. El-Megharbel, S. M.; Alsawat, M.; Al-Salmi, F. A.; Hamza, R. Z., Utilizing of (Zinc Oxide Nano-Spray) for Disinfection against "SARS-CoV-2" and Testing Its Biological Effectiveness on Some Biochemical Parameters during (COVID-19 Pandemic)—" ZnO Nanoparticles Have Antiviral Activity against (SARS-CoV-2)". *Coatings* **2021,** *11* (4), 388.

19. Gopal, V.; Nilsson-Payant, B. E.; French, H.; Siegers, J. Y.; Yung, W.-s.; Hardwick, M.; Te Velthuis, A. J., Zinc-Embedded Polyamide Fabrics Inactivate SARS-CoV-2 and Influenza A Virus. *ACS Appl. Mater. Interfaces* **2021**.

20. Aydin Sevinç, B.; Hanley, L., Antibacterial activity of dental composites containing zinc oxide nanoparticles. *J. Biomed. Mater. Res., Part B* **2010,** *94* (1), 22-31.

21. Seil, J. T.; Webster, T. J., Antibacterial effect of zinc oxide nanoparticles combined with ultrasound. *Nanotechnology* **2012,** *23* (49), 495101.

22. Antoine, T. E.; Hadigal, S. R.; Yakoub, A. M.; Mishra, Y. K.; Bhattacharya, P.; Haddad, C.; Valyi-Nagy, T.; Adelung, R.; Prabhakar, B. S.; Shukla, D., Intravaginal zinc oxide tetrapod nanoparticles as novel immunoprotective agents against genital herpes. *J. Immunol.* **2016,** *196* (11), 4566-4575.

23. Ghaffari, H.; Tavakoli, A.; Moradi, A.; Tabarraei, A.; Bokharaei-Salim, F.; Zahmatkeshan, M.; Farahmand, M.; Javanmard, D.; Kiani, S. J.; Esghaei, M., Inhibition of H1N1 influenza virus infection by zinc oxide nanoparticles: another emerging application of nanomedicine. *J. Biomed. Sci.* **2019,** *26* (1), 1-10.

24. Applerot, G.; Perkas, N.; Amirian, G.; Girshevitz, O.; Gedanken, A., Coating of glass with ZnO via ultrasonic irradiation and a study of its antibacterial properties. *Appl. Surf. Sci.* **2009,** *256* (3), S3-S8.

25. Merkl, P.; Long, S.; McInerney, G. M.; Sotiriou, G. A., Antiviral Activity of Silver, Copper Oxide and Zinc Oxide Nanoparticle Coatings against SARS-CoV-2. *Nanomaterials* **2021,** *11* (5), 1312.

26. Wu, W.; Liu, T.; He, H.; Wu, X.; Cao, X.; Jin, J.; Sun, Q.; Roy, V. A.; Li, R. K., Rhelogical and antibacterial performance of sodium alginate/zinc oxide composite coating for cellulosic paper. *Colloids Surf., B* **2018,** *167*, 538-543.

27. Rahman, M. M., Polyurethane/Zinc Oxide (PU/ZnO) Composite—Synthesis, Protective Propertyand Application. *Polymers* **2020,** *12* (7), 1535.

28. Schwartz, V. B.; Thétiot, F.; Ritz, S.; Pütz, S.; Choritz, L.; Lappas, A.; Förch, R.; Landfester, K.; Jonas, U., Antibacterial surface coatings from zinc oxide nanoparticles embedded in poly (n-isopropylacrylamide) hydrogel surface layers. *Adv. Funct. Mater.* **2012,** *22* (11), 2376-2386.

29. Ghimire, P. P.; Jaroniec, M., Renaissance of Stöber Method for Synthesis of Colloidal Particles: New Developments and Opportunities. *Journal of Colloid and Interface Science* **2020**.

30. Stöber, W.; Fink, A.; Bohn, E., Controlled Growth of Monodisperse Silica Spheres in The Micron Size Range. *Journal of colloid and interface science* **1968,** *26* (1), 62-69.

31. Mecklenburg, M.; Schuchardt, A.; Mishra, Y. K.; Kaps, S.; Adelung, R.; Lotnyk, A.; Kienle, L.; Schulte, K., Aerographite: ultra lightweight, flexible nanowall, carbon microtube material with outstanding mechanical performance. *Adv. Mater.* **2012,** *24* (26), 3486-3490.

32. Chatterjee, S.; Murallidharan, J. S.; Agrawal, A.; Bhardwaj, R., Why coronavirus survives longer on impermeable than porous surfaces. *Phys. Fluids* **2021,** *33* (2), 021701.

33. FDA Code of Federal Regulations Title.21. https://www.accessdata.fda.gov/scripts/cdrh/cfdocs/cfcfr/CFRSearch.cfm?CFRPart=582&showFR=1.

34. Agarwal, H.; Menon, S.; Kumar, S. V.; Rajeshkumar, S., Mechanistic study on antibacterial action of zinc oxide nanoparticles synthesized using green route. *Chem.-Biol. Interact.* **2018,** *286*, 60-70.

35. Xie, Y.; He, Y.; Irwin, P. L.; Jin, T.; Shi, X., Antibacterial activity and mechanism of action of zinc oxide nanoparticles against Campylobacter jejuni. *Appl. Environ. Microbiol.* **2011,** *77* (7), 2325-2331.

36. Raghupathi, K. R.; Koodali, R. T.; Manna, A. C., Size-dependent bacterial growth inhibition and mechanism of antibacterial activity of zinc oxide nanoparticles. *Langmuir* **2011,** *27* (7), 4020-4028.

37. Sirelkhatim, A.; Mahmud, S.; Seeni, A.; Kaus, N. H. M.; Ann, L. C.; Bakhori, S. K. M.; Hasan, H.; Mohamad, D., Review on zinc oxide nanoparticles: antibacterial activity and toxicity mechanism. *Nano-Micro Lett.* **2015,** *7* (3), 219-242.

38. Patra, J. K.; Baek, K.-H., Antibacterial activity and synergistic antibacterial potential of biosynthesized silver nanoparticles against foodborne pathogenic bacteria along with its anticandidal and antioxidant effects. *Front. Microbiol.* **2017,** *8*, 167.

39. Amro, N. A.; Kotra, L. P.; Wadu-Mesthrige, K.; Bulychev, A.; Mobashery, S.; Liu, G.-y., High-resolution atomic force microscopy studies of the Escherichia coli outer membrane: structural basis for permeability. *Langmuir* **2000,** *16* (6), 2789-2796.

40. Jin, S.-E.; Jin, H.-E., Antimicrobial Activity of Zinc Oxide Nano/Microparticles and Their Combinations against Pathogenic Microorganisms for Biomedical Applications: From Physicochemical Characteristics to Pharmacological Aspects. *nanomaterials* **2021,** *11* (2), 263.

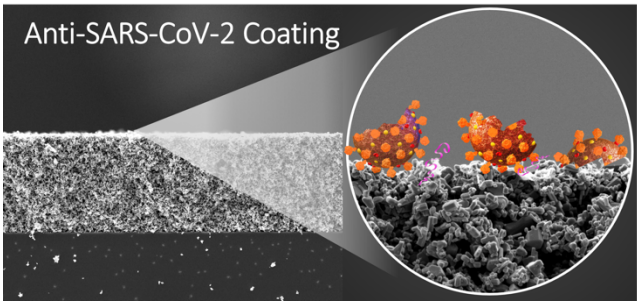
41. Ciołek, L.; Biernat, M.; Jaegermann, Z.; Zaczyńska, E.; Czarny, A.; Jastrzębska, A.; Olszyna, A., The studies of cytotoxicity and antibacterial activity of composites with ZnO-doped bioglass. *Int. J. Appl. Ceram. Technol.* **2019,** *16* (2), 541-551.

42. Huang, Y.-W.; Wu, C.-h.; Aronstam, R. S., Toxicity of transition metal oxide nanoparticles: recent insights from in vitro studies. *Materials* **2010,** *3* (10), 4842-4859.

43. Riddell, S.; Goldie, S.; Hill, A.; Eagles, D.; Drew, T. W., The effect of temperature on persistence of SARS-CoV-2 on common surfaces. *Virol. J.* **2020,** *17* (1), 1-7.

44. Lin, K.; Marr, L. C., Humidity-dependent decay of viruses, but not bacteria, in aerosols and droplets follows disinfection kinetics. *Environ. Sci. Technol.* **2019,** *54* (2), 1024-1032.

For Table of Contents Use Only



7.6. SUPPORTING INFORMATION

Reduction of Infectivity of SARS-CoV-2 by Zinc Oxide Coatings

Mohsen Hosseini[1†], Saeed Behzadinasab[†1], Alex W.H. Chin[†2,3], Leo L.M. Poon*[2,3,4], and William A. Ducker*[1]

[†] These authors contributed equally

*Corresponding Authors' Email: Leo Poon llmpoon@hku.hk; William Ducker wducker@vt.edu

[1]Dept. of Chemical Engineering and Center for Soft Matter and Biological Physics, Virginia Tech, VA, 24061, USA

[2]School of Public Health, LKS Faculty of Medicine, The University of Hong Kong, Hong Kong Special Administrative Region, China.

[3]Centre for Immunity and Infection, Hong Kong Science Park, Hong Kong, China

[4]HKU-Pasteur Research Pole, LKS Faculty of Medicine, The University of Hong Kong, Hong Kong, China

Keywords: SARS-CoV-2, zinc oxide, zinc oxide tetrapod, coating, coronavirus, antiviral, COVID-19

7.6.1. Materials and Methods

7.6.1.1. Materials

100% Ethanol (ACS grade), 70% ethanol (Reagent grade) 70% nitric acid, and glass slides (Model number 48300-026) were Purchased from VWR. Tetraethyl orthosilicate 99.999% (TEOS) was purchased from Sigma Aldrich and Ammonium hydroxide (Certified ACS Plus) was obtained from Fisher Scientific. Commercial polyurethane (PU) (Miniwax, Fast-Drying Polyurethane, clear satin) was obtained from Lowes Home Improvement Store. Zinc Oxide particle (average particle size 296 nm and the median size 249 nm, see Figure S7-7) was purchased from US Research Nanomaterials and zinc oxide particles tetrapod (ZnO-T) with the average size of 10 μm (grade: WZ-0501) were purchased from Dreytek Inc. Smooth crushed glass (270-1000 grit, catalog number 64223704) was obtained from MSC Industrial Supply Company. The crushed glass was milled for 95 hours in a generic mill jar (U.S. Stoneware roller mill) with alumina milling media with the rate of 0.5 rotation per sec to obtain small glass particles. Deionized (DI) water was purified by Milli-Q Reference system.

7.6.1.2. Fabrication of ZnO/Silica

Glass slides were initially cut into 12×12 mm pieces, which we refer to as substrates, and cleaned using the following method. The substrates were first rinsed three time times in DI water and left in 70% ethanol for 15 minutes, rinsed completely with DI water, soaked in a 6M nitric acid for 20 minutes, rinsed with water to ensure that acid was removed from the surface, and, finally, dried with a nitrogen gas.

The key design feature is for the binding material to not engulf the entire surface of the active material. To achieve this feature, we produced liquid menisci between the particles and then solidified the menisci in place using a gas phase catalyst that was a variant of the Stöber method.[1,2] . A 20% (vol/vol) TEOS in ethanol solution was sonicated for five minutes before sub-micron ZnO particles were added to produce a final ZnO loading of 0.16 g/mL suspension. The suspension was sonicated for 15 minutes to yield a uniform colloidal system prior to the application on the surface. The glass substrates were activated with 5-minutes of oxygen plasma cleaning at P<200 mTorr and 100 W on glass slides to create reactive groups that are the active sites for the adhesion through sol-gel process.[3] Immediately after the plasma cleaning 50 µL of the ethanol/TEOS/ZnO suspension was applied on each glass piece in a leveled container and left to dry for 3 hours. Samples were then exposed to vapors of 8 M DI water in ethanol and 7.62 M ammonia in DI Water for 20 hours. Following this, a one-hour heat treatment step at 160 °C was applied to generate the silica menisci. Samples were then blown with nitrogen to remove unattached particles, rinsed in DI water for 10 minutes and dried using a stream of nitrogen gas.

7.6.1.3. Fabrication of ZnO-T/PU

The ZnO-T/PU was made as follows**:** first, a thin layer of polyurethane was cast on a glass slide (25 x 75 mm) with a sponge. It was allowed to partially cure at room temperature for approximately 6-8 minutes. After this time, the film shows only slight marking when it was touched with a gloved hand. ~1.4 mL of ZnO-T suspension in ethanol (8%w/w) was then drop cast on the PU film. The film was left to partially dry for about 7-8 minutes at room temperature. Subsequently, it was heat treated in an oven for 2 hours at 120 °C to complete the curing. The coating was then blown with high pressure nitrogen gas, washed thoroughly with DI water, and

dried with nitrogen gas. The glass film was broken into smaller sizes (≈ 12×12 mm pieces) and each piece was cleaned with argon plasma for 3 min at ≈ 100 W and <200 mTorr (See Figure S7-6).

7.6.1.4. Fabrication of porous glass surfaces

Glass slides were cut into 15×15 mm pieces, rinsed with DI water and dried using a nitrogen stream. A 10.5 wt.% milled glass in ethanol suspension was sonicated for 6 min and then 280 µL suspension was applied on the glass substrate. Upon the evaporation of ethanol at room temperature, the samples were put in a furnace at 120° with gradual increasing of the temperature up to 617 °C to generate early stage necks between the particles. After 2 hours, the furnace was switched off and the samples cooled down overnight. Samples were the rinsed with DI water and dried using a nitrogen stream. Figure S7-9 shows the elemental comparison of flat and porous glass samples and also SEM image of porous glass surface, clearly confirming the porous nature of it.

7.6.1.5. Characterization

Scanning Electron Microscope (SEM, JEOL IT500 SEM) equipped with Energy Dispersive X-ray Spectrometer (EDS, Oxford Instruments NanoAnalysis) was used to characterize the morphology and the composition of the coatings. X-ray photoelectron spectroscopy (XPS, PHI VersaProbe III with a monochromatic Al Kα source of 1486.6 eV) was utilized to evaluate the outer few nanometers composition of the samples. A Bruker D8 ADVANCE diffractometer (monochromatic Cu Kα X-rays, wavelength = 1.5418 Å) was used to obtain the X-ray diffraction pattern. The contact angles of a 5 µL DI water droplet on the samples were measured using a First Ten Angstroms FTA125 device.

7.6.1.6. Preparation of SARS-CoV-2 culture

The SARS-CoV-2 strain was isolated from the index case of Hong Kong. 2% fetal bovine serum and 1% v/v penicillin-streptomycin were added to the Dulbecco's Modified Eagle Medium. The virus stock was prepared in Vero-E6 cells cultured in DMEM At 37°C under 5% CO_2.

7.6.1.7. Inactivation of SARS-CoV-2

Our viral assay methods were done as described previously.[4-6] In brief, prior to the SARS-CoV-2 stability tests, all of the surfaces and coatings were sterilized with 70% ethanol. The environmental conditions were set to 22-23°C and 60–70% relative[7] humidity. A 5 µL droplet containing 6.2 x 10^7 (7.8 $\log_{10}$ unit) $TCID_{50}$/mL of SARS-CoV-2 was placed on the test solids. After a predefined period of time, the tests solids were eluted in 300 µL of viral transport medium at room temperature (approximately 22 °C). The zero time point data was eluted within one minute. We used Earle's balanced salt solution (pH 7.4) supplemented with 0.5%(w/v) bovine serum albumin and 0.1%(w/v) glucose as the viral transport medium. Subsequently, the eluted virus was titrated using 50% tissue culture infective dose ($TCID_{50}$) assay in Vero E6 cells.[8,9]

Three independent coated samples were tested at each time point. For each sample, four replicate plaque measurements were done and assessed by the Reed-Muench method.[10] We conducted a statistical analysis and found that a log transformation is needed to obtain a normally distributed residuals of errors. Therefore, all averages values were calculated from the log of the titers. For log reduction, the titers have been divided through by the units, and the same procedure and units have been used for all samples.

7.6.1.8. ASTM D3359 adhesion test

We tested the adhesion of our coatings according to ASTM D3359 standard. In this test, a pattern is cut on the coating using a razor blade, blushed softly and then a piece of tape is placed on the cut portion. The tape is rubbed using a rubber eraser to ensure adhesion to the coating. Within 60 second of application, the tape is peeled off such that it makes a 180° angle with the test solid. Finally, the coating condition before and after the application of tape is evaluated for any defects and the coating is rated according to ASTM D3359 tables. The pattern that is cut depends on thickness of the coating. For coatings with thickness below 50 microns (e.g., ZnO/Silica), a cross hatch pattern is cut on coatings to generate a 10×10 grid of 1 mm^2 coated regions. For coatings with thickness greater than 125 microns (e.g., ZnO-T-PU), an X pattern with the smaller angle between 30° and 45° is cut on the coating.

7.6.1.9. Statistical Tests

All uncertainties, including error bars, are 95% confidence intervals. Error bars in Figures 2 and 3 are the 95% confidence interval of all the residuals between data points and the mean of each group. Data from groups where data was below the detection limit was not included in calculation of the confidence interval. The level of significance was 95%, e.g., $p < 0.05$.

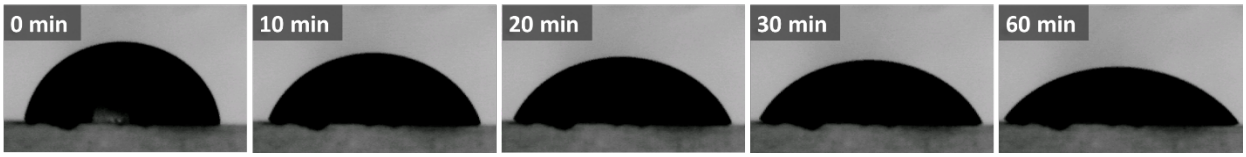


Figure S7-1. Time series of photographs showing imbibition of a 5 μL droplet on ZnO/TEOS coating in a highly humid environment. Note that there is a slight loss in volume of visible droplet after 60 minutes. This is not due to evaporation, as the surrounding air is approaching 100% relative humidity. The loss is due to imbibition of the liquid into the ZnO coating, see Figure S7-3.

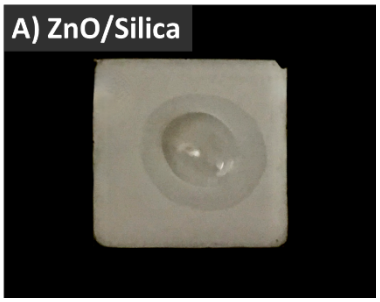


Figure S7-2. Droplet on ZnO/TEOS coating after 60 minutes at 30% relative humidity and 22°C. There is a wet ring around the droplet showing where the water has partially imbibed into a disk around, and presumably under, the droplet. The brightness and contrast of the image were slightly altered to better show the disc around the droplet.

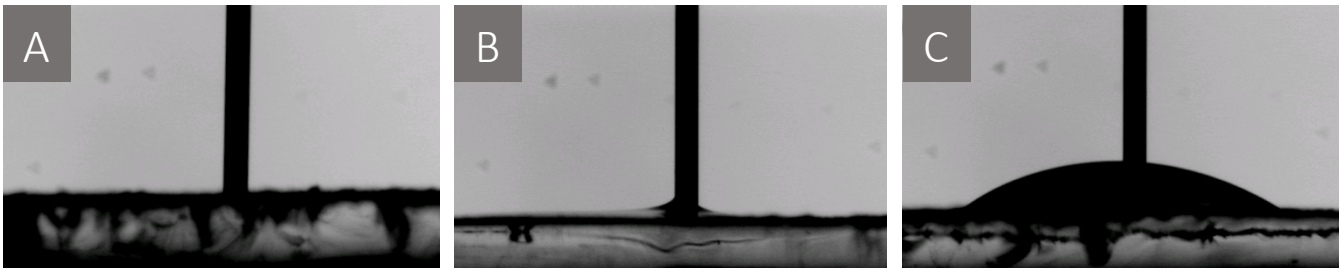


Figure S7-3. Images of advancing contact angles of the porous ZnO-T/PU coating using a 10 μm droplet. A) day 0, immediately after plasma-treatment, the droplet is not visible because it has imbibed into the coating within a few seconds. B) Day 11 after plasma treatment, the droplet still imbibes into the coating. C) A different sample to A and C on Day 11 after plasma treatment. For the sample shown in C there is only partial imbibition. Of the ten samples that we tested, 7 imbibed the entire droplet immediately, even if the sample was aged for 7 days prior to testing, and 3 caused partial imbibition with about 40º advancing contact angle and 0°receding angle. For all samples there was little to no change in contact angle over 11 days.

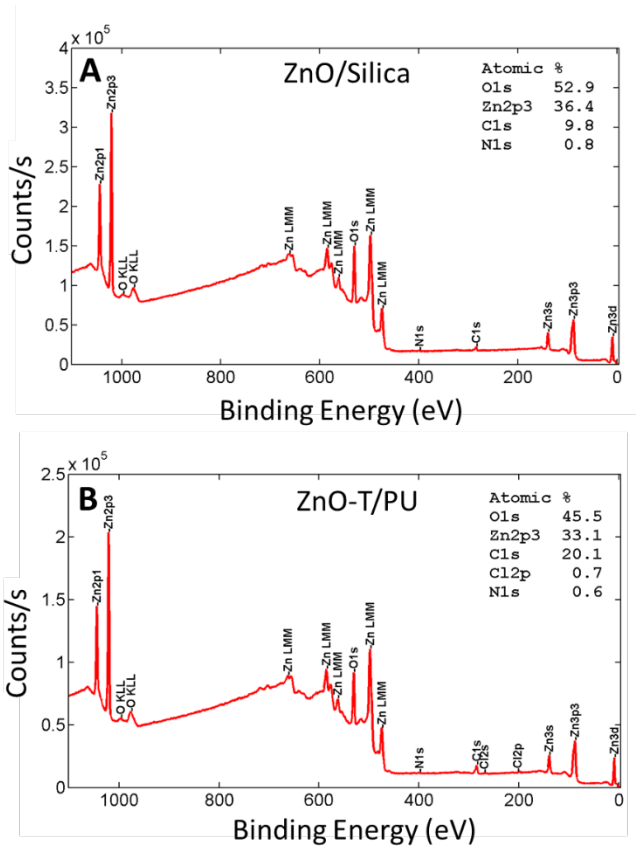


Figure S7-4. XPS spectra and the elemental analysis of the outer surface of A) ZnO/Silica and B) ZnO-T/PU.

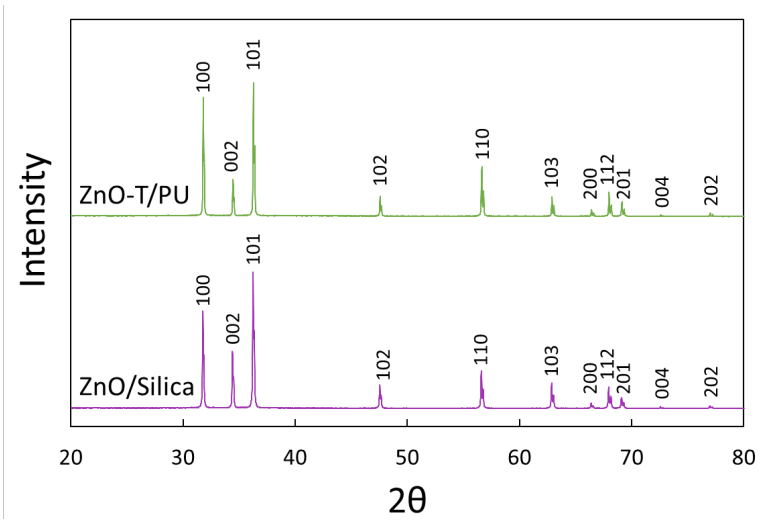


Figure S7-5. XRD pattern of the coatings. A) ZnO/TEOS and B) ZnO-T/PU. The XRD patten of both coatings match the wurtzite structure of zinc oxide in the literature.[11-13] The numbers on top of the peaks indicate the Miller indices.

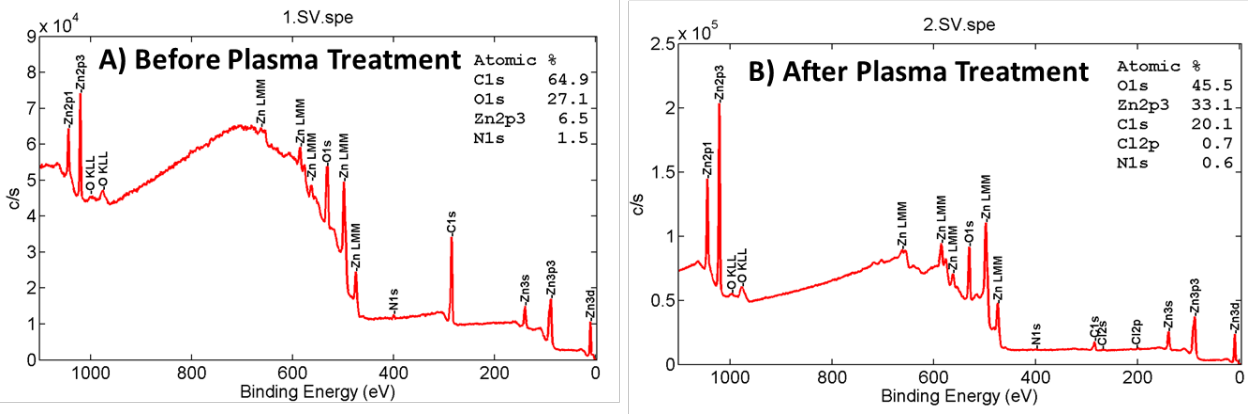


Figure S7-6. XPS survey spectra of the ZnO-T/PU surfaces of (A) before and (B) after plasma treatment. The tables in the insets show elemental atomic %. The elemental percentage of zinc oxide increases after plasma treating the surface, and the scale has been increased in (B) to accommodate the larger Zn peak.

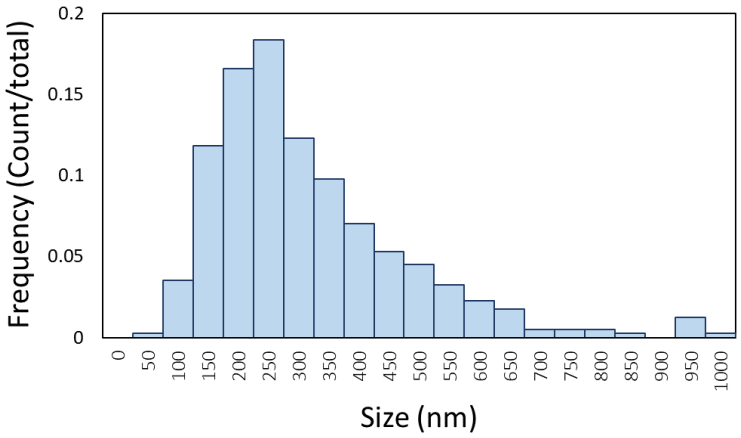


Figure S7-7. Size distribution histogram of ZnO sub-micron particles using to form the ZnO-silica coating. The average particle size is 296 nm and the median size is 249 nm. 200 particles were counted.

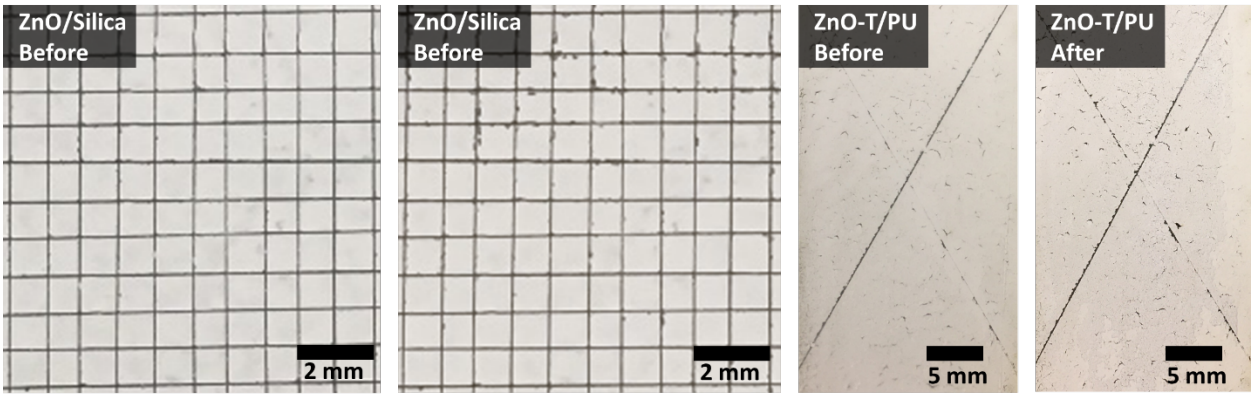


Figure S7-8. ASTM D3359 adhesion test result for ZnO coatings. Photographs are shown for samples before and after the peel test. There is little damage to the coating as a result of the peel. Three independent sample of each coating were tested and both coatings demonstrated a satisfactory adhesion, where the adhesion for ZnO/Silica and ZnO-T/PU were rated more than 3B and 3A respectively, corresponding to more than 85% adhesion.

Element	Porous Glass	Glass Slide
O	58.2	60.9
Si	21.1	22.7
C	13.9	12
Na	3.5	1.9
Ca	1.3	0.9
Mg	1.3	0.7
Zn	0.6	0
N	-	0.5
Cl	0.2	-
Al	-	0.4

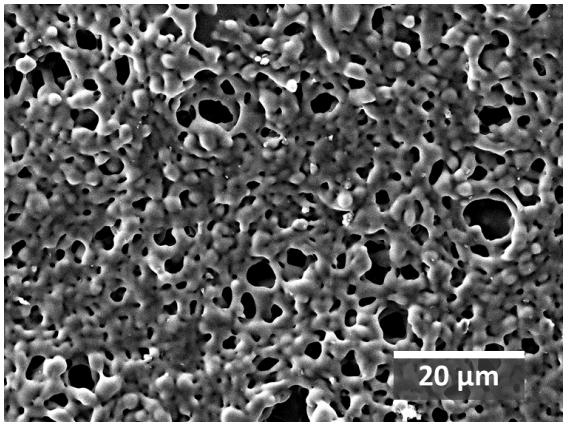


Figure S7-9. Left: Table comparing the elemental composition of porous glass and uncoated glass slide measured by XPS. Results show that the chemistry of these two samples are very similar and confirms the porous nature of this sample. Right: SEM image of porous glass.

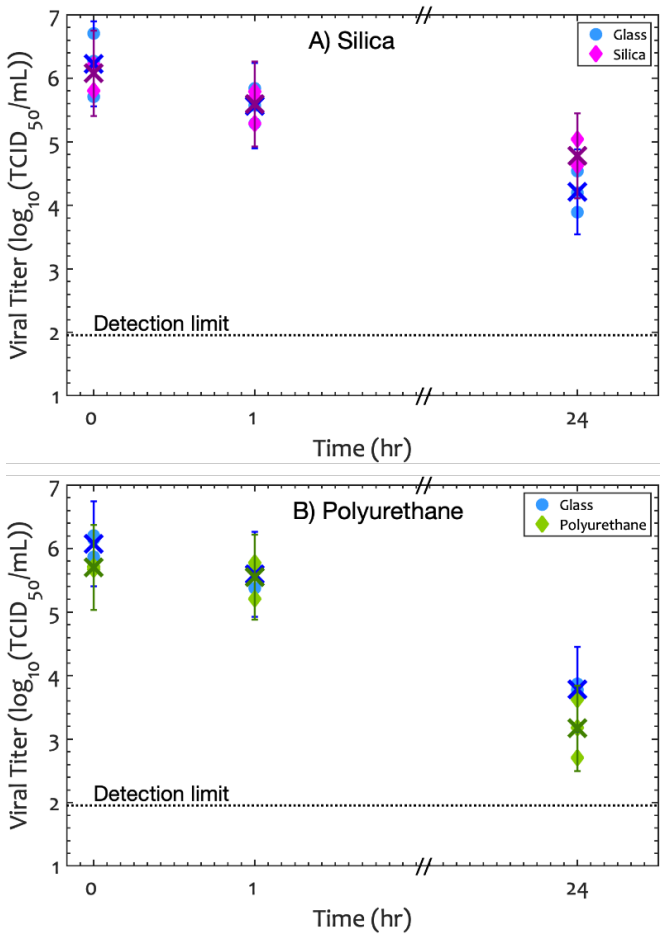


Figure S7-10. Decay of SARS-CoV-2 $TCID_{50}$ titer on A) silica and B) polyurethane compared to glass. The viral titer data on silica and polyurethane was not statistically different from that of glass at each time point. The polyurethane figure data has been extracted from our previous work[4].

Material	Time		$TCID_{50}$/ml			log ($TCID_{50}$/ml)		
Nil (virus input control)	---	1.178×10^{6}	2.358×10^{6}	1.607×10^{6}		6.07	6.37	6.20
Glass	0	5.081×10^{6}	5.081×10^{5}	1.855×10^{6}		6.71	5.71	6.27
	1 h	6.927×10^{5}	1.947×10^{5}	3.7267×10^{5}		5.84	5.28	5.57
	24 h	7.824×10^{3}	3.461×10^{4}	1.559×10^{4}		3.89	4.53	4.19
(ZnO/Silica)	0	1.947×10^{5}	5081×10^{4}	1.607×10^{5}		5.29	4.71	5.21
	1 h	<	<	<		<	<	<
	24 h	<	<	<		<	<	<
(ZnO-T/PU)	0	6.927×10^{5}	4.728×10^{5}	7.458×10^{5}		5.84	5.67	5.87
	1 h	<	<	187		<	<	2.27
	24 h	<	<	<		<	<	<

Table S7-1. TCID50/mL data for figure 2. The sign "<" means "below the detection limit", which was TCID50/ml = 90, which corresponds to log (TCID50/ml) = 1.95

Material	Time	$TCID_{50}$/ml				log ($TCID_{50}$/ml)		
Nil (virus input control)	---	5.081×10^5	5.081×10^5	1.496×10^6		5.71	5.71	6.17
Glass	0	1.607×10^6	1.167×10^6	6.156×10^5		6.21	6.07	5.79
	1 h	4.194×10^5	4.728×10^5	2.358×10^5		5.62	5.67	5.37
	24 h	7.458×10^4	5.081×10^4	1.178×10^5		4.87	4.71	5.07
Porous glass	0	1606	1606	2022		3.21	3.21	3.31
	1 h	160	1326	381		2.21	3.12	2.58
	24 h	<	<	<		<	<	<

Table S7-2. $TCID_{50}$/mL data for figure 3. The sign "<" means "below the detection limit", which was TCID50/ml = 90, which corresponds to log ($TCID_{50}$/ml) = 1.95. There are minor differences between the glass measurement in Tables S1 and S2. Comparisons between data on flat and porous glass in the manuscript used data in Table S2 only.

References

[1] Pramila P Ghimire and Mietek Jaroniec, Journal of Colloid and Interface Science (2020).

[2] Werner Stöber, Arthur Fink, and Ernst Bohn, Journal of colloid and interface science **26** (1), 62 (1968).

[3] Yow-Ren Chang, Shane Taylor, Scott Duncan, Dan A Mazilu, AL Ritter, and William A Ducker, Colloids Surf., A **514**, 185 (2017).

[4] Saeed Behzadinasab, Alex Chin, Mohsen Hosseini, Leo Poon, and William A Ducker, ACS Appl. Mater. Interfaces **12** (31), 34723 (2020).

[5] Mohsen Hosseini, Alex WH Chin, Saeed Behzadinasab, Leo LM Poon, and William A Ducker, ACS Appl. Mater. Interfaces **13** (5), 5919 (2021).

[6] Alex W. H. Chin, Julie T. S. Chu, Mahen R. A. Perera, Kenrie P. Y. Hui, Hui-Ling Yen, Michael C. W. Chan, Malik Peiris, and Leo L. M. Poon, Lancet Microbe **1** (1), e10 (2020).

[7] Johns Hopkins University (JHU), 2020. https://coronavirus.jhu.edu/map.html

[8] KH Chan, ST Lai, LLM Poon, Y Guan, KY Yuen, and JSM Peiris, J. Clin. Virol. **45** (3), 205 (2009).

[9] Hana Malenovska, J. Virol. Methods **191** (2), 136 (2013).

[10] Lowell Jacob Reed and Hugo Muench, Am. J. Epidemiol. **27** (3), 493 (1938).

[11] Kai-sheng Yu, Jian-ying Shi, Zai-li Zhang, Yong-mei Liang, and Wei Liu, J. Nanomater. **2013** (2013).

[12] Rajeswari Yogamalar, Ramasamy Srinivasan, Ajayan Vinu, Katsuhiko Ariga, and Arumugam Chandra Bose, Solid State Commun. **149** (43-44), 1919 (2009).

[13] Mehdi Zareie, Abed Gholami, Mohammad Bahrami, Amir Hossein Rezaei, and Mohammad Hossein Keshavarz, Mater. Lett. **91**, 255 (2013).

Chapter 8. Antimicrobial Mechanism of Cuprous Oxide (Cu_2O) Coatings

Saeed Behzadinasab[1,2,3], Myra D. Williams[4], Joseph O. Falkinham III[4], and William A. Ducker*[1,2,3]

[1]Department of Chemical Engineering, Virginia Tech, Blacksburg, Virginia, 24061, USA

[2]Center for Soft Matter and Biological Physics, Virginia Tech, Blacksburg, Virginia, 24061, USA

[3]Macromolecules Innovation Institute, Virginia Tech, Blacksburg, Virginia, 24061, USA

[4]Department of Biological Sciences, Virginia Tech, Blacksburg, Virginia, 24061, USA

Authors' Email: Saeed Behzadinasab saeedb@vt.edu; Joseph Falkinham jofiii@vt.edu; William Ducker wducker@vt.edu

Keywords: mechanism, Cu2O, copper, copper oxide, antibacterial, antimicrobial, coating, bacteria, surface

ORCIDs:

Saeed Behzadinasab: 0000-0002-6271-2623

Joseph O. Falkinham III: 0000-0002-4391-9012

William A. Ducker: 0000-0002-8207-768X

8.1. Abstract

Some very effective antimicrobial coatings exploit copper or cuprous oxide (Cu_2O) as the active agent. The aim of this study is to determine the active chemical species that arises from Cu_2O, with the aim of improving the efficacy of these coatings. We investigated three mechanistic routes that have been proposed previously: ion leaching, contact killing, and generation of reactive oxygen species (ROSs) against *Pseudomonas aeruginosa*. We conclude that ion leaching is an important antimicrobial mechanism and that the most potent species is Cu^+. The concentration of copper species leached from Cu_2O into aqueous solution depends strongly on the composition of the aqueous solution, and for a range of solution buffers, the killing of *P. aeruginosa* was highly correlated with the concentration of copper in the leachate. This killing occurred without contact between the bacterium and the solid, demonstrating that contact with Cu_2O is not necessary for efficacy. However, further experiments show that contact with solid Cu_2O aids killing (reduction of 99.2% in 10 min compared to uncoated control). We attribute part of this benefit to the ability of the solid to quickly raise the concentration of soluble copper species near the bacterium. When we blocked access of the bacteria to solid Cu_2O by coating the solid with a 0.7 μm thick layer of the polymer, carboxymethylcellulose (CMC) there was still a reduction of 99.6% of *P. aeruginosa* in 10 min. This demonstrates that molecular contact between the bacterium and the solid surface is not necessary. Finally, measurements also showed that generation of ROSs and the exposure to light were not significant contributors to the killing action of Cu_2O surfaces against *P. aeruginosa*.

8.2. Introduction

Microorganisms on surfaces in hospitals and healthcare facilities are sources of infections.[1-4] Touch screens are an example of such surfaces that are touched by multiple individuals in a short period of time. Antimicrobial surface coatings have emerged as a tool combat the human to human transmission of microbes and viruses via contaminated solids that are touched by more than one person.[5-6] They have been shown to decrease the incidence of disease and infections in healthcare units,[7] and lead to a significant decrease[8] in aerobic bacteria, where they were applied. The traditional method of combatting such transfer is to use disinfectants such as bleach, 70% ethanol, and/or quaternary ammonium ions. Antimicrobial coatings are distinguished from these common disinfectants by the ability to offer long-lasting killing activity. A disinfectant only kills microbes that were present prior to disinfection (or perhaps for a few minutes afterward). An antimicrobial coating is designed with two timescales in mind. The first is a quick kill in a few minutes (as for traditional disinfectants) and the second is a long timescale of days, weeks, months, or years over which the antimicrobial coatings will continue to provide the minute-scale kill. This ongoing kill provides a better, continuous, protection, and is also cost-effective by reducing or eliminating the labor cost of frequently wiping surfaces with disinfectant.

A wide variety of materials or chemicals have been exploited as the active ingredient in antimicrobial coatings. Examples are polymers that possess antimicrobial properties, such as polyamines,[9-10] polyimines,[11-12], layer by layer fabrication of polycations and polyanions,[13-14] and side chain modified polyacrylates[15], and inorganic materials containing metal ions, including copper,[16-17] silver,[18-19] zinc,[20] gold,[21] their oxides,[22-24] or alloys.

In this work, we specifically consider copper in its lower oxidation state, cuprous oxide (Cu_2O). The native surface of metallic copper is oxidized and it is likely that many copper metal surfaces that have been studied have a surface that is primarily oxidized copper. Metallic copper and its oxides have shown antimicrobial activity against a broad range of pathogens, including bacteria, mycobacteria, and fungi.[16-17, 22-23, 25-32] We focus on microparticles (1 μm < diameter < 10 μm) in order to avoid the possible hazards of nanoparticles. An epidemiological study has shown a reduced incidence of infections subsequent to the implementation of Cu_2O coatings in a clinical setting,[33] and its use in clinical settings has been reviewed.[25] Copper and its oxides are also abundant and inexpensive, which makes them attractive active antimicrobial agents. Finally their toxicity to humans is low, [34-35]. and copper is already present in human blood.[36] The main disadvantage is toxicity to aquatic lifeforms, which are not commonly present in hospital applications but may be ultimately be impacted by waste water.

In order to optimize the action of copper-based antimicrobials, it would be beneficial to understand their mechanism of action. Here we limit our scope to understanding the nature of the active species, not the metabolic consequences of exposure of microbial cells to Cu_2O. Prior research suggests metals and metal oxides have three routes to killing microbes and has been reviewed by several authors:[24, 37-39] (1) leaching of active agents such as metal cations, (2) killing by contact or adsorption with the solid,[40] and (3) generation of reactive oxygen species (ROSs), which then go on to kill the microbes. In the design of antimicrobials, it would, for example, be useful to know whether direct contact of the microbe was required, or whether it is beneficial for cations to diffuse to the microbes.

The current literature on mechanism of action of metal (oxide) particles is heavily focused on the mechanism that occurs when both particles and bacteria are in suspension,[37, 41]

whereas we believe that the most likely application is antimicrobial solids. Suspension and surface killing differ in several important aspects. In suspension, both the active ingredient and the microbe transport through the liquid, and active mixing is often implemented in experiments. On a solid, there is no active mixing, therefore passive transport dominates. Fomite infection occurs when droplets contaminate solids, so the dynamics of droplets also influences activity. For example, wetting affects contact with the solid and evaporation causes natural mixing, concentrates active ingredients, and can change the temperature.

The ion leaching mechanism occurs when metal- or metal-containing-ions are solubilized in the aqueous solution, and cause damage to cells. While low concentrations of various metal ion are beneficial or necessary for cell function, when the concentration of these ions increases, they become toxic to the cell. It has been demonstrated that metal leaching causes damage to membranes,[42-43] enzyme modification,[44-45] or DNA/RNA effects.[46-47]

Ion leaching from metals is dependent upon the characteristics of the environment,[48-50] such as the pH,[51-52] composition of the liquid,[53-54] or temperature.[53, 55] The current literature contains conflicting evidence regarding the effect of particle characteristics (such as particle size) on dissolution, this conflict is largely about nano-sized particles,[49-50, 56-59] whereas this work focuses on microparticles. Recent work by our group showed that chelation of Cu^{+} ions reduced the efficacy of Cu_2O coatings, demonstrating the role of free Cu^{+} ions in killing cells.[26] That work concluded that drying of liquid droplets was critical for efficacy: bacteria did not die as quickly if they were suspended in droplets that were prevented from drying as they did in drying droplets[26]

Here we use the term “contact killing” to describe the killing of cells due to direct contact between the cell and solid antimicrobial particle. Note that some authors use contact killing to mean killing that occurs on solids, which could include all three mechanisms.[40] During contact killing, the cell wall or membrane can be damaged[40] or small nano-sized metal particles can be formed inside the cell.[60] Also, the DNA molecule of the microbe can be damaged.[40] Sunada *et al* concluded that direct contact was the antimicrobial mechanism for Cu_2O.[31] This was primarily based on experiments showing antimicrobial efficacy when Cu_2O was physically separated from the pathogen.

Another mechanism is the generation of reactive oxygen species (ROSs). ROSs are highly reactive species that can damage biological structures through oxidation.[61] ROSs include hydrogen peroxide (H_2O_2), superoxide ($^{\bullet}O_2^-$), hydroxyl radical ($^{\bullet}OH$) and singlet oxygen ($^1O_2$).[61] These ROS have very short half-lives;[62] the half-life for singlet oxygen in water is ~ 4 μs and for hydroxyl radicals 1 μs. Almost all cells, including bacterial cells, produce H_2O_2. Cu^+ is known to interact with H_2O_2, through the following “Fenton-like” reaction that produces hydroxide radicals:[31, 63]

$$Cu^+ + H_2O_2 \rightarrow Cu^{2+} + OH^- + {\bullet}OH$$

The standard reduction potential of Cu^{2+} is only 0.15 V so it can move between valence states easily (oxidize Cu^+ or to reduce Cu^{2+}) within the physiological conditions of microorganisms encountered in hospital and healthcare facilities.[64] While the ROSs can affect survival of bacteria,[65] current literature concludes that ROSs do not play a role in inactivation of viruses,[31, 66] Viruses are metabolically inert, so have reduced levels of H_2O_2 for reaction with metal cations. Sunada et al demonstrated that the efficacy of cuprous oxide against viruses was

unaffected by the use of an oxygen free environment, leading them to conclude that that ROS do not affect cuprous oxide efficacy.[31] In their work, cuprous oxide was separated in two different experiments, one with a filter and the other by reaction with the passivating agent 1H-benzotriazole. We note that 1H-benzotriazole also passivates the solid, so that dissolution of copper cations may have been inhibited in this experiment, thereby preventing two mechanisms.

Mechanisms of killing by Cu_2O surfaces may vary by species and in this work we focused (exclusively) on *Pseudomonas aeruginosa (P. aeruginosa*; strain DSM-9644), which is the organism used by the US Environmental Protection Agency (EPA) in assessment of antimicrobial efficacy, [67-68] and *P. aeruginosa* is considered a "Serious Threat" by the US CDC.[69-71]

Our method was to examine each of the three mechanisms separately. To examine dissolved ions only, we leached ions out of Cu_2O solid, then removed the solid by filtration and centrifugation. We found that leachate in PBS does not influence killing of *P. aeruginosa*. However, we also found that the concentration of dissolved copper in the leachate is strongly affected by the presence of other soluble species and can be increased greatly. In the presence of Dulbecco's Modified Eagle Medium (DMEM, a common medium for mammalian cell growth[72]), there was 1000× as much copper and much better killing. This shows that it is not necessary for *P. aeruginosa* to make direct contact with Cu_2O. Additionally, we found that the generation of ROSs are not involved in the mechanism of Cu_2O surfaces against *P. aeruginosa*.

8.3. Results and Discussion

8.3.1. The Concentration of Dissolved Copper Species is a Strong Function of the Solution Composition.

We began our study of the effect of dissolved copper species (leachate) by measuring the concentration of copper in equilibrium with solid Cu_2O. It is well-known that the rate of leaching of metal ions depends on the pH and the chemical composition of the solution,[73-74] so we investigated a variety of solution compositions. We used inductively-coupled-plasma mass-spectroscopy (ICP-MS) to measure the total copper in equilibrium with the Cu_2O microparticles for a variety of aqueous solutions. The disadvantage of ICP-MS is that it does not discriminate between various copper species. Copper has two oxidations states (Cu^+ and Cu^{2+}) plus a variety of hydroxides and chloride complexes[75] and ICP-MS measures the total of all these forms of soluble copper. Dissolved Cu^+ spontaneously disproportionates into Cu^{2+} and Cu[75-76] so, in any case, it is difficult to reliably obtain separate concentrations of Cu^+ and Cu^{2+}, as described previously.[77]

Our experiments show that the concentration of copper leachates is a strong function of the other species present in the test liquid (see Table 8-1). For distilled (DI) water, the concentration was 300 μM whereas in phosphate buffered saline (PBS), it was only 3 μM. In contrast, we found a very large concentration of copper, 4,200 μM leached into Dulbecco's Modified Eagle Medium (DMEM), which is a widely used growth medium for mammalian cells,[72] and therefore is also used as a medium for testing pathogens of mammals.[23] Therefore, our first conclusion is that the concentration of dissolved copper that is presented to bacterial cells in suspension by Cu_2O depends critically on the buffer that is used to suspend the cells.

The observed effect of diminished copper solubility with added electrolyte is the opposite direction and too large an effect to be explained Debye-Huckle theory ("salting in"). The magnitude is too small, and the concentration of salt in the buffers is low compared to the levels usually experienced for a generic "salting out" effect. Thus, we attribute the buffer effects on the solubility to chemical interactions between copper and the species in the buffers (the "common ion" effect). PBS contains 137 mM NaCl, 2.7 M KCl, 10 mM Na_2HPO_4 and 1.80 mM K_2HPO_4. Cu^+ forms a relatively insoluble compound with Cl^- (the solubility product (K_{sp}) of Cu(I) chloride is only 1.2×10^{-6} at 25 ºC) and very insoluble compounds with PO_4^{2-}.[78] Both Cl^- and PO_4^{2-} will limit the solubility of Cu^+ until the finite amount of these ions in solution has depleted by formation of insoluble solid. The very low concentration of copper leachate in PBS is likely due to the very low solubility of Cu^+-phosphate, but the measurable amount of Cu^+ in PBS suggests that most of the phosphate has been depleted. More Cu^+ was measured in 0.15 M NaCl. In this case, we expect the concentration to be limited by Cl^-. For unit activity coefficient, the solubility of Cu^+ in 0.15 M Cl^- should be only 8 μM whereas we measure 20 μM Cu^+ in the NaCl solution. Some of the increased solubility will be due to a decreased activity coefficient in the NaCl solution, but it is likely that some Cl^- has been depleted. In summary, the solubility of Cu^+ decreases in PBS and NaCl compared to water in qualitative accordance with the known solubility of Cu^+ species. Therefore, we expect the antimicrobial efficacy of Cu_2O leachate to depend on the leaching solution.

The very high dissolution of copper species from DMEM is intriguing and worthy of further investigation. DMEM is a mixture of many components (see Table S8-1) including 0.9 mM $NaHPO_4$ and a concentration of Cl^- similar to that in PBS or the NaCl solution we tested, so it is at first surprising that it solubilizes so much copper. We examined two of these components,

$NaHCO_3$ and Fetal Bovine Serum (FBS) and combinations of these with NaCl at the concentrations used in DMEM. We found that both $NaHCO_3$ solution (150 μM) and FBS solution (120 μM) leached a considerable concentration of copper. When NaCl was added to either $NaHCO_3$ or FBS, the copper concentration remained high, which leads us to believe that $NaHCO_3$ and FBS each solubilized copper in a form that was not the simple Cu^+ ion.

So, we conclude that DMEM leaches much more copper than PBS because various agents in the mixture bind or chelate the copper in a soluble form. To further examine this hypothesis, we examined leaching into 6 mM solutions of two known chelating agents: ethylenediaminetetraacetic (EDTA) and BCCA (bicinchoninic acid) that form soluble complexes with Cu^+. EDTA can chelate both Cu^+ and Cu^{2+}, whereas BCCA is a Cu^+-selective chelator.[79] EDTA leaches slightly more copper (5,700 μM) than DMEM and BCCA slightly less (2,300 μM). The ability of the ICP-MS to detect chelated copper from Cu_2O provides indirect support that chelation is also occurring in DMEM.

Liquid	Cu concentration (μM)
PBS	3 ± 1
$NaCl_{(aq)}$	$(2.1 \pm 1.4) \times 10^1$
DI water	$(3 \pm 1) \times 10^2$
$NaHCO_{3(aq)}$ (44 mM)	$(1.50 \pm 0.01) \times 10^2$
$NaHCO_{3(aq)}$ (88 mM)	$(4.0 \pm 0.1) \times 10^2$
$BCCA_{(aq)}$ (6 mM)	$(2.3 \pm 0.3) \times 10^3$
DMEM	$(4.2 \pm 0.2) \times 10^3$
$EDTA_{(aq)}$ (6 mM)	$(5.7 \pm 0.3) \times 10^3$
PBS and CMC-coated Cu_2O	8 ± 2

Table 8-1. Total copper concentration as measured by ICP-MS. The medium has a strong effect on the equilibrium copper concentration. The error is the standard deviation rounded to one significant figure. The final entry in the table is for leaching from CMC-coated particles into PBS solution. Additional data is shown in Table S8-2.

8.3.2. Leaching and Drying Can Alter the Oxidation State of Copper

As described earlier, the reduction potential of Cu^+ is very low and Cu^+ can disproportionate, which makes it difficult to control or measure which of Cu^+ and Cu^{2+} species are present in solution. X-ray photoelectron spectroscopy (XPS) is a useful technique in this regard because it can differentiate the two oxidation states. We utilized XPS to determine the Cu^+/Cu^{2+} composition in droplets of leachate from Cu_2O that were dried onto a solid. The solid was polyethylene, which contains no copper, the volume was 10 μL, the same volume used for

antimicrobial tests. A difficulty is that the x-ray beam itself may oxidize materials,[80] so we first conducted controls to determine the composition of dried $CuCl_2$ droplets (Figure S8-2). Some Cu^{2+} in each case was reduced to Cu^{+}, which complicates interpretation. XPS of dried droplets of leachate of Cu_2O into DMEM showed that all the copper was in the form of Cu^{+} (no Cu^{+2}), whereas leachate of Cu_2O into water was about half of each of Cu^{+} and Cu^{2+} (see Figure 8-1). This showed that the chelating agent in DMEM protects the Cu^{+} from oxidation during drying and XPS.

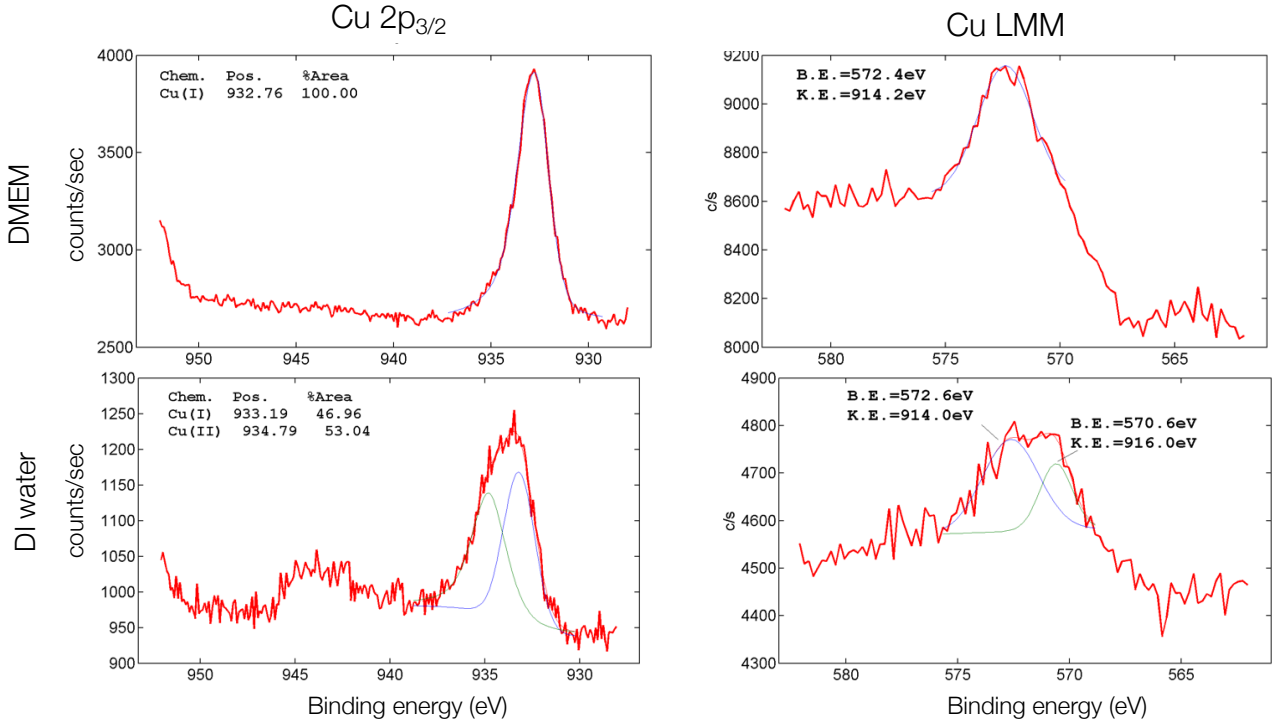


Figure 8-1. XPS spectra of an aqueous droplet dried onto polyethylene (red lines). Each droplet contained leachate from Cu_2O into DMEM (top) or DI water (bottom). For DMEM, the leachates are Cu^{+}, whereas for DI water, the leachates are a mixture of Cu^{+} and Cu^{2+}. Blue lines are fitted Cu(I) spectra and the green lines are fitted Cu(II) spectra.

8.3.3. Killing of *P. aeruginosa* Depends on the Buffer and is Correlated with the Buffer Copper Content.

Being now aware that the concentration of copper ions leached from Cu_2O depends on the buffer, we tested the antimicrobial properties of leachate from each of the buffers. The filtered leachate (no Cu_2O particles) was mixed with suspensions of P. *aeruginosa* and the survival was measured after 60 min. Copper leached into PBS did not kill bacterial cells (p = 0.45), whereas the $NaHCO_3$ leachate killed 99.86% (2.85 logs, p = 0.004) and the DMEN-leachate killed >99.99% (4.1 logs, p = 0.011). Recall that this is the same trend as for the copper concentration measured by ICP (Table 8-1). Figure 8-2 is a plot log kill as a function of log concentration of copper as measured by ICP-MS. Log concentration is plotted because the activity of an ideal solution species scales with log concentration. The plot shows a roughly linear relationship, which suggests that soluble copper kills *P. aeruginosa.* This result is in contrast to those of Sunada et al, who concluded that bacteriophage Qβ required contact with Cu_2O to be inactivated in SM buffer (0.1 M NaCl, 8 mM $_{MgSO4}$, 50 mM Tris–HCl [pH 7.5], and 0.1% gelatin).[31] One complication in that work was that the state of the copper was not reported, but for DMEM, our XPS suggest that the copper is Cu^+. Prior research on *Escherichia coli* also suggested that the active species was Cu^+.[26] Here we also tested known concentrations of Cu^+ and Cu^{2+} solutions against *P. aeruginosa*. Cu^+ was effective against the bacterium, but Cu^{2+} was ineffective; the kill falls below the 95% confidence interval of the linear trend obtained for the leachate solutions. This is consistent with prior work showing that cupric ions are weak antimicrobials.[81]

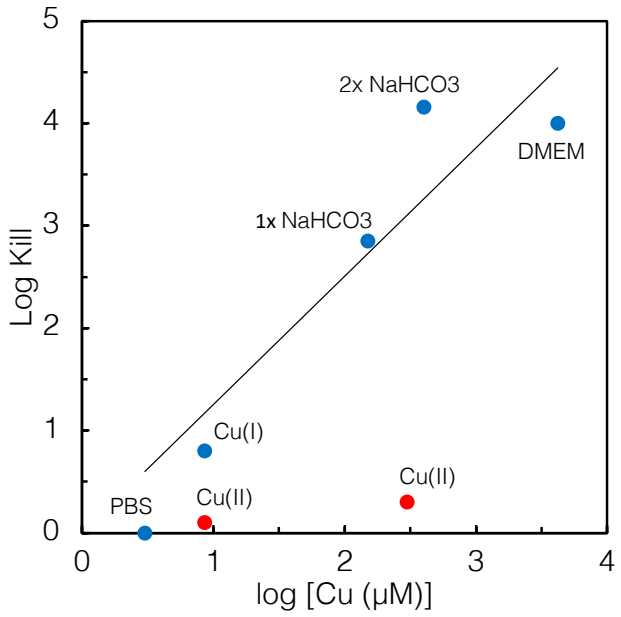


Figure 8-2. Effect of leachate solution on bacterial kill. Aqueous solution where indicated. Kill was measured by CFU and copper concentrations were measured by ICP-MS. Points labelled Cu were prepared form solid Cu compounds; no leaching was done. The kill depends strongly on the leaching solution and there is a linear relationship between log kill and the log soluble copper (slope = 1.3 $\pm$ 0.4, excluding Cu(II) points). The copper solutions were CuCl and $CuCl_2$. Higher concentrations of Cu^+ could not be prepared from CuCl because of the solubility limit.

Additional control experiments were also performed. First, DMEM alone (no copper) did not kill *P. aeruginosa* cells, so the leachate contains the active ingredient. Previously the $NaHCO_3$ concentration was set to match the concentration in DMEM. We also tested a $NaHCO_3$ at twice the concentration (88 mM). At twice $NaHCO_3$ concentration, the copper concentration increased (to 4×10^2 μM) and there was increase in killing (4.16 logs or >99.99%). $NaHCO_3$ is a base and 88 mM $NaHCO_3$ has a pH of 9.7, so the increase in killing may have been due to the high pH. A further control experiment with 88 mM $NaHCO_3$ at pH 7.4 (addition of 2 M HCl prior to exposure to *P. aeruginosa*) led to the same level of killing (p = 0.035) as the solution at pH 9.7, so the pH was not the cause (Figure 8-3). While these tests clearly indicate the pH does

not play a role in killing of *P. aeruginosa* directly or via ion leachate, we cannot rule out some synergy between carbonate species and leachate as all our highly leaching solutions contain some carbonate.

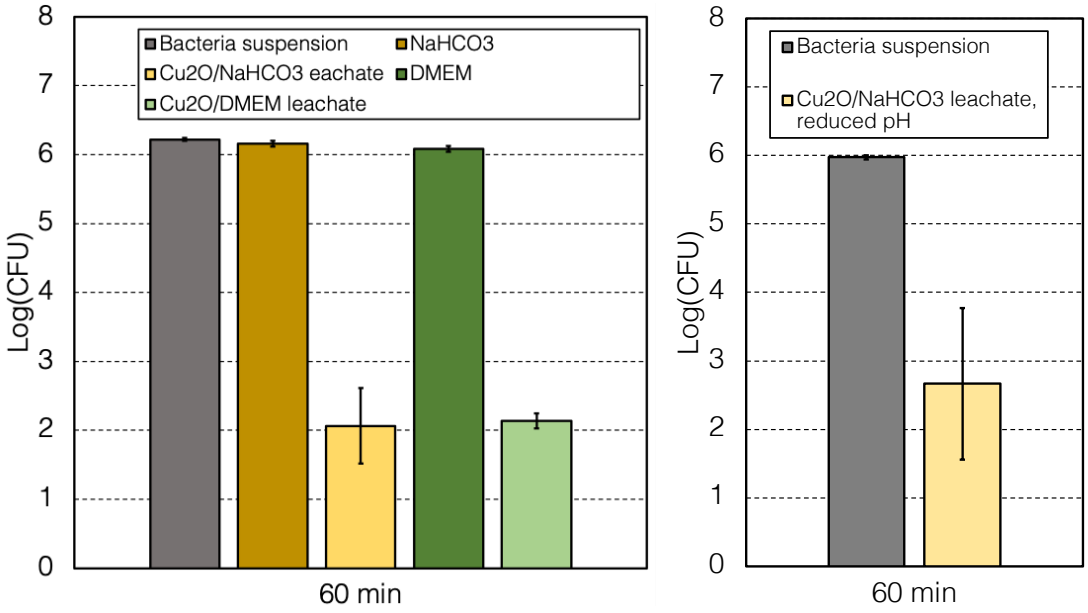


Figure 8-3. Bacterial (*P. aeruginosa*) test with leached copper at various conditions. The sodium bicarbonate concentration was 88 mM and the DMEM included 2% v/v FBS. The detection limit (i.e., all bacteria are dead) is log CFU = 1.7.

Our results thus far suggest that Cu^{+} is the active species. If this is correct, then removal of Cu^{+} from the Cu_2O leachate should decrease the kill. We tested this hypothesis by using the chelating agent, bicinchoninic acid disodium salt hydrate (BCCA) which complexes Cu^{+}.[82] BCCA is thought to be selective for Cu^{+} and not Cu^{2+}.[83] After leaching the copper from Cu_2O in various buffers, we added BCCA to chelate Cu^{+} and then tested the antimicrobial efficacy. Two concentrations of BCCA were used, 1.5 or 10 equivalents of the measured copper concentration in that particular leachate. The results for 10 equivalents are shown in Figure 8-4 and very

similar data for 1.5 equivalents is shown in Figure S8-2. First, we found that 10 equivalents of BCCA did not harm the cells because there was no killing in bicarbonate/BCCA. Second, after introduction of BCCA, the leachate become only a mild antimicrobial, killing only 0.7 log in $NaHCO_3$ and about 0.07 log in DMEM. So we conclude that Cu^+ is the highly antimicrobial species that dissolves from Cu_2O, but there is another more mild antimicrobial species. Possibilities are the Cu^+-BCCA complex, which is an artifact of the current test, or another dispersed species such as copper hydroxides or small nanoparticles of Cu_2O.

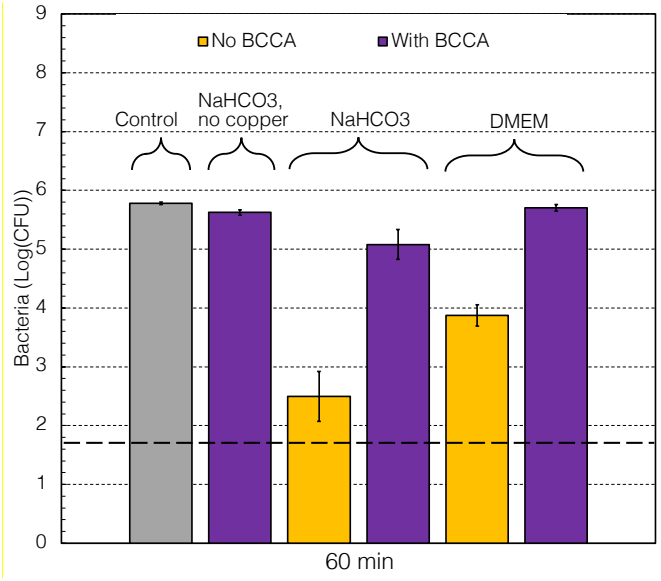


Figure 8-4. Effect of 10 equivalents of BCCA chelating agent on the antimicrobial activity of Cu_2O leachate. The concentration of BCCA used was 10 times the amount of copper that was measured by ICP-MS in that solution. BCCA reduces the antimicrobial effect of the leachate into both DMEM and bicarbonate (44 mM), which suggests that Cu^+ is the potent antimicrobial that leaches from Cu_2O. Data for 1.5 equivalents of BCCA is shown in Figure S8-2.

8.3.4. Cu_2O Solid Surfaces Kill Bacteria in PBS.

Our previous work showed that coatings containing Cu_2O caused very rapid killing of bacterial cells that were suspended in PBS,[16, 22-23] whereas in the current manuscript we found very weak killing of bacteria by leachate into PBS. This suggests that copper leachate is not the entire mechanism. So we repeated tests of the antimicrobial activity of a coating (Cu_2O/PU) that was prepared using polyurethane (PU), and cuprous oxide particles (Cu_2O). The bacterial cells were initially suspended in PBS, and then a 10 μL suspension droplet was placed on the coating. The coating caused a 99.2% reduction in the number of surviving cells of *P. aeruginosa* in only 10 min (see Figure 8-5) which is far superior to the effect of the PBS leachate Therefore, either (1) the killing was achieved by contact with the solid, or (2) the partial drying of the bacterial suspension on the solid kills microbes. However, the mere process of partial drying cells does not have any significant effect on *P. aeruginosa* bacterial cells because there is no kill when the bacteria are simply dried on glass for 10 min (Figure 8-5) Therefore, if drying has an effect, the effect arises from the combination of drying and the copper solid. One possibility is that the drying concentrates the Cu^+ near the bacteria by reducing the volume available to both ion and bacterium.

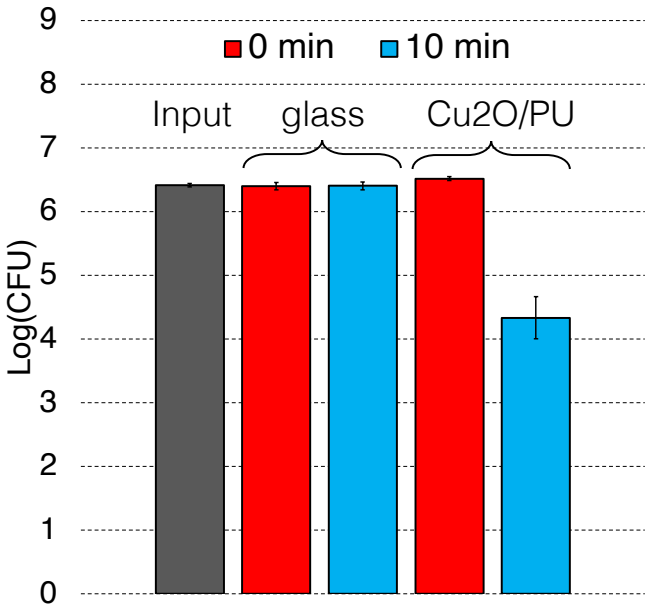


Figure 8-5. Killing of *P. aeruginosa* from droplets on Cu_2O-coated surfaces. The Cu_2O/PU coating causes a reduction of 99.16% in 10 min ($p = 0.0069$). The detection limit is log CFU = 1.7.

8.3.5. Direct Contact with Cu_2O is not Necessary for Killing by Cu_2O

To accurately examine the effect of contact killing, we followed the work of Sunada et al by placing a barrier between the bacterial cells and the solid Cu_2O surface.[31] We utilized an adsorbed layer carboxymethyl cellulose (CMC) on the Cu_2O/PU coating because it allows for penetration of ions and other species.[84] Cells have diffuse outer layers of polymer, so we made a thick layer of CMC, 0.7 ± 0.4 µm (see Figure S8-3), to hinder progress of the cells, their diffuse polymer layers and appendages to contact Cu_2O. After the deposition of CMC, some copper was still detected by XPS (4% Cu on CMC coated Cu_2O/PU compared to 35% on uncoated Cu_2O/PU, Figure S8-3). High resolution XPS showed that copper had the same chemical state with and without the CMC layer (Figures S4 and S5). The layer of CMC is sufficiently thick that there should be no XPS signal from the underlying solid Cu_2O.

Bacterial CFU results showed that the Cu_2O/PU with the CMC layer killed *P. aeruginosa* as effectively (99.6% reduction) as without the layer (99.1% reduction) in 10 min ($p = 0.74$, Figure 8-6). These experiments directly demonstrate that direct contact between the cells and Cu_2O particles is not necessary for killing.

XPS reveals the mechanism for killing when the CMC layer is present: copper (probably Cu^+) dissolved out of the Cu_2O, and became associated with the CMC polymer layer, even the topmost few nanometers that are sensed by XPS. Therefore, we conclude that there is nothing unique about the ability of $Cu_2O_{(s)}$ to kill *P. aeruginosa* – a CMC-Cu^+ compound can also kill. We speculate that the carboxylic acid groups of CMC are responsible for holding a high density of Cu^+.

Our results are consistent with the idea that the key to killing is a concentrated source of solubilizable copper near the bacterium. Even though solubility may limit the concentration of Cu^+ available to kill the bacterium, the speed of killing also depends on the rate of delivery (transport) of copper to the bacteria. In non-steady conditions, this will also depend on the distance between the source of Cu^+ and the bacterium. As reviewed in recent work by Hofmann et al,[85] *P. aeruginosa* maintains a set of strategies to regulate the copper, which hinder the deleterious effect of high copper concentrations in the environment. It is reasonable that a nearby source of copper ions could provide a sufficient flux to overwhelm these defenses.

The XPS results also provide some insight into what may happen to the bacteria when they adsorb onto $Cu_2O_{(s)}$. The surface of bacteria is not the same as CMC but there are similarities. Bacterial cells walls contain peptidoglycan, which in common with CMC is a polysaccharide with carboxylic acid and ester groups. XPS demonstrated that CMC adsorbed to

$Cu_2O_{(s)}$ became enriched in copper; it may be that the bacterial peptidoglycan also becomes concentrated in copper that dissolves from the solid. This may delay a deadly increase in copper concentration within the cell, but ultimately an increase in copper in the peptidoglycan or within the cell kills the bacteria, direct contact with the solid is not required.

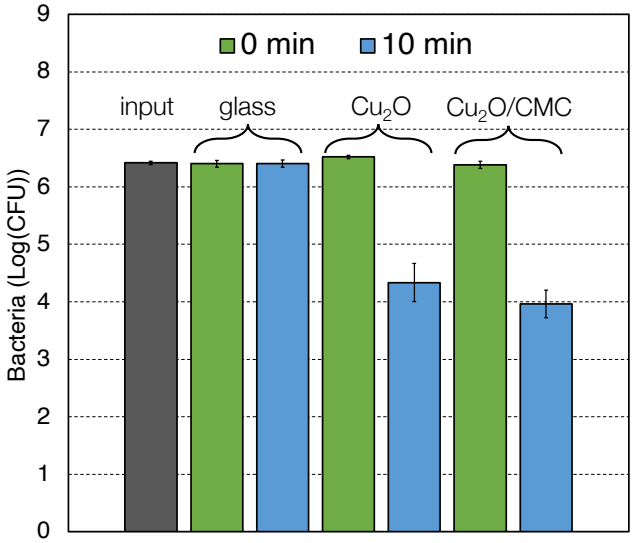


Figure 8-6. Effect of a CMC layer on the ability of Cu_2O/PU coatings to kill of *P. aeruginosa*. The Cu_2O/PU coating is good at killing, whether or not it is coated in CMC. With the CMC layer, the Cu_2O/PU caused a reduction of 99.2% and without the CMC layer, there was a reduction of 99.6% in 10 min and we did not resolve a difference ($p = 0.739$). The detection limit is log CFU = 1.7. 2-way ANOVA resulted in the following p-values: $p_{time} < 10^{-9}$, $p_{coating} < 10^{-7}$, and $p_{interaction} < 10^{-7}$.

8.3.6. Generation of ROSs is not Involved in the Mechanism

As described in the Introduction, ROSs include hydrogen peroxide and byproducts, and the formation of these byproducts can be accelerated by Cu^+. One potential mechanism is that copper species on the solid or dissolved in solution interact with hydrogen peroxide to kill *P. aeruginosa*. We first measured the concentration of hydrogen peroxide in the suspension of *P.*

aeruginosa in the absence of copper solid or leachate. The concentration was very low, only 0.3 μM. We then examined the effect of removing ROSs from the bacterial suspension by adding ascorbic acid (50% excess of the concentration of H_2O_2), which is an excellent antioxidant and ROS scavenger,[86-88] prior to placing the droplet on Cu_2O/PU coating. The removal of ROSs did not affect the killing of bacteria (p = 0.82, see Table 8-2). Controls showed that ascorbic acid has very little effect on the *P. aeruginosa* cells or their survival on uncoated glass control.

Sample	Log (CFU) Ascorbic acid in droplet	VS	Log (CFU) Regular droplet	p-value
Suspension	6.31 ± 0.04		6.24 ± 0.04	0.122
Uncoated glass	6.25 ± 0.08		6.18 ± 0.02	0.269
Cu_2O/PU	4.83 ± 0.86		4.98 ± 0.61	0.819

Table 8-2. Total Effect of ascorbic acid on the CFUs of *P. aeruginosa* that were placed in suspension on Cu_2O. The addition of ascorbic acid in bacteria suspension did not impact the killing of bacteria in 10 min, which suggests that ROSs were not important for killing.

It is possible that somehow ascorbic acid, H_2O_2, or their combination affected the Cu_2O/PU coating, so we performed various controls by pre-treated the coating, rinsing to remove any reaction products then exposing *P. aeruginosa* to the coating. As shown in Table 8-3, there was no effect.

Treatment	treated Cu_2O/PU	vs	regular Cu_2O/PU	p-value
Added H_2O_2 to coating, and rinsed	4.51 ± 0.18		4.98 ± 0.61	0.308
Added ascorbic acid to coating, and rinsed	3.85 ± 0.63		4.98 ± 0.61	0.089
Added mix of H_2O_2 and ascorbic acid to coating, and rinsed	4.94 ± 0.17		4.98 ± 0.61	0.916

Table 8-3. Total Control experiments for ROSs mechanism Data shows CFU of *P. aeruginosa* after various treatments of Cu_2O/PU. Treatment with H_2O_2, ascorbic acid, or a mixture of the two does not affect the killing of bacteria.

8.3.7. Effect of Light on the ability of Cu2O to Kill *P. aeruginosa*

Semiconductors can absorb photons to produce excited electrons that go on to oxidize materials. For example, titanium dioxide (TiO_2)[89] has antimicrobial activity that is effected by UV light absorption. Cu_2O has a bandgap of 1.8–2.6 eV[90-91] corresponding to photons in the range 688– 476 nm which overlaps with both sunlight and room light. Therefore, it is possible that photoexcited electrons play a role in the antimicrobial activity of Cu_2O under normal test conditions. To test this hypothesis, we examined antimicrobial properties in the dark, in room light and in the presence of a lamp that produced 365 nm photons (UV). Note that photons of wavelength shorter than the wavelength of the bandgap produce photoelectrons, so the UV excitation was designed to excite even the largest reported band gap of Cu_2O. As shown in Figure 8-7, the Cu_2O/PU coating had a very strong killing effect for all light conditions. 2 factor ANOVA showed a significant effect of the illumination on the copper surfaces, but the effect is

minor compared to the kill produced by Cu_2O. Therefore, we conclude the copper does not rely on illumination for the killing effect; the main effect comes from dissolution of Cu^+ ions.

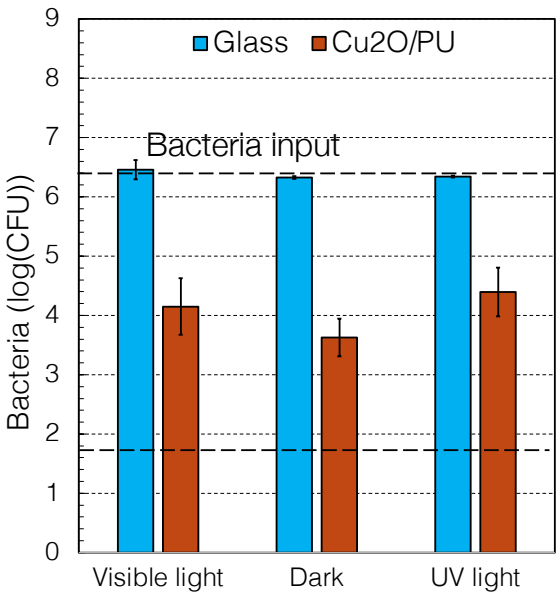


Figure 8-7. Effect of illumination on the antimicrobial properties of Cu_2O. The coating kills *P. aeruginosa* very well under the three light conditions we studied. The bottom dotted line shows the detection limit, which was 50 CFU.

8.4. Conclusion

Our overall conclusion is that solubilized Cu^+ is the most potent active agent for Cu_2O. Direct contact between the solid and the bacteria is not necessary, as shown by the ability of CMC-coated Cu_2O/PU to kill *P. aeruginosa.* However, close contact between Cu_2O and the bacteria enhances killing, presumably by quickly raising and then maintaining the local concentration of Cu^+ at the site of the bacteria.

A greater concentration of dissolved copper species enhances killing, and different buffers extract orders of magnitude differences in concentration of dissolved species. This is important because a variety of media (buffers) is used in antimicrobial testing, and those media is not always the same as the bodily fluid that carries the microbes or viruses. We find that the concentration of copper dissolved into DMEM, a common mammalian cell culture medium, is about 1000 × greater than the concentration dissolved in PBS, a common buffer that maintains the pH and ionic strength of serum. These two solutions have a very different effect on *P. aeruginosa*. Leachate from Cu_2O into DMEM was very effective at killing the bacterium (>99.99% killing in 60 min) whereas leachate of Cu_2O in PBS was ineffectual against the bacterium. Sifting through the components of DMEM, we found that sodium bicarbonate was effective at solubilizing Cu_2O and that the leachate into sodium bicarbonate was also effective at killing *P. aeruginosa.*

From the above, we conclude that the equilibrium concentration of dissolved copper had a strong impact on killing, but this is not the entire story: contact with Cu_2O also has a large effect. When a bacterial suspension in PBS is placed directly on Cu_2O/PU, there is a reduction of 99.2% in viable cells in only 10 min, despite the fact that very little copper solubilized into PBS,

and that concentration of copper is very poor at killing *P. aeruginosa.* Thus, proximity to the solid is important. However, insertion of a porous, 0.7 μm-thick coating of CMC polymer on the Cu_2O/PU, designed to block the bacterial cells from touching the Cu_2O but allowing passage of dissolved species, had little effect on killing (99.6% of *P. aeruginosa* in 10 min.). So, the bacteria do not need to be in direct contact with Cu_2O, they just need to be close to a source of copper ions. This effect was understood with the help of XPS measurements, which showed that the CMC had become impregnated with copper.

Combining all these experiments, we find that dissolved copper species, probably Cu^+, is the primary route by Cu_2O kills *P. aeruginosa.* Proximity to source of Cu^+ enables rapid killing, probably because of the supply of Cu^+ to the bacterium occurs rapidly and is maintained despite bacterial defenses, not because physical contact with the solid is required. Finally, we found no evidence that ROSs or light were important in the mechanism for killing *P. aeruginosa* with Cu_2O under normal lab conditions.

8.5. Materials and Methods

8.5.1. Materials

The following items were purchased from VWR: glass slides (25 × 75 × 1 mm), ethanol (200 proof), nitric acid (70%, ACS grade). Glass slides were cleaned using the following series: DI water, 70% ethanol, DI water, nitric acid (6 M), DI water, and drying with N_2 gas. Cuprous oxide (Cu_2O) particles (Chem Copp HP III UltraFine Type -5; avg size = 5.4μm) were obtained from American Chemet Corporation, and polyurethane (PU; Miniwax, Fast-Drying Polyurethane, clear satin) was obtained from Lowe's Home Improvement department store. Nitric acid (trace metal grade), copper(I) chloride (99%), sodium carboxymethyl cellulose (CMC; average M.W. 90,000 g/mol), glycerol (99+%), ascorbic acid (99+%), bicinchoninic acid disodium salt hydrate (BCCA; 98+%), Dulbecco's Modified Eagle Medium (DMEM), fetal bovine serum (FBS), and penicillin-streptomycin were purchased from Fisher Scientific. Tryptic Soy Agar (TSA), Tryptic soy broth (TSB), and DE broth were obtained from BD (Sparks, MD). The following were obtained from Sigma Aldrich: syringe filter (Whatman Anotop 10), copper (II) chloride (97%), and ethylenediaminetetraacetic acid disodium salt dihydrate (EDTA, 99+%). In house DI water was further purified by a Milli-Q Reference system.

There are several versions of DMEM. The DMEM we used here consisted of DMEM purchased from Fisher Scientific + 2% v/v FBS + 1% v/v penicillin-streptomycin (unless otherwise noted).

8.5.2. Light/Dark Experiments

Experiments with exposure to UV were performed with a lamp that emitted 365 nm photons (Arthur H. Thomas Co). The lamp was held 18 cm from the samples while the bacterial suspension droplet was on the samples. In both the dark and UV experiments, the room lights were off, the windows were covered, and the laboratory was very dark except for a faint red light to allow the pipetting of the bacterial suspensions. There was also some light from a Bunsen burner in all experiments.

8.5.3. Preparation of the Antimicrobial Cu_2O/PU Coating

The antimicrobial cuprous oxide/polyurethane (Cu_2O/PU) coating was prepared according to our previous publications.[22-23] A thin film of PU was cast on a glass slide by a sponge. Subsequently, the film was left in air for a few min to partially dry, after which a 10% (w/w) suspension of Cu_2O in ethanol was slowly added to cover the whole glass. The film was left in air at room temperature for a few minutes to dry partially. The sample was heated at 120 ˚C for 2 h, blown with pressurized N_2 gas after it cooled down to room temperature, and thoroughly rinsed with DI water. The coated glass was then cut to ≈ 12×12 mm pieces, and each sample was cleaned with argon plasma (100 W, <200 Torr, for 3 min).

8.5.4. Preparation of CMC-coated Cu_2O/PU

The carboxymethyl cellulose (CMC) solution was prepared following a procedure from the literature:[92-93] a solution of CMC (1 g/L) in DI water was heated to 80˚C for 30 min to allow for full dissolution of the CMC molecules. Subsequently the solution was removed from the heating plate, then glycerol was added to achieve a final concentration of 0.03 g/L. Freshly plasma treated Cu_2O/PU coatings (12 x 12 mm) were covered with 90 µL of CMC solution at room temperature, and left to dry in air for 24 hr.

8.5.5. Characterization of Coatings

Electron microscopy (SEM, model: JEOL IT500) and XPS (models: PHI VersaProbe III using a monochromatic Al Kα source of 1486.6 eV or PHI Quantera SXM (Physical Electronics) with a monochromatic Al K(alpha) x-ray (1486.6 eV)) were utilized to characterize the coatings. Prior to SEM characterization, samples were sputter-coated with 5 nm of Pt/Pd. ICP-MS (Model: Agilent 7900) was used to quantify concentration of copper.

8.5.6. Preparation of Solutions for Ion Leaching Experiments

Cu_2O particles were mixed with one of the test liquids at a mass ratio of 1:4 (Cu_2O particles to liquid) using a laboratory tube rotator. The mixing was continued for 20 min. (unless otherwise mentioned) at a rate of 40 RPM. We wanted to measure the dissolved content, so it was important to remove suspended particles. To achieve this, the suspension was centrifuged at

4000 RPM for 4 min, and then the supernatant was carefully separated using a syringe. Subsequently, the solution was filtered with an 0.02 µm filter into a polyethylene vial. We chose 20 min because it is the typical time for a 10 µL droplet to evaporate on a solid in our lab. As a preliminary experiment, we measured the copper concentration for the leachate into PBS after 20 min and 24 h, and found them to be similar, so we assumed that equilibrium was established after 20 minutes.

8.5.7. Preparation of ICP-MS Samples

To quantify the copper content of an analyte, the liquid as prepared in the previous step was used. The liquid was diluted 100 times in 2% w/v nitric acid (trace metal grade). The sample was then shaken, vortexed, and characterized by ICP-MS. The results section reports the original concentration of copper, not the diluted concentration.

8.5.8. Measurement of Antimicrobial Activity

8.5.8.1. Growth of Microbial Strains

P. aeruginosa was grown in TSB (5 mL) at 37° C with aeration at 60 rpm to mid-exponential phase. Following this step, the bacteria was streaked on TSA agar plates (incubated at 37° C for 48 h) so that visual characteristics of the colonies could be used to assess contamination.

8.5.8.2. Preparation of Microbial Cells

Bacterial cells were separated from the growth medium and suspended them in sterile PBS as follows. The cells were centrifuged at 5,000 g for 20 min, and then its supernatant was discarded. Subsequently, the bacterial cells were resuspended in PBS (5 mL) using vortexing for 60 s. Then, the suspensions were centrifuged for 20 min (5,000 x g), and again the supernatant was discarded. The washed cells were suspended in sterile PBS (5 mL) using vortexing for 60 s. Subsequently, the cell density was modified by dilution to McFarland No. 1 Standard. A typical cell count was 3.3×10^5–$1.2x10^6$ CFU/ mL.

8.5.8.3. Measurement of Killing by Leached Copper

The leached copper in liquid form that was described in Section 4.6 was mixed with bacterial suspension at a 1:1 ratio. This suspension was vortexed and at defined time points, 10 µL was transferred to a 50 mL centrifuge tube that contained 5 mL PBS. The tube was vortexed (30 sec), sonicated (5 min), and the CFU/mL was quantified as described above. As a control to account for this 1:1 dilution, a small quantity of bacterial suspension in PBS was diluted with PBS at a ratio of 1:1 the CFU/mL was measured. This was shown on the relevant figures in this work with the label ‘bacteria suspension’. For experiments where BCCA was used, BCCA was added to the leachate after filtration and before combining with the bacterial suspension.

8.5.8.4. Measurement of Surface-Killing

A droplet (10 µL) of cell suspension in PBS was placed on each test sample. At a later time (specified for each result) the sample was transferred to a sterile centrifuge tube (50 mL) that contained 5 mL of PBS. The tube was then vortexed (30 sec), sonicated (5 min), and the CFU/mL of the suspension measured as mentioned above. Following incubation of the plates (48 h), colonies were counted, the CFU/mL of suspension calculated, and the survival calculated as described below. CFUs were measured for three independent coupons at each time point, and figures show the average of the log of each of these CFU measurements. Three replicates of CFU plating were done for each sample, and the results averaged.

8.5.9. Statistical Analysis

All statistical measures were calculated from log CFU, and Student's t-tests were two-tailed and heteroscedastic with a significance level of 0.05. The error bars in figures are the standard deviation of independent replicates, and in the text, the number following the ± symbol is the standard deviation.

8.5.10. Calculation of Microbial Reduction

The CFU counting technique counts cells that can reproduce enough times to form a visible bacterial colony. We use the term "kill" as a shorthand for cells that cannot form a

colony. Percentage kill is a comparison of the CFU measured after a specific time to the CFU of the input suspension:

$$\log \text{kill} = \text{mean}\left[\log_{\mathbf{10}}\left(\frac{\text{input titer}}{\text{units}}\right)\right] - \text{mean}\left[\log_{\mathbf{10}}\left(\frac{\text{sample titer}}{\text{units}}\right)\right] \quad \text{Equation 8-1}$$

$$\%\ \text{kill} = \left[1 - 10^{-\log \text{kill}}\right] \times 100 \quad \text{Equation 8-2}$$

The term "reduction" compares bacterial CFU at a specific timepoint for a coated sample vs an uncoated control surface. Thus, reduction was calculated by:

$$\log \text{reduction} = \text{mean}\left[\log_{\mathbf{10}}\left(\frac{\text{uncoated surface titer}}{\text{units}}\right)\right] - \text{mean}\left[\log_{\mathbf{10}}\left(\frac{\text{sample titer}}{\text{units}}\right)\right] \quad \text{Equation 8-3}$$

$$\%\ \text{reduction} = \left[1 - 10^{-\log \text{Reduction}}\right] \times 100 \quad \text{Equation 8-4}$$

Acknowledgments

This work was supported by the Virginia Tech Proof of Concept (POC) Grant No. 238079 and Virginia Tech GRDP program under grant number 118965. We thank Mr. McAlister Council-Troche for capturing ICP-MS data at Analytical Chemistry Research Lab at the VA-MD College of Veterinary Medicine. This work used shared facilities at the Virginia Tech National Center for Earth and Environmental Nanotechnology (NCFL) Infrastructure supported by the NSF (ECCS 1542100 and ECCS 2025151). We also thank Dr. Xu Feng (at the Surface Analysis Laboratory, supported by NSF (CHE-1531834), in the Department of Chemistry at VT and Weinan Leng at NCFL at VT, who captured XPS spectra.

Conflict of Interest

Authors declare no conflict of interest.

Supporting Information

The Supporting Information is available free of charge at Journal's website.

REFERENCES

(1) Centers for Disease Control and Prevention Covid-19: U.S. Impact on Antimicrobial Resistance, Special Report 2022. https://www.cdc.gov/drugresistance/pdf/covid19-impact-report-508.pdf (accessed Sep 29, 2022).

(2) Centers for Disease Control and Prevention Covid-19 & Antibiotic Resistance. https://www.cdc.gov/drugresistance/covid19.html (accessed Sep 28, 2022).

(3) Weiner-Lastinger, L. M.; Pattabiraman, V.; Konnor, R. Y.; Patel, P. R.; Wong, E.; Xu, S. Y.; Smith, B.; Edwards, J. R.; Dudeck, M. A. The Impact of Coronavirus Disease 2019 (Covid-19) on Healthcare-Associated Infections in 2020: A Summary of Data Reported to the National Healthcare Safety Network. *Infect. Control Hosp. Epidemiol.* **2022,** *43* (1), 12-25.

(4) Centers for Disease Control and Prevention 2020 National and State Healthcare-Associated Infections Progress Report. https://www.cdc.gov/hai/data/archive/2020-HAI-progress-report.html (accessed May 5, 2023).

(5) Behzadinasab, S.; Chin, A. W. H.; Hosseini, M.; Poon, L. L. M.; Ducker, W. A. Sars-Cov-2 Virus Transfers to Skin through Contact with Contaminated Solids. *Sci. Rep.* **2021,** *11* (1), 22868, DOI: https://doi.org/10.1038/s41598-021-00843-0.

(6) Lopez, G. U.; Gerba, C. P.; Tamimi, A. H.; Kitajima, M.; Maxwell, S. L.; Rose, J. B. Transfer Efficiency of Bacteria and Viruses from Porous and Nonporous Fomites to Fingers under Different Relative Humidity Conditions. *Appl. Environ. Microbiol.* **2013,** *79* (18), 5728-5734.

(7) Ellingson, K. D.; Pogreba-Brown, K.; Gerba, C. P.; Elliott, S. P. Impact of a Novel Antimicrobial Surface Coating on Health Care–Associated Infections and Environmental Bioburden at 2 Urban Hospitals. *Clin. Infect. Dis.* **2020,** *71* (8), 1807-1813.

(8) Ejerhed, L.; Roshani, L.; Andersson, A. E. Antimicrobial Coating Is Associated with Significantly Lower Aerobic Colony Counts in High-Touch Areas in an Orthopedic Ward Environment. *Ann. Clin. Microbiol. Antimicrob.* **2020,** *19* (1), 1-7.

(9) Iarikov, D. D.; Kargar, M.; Sahari, A.; Russel, L.; Gause, K. T.; Behkam, B.; Ducker, W. A. Antimicrobial Surfaces Using Covalently Bound Polyallylamine. *Biomacromolecules* **2014,** *15* (1), 169-176.

(10) Andrews, M. A.; Figuly, G. D.; Chapman, J. S.; Hunt, T. W.; Glunt, C. D.; Rivenbark, J. A.; Chenault, H. K. Antimicrobial Hydrogels Formed by Crosslinking Polyallylamine with Aldaric Acid Derivatives. *J. Appl. Polym. Sci.* **2011,** *119* (6), 3244-3252.

(11) Haldar, J.; An, D.; de Cienfuegos, L. A.; Chen, J.; Klibanov, A. M. Polymeric Coatings That Inactivate Both Influenza Virus and Pathogenic **B**acteria. *Proceedings of the National Academy of Sciences* **2006,** *103* (47), 17667-17671.

(12) Liu, J.; Duan, W.; Song, J.; Guo, X.; Wang, Z.; Shi, X.; Liang, J.; Wang, J.; Cheng, P.; Chen, Y. Self-Healing Hyper-Cross-Linked Metal–Organic Polyhedra (Hcmops) Membranes with Antimicrobial Activity and Highly Selective Separation Properties. *Journal of the American Chemical Society* **2019,** *141* (30), 12064-12070.

(13) Wong, S. Y.; Li, Q.; Veselinovic, J.; Kim, B.-S.; Klibanov, A. M.; Hammond, P. T. Bactericidal and Virucidal Ultrathin Films Assembled Layer by Layer from Polycationic N-

Alkylated Polyethylenimines and Polyanions. *Biomaterials* **2010,** *31* (14), 4079-4087, DOI: 10.1016/j.biomaterials.2010.01.119.

(14) Escobar, A.; Muzzio, N.; Moya, S. E. Antibacterial Layer-by-Layer Coatings for Medical Implants. *Pharmaceutics* **2020,** *13* (1), 16.

(15) Ikeda, T.; Yamaguchi, H.; Tazuke, S. New Polymeric Biocides: Synthesis and Antibacterial Activities of Polycations with Pendant Biguanide Groups. *Antimicrobial agents and chemotherapy* **1984,** *26* (2), 139-144.

(16) Behzadinasab, S.; Williams, M. D.; Hosseini, M.; Poon, L. L.; Chin, A. W.; Falkinham III, J. O.; Ducker, W. A. Transparent and Sprayable Surface Coatings That Kill Drug-Resistant Bacteria within Minutes and Inactivate Sars-Cov-2 Virus. *ACS Appl. Mater. Interfaces* **2021,** *13* (46), 54706-54714, DOI: https://doi.org/10.1021/acsami.1c15505.

(17) Borkow, G.; Gabbay, J. Copper, an Ancient Remedy Returning to Fight Microbial, Fungal and Viral Infections. *Curr. Chem. Biol.* **2009,** *3* (3), 272-278.

(18) Lara, H. H.; Garza-Treviño, E. N.; Ixtepan-Turrent, L.; Singh, D. K. Silver Nanoparticles Are Broad-Spectrum Bactericidal and Virucidal Compounds. *Journal of nanobiotechnology* **2011,** *9*, 1-8.

(19) Burdușel, A.-C.; Gherasim, O.; Grumezescu, A. M.; Mogoantă, L.; Ficai, A.; Andronescu, E. Biomedical Applications of Silver Nanoparticles: An up-to-Date Overview. *Nanomaterials* **2018,** *8* (9), 681.

(20) Almoudi, M. M.; Hussein, A. S.; Hassan, M. I. A.; Zain, N. M. A Systematic Review on Antibacterial Activity of Zinc against Streptococcus Mutans. *The Saudi dental journal* **2018,** *30* (4), 283-291.

(21) Zhang, Y.; Shareena Dasari, T. P.; Deng, H.; Yu, H. Antimicrobial Activity of Gold Nanoparticles and Ionic Gold. *J. Environ. Sci. Health, Pt. C* **2015,** *33* (3), 286-327.

(22) Behzadinasab, S.; Hosseini, M.; Williams, M.; Ivester, H.; Allen, I.; Falkinham III, J.; Ducker, W. Antimicrobial Activity of Cuprous Oxide-Coated and Cupric Oxide-Coated Surfaces. *J. Hosp. Infect.* **2022,** *129*, 58-64, DOI: https://doi.org/10.1016/j.jhin.2022.07.022.

(23) Behzadinasab, S.; Chin, A.; Hosseini, M.; Poon, L.; Ducker, W. A. A Surface Coating That Rapidly Inactivates Sars-Cov-2. *ACS Appl. Mater. Interfaces* **2020,** *12* (31), 34723-34727, DOI: https://doi.org/10.1021/acsami.0c11425.

(24) Mendes, C. R.; Dilarri, G.; Forsan, C. F.; Sapata, V. d. M. R.; Lopes, P. R. M.; de Moraes, P. B.; Montagnolli, R. N.; Ferreira, H.; Bidoia, E. D. Antibacterial Action and Target Mechanisms of Zinc Oxide Nanoparticles against Bacterial Pathogens. *Sci. Rep.* **2022,** *12* (1), 2658.

(25) Arendsen, L. P.; Thakar, R.; Sultan, A. H. The Use of Copper as an Antimicrobial Agent in Health Care, Including Obstetrics and Gynecology. *Clin. Microbiol. Rev.* **2019,** *32* (4), e00125-18.

(26) Benmamoun, Z.; Wyhopen, T.; Li, Y.; Ducker, W. A. Mechanism and Efficacy of Cu2o-Treated Fabric. *Antibiotics* **2022,** *11* (11), 1633.

(27) Borkow, G.; Zhou, S. S.; Page, T.; Gabbay, J. A Novel Anti-Influenza Copper Oxide Containing Respiratory Face Mask. *PLoS One* **2010,** *5* (6), e11295.

(28) Champagne, V. K.; Helfritch, D. J. A Demonstration of the Antimicrobial Effectiveness of Various Copper Surfaces. *J. Biol. Eng.* **2013,** *7* (1), 1-7.

(29) Sousa, B. C.; Cote, D. L. Antimicrobial Copper Cold Spray Coatings and Sars-Cov-2 Surface Inactivation. *MRS Adv.* **2020,** *5* (56), 2873-2880.

(30) Vincent, M.; Duval, R. E.; Hartemann, P.; Engels-Deutsch, M. Contact Killing and Antimicrobial Properties of Copper. *J. Appl. Microbiol.* **2018,** *124* (5), 1032-1046.

(31) Sunada, K.; Minoshima, M.; Hashimoto, K. Highly Efficient Antiviral and Antibacterial Activities of Solid-State Cuprous Compounds. *J. Hazard. Mater.* **2012,** *235*, 265-270.

(32) Behzadinasab, S.; Williams, M. D.; Aktuglu, M.; Falkinham III, J. O.; Ducker, W. A. Porous Antimicrobial Coatings for Killing Microbes within Minutes. *ACS Appl. Mater. Interfaces* **2023,** *15* (12), 15120–15128, DOI: https://doi.org/10.1021/acsami.2c22240.

(33) Marik, P.; Shankaran, S.; King, L. The Effect of Copper-Oxide-Treated Soft and Hard Surfaces on the Incidence of Healthcare-Associated Infections: A Two-Phase Study. *J. Hosp. Infect.* **2020,** *105* (2), 265-271.

(34) U.S. Department of Health and Human Services,Public Health Service, Toxicological Profile for Copper. Agency for Toxic Substances and Disease Registry, Division of Toxicology/Toxicology Information Branch, Atlanta, Georgia, P 272 2004.

(35) Ufelle, A. C.; Barchowsky, A. T. Toxic Effects of Metals. In *Casarett & Doull's Toxicology, the Basic Science of Poisons*; Klaassen, C. D., Ed.; McGraw Hill Education: New York,, 2019; pp 1107 -1161.

(36) Nelson, L. S. Copper. In *Goldfrank's Toxicologic Emergencies* Hoffman, R. S.; Howland, M. A.; Lewin, N. A.; Nelson, L. S.; Goldfrank, L. R., Eds.; McGraw Hill Education: New York, 2015; pp 1210-1218.

(37) Yin, I. X.; Zhang, J.; Zhao, I. S.; Mei, M. L.; Li, Q.; Chu, C. H. The Antibacterial Mechanism of Silver Nanoparticles and Its Application in Dentistry. *International journal of nanomedicine* **2020**, 2555-2562.

(38) Raghunath, A.; Perumal, E. Metal Oxide Nanoparticles as Antimicrobial Agents: A Promise for the Future. *Int. J. Antimicrob. Agents* **2017,** *49* (2), 137-152.

(39) Ermini, M. L.; Voliani, V. Antimicrobial Nano-Agents: The Copper Age. *ACS nano* **2021,** *15* (4), 6008-6029.

(40) Grass, G.; Rensing, C.; Solioz, M. Metallic Copper as an Antimicrobial Surface. *Appl. Environ. Microbiol.* **2011,** *77* (5), 1541-1547.

(41) Raffi, M.; Mehrwan, S.; Bhatti, T. M.; Akhter, J. I.; Hameed, A.; Yawar, W. Investigations into the Antibacterial Behavior of Copper Nanoparticles against Escherichia Coli. *Ann. Microbiol.* **2010,** *60* (1), 75-80.

(42) Li, W.-R.; Xie, X.-B.; Shi, Q.-S.; Zeng, H.-Y.; Ou-Yang, Y.-S.; Chen, Y.-B. Antibacterial Activity and Mechanism of Silver Nanoparticles on Escherichia Coli. *Applied microbiology and biotechnology* **2010,** *85*, 1115-1122.

(43) Hong, R.; Kang, T. Y.; Michels, C. A.; Gadura, N. Membrane Lipid Peroxidation in Copper Alloy-Mediated Contact Killing of Escherichia Coli. *Appl. Environ. Microbiol.* **2012,** *78* (6), 1776-1784.

(44) Macomber, L.; Imlay, J. A. The Iron-Sulfur Clusters of Dehydratases Are Primary Intracellular Targets of Copper Toxicity. *Proceedings of the National Academy of Sciences* **2009,** *106* (20), 8344-8349.

(45) Harrison, J. J.; Tremaroli, V.; Stan, M. A.; Chan, C. S.; Vacchi-Suzzi, C.; Heyne, B. J.; Parsek, M. R.; Ceri, H.; Turner, R. J. Chromosomal Antioxidant Genes Have Metal Ion-Specific Roles as Determinants of Bacterial Metal Tolerance. *Environ. Microbiol.* **2009,** *11* (10), 2491-2509.

(46) Asakura, K.; Satoh, H.; Chiba, M.; Okamoto, M.; Serizawa, K.; Nakano, M.; Omae, K. Genotoxicity Studies of Heavy Metals: Lead, Bismuth, Indium, Silver and Antimony. *J. Occup. Health* **2009,** *51* (6), 498-512.

(47) Feng, Q. L.; Wu, J.; Chen, G. Q.; Cui, F.; Kim, T.; Kim, J. A Mechanistic Study of the Antibacterial Effect of Silver Ions on Escherichia Coli and Staphylococcus Aureus. *J. Biomed. Mater. Res.* **2000,** *52* (4), 662-668.

(48) Kent, R. D.; Vikesland, P. J. Dissolution and Persistence of Copper-Based Nanomaterials in Undersaturated Solutions with Respect to Cupric Solid Phases. *Environ. Sci. Technol.* **2016,** *50* (13), 6772-6781.

(49) Yang, Z.; Xie, C. Zn2+ Release from Zinc and Zinc Oxide Particles in Simulated Uterine Solution. *Colloids Surf. B. Biointerfaces* **2006,** *47* (2), 140-145.

(50) Ivask, A.; Kurvet, I.; Kasemets, K.; Blinova, I.; Aruoja, V.; Suppi, S.; Vija, H.; Käkinen, A.; Titma, T.; Heinlaan, M. Size-Dependent Toxicity of Silver Nanoparticles to Bacteria, Yeast, Algae, Crustaceans and Mammalian Cells in Vitro. *PLoS One* **2014,** *9* (7), e102108.

(51) Komonweeraket, K.; Cetin, B.; Aydilek, A. H.; Benson, C. H.; Edil, T. B. Effects of Ph on the Leaching Mechanisms of Elements from Fly Ash Mixed Soils. *Fuel* **2015,** *140*, 788-802.

(52) Mahedi, M.; Cetin, B.; Dayioglu, A. Y. Leaching Behavior of Aluminum, Copper, Iron and Zinc from Cement Activated Fly Ash and Slag Stabilized Soils. *Waste Management* **2019,** *95*, 334-355.

(53) Hao, J.; Wang, X.; Wang, Y.; Wu, Y.; Guo, F. Optimizing the Leaching Parameters and Studying the Kinetics of Copper Recovery from Waste Printed Circuit Boards. *ACS omega* **2022,** *7* (4), 3689-3699.

(54) Cui, H.; Anderson, C. G. Literature Review of Hydrometallurgical Recycling of Printed Circuit Boards (Pcbs). *J. Adv. Chem. Eng* **2016,** *6* (1), 142-153.

(55) Bas, A. D.; Deveci, H.; Yazici, E. Y. Treatment of Manufacturing Scrap Tv Boards by Nitric Acid Leaching. *Sep. Purif. Technol.* **2014,** *130*, 151-159.

(56) Yamaki, K.; Yoshino, S. Comparison of Inhibitory Activities of Zinc Oxide Ultrafine and Fine Particulates on Ige-Induced Mast Cell Activation. *Biometals* **2009,** *22*, 1031-1040.

(57) Peng, X.; Palma, S.; Fisher, N. S.; Wong, S. S. Effect of Morphology of Zno Nanostructures on Their Toxicity to Marine Algae. *Aquat. Toxicol.* **2011,** *102* (3-4), 186-196.

(58) Azam, A.; Ahmed, A. S.; Oves, M.; Khan, M.; Memic, A. Size-Dependent Antimicrobial Properties of Cuo Nanoparticles against Gram-Positive and-Negative Bacterial Strains. *International journal of nanomedicine* **2012**, 3527-3535.

(59) Osonga, F. J.; Akgul, A.; Yazgan, I.; Akgul, A.; Eshun, G. B.; Sakhaee, L.; Sadik, O. A. Size and Shape-Dependent Antimicrobial Activities of Silver and Gold Nanoparticles: A Model Study as Potential Fungicides. *Molecules* **2020,** *25* (11), 2682.

(60) Chang, T.; Babu, R. P.; Zhao, W.; Johnson, C. M.; Hedstrom, P.; Odnevall, I.; Leygraf, C. High-Resolution Microscopical Studies of Contact Killing Mechanisms on Copper-Based Surfaces. *ACS Appl. Mater. Interfaces* **2021,** *13* (41), 49402-49413.

(61) Juan, C. A.; Pérez de la Lastra, J. M.; Plou, F. J.; Pérez-Lebeña, E. The Chemistry of Reactive Oxygen Species (Ros) Revisited: Outlining Their Role in Biological Macromolecules (DNA, Lipids and Proteins) and Induced Pathologies. *Int. J. Mol. Sci.* **2021,** *22* (9), 4642.

(62) Bhattacharjee, S. The Language of Reactive Oxygen Species Signaling in Plants. *Journal of Botany* **2012,** *2012*.

(63) Pham, A. N.; Xing, G.; Miller, C. J.; Waite, T. D. Fenton-Like Copper Redox Chemistry Revisited: Hydrogen Peroxide and Superoxide Mediation of Copper-Catalyzed Oxidant Production. *J. Catal.* **2013,** *301*, 54-64.

(64) Chang, R. C. *Chemistry*, Fourth ed.; McGraw Hill: New York, 1991, page 803.

(65) Salah, I.; Parkin, I. P.; Allan, E. Copper as an Antimicrobial Agent: Recent Advances. *RSC Adv.* **2021,** *11* (30), 18179-18186.

(66) Warnes, S. L.; Keevil, C. W. Inactivation of Norovirus on Dry Copper Alloy Surfaces. *PLoS One* **2013,** *8* (9), e75017.

(67) Environmental Protection Agency Antimicrobial Testing Methods & Procedures: Interim Method for Evaluating the Efficacy of Antimicrobial Surface Coatings https://www.epa.gov/pesticide-analytical-methods/antimicrobial-testing-methods-procedures-interim-method-evaluating (accessed Sep 2, 2022).

(68) Environmental Protection Agency Protocol for the Evaluation of Bactericidal Activity of Hard, Non-Porous Copper Containing Surface Products. https://www.epa.gov/sites/production/files/2016-02/documents/copper_and_copper-alloy_surface_protocol_revised_012916.pdf (accessed Sep 2, 2022).

(69) Centers for Disease Control and Prevention Multidrug-Resistant Pseudomonas Aeruginosa https://www.cdc.gov/drugresistance/pdf/threats-report/pseudomonas-aeruginosa-508.pdf (accessed Mar 20, 2023).

(70) Restrepo, M. I.; Babu, B. L.; Reyes, L. F.; Chalmers, J. D.; Soni, N. J.; Sibila, O.; Faverio, P.; Cilloniz, C.; Rodriguez-Cintron, W.; Aliberti, S. Burden and Risk Factors for Pseudomonas Aeruginosa Community-Acquired Pneumonia: A Multinational Point Prevalence Study of Hospitalised Patients. *Eur. Respir. J.* **2018,** *52* (2), 1701190, DOI: https://doi.org/10.1183/13993003.01190-2017.

(71) Chatzinikolaou, I.; Abi-Said, D.; Bodey, G. P.; Rolston, K. V.; Tarrand, J. J.; Samonis, G. Recent Experience with Pseudomonas Aeruginosa Bacteremia in Patients with Cancer: Retrospective Analysis of 245 Episodes. *Arch. Intern. Med.* **2000,** *160* (4), 501-509.

(72) Eagle, H. Amino Acid Metabolism in Mammalian Cell Cultures. *Science* **1959,** *130* (3373), 432-437.

(73) Halli, P.; Hamuyuni, J.; Revitzer, H.; Lundström, M. Selection of Leaching Media for Metal Dissolution from Electric Arc Furnace Dust. *Journal of Cleaner Production* **2017,** *164*, 265-276.

(74) Zheng, S.-a.; Zheng, X.; Chen, C. Leaching Behavior of Heavy Metals and Transformation of Their Speciation in Polluted Soil Receiving Simulated Acid Rain. *PLoS One* **2012,** *7* (11), e49664.

(75) Ahrland, S.; Rawsthorne, J. The Stability of Metal Halide Complexes in Aqueous Solution. *Acta Chem. Scand* **1970,** *24* (157), 24-0157.

(76) Tilley, I. T. Copper (I) in Solution. Ph.D. Australian National University, 1974.

(77) Moffett, J. W.; Zika, R. G. Oxidation Kinetics of Cu (I) in Seawater: Implications for Its Existence in the Marine Environment. *Mar. Chem.* **1983,** *13* (3), 239-251.

(78) Haynes, W. M. *Crc Handbook of Chemistry and Physics*, CRC press: 2016.

(79) Mathews, S.; Kumar, R.; Solioz, M. Copper Reduction and Contact Killing of Bacteria by Iron Surfaces. *Appl. Environ. Microbiol.* **2015,** *81* (18), 6399-6403.

(80) Li, X.; Zhang, H.; Ran, Y.; Ye, M.; Yang, F.; Han, Y.; Liu, Z. Beam-Induced Effects on Platinum Oxidation During Ambient-Pressure X-Ray Photoelectron Spectroscopy. *The Journal of Physical Chemistry Letters* **2022,** *13* (24), 5677-5682.

(81) Karlsson, H. L.; Cronholm, P.; Gustafsson, J.; Moller, L. Copper Oxide Nanoparticles Are Highly Toxic: A Comparison between Metal Oxide Nanoparticles and Carbon Nanotubes. *Chem. Res. Toxicol.* **2008,** *21* (9), 1726-1732.

(82) Tikhonov, V. N. High Selective Titration Mehod for Determining Copper with 2,2-Bicinchonic Acid *Zhurnal Analiticheskoi Khimii* **1972,** *27* (4), 673-+.

(83) Smith, P. e.; Krohn, R. I.; Hermanson, G.; Mallia, A.; Gartner, F.; Provenzano, M.; Fujimoto, E.; Goeke, N.; Olson, B.; Klenk, D. Measurement of Protein Using Bicinchoninic Acid. *Anal. Biochem.* **1985,** *150* (1), 76-85.

(84) Saifur, R. M.; Saif, H. M.; Sutradhar, N. A.; Sunghyun, N.; Krishna, K. A.; Shameem, A. M.; Boshir, A. M. Recent Developments of Carboxymethyl Cellulose. **2021**.

(85) Hofmann, L.; Hirsch, M.; Ruthstein, S. Advances in Understanding of the Copper Homeostasis in Pseudomonas Aeruginosa. *Int. J. Mol. Sci.* **2021,** *22* (4), 2050.

(86) Darr, D.; Combs, S.; Dunston, S.; Manning, T.; Pinnell, S. Topical Vitamin C Protects Porcine Skin from Ultraviolet Radiation-Induced Damage. *Br. J. Dermatol.* **1992,** *127* (3), 247-253.

(87) Frei, B. Reactive Oxygen Species and Antioxidant Vitamins: Mechanisms of Action. *The American journal of medicine* **1994,** *97* (3), S5-S13.

(88) Deutsch, J. C. Ascorbic Acid Oxidation by Hydrogen Peroxide. *Anal. Biochem.* **1998,** *255* (1), 1-7.

(89) Adams, L. K.; Lyon, D. Y.; Alvarez, P. J. Comparative Eco-Toxicity of Nanoscale Tio2, Sio2, and Zno Water Suspensions. *Water Res.* **2006,** *40* (19), 3527-3532.

(90) Oudah, M.; Hasan, M.; Abd, A. In *Synthesis of Copper Oxide Thin Films by Electrolysis Method Based on Porous Silicon for Solar Cell Applications*, IOP Conference Series: Materials Science and Engineering, IOP Publishing: 2020; p 012051.

(91) Murali, D. S.; Kumar, S.; Choudhary, R.; Wadikar, A. D.; Jain, M. K.; Subrahmanyam, A. Synthesis of Cu2o from Cuo Thin Films: Optical and Electrical Properties. *AIP advances* **2015,** *5* (4), 047143.

(92) Wang, L.-F.; Rhim, J.-W. Functionalization of Halloysite Nanotubes for the Preparation of Carboxymethyl Cellulose-Based Nanocomposite Films. *Applied Clay Science* **2017,** *150*, 138-146.

(93) Bifani, V.; Ramírez, C.; Ihl, M.; Rubilar, M.; García, A.; Zaritzky, N. Effects of Murta (Ugni Molinae Turcz) Extract on Gas and Water Vapor Permeability of Carboxymethylcellulose-Based Edible Films. *LWT-Food Science and Technology* **2007,** *40* (8), 1473-1481.

8.6. SUPPORTING INFORMATION

Antimicrobial Mechanism of Cuprous Oxide (Cu_2O) Coatings

Saeed Behzadinasab[1,2,3], Myra D. Williams[4], Joseph O. Falkinham III*[4], and William A. Ducker*[1,2,3]

[1]Department of Chemical Engineering, Virginia Tech, Blacksburg, Virginia, 24061, USA

[2]Center for Soft Matter and Biological Physics, Virginia Tech, Blacksburg, Virginia, 24061, USA

[3]Macromolecules Innovation Institute, Virginia Tech, Blacksburg, Virginia, 24061, USA

[4]Department of Biological Sciences, Virginia Tech, Blacksburg, Virginia, 24061, USA

Authors' Email: Saeed Behzadinasab saeedb@vt.edu; Joseph Falkinham jofiii@vt.edu; William Ducker wducker@vt.edu

Keywords: mechanism, Cu2O, copper, copper oxide, antibacterial, antimicrobial, coating, bacteria, surface

8.6.1. Composition of DMEM

Components	Molecular Weight	Concentration (mg/L)	mM
Amino Acids			
Glycine	75.0	30.0	0.4
L-Arginine hydrochloride	211.0	84.0	0.39810428
L-Cystine 2HCl	313.0	63.0	0.20127796
L-Glutamine	146.0	584.0	4.0
L-Histidine hydrochloride-H2O	210.0	42.0	0.2
L-Isoleucine	131.0	105.0	0.8015267
L-Leucine	131.0	105.0	0.8015267
L-Lysine hydrochloride	183.0	146.0	0.7978142
L-Methionine	149.0	30.0	0.20134228
L-Phenylalanine	165.0	66.0	0.4
L-Serine	105.0	42.0	0.4
L-Threonine	119.0	95.0	0.79831934
L-Tryptophan	204.0	16.0	0.078431375
L-Tyrosine disodium salt dihydrate	261.0	104.0	0.39846742
L-Valine	117.0	94.0	0.8034188
Vitamins			
Choline chloride	140.0	4.0	0.028571429
D-Calcium pantothenate	477.0	4.0	0.008385744
Folic Acid	441.0	4.0	0.009070295
Niacinamide	122.0	4.0	0.032786883
Pyridoxine hydrochloride	206.0	4.0	0.019417476
Riboflavin	376.0	0.4	0.0010638298
Thiamine hydrochloride	337.0	4.0	0.011869436
i-Inositol	180.0	7.2	0.04

Inorganic Salts			
Calcium Chloride (CaCl2) (anhyd.)	111.0	200.0	1.8018018
Ferric Nitrate (Fe(NO3)3"9H2O)	404.0	0.1	2.4752476E-4
Magnesium Sulfate (MgSO4) (anhyd.)	120.0	97.67	0.8139166
Potassium Chloride (KCl)	75.0	400.0	5.3333335
Sodium Bicarbonate (NaHCO3)	84.0	3700.0	44.04762
Sodium Chloride (NaCl)	58.0	6400.0	110.344826
Sodium Phosphate monobasic (NaH2PO4-H2O)	138.0	125.0	0.9057971
Other Components			
D-Glucose (Dextrose)	180.0	4500.0	25.0
Phenol Red	376.4	15.0	0.039851222

Table S8-1. Screenshot of the composition of DMEM sold by Sigma-Aldrich in 2023. The composition was obtained from the Sigma Aldrich website.[1]

8.6.2. Supplementary Results

8.6.2.1. Supplementary ICP-MS data

Liquid	Cu concentration (µM)
NH_4OH	9.52E+01
FBS	1.21E+02
NaCl + $NaHCO_3$	1.75E+02
NaCl + FBS	4.51E+01
$NaHCO_3$ + FBS	2.97E+02
NaCl + $NaHCO_3$ + FBS	3.25E+02

Table S8-2. Additional measurements of dissolved copper leached from Cu_2O. These measurements were performed to identify why DMEM leached a large amount of copper, and so the solution concentrations match those in DMEM. NH_4OH was used as a generic amine ligand to mimic the many amino acids in DMEM. The concentrations of each component are as follows: NaCl = 6.4 g/L, $NaHCO_3$ (3.7 g/L), and FBS (2% v/v). The concentrations are according to each constituting component found in DMEM. Data measured by ICP-MS.

8.6.2.2. Supplementary XPS data

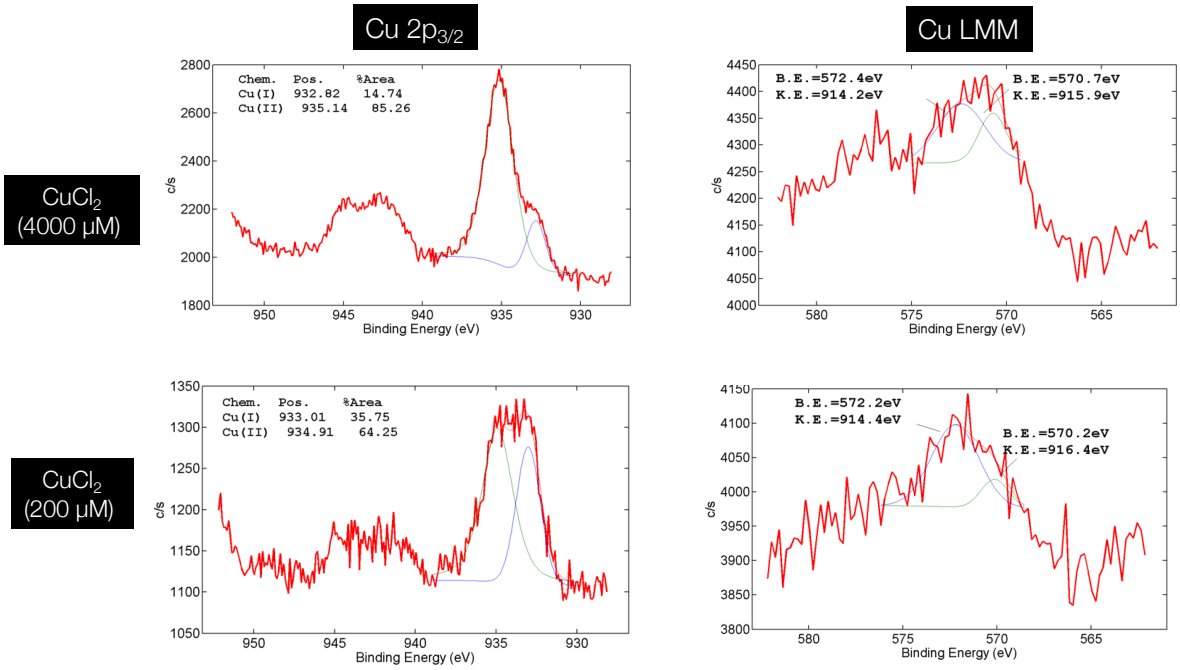


Figure S8-1. XPS data of a $CuCl_2$ droplet that was dried on a polyethylene support. The data shows most of the copper is Cu^{2+}, and some of the Cu^{2+} has converted to Cu^{+}.

8.6.2.3. Addition of BCCA to Cu_2O leachates

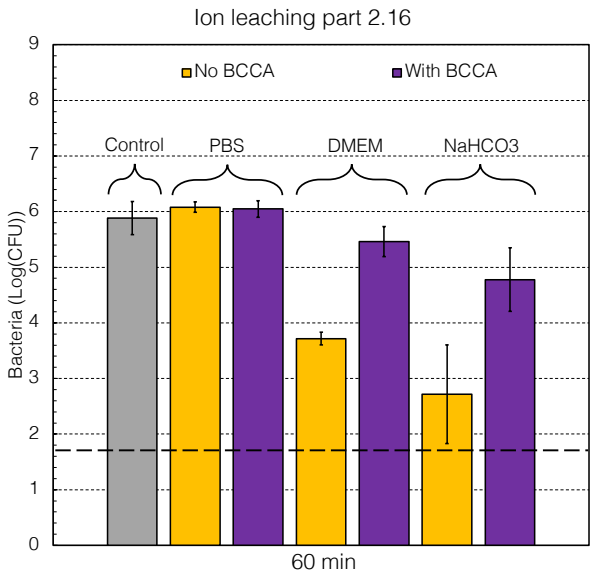


Figure S8-2. Cross Bacterial test with and without addition of BCCA. Addition of BCCA (chelating agent) reduces the killing of bacteria by leached copper with both DMEM and bicarbonate (3.7 g/L). BCCA selectively chelates Cu^{+}.

8.6.2.4. SEM images of CMC coating

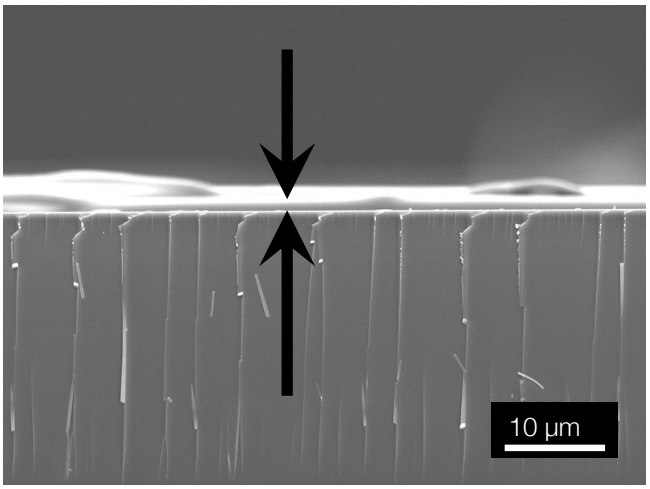


Figure S8-3. Cross section SEM image of CMC layer on glass. The vertical lines are fracture lines in the glass. The CMC is the thin layer between the arrows.

8.6.2.5. Supplementary XPS data

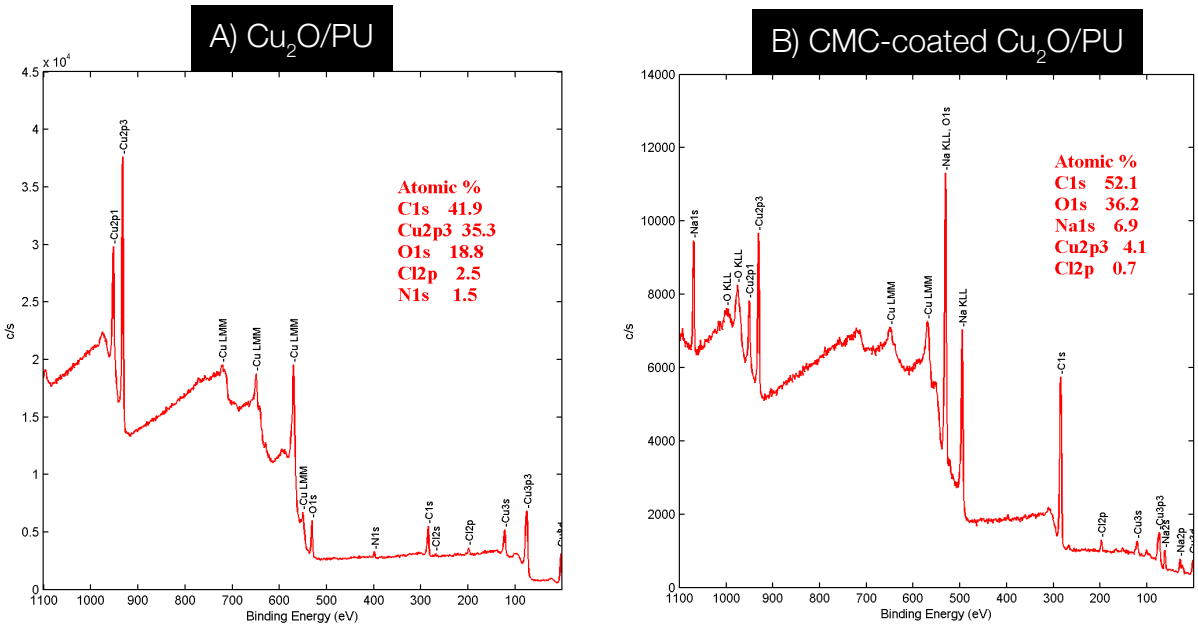


Figure S8-4. XPS Survey showing copper content on the surface of Cu_2O/PU and CMC-coated Cu_2O/PU. Copper is detected even with the CMC-layer present on Cu_2O/PU.

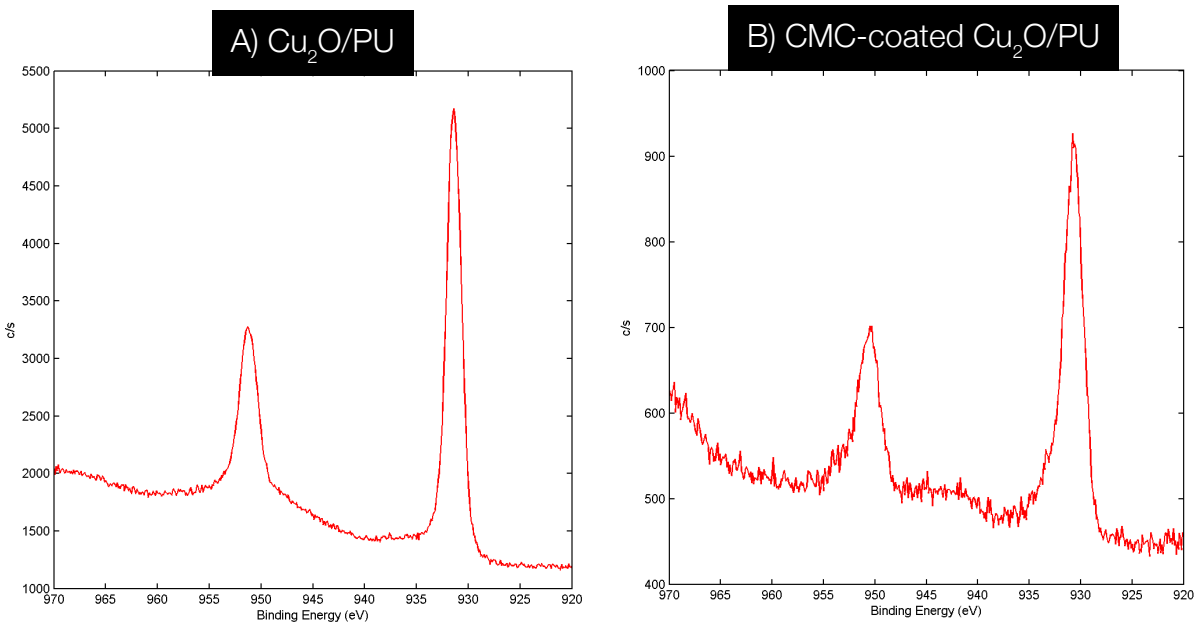


Figure S8-5. High resolution XPS spectra of Cu_2O/PU and CMC-coated Cu_2O/PU. The high-resolution Cu 2p data shows a similar state for copper on the surface of both samples.

References

(1) Sigma Aldrich Technical Resources. 11965 - Dmem, High Glucose.

https://www.thermofisher.com/us/en/home/technical-resources/media-formulation.8.html

(accessed Mar 15, 2023).

Chapter 9. SARS-CoV-2 virus transfers to skin through contact with contaminated solids

Saeed Behzadinasab[†1], Alex W.H. Chin[†2], Mohsen Hosseini[1], Leo L.M. Poon*[2,3], and William A. Ducker*[1]

[†] These authors contributed equally

*Corresponding Authors' Email: Leo Poon llmpoon@hku.hk; William Ducker wducker@vt.edu

[1]Dept. of Chemical Engineering and Center for Soft Matter and Biological Physics, Virginia Tech, VA, 24061, USA

[2]School of Public Health, LKS Faculty of Medicine, The University of Hong Kong, Hong Kong Special Administrative Region, China.

[3]HKU-Pasteur Research Pole, LKS Faculty of Medicine, The University of Hong Kong, Hong Kong, China

Keywords: SARS-CoV-2, transfer, skin, coronavirus, COVID-19, hand, fomite

9.1. Abstract

Transfer of SARS-CoV-2 from solids to fingers is one step in infection via contaminated solids, and the possibility of infection from this route has driven calls for increased frequency of handwashing during the COVID-19 pandemic. To analyze this route of infection, we measured the percentage of SARS-CoV-2 that was transferred from a solid to an artificial finger. A droplet of SARS-CoV-2 suspension (1 μL) was placed on a solid, and then artificial skin was briefly pressed against the solid with a light force (3 N). Transfer from a variety of solids was detected, and transfer from the non-porous solids, glass, stainless steel, and Teflon, was substantial when the droplet was still wet. The viral titer for the finger was 13–16 % or 0.8–0.9 log less than for the input droplet Transfer still occurred after the droplet evaporated, but was smaller, 3–9 %. We found a lower level of transfer from porous solids but did not find a significant effect of solid wettability for non-porous solids.

9.2. Introduction

In the period January 2020 to May 2021, about 170 million people contracted COVID-19, and about 3.6 million have died as a result of the illness.[1] The disease is caused by a virus, SARS-CoV-2 (severe acute respiratory syndrome coronavirus 2). In 2020, the US CDC stated that the primary mechanism for transmission is close contacts or inhalation of respiratory droplets.[2] Some diseases can also be transferred via contaminated solids (fomites), and the World Health Organization states that "fomite transmission is considered a likely mode of transmission for SARS-CoV-2".[3] A study on hamsters showed that direct inhalation is the main mechanism, but infection via fomite transmission also occurred [4]. Modelling of the pandemic and disease transmission found that up to 25% of the disease transmissions during lockdown was via fomites [5]. Studies have shown that SARS-CoV-2 remains infective up to 7 days after a droplet is placed on some solids [6,7], indicating the window of possible infection from solids may be large. This has led to widespread fear of touching communal objects and to health authorities suggesting that people increase the frequency and quality of their hand-washing [8]. A parallel approach is to design coatings for solids that inactivate the virus and to apply these coatings to communal objects [9-12].

An important question remains unanswered: does the virus actually transfer from contaminated objects to a person's hand? The transfer of virus from the contaminated solid surface to the body is necessary for infection via fomites. In this article, we describe measurements of the percentage transfer of SARS-CoV-2 to skin from a variety of solids.

Following biosafety protocols, we were not able to examine transfer to the skin of living humans. We instead used Vitro-skin® an artificial skin for a number of reasons. First, many of

its characteristics are similar to human skin. Vitro-skin® has similar wettability [13], mechanical properties [14], textural features, and chemistry to human skin (see Supplementary Information.) Others have found Vitro-skin® to be a good model for human skin [14,15]. An additional advantage of using an artificial skin is that human skin varies from place to place on the body, between individuals, and depends on the state of the individual. Use of a constant skin sample enables better resolution of the variations in transfer from different inanimate objects.

We made an artificial finger from polydimethylsiloxane (PDMS) with a modulus similar to human skin and attached the Vitro-skin® to the PDMS. We contaminated each solid with 1 µL of SARS-CoV-2 in suspension in buffer. 1 µL is the upper end of the size range of respiratory droplets [16], much smaller droplets did not allow sufficient resolution of the viral titer.

As described below, our experiments do show that SARS-CoV-2 transfers from solids to skin, even when contact is made after the droplet has evaporated.

9.3. Materials and Methods

Details of the materials and their characterization are in Supplementary Information.

9.3.1. Artificial Skin

Vitro-Skin® was purchased from IMS Division of Florida Skincare Testing Inc. (Florida, USA). In this manuscript "artificial skin" refers to Vitro-Skin®. As-received Vitro-Skin® needs to be hydrated to be a good model for human skin. Hydration was achieved in a sterilized, sealed

chamber that contains 15% w/w glycerin in water for 16-24 hrs [14]. Artificial skin was sterilized with 70% ethanol prior to the hydration step.

9.3.2. Artificial Finger

PDMS was chosen as support for the skin because we were able to make a PDMS support that had about the same deformation as a human finger when subjected to a 3 N load. Sylgard 184 (base to curing agent = 10:1) and Sylgard 527 (part A to part B = 1:1) were prepared separately and the two were thoroughly mixed with a ratio of Sylgard 527:184 = 5:1. Subsequently the mixture was poured into hemicylindrical-shaped molds (plastic centrifuge tube, diameter = 15 mm) and heated at 80ºC for 9 hours to cure. The resulting PDMS had a hemicylindrical shape, and the curved side faced the test solid during the transfer (See Supplementary Figure 9-5). The in vivo elastic modulus of human skin is 0.04-0.22 MPa [17,18]. which spans the range of 0.13 MPa measured for Sylgard 527:184 = 5:1 [19]. The sterilized and hydrated artificial skin was attached to the PDMS hemicylinder using double-sided tape to create the artificial finger.

9.3.3. Transfer Experiment

A 1 μL SARS-CoV-2 droplet (at $\log_{10}$ 7.8 $TCID_{50}$/ml) was placed on each test solid (glass, etc.) at 22-23°C and relative humidity of 60-70%, and then the artificial skin was contacted to the test solid after waiting for either 10 sec or 30 min. After 10, the droplet evaporation was negligible, and so we describe the test solid as “wet”; after 30 min, the droplet had evaporated so the test solid was dry, which we refer to as “evaporated” or “dry”. Artificial

skin was attached to the curved side of the PDMS immediately before the touch experiment. Contact between artificial skin and the test solid was for 5 sec with a mass of 300 g, i.e., with a force of ≈ 3N (See Supplementary Figure 9-5C). This contact force was chosen after measuring the force that we used to press a checkout credit-card machine button. The 5 sec contact time was longer than what we use to press a credit card reader button, but was chosen to achieve a smaller percentage variation in contact time. The contact area was roughly 1.2 cm x 0.3 cm, resulting in an average pressure of about 1 atm. The flat-cylinder contact was chosen to achieve a well-defined contact. A flat–flat contact would depend critically on alignment; a sphere–flat contact was not possible with the flat sheets of artificial skin that we utilized. An additional critical aspect was that that we needed to ensure that, during contact, the droplet did not run off the edges of the test solid; that would not allow accurate or reproducible accounting of the transfer. The use of a curved skin substrate provided more space within the liquid meniscus for the droplet to remain between the solids during contact. This was confirmed using dye tests prior to the experiments (Supplementary Figure 9-5C).

9.3.4. SARS-CoV-2 Assay

After the finger was separated from the test solid, the artificial skin was removed from the PDMS and the skin was soaked in 200 μL of viral transport medium (Earle's balanced salt solution, which was supplemented with 0.5%(w/v) bovine serum albumin and 0.1%(w/v) glucose, pH = 7.4) at room temperature for 30 minutes to elute the SARS-CoV-2 virus (from the Hong Kong index case). Subsequently, the eluted viral suspension was assayed by 50% tissue culture infective dose ($TCID_{50}$) assay in Vero E6 cells to determine how effective the eluent was

in infecting mammalian cells [20,21]. Supplementary Information, contains further information on the SARS-CoV-2 culture.

9.3.5. Statistical analysis

We and others find that the errors in log ($TCID_{50}$) are distributed normally, and therefore all statistics were obtained after a log transformation of the raw $TCID_{50}$ data. Data for Figure 9-2, Supplementary Figure 9-8, and Supplementary Figure 9-9 was analyzed using N-way ANOVA in MATLAB with two factors, material (glass, stainless steel, etc.) and wet/evaporated. The population marginal means were estimated using Post Hoc multiple comparison (Dunn-Sidák's approach). Additionally, we did a regression analysis with three factors – porosity (categorical), wettability (numerical from contact angle) and wet/evaporated. $p < 0.001$ for coefficients for porosity and wet/dry.

9.4. RESULTS

When a droplet of SARS-CoV-2 suspension is placed on a solid, the virus can be transferred to a finger, even when the finger has only a brief (5 sec) and light (3 N) touch to the solid that one may do when pressing a button. Figure 9-1 shows the transfer ratio, *T*, which is the ratio of the infectivity on the finger compared to the infectivity of the original droplet:

$$T = \frac{N_{\text{finger}}}{N_{\text{initial}}} \times \frac{1}{R} \times 100\% \qquad \text{Equation 9-1}$$

where N_{finger} is the infectivity measured from liquid extracted from the finger after contact with the solid, as measured by $TCID_{50}$ assay in Vero E6 (African green monkey) cells, and N_{initial} is the infectivity measured in the droplet that was initially placed on the test solid. R is the recovery rate for extracting virus from the finger. More detail is provided in Supplementary Information.

We examined transfer for two conditions: (1) when it was freshly placed on the solid (after 10 sec) and (2) after it had evaporated (30 min). The transfer percentage for wet droplets on the three common non-porous solids – glass, stainless steel and Teflon – are in the range 13–16% (0.8–0.9 log less than the input) (Figure 9-1). These numbers are quite high: the amount of virus transferred to the skin after touching the solid is about 15% as great as if the droplet landed directly on the finger. When the droplet was allowed to dry, about 3–9% (1–1.5 log less than the input) was transferred. This evokes the scenario when an infected individual deposits a droplet and half an hour later a second individual who touches the dry surface could still transfer 3–9% of the original virus onto their fingers. This is not a large reduction by microbiological standards; for comparison, sanitizers and disinfectants are considered effective when they leave less than 0.1% of the germ, i.e., at least a 30–150 times greater reduction. The results reinforce the idea that hand-washing is important before touching one's face. Note that our method of calculating the transfer includes any inactivation of the virus that occurs on the test solid prior to contact with the finger. In some cases, this could be substantial. For example, in our prior work, we showed that only 31% of the virus was recovered from glass after 30 minutes, even with no skin contact[10]. We think that the fraction of the initial dose that ends up on the finger is the relevant quantity. We note that for the transfer percentage of the dried droplets may be slightly greater

than indicated, as described in Supplementary Information. A separate experiment with $1/5^{th}$ of the viral loading on glass revealed that, in this range, the load did not affect the transfer.

For the remaining results, we directly compare $TCID_{50}$/mL values, which are shown in Figure 9-2. Figure 9-2, Supplementary Figure 9-8, and Supplementary Figure 9-9 also show population marginal means. There is a significant decrease in viral transfer after the droplet evaporates (p <0.0001), which is more clearly shown in Supplementary Figure 9-8. This is as expected; once the liquid evaporates, there is no liquid meniscus to transport the virus to the finger.

We originally hypothesized that a more hydrophobic solid, i.e., a solid with a greater water receding angle, would transfer more virus. This was based on the idea that a greater volume of liquid would transfer from a hydrophobic solid, and therefore, more virus could be transferred in that greater volume. We examined this hypothesis by including Teflon as one of the samples. Teflon has an unusually high receding angle (96º ± 9º) whereas clean glass has a low contact angle, 11º ± 7º (Table 9-1). There was no significant difference between the transfer for the two substances (see Figure 9-2 and Supplementary Figure 9-9). We then tested the mass of liquid that was transferred (Supplementary Figure 9-7), and found that the mass transfer was also similar, which possibly explains why the viral titer did not depend on the contact angle for non-porous solids.

Porosity, however, does play a key role. We examined three porous objects (tissue, wood, and porous glass) that were sufficiently hydrophilic that the droplet could penetrate into the solid. Each of these porous solids had less transfer than each of the three non-porous solids (glass, stainless steel, or Teflon). This is evident for wet and dried solids considered separately

(Figure 9-1) and for wet and dried samples considered together (Supplementary Figure 9-9). The most direct comparison is between porous and non-porous glass, where the material is the same yet the transfer is completely different. The explanation is fairly simple. For wet surfaces, the droplet is mainly within the porosity and less of the droplet is transferred to skin. For dried droplets, we expect that much of the virus is dried into the interior of the porosity and is not available on the surface for dry, solid-to-solid transfer. We did some further tests on the effect of porosity using real time quantitative polymerize chain reaction (RT-qPCR) measurements that confirm that the virus does become trapped in interior pores (see Supplementary Figure 9-10). We expect that the effect of porosity would be contingent on the interior pores of the solid being wettable. Thus, we would not expect the droplet to penetrate porous Teflon, so we predict transfer would still be high from this material.

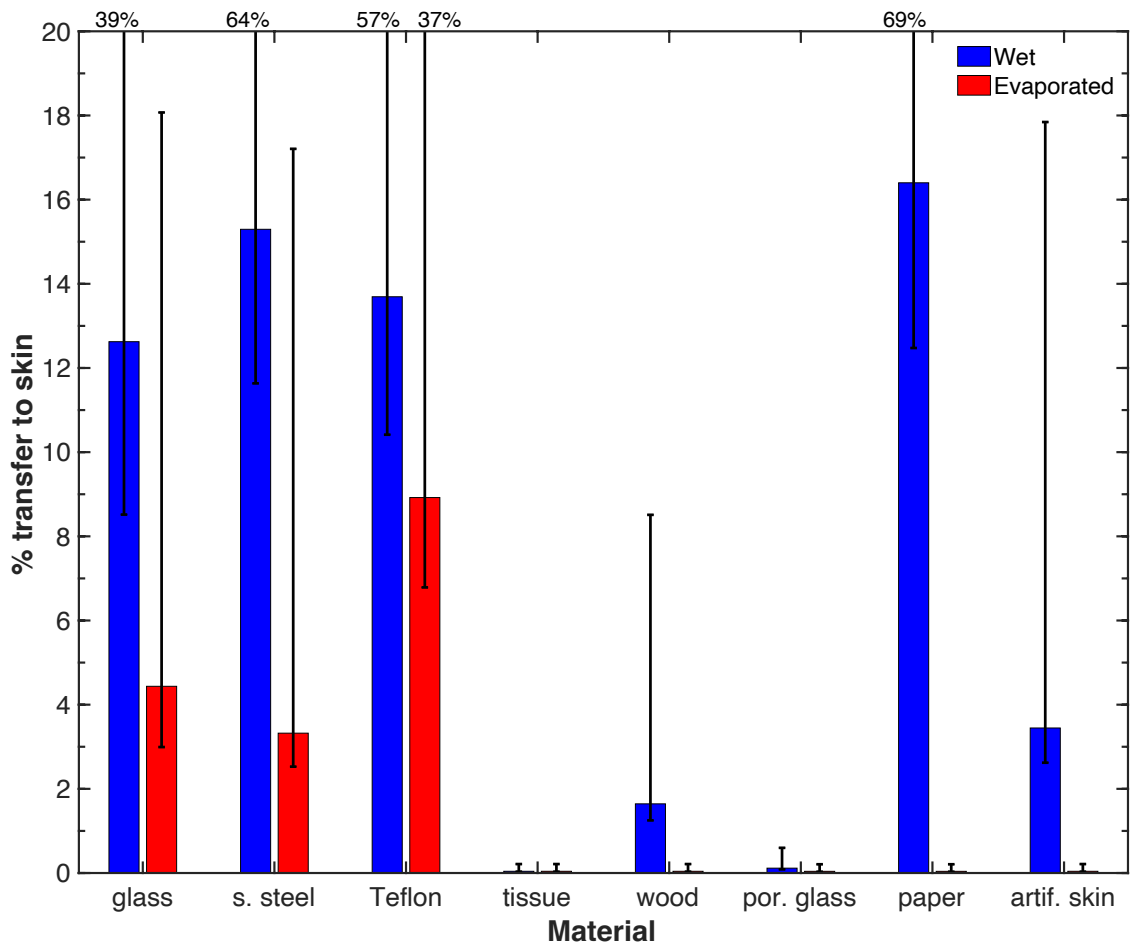


Figure 9-1. Mean percentage transfer to an artificial finger from various solid material during a 5 sec contact with a 3 N (300 g) load with no lateral motion (i.e., no rubbing). Error bars are the comparison intervals from ANOVA with two factors: the material and the time, which corresponds to wet or evaporated. The error bar is asymmetric because of the exponential distribution of measurement residuals. When the upper bound is off-scale, it is indicated by a number. The time to adsorb the droplet on porous surfaces was as follows: tissue and porous glass, immediate; wood, 1-2 min; and paper, 2.5 min. Note that the transfer is high for non-porous solids and is measurable when the 1 μL test drop is wet (10 sec) or has evaporated (30 min). Each data point was obtained from three independent measurements that are tabulated in Supplementary Table 9-1.

Solids	Contact angle	
	Advancing	**Receding**
glass	26 ± 13	11 ± 7
stainless steel	84 ± 15	40 ± 23
Teflon	111 ± 6	96 ± 9
porous glass	0	0
paper	96 ± 12	11 ± 3
artificial skin	89 ± 6	<10

Table 9-1. Mean water contact angle measurements of test solids. The figure after ± sign is the 95% confidence interval. The contact angle was measured 10 seconds after the droplet was placed on the solid.

Recent work has also tested the transfer of SARS-CoV-2 from cardboard or plastic to pig skin.[22] That work showed that transfer was greater from plastic than from cardboard. The authors state that the plastic was non-porous and that the cardboard was porous, and make a similar conclusion that the lack of transfer for cardboard is due to the drop being imbibed into the porous surface.

The paper material provides an interesting example of a porous material. Transfer from paper was initially (after 10 s) very high whereas transfer after the droplet evaporated (30 min) was very low. This is explained though an understanding of how the wettability of the material affects access to the porosity. If the chemistry of pores is sufficiently hydrophobic, then the water cannot spontaneously enter the pores and the porosity is not accessed. Although paper is porous, there is an induction time for wetting: for the particular paper that we used, the paper goes from non-wetting and impermeable to wetting and permeable after about 2.5 minutes of

contact with a 1 μL droplet (See Supplementary Figure 9-12). Our "wet" experiment was conducted after 10 s, during the impermeable period. Without access to the porosity, the SARS-CoV-2 suspension behaved like it was on a non-porous solid, the droplet was transferred to the finger and we recorded a high transfer ratio. After 2.5 min., the viral suspension penetrated into the paper, and subsequently dried into the pore space, presumably depositing the virus onto the paper fibers on the interior of the paper. The transfer experiment after 30 minutes showed a very low level of transfer because those interior surfaces were not accessible to the finger during transfer.

A further interesting aspect of porosity concerns the fate of the SARS-CoV-2 in the porosity. We also measured the $TCID_{50}$ of liquid used to extract virus from the dried solids after contact with the finger (data not shown) using the same procedure as for extraction from the skin. We were not surprised that the levels were very low for porous solids. For porous glass, tissue, and wood, $TCID_{50}$/mL was below the detection limit. However, for paper, log[$TCID_{50}$/mL] was 3.5. This indicates that SARS-CoV-2 can, to some extent, be stored in dried paper, and resuspended in an active state.

Finally, we used linear regression to make a predictive model for the transfer as a function of the wet/dry state, the porosity, and the wettability. This model performed well and is described in Supplementary Figure 9-13.

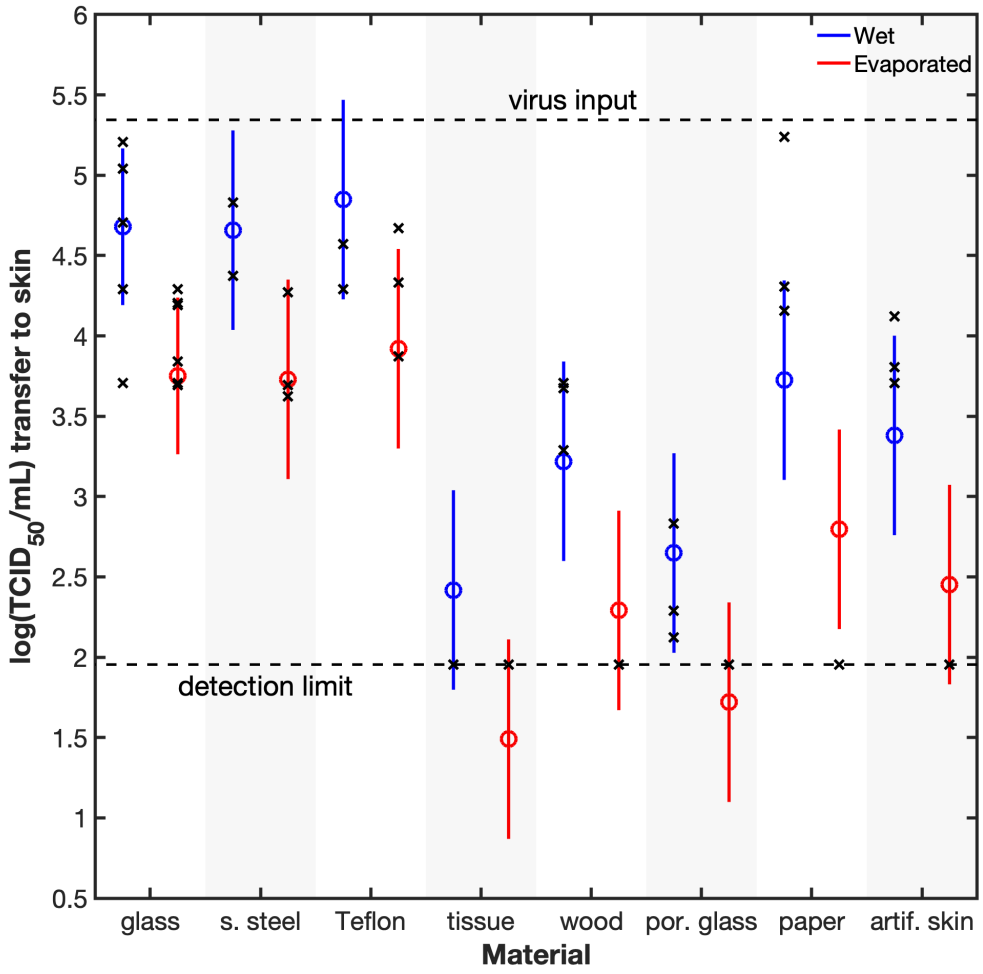


Figure 9-2. Log($TCID_{50}$/mL) values (x) and population marginal means (o) on artificial skin after transfer from various solids. The population marginal means were calculated from Post Hoc comparison using N-way ANOVA (two factors: material and wet/evaporated) in MATLAB using the Dunn-Sidák's approach. The bars represent the comparison interval; two groups are statistically different if their intervals do not overlap. Transfer is detectable for all solids, except tissue, wood (dry), porous glass (dry), and paper (dry), and these data points have been plotted on the detection limit of 90. Transfer is greater for wet solids than for dry and there is no significant difference among common non-porous solids.

9.5. Discussion

People use a huge range of contact trajectories when touching surfaces, for example, different pressures, different times of contact, and different rubbing actions. In this study we considered only brief and low-pressure contact with no rubbing or translation in contact. It is well-established that rubbing causes friction and increases wear and transfer between solids, and in particular that microbial transfer is increased significantly by rubbing [23]. We therefore expect that transfer of SARS-CoV-2 would also be enhanced by rubbing.

Infected patients can shed droplets with high concentrations of SARS-CoV-2 [24,25]. For example, Pan *et al*. showed a median of 7.5 x 10^5 and a high of 10^7 gene copies per mL in sputum [24]. Our research shows that, on non-porous solids, 13–16% of this virus can be transferred to skin after being deposited on a solid when the drop is still wet and 3–9% can be transferred even 30 minutes later, when the droplet is dry. This still leaves a large dose of virus on the finger. Clearly one more step is required to transfer the virus to the respiratory system: transfer from the finger to the nose or mouth. The overall transmission from solid to skin to respiratory system depends on the product of the individual transfer rates, and would be lower. The final dose transferred to the respiratory system should be compared to the infectious dose for a human, which unfortunately is not known. Studies of Syrian hamsters indicate that the infective does for these susceptible animals is only 5 infectious particles [26]. Clearly hand washing can reduce both the contamination of surfaces and intercept the virus before it is transferred from fingers to the respiratory system.

Infection via fingers depends also on the longevity of the virus on human skin: the virus must survive long enough on skin to be transferred. Harbourt et al. reported the stability of

SARS-CoV-2 on dead porcine (pig) skin [27]. They found the virus remains stable for 4 days at 22±2°C, and 8 h at 37±2°C (relative humidity of 40-50%). Hirose et al. measured survival of the SARS-CoV-2 virus on a dead human skin model [28]. They showed the virus can survive on the skin model for up to 9 hours at 25°C and relative humidity of 45–55%. These longevity studies suggest that once SARS-CoV-2 has been transferred to the skin, there is a long period of vulnerability.

9.6. Conclusions

In summary, our research demonstrates substantial transfer of SARS-CoV-2 virus from a variety of solids to an artificial finger, even when the surface has dried after application of a viral suspension and for a brief, light force and no rubbing. When the droplet penetrates a porous solid, such as wood or tissue, the transfer is low.

Data availability:

The data that supports the findings of this study are available within the Supplementary Information.

REFERENCES

1 World Health Organization. *WHO Coronavirus Disease (COVID-19) Dashboard*, <https://covid19.who.int/> (2021).

2 Center for Disease Control. *Cleaning and Disinfection for Households*, <https://www.cdc.gov/coronavirus/2019-ncov/prevent-getting-sick/cleaning-disinfection.html> (2020).

3 World Health Organization. *Transmission of SARS-CoV-2: implications for infection prevention precautions*, <https://www.who.int/news-room/commentaries/detail/transmission-of-sars-cov-2-implications-for-infection-prevention-precautions> (2020).

4 Sia, S. F. *et al.* Pathogenesis and transmission of SARS-CoV-2 in golden hamsters. *Nature* **583**, 834-838 (2020).

5 Meiksin, A. Dynamics of COVID-19 transmission including indirect transmission mechanisms: a mathematical analysis. *Epidemiol. Infect.* **148**, e257, doi:10.1017/S0950268820002563 (2020).

6 Van Doremalen, N. *et al.* Aerosol and surface stability of SARS-CoV-2 as compared with SARS-CoV-1. *N. Engl. J. Med.* **382**, 1564-1567 (2020).

7 Chin, A. W. H. *et al.* Stability of SARS-CoV-2 in different environmental conditions. *The Lancet Microbe* **1**, e10, doi:10.1016/S2666-5247(20)30003-3 (2020).

8 Alzyood, M., Jackson, D., Aveyard, H. & Brooke, J. COVID-19 reinforces the importance of handwashing. *J. Clin. Nurs.* **29**, 2760-2761, doi:10.1111/jocn.15313 (2020).

9 Behzadinasab, S., Chin, A., Hosseini, M., Poon, L. & Ducker, W. A. A surface coating that rapidly inactivates SARS-CoV-2. *ACS Appl. Mater. Interfaces* **12**, 34723-34727 (2020).

10 Hosseini, M., Chin, A. W., Behzadinasab, S., Poon, L. L. & Ducker, W. A. Cupric oxide coating that rapidly reduces infection by SARS-CoV-2 via solids. *ACS Appl. Mater. Interfaces* **13**, 5919-5928 (2021).

11 Hutasoit, N. *et al.* Sars-CoV-2 (COVID-19) inactivation capability of copper-coated touch surface fabricated by cold-spray technology. *Manuf. Lett.* **25**, 93-97 (2020).

12 Hasan, J. *et al.* Antiviral Nanostructured Surfaces Reduce the Viability of SARS-CoV-2. *ACS Biomater. Sci. Eng.* **6**, 4858-4861 (2020).

13 Ginn, M., Noyes, C. & Jungermann, E. The contact angle of water on viable human skin. *J. Colloid Interface Sci.* **26**, 146-151 (1968).

14 Jermann, R., Toumiat, M. & Imfeld, D. Development of an in vitro efficacy test for self-tanning formulations. *Int. J. Cosmet. Sci.* **24**, 35-42 (2002).

15 Chen, S. & Bhushan, B. Nanomechanical and nanotribological characterization of two synthetic skins with and without skin cream treatment using atomic force microscopy. *J. Colloid Interface Sci.* **398**, 247-254 (2013).

16 Duguid, J. The size and the duration of air-carriage of respiratory droplets and droplet-nuclei. *Epidemiol. Infect.* **44**, 471-479 (1946).

17 Pailler-Mattei, C., Bec, S. & Zahouani, H. In vivo measurements of the elastic mechanical properties of human skin by indentation tests. *Med. Eng. Phys.* **30**, 599-606 (2008).

18 Diridollou, S. *et al.* In vivo model of the mechanical properties of the human skin under suction. *Skin Res. Technol.* **6**, 214-221 (2000).

19 Palchesko, R. N., Zhang, L., Sun, Y. & Feinberg, A. W. Development of polydimethylsiloxane substrates with tunable elastic modulus to study cell mechanobiology in muscle and nerve. *PLoS One* **7**, e51499 (2012).

20 Chan, K. *et al.* Analytical sensitivity of rapid influenza antigen detection tests for swine-origin influenza virus (H1N1). *J. Clin. Virol.* **45**, 205-207 (2009).

21 Malenovska, H. Virus quantitation by transmission electron microscopy, TCID50, and the role of timing virus harvesting: a case study of three animal viruses. *J. Virol. Methods* **191**, 136-140 (2013).

22 Johnson, G. T. *et al.* Evaluation of the Survivability of SARS-CoV-2 on Cardboard and Plastic Surfaces and the Transferability of Virus from Surface to Skin. *Occup. Dis. Environ. Med.* **9**, 63-73 (2021).

23 Zhao, P. *et al.* Physical factors that affect microbial transfer during surface touch. *Build. Environ.* **158**, 28-38 (2019).

24 Pan, Y., Zhang, D., Yang, P., Poon, L. L. & Wang, Q. Viral load of SARS-CoV-2 in clinical samples. *Lancet Infect. Dis.* **20**, 411-412 (2020).

25 Yu, F. *et al.* Quantitative detection and viral load analysis of SARS-CoV-2 in infected patients. *Clin. Infect. Dis.* **71**, 793-798 (2020).

26 Rosenke, K. *et al.* Defining the Syrian hamster as a highly susceptible preclinical model for SARS-CoV-2 infection. *Emerg. Microbes Infect.* **9**, 2673-2684 (2020).

27 Harbourt, D. E. *et al.* Modeling the stability of severe acute respiratory syndrome coronavirus 2 (SARS-CoV-2) on skin, currency, and clothing. *PLoS Negl. Trop. Dis.* **14**, e0008831 (2020).

28 Hirose, R. *et al.* Survival of severe acute respiratory syndrome coronavirus 2 (SARS-CoV-2) and influenza virus on human skin: importance of hand hygiene in coronavirus disease 2019 (COVID-19). *Clin. Infect. Dis.*, doi:10.1093/cid/ciaa1517 (2020).

Acknowledgments

The authors acknowledge use of Microscopy facilities within the NCFL at Virginia Tech. We thank Professor Thomas Staley for grinding the glass particles to an appropriate size, Kevin Holshouser for fabricating the transfer apparatus, and Matty Ducker for the linear regression. This work was supported by the National Science Foundation under Grant No. CBET-1902364, the Health and Medical Research Fund (COVID190116), and the National Institute of Allergy and Infectious Diseases (contract HHSN272201400006C)

Author Contributions

WD and LLMP conceived of the experiments and WD designed the transfer apparatus. WD and SB designed the artificial finger and designed the experiments. SB prepared and characterized the samples unless otherwise noted. MH fabricated the porous glass samples. Analysis of data was done by WD, SB, AWHC, and LLMP. The preparation of SARS-CoV-2 and experiments containing the virus were done by AWHC. Supervision was done by WAD and LLMP. The manuscript was written by SB and WD with input from all authors.

Additional Information

Competing interests: WD declares part ownership in a startup company to produce surface coatings. No other authors declare competing interests.

Supplementary Information: see Supplementary Information for further information about Supplementary Materials and Methods, Characterization of Samples, Transfer Apparatus, Statistical analysis, Data Analysis, Mass Balance for Transfer Efficiency, Calculation of the transfer ratio by another method, Data tables, and Additional figures.

ORCID

Saeed Behzadinasab: 0000-0002-6271-2623

Alex W.H. Chin: 0000-0002-6556-9092

Mohsen Hosseini: 0000-0002-9482-0215

Leo Poon: 0000-0002-9101-7953

William A. Ducker: 0000-0002-8207-768X

9.7. SUPPLEMENTARY INFORMATION

SARS-CoV-2 virus transfers to skin through contact with contaminated solids

Saeed Behzadinasab[†1], Alex W.H. Chin[†2], Mohsen Hosseini[1], Leo L.M. Poon*[2,3], and William A. Ducker*[1]

[†] These authors contributed equally

*Corresponding Authors' Email: Leo Poon llmpoon@hku.hk; William Ducker wducker@vt.edu

[1]Dept. of Chemical Engineering and Center for Soft Matter and Biological Physics, Virginia Tech, VA, 24061, USA

[2]School of Public Health, LKS Faculty of Medicine, The University of Hong Kong, Hong Kong Special Administrative Region, China.

[3]HKU-Pasteur Research Pole, LKS Faculty of Medicine, The University of Hong Kong, Hong Kong, China

Keywords: SARS-CoV-2, transfer, skin, coronavirus, COVID-19, hand, wash

Supplementary Materials and Methods

9.7.1. Materials

The following items were purchased from VWR: glass slides (25 × 75 × 1 mm), acetone (ACS grade), nitric acid (70%, ACS grade), 70% ethanol, and ethanol (200 Proof). Polydimethylsiloxane (PDMS) Sylgard 184 and 527 were obtained from Dow Corning. Tissue was purchased from Vinda (Hong Kong). Wood was part of a disposable tongue depressor purchased from Navy (Hong Kong). The test solid of paper was TRU RED^{TM} printer paper (SKU# 13585, 75 g/m^2). Water was purified by Milli-Q Reference system. Glass slides were cut into 12x12 mm, rinsed with water (3 times), immersed in 70% ethanol for 15 min. Subsequently, rinsed with water (3 times), soaked in 6 M nitric acid for 20 min and rinsed with water. Fatigue-resistant 301 stainless steel (301 SS, 6”x6”, ½ hard temper, 0.015” thick) and chemical resistant PTFE (Teflon) sheet (12”x12”x1/16”) were purchased from McMaster-Carr. 301 SS was cut into 12x12 mm pieces, washed with soapy water, rinsed with water. Teflon was cut into 12x12 mm pieces, washed with a soap solution in water, rinsed with water, immersed in and rinsed with ethanol and then acetone.

SARS-CoV-2 virus (BetaCoV/Hong Kong/VM20001061/2020) was isolated from a confirmed COVID-19 patient in Hong Kong. DMEM, fetal bovine serum, penicillin-streptomycin, Earle’s balanced salt solution, bovine serum albumin, and glucose were purchased from Sigma Aldrich.

9.7.2. Methods

9.7.2.1. Characterization

Contact angles were measured using a First Ten Angstroms FTA125. Scanning Electron Microscope (SEM, JEOL IT500 SEM) was used to characterize the morphology. The porous glass sample was sputtered with 5 nm of Au/Pt prior to SEM imaging.

The following methods were used to determine the similarity between Vitro-Skin® (artificial skin) and human skin: Attenuated Total Reflectance-Fourier Transform Infrared (ATR-FTIR, Varian 670-FTIR), optical microscopy (Zeiss Axio Imager.M2 upright fluorescent microscope equipped with a 10 × objective).

9.7.2.2. Fabrication of porous glass test solids

Smooth crushed glass (270-1000 grit, catalog number 64223704) was purchased from MSC Industrial Supply Company. The crushed glass was milled in U.S. Stoneware roller mill with alumina milling media at 0.5 rotations per sec. The attachment of the particles to glass slides was accomplished as follows. A suspension of 10.5 wt.% milled glass in ethanol was sonicated for five minutes, 280 µL of suspension applied on 15×15 mm pieces of glass slide, and then the samples were dried at room temperature for 30 minutes. Early-stage sintering of particles to each other and to the slide was achieved by heat treatment at 120°C for 10 minutes, then at 320°C for 10 minutes, and finally at 617°C for 2 hours. Next, the furnace was switched off and samples were cooled gradually to room temperature. Finally, the porous glass test solids were cleaned in the same way as the glass slides.

9.7.2.3. Preparation of SARS-CoV-2 culture

Our viral assay methods were described previously [1-3]. In summary, all of the surfaces were sterilized with 70% ethanol and dried in air before testing with the virus, unless otherwise noted.

The SARS-CoV-2 strain was from the index case of Hong Kong. The stock virus was prepared in Vero-E6 cells cultured in Dulbecco's Modified Eagle Medium (DMEM, with 2% fetal bovine serum and 1% v/v penicillin-streptomycin) at 37°C with 5% CO_2.

9.7.2.4. SARS-CoV-2 assay

After the finger was separated from the test solid, the artificial skin was removed from the PDMS and the skin was soaked in 200 µL of viral transport medium (Earle's balanced salt solution, which was supplemented with 0.5%(w/v) bovine serum albumin and 0.1%(w/v) glucose, pH = 7.4) at room temperature for 30 minutes to elute the SARS-CoV-2 virus (from Hong Kong index case). Subsequently, the eluted viral suspension was assayed by 50% tissue culture infective dose ($TCID_{50}$) assay in Vero E6 cells to determine how effective the elutant was in infecting mammalian cells [4,5].

Briefly, the liquid containing the virus was serially diluted in quadruplicates and infected confluent Vero E6 cells on 96-well plates. Subsequently, the infected cells were incubated at 37°C with 5% CO_2. On day 5 post-infection, the cells were examined for a cytopathic effect. The $TCID_{50}$/ml is the dilution that caused a cytopathic effect in 50% of treated Vero E6 cell cultures (N=4 per each dilution; Reed-Muench method [6]). Three independent tests were done at each

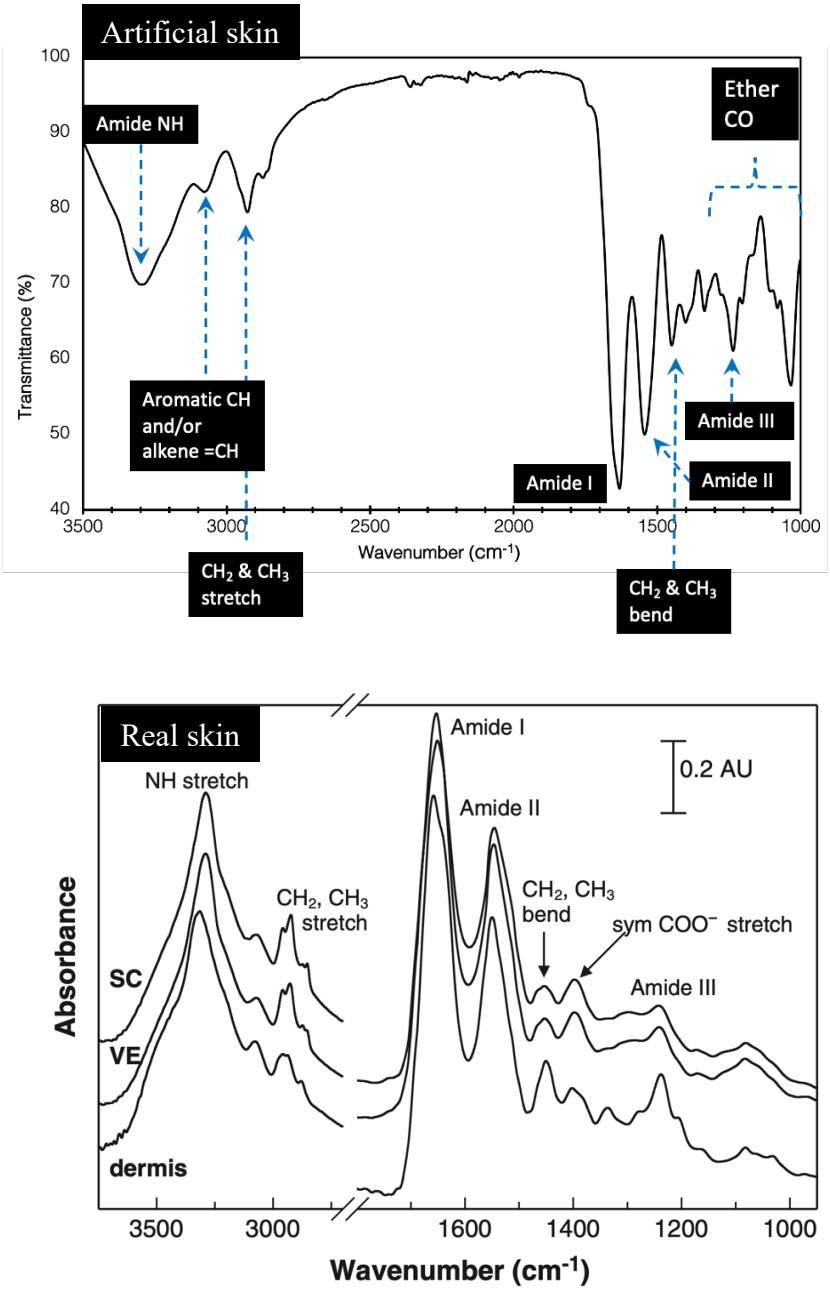
condition. Error residuals were approximately normally distributed after a log transformation, so all statistics were calculated from the log of the titers

9.7.2.5. qPCR test

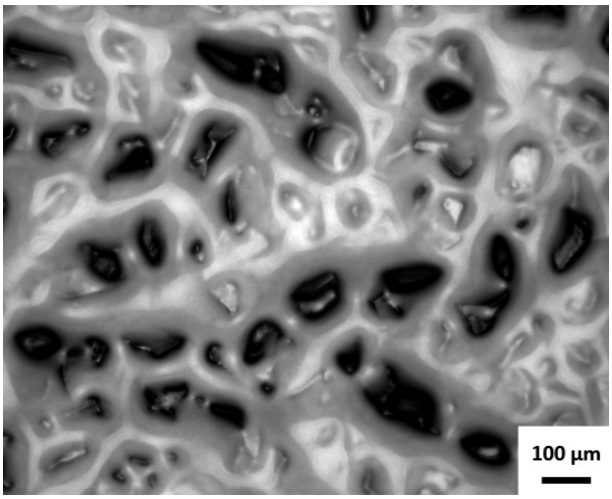
Viral RNA was extracted from 70 ml of VTM containing the virus using QIAamp Viral RNA Mini Kit (Qiagen) and eluted in 30 ml elution buffer. Two ml of the eluted viral RNA was subjected to quantitative RT-PCR to quantify the N gene of SARS-CoV-2 using TaqMan Fast Virus 1-step Master Mix (Thermo Fisher). The primers and probe for the assay are: 5′-TAATCAGACAAGGAACTGATTA-3′ (Forward), 5′-CGAAGGTGTGACTTCCATG-3′ (Reverse) and 5′-GCAAATTGTGCAATTTGCGG-3′ (Probe in 5'-FAM/ZEN/3'-IBFQ format), as described in[7].

9.7.3. Characterization of Samples

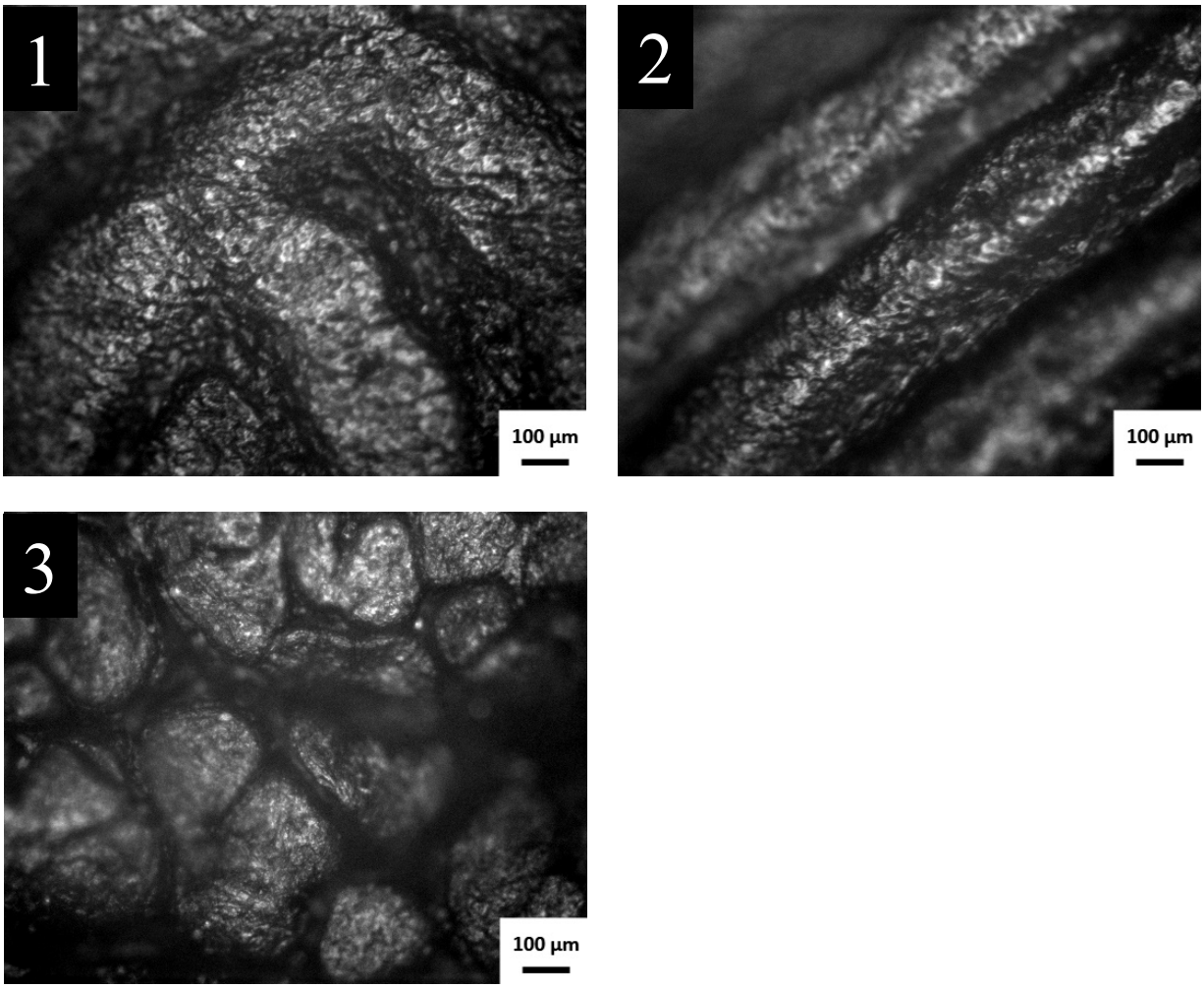
9.7.3.1. Vitro-Skin®



Supplementary Figure 9-1. IR spectra of (top) artificial skin and (bottom) real human skin. Note that the Vitro-Skin® data is presented as transmittance, whereas the real skin data is presented as absorbance. The artificial skin and real human skin have similar IR spectra, which is consistent with similar chemistry. (IR of real skin was reused with permission from Ref. 8, © 2012 Wiley).

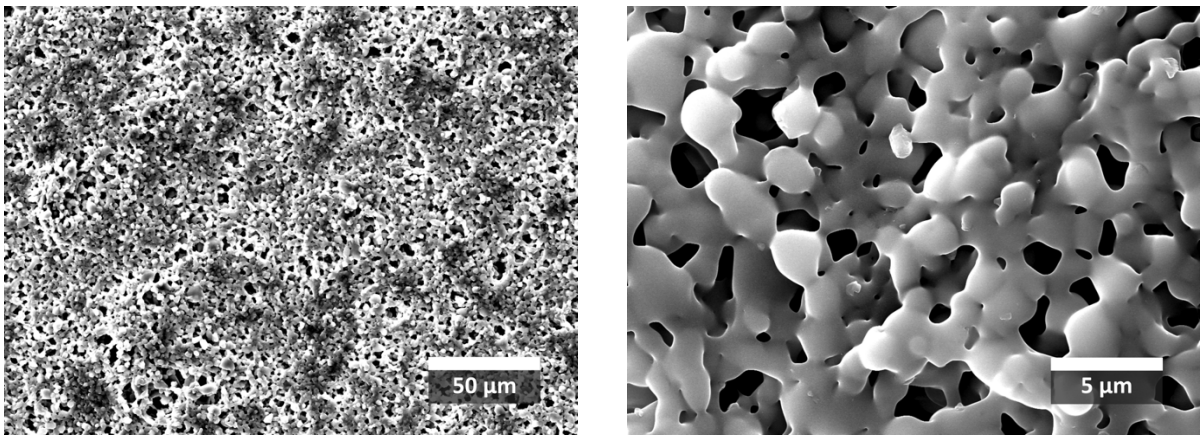


Supplementary Figure 9-2. Optical image of Vitro-Skin®.



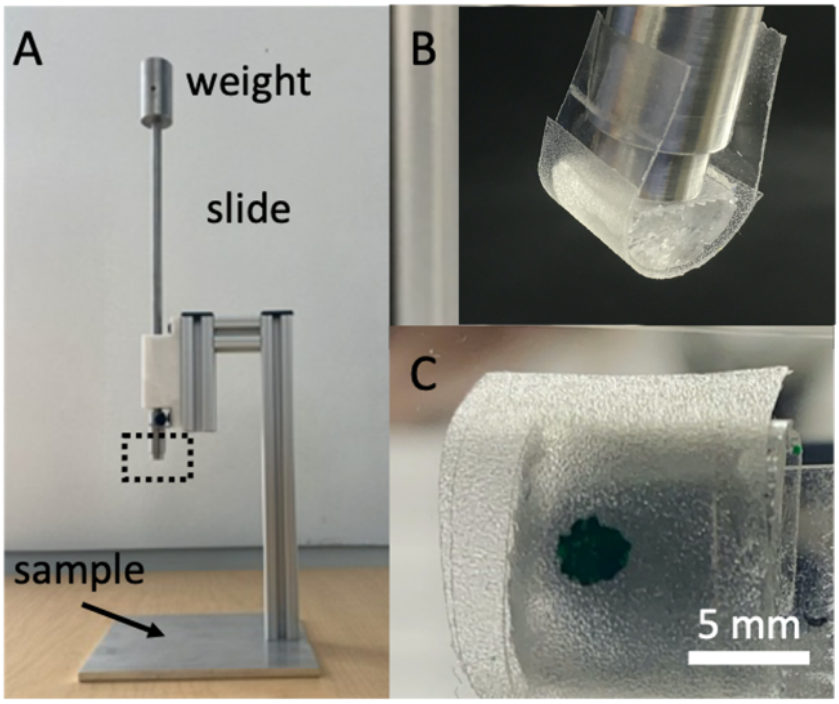
Supplementary Figure 9-3. Optical images of human hand skin. Number 1 and 2 show two regions of the finger-print region of index finger of a right-hand. Number 3 shows skin on the nail-side of the right-hand index finger. Human skin topography varies depending on the location. The subject's hand was washed with antibacterial soap (twice) immediately before imaging. The feature size is similar on human skin and Vitro-Skin®, but Vitro-Skin® does not have fingerprints.

9.7.3.2. Porous Glass



Supplementary Figure 9-4. SEM images of the porous glass sample. The images show the pore size ranges from sub-µm to above to a few µm.

9.7.4. Transfer Apparatus



Supplementary Figure 9-5. Photographs of apparatus. (A) Device for applying 3 N constant force. Square box shows area of detail in (B). (B) higher magnification view of the imitation finger showing semicircular cross-section. (C) The finger in contact with a glass slide. The slide was moved down so that the artificial finger contacted the sample with a known force of 3 N. For this photograph, the droplet was dyed green for easier visibility. The PDMS cylinder is flattened by the load.

9.7.5. Data Analysis

As described in the manuscript, we defined Transfer Efficiency as:

$$T = \frac{N_{\text{skin}}}{N_{\text{initial}}} \times \frac{1}{R} \times 100\% \qquad \text{(Supplementary Eq. 1)}$$

where N_{skin} is the $TCID_{50}$ measured on skin after contact with the solid and N_{initial} is the $TCID_{50}$ measured in the droplet that was initially placed on the solid. The $TCID_{50}$ technique is not a measure of viral numbers but a measure of infectivity. The exact relationship between $TCID_{50}$ and number of virions is unknown, but if we assume that it is linear, then the proportionality cancels in Supplementary Information and the Transfer ratio represents the fraction of virions that are transferred. When comparing N_{skin} to N_{initial} it is important to note that N_{skin}depends on our ability to recover the virus from a solid, whereas N_{initial} does not, so we need to account for fraction of virus recovered from the skin, R_{skin}, which was calculated as follows (see Supplementary Figure 9-6). This was determined in a separate experiment by placing a viral suspension of known $TCID_{50}$ directly on the artificial finger (i.e., no contact with a test solid) and then eluting the droplet in the same way as was done for skin after each transfer experiment. $R_{\text{skin}}$was calculated from:

$$R_{\text{skin}} = \frac{N_{\text{skin}}}{N_{\text{initial}}} \qquad \text{(Supplementary Eq. 2)}$$

where N_{skin} is the $TCID_{50}$ for the liquid eluted from the skin, and N_{initial} is the $TCID_{50}$ from the original droplet that was placed on the skin. In principle, N_{initial} from Supplementary Eq. 1 and Supplementary Eq. 2 could be measured at the same time, but in practice they were measured at different times and therefore are slightly different. Note that the N values in Supplementary Eq.

1 and Supplementary Eq. 2 are the averages of 3 independent $TCID_{50}$measurements, and because the residuals are distributed normally after a log transformation are calculated from:

$$N = \text{antilog}\left[\text{average}\left(\log(\text{TCID}_{50})\right)\right] \qquad \text{(Supplementary Eq. 3)}$$

The value of R_{skin} was 0.99 and $TCID_{50}$ of virus recovered from artificial skin after is not significantly different than from the droplet was placed on the skin. We have not devised a method for determining R_{skin} for a solid when dried virus is transferred so we have used the value of R_{skin} for the transfer from a wet solid. We expect that the extraction will be more difficult for dried virus so we consider the reported transfer for virus from various dried solids to be lower bounds. An alternate method for calculating the Transfer Ratio, that was discarded by us, is described in S6.

We and others find that the errors in log ($TCID_{50}$) are distributed normally, and therefore all statistics were obtained after a log transformation of the raw $TCID_{50}$ data, i.e.:

$$N = \text{antilog}\left[\text{average}\left(\log(\text{TCID}_{50})\right)\right] \qquad \text{(Supplementary Eq. 3)}$$

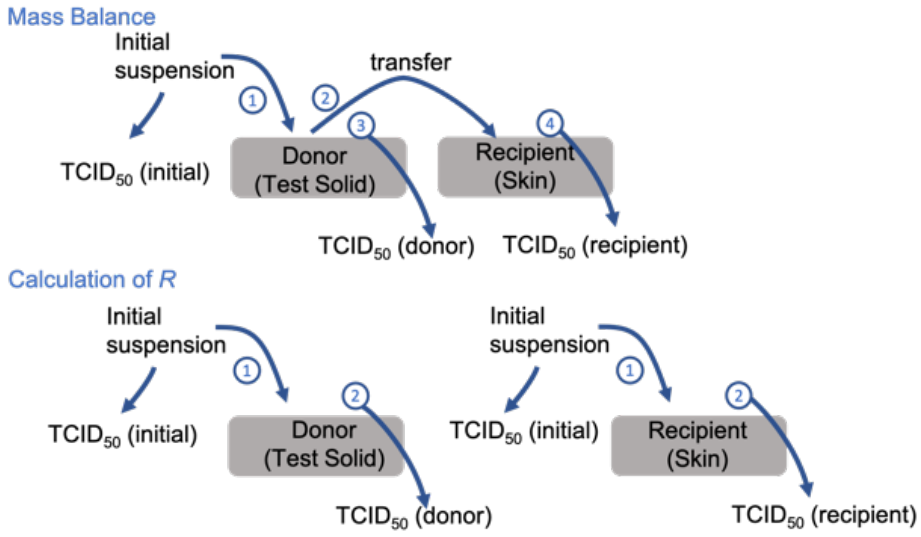
9.7.6. Mass Balance for Transfer Efficiency

To validate our approach for Supplementary Eq. 1, we examined the mass balance for the virus for transfer from two solids, the glass and the stainless steel. For these two materials, we have R_{fraction} from prior work [3]. If no virus is lost and our assumptions for Supplementary Eq. 1 were correct, then the sum of the amount recovered from the donor surface and from the skin should equal the amount originally added to the donor. To utilize the $TCID_{50}$ data we must make

the additional assumption that the $TCID_{50}$ values are additive, which rests on the unproved idea that the dose response of the Vero E6 cells to SARS-CoV-2 is linear. Making this assumption:

$$\mathrm{TCID}_{50}(\mathrm{final}) = \frac{\mathrm{TCID}_{50}(\mathrm{donor})}{R_{\mathrm{donor}}} + \frac{\mathrm{TCID}_{50}(\mathrm{recipient})}{R_{\mathrm{recipient}}} \quad \text{(Supplementary Eq. 4)}$$

Supplementary Eq. 4 again assumes that the $TCID_{50}$ values are additive. Supplementary Figure 6 is a schematic of the mass balance experiment.



Supplementary Figure 9-6. schematic of the mass balance experiment

Supplementary Table 9-2 shows relevant data for the calculation. We compare the $TCID_{50}$ (final) from Supplementary Eq. 4, to the $TCID_{50}$ of the suspension droplet that we placed on the surface (initial). For wet glass we obtain 44% in the first measurement and 41% in the second experiment. For dry glass, we account for 109% in the first experiment and 170% in the

second experiment. For wet stainless steel, we account for 33%. We do not have data to calculate mass balance for the other combinations. Possible reasons for the lack of mass balance are that the dose-response is highly non-linear and it is not valid to perform the sum in Supplementary Eq. 4. Also, there is a large uncertainty in R values. We note that we do not use Supplementary Eq. 4 in our data analysis.

9.7.7. Calculation of the transfer ratio by another method.

Another potential method for calculating transfer ratio is from:

$$\frac{\frac{\mathrm{TCID}_{50}(\mathrm{recipient})}{R_{\mathrm{recipient}}}}{\left(\frac{\mathrm{TCID}_{50}(\mathrm{recipient})}{R_{\mathrm{recipient}}}+\frac{\mathrm{TCID}_{50}(\mathrm{donor})}{R_{\mathrm{donor}}}\right)}.$$

We reject this method because:

(a) The TCID values are not necessarily additive, making the calculation in the denominator problematic.

(b) There are very large uncertainties in calculating R and therefore in correctly weighting the various terms. The mass balance calculation above demonstrates this.

(c) There is large variation in the measured values of transfer ratios for repeat measurements.

9.7.8. Data tables

		TCID50/ml				log (TCID50/ml)		
Nil (virus input control)		419371.2	160669	160669		5.622599	5.205932	5.205932
Material								
Glass (wet)		5080.798	5080.798	160669		3.705932	3.705932	5.205932
Glass (dry)		6927.034	5080.798	15587.41		3.840547	3.705932	4.192774
Stainless steel (wet)		23582.98	23582.98	67753.53		4.372599	4.372599	4.830932
Stainless steel (dry)		18694.83	4193.712	4929.173		4.271721	3.622599	3.692774
Teflon (wet)		19465.49	37266.33	37266.33		4.289265	4.571317	4.571317
Teflon (dry)		7457.592	46796.96	21425.55		3.872599	4.670218	4.330932
Artificial skin (wet)		13261.68	5080.798	6396.346		4.122599	3.705932	3.805932
Artificial skin (dry)		<	<	<		<	<	<
Tissue (wet)		<	<	<		<	<	<
Tissue (dry)		<	<	<		<	<	<
Wood (wet)		4728.049	1946.549	5080.798		3.674682	3.289265	3.705932

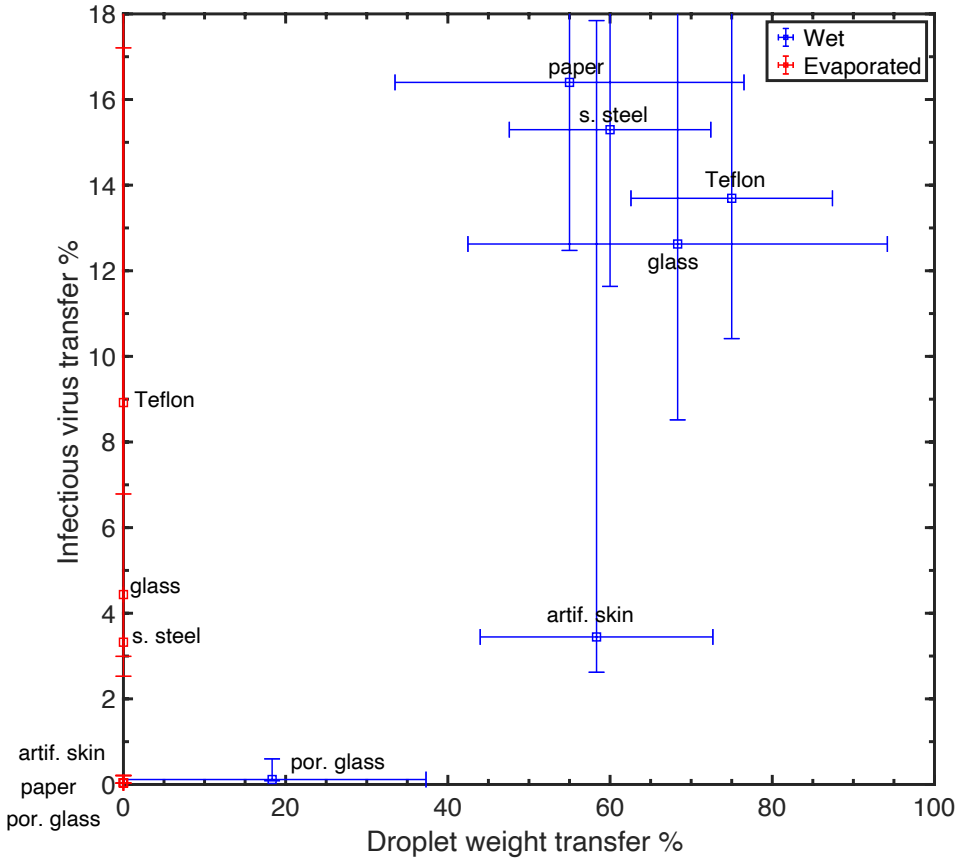
Wood (wet)		<	<	<		<	<	<
Nil (virus input control)		160669	194654.9	372663.3		5.205932	5.289265	5.571317
Material								
Glass (wet)		19465.49	109462.5	50807.98		4.289265	5.039265	4.705932
Glass (dry)		4929.173	19465.49	16066.9		3.692774	4.289265	4.205932
Porous glass (wet)		194.6549	677.5353	132.6168		2.289265	2.830932	2.122599
Porous glass (dry)		<	<	<		<	<	<
Paper (wet)		172656.1	14319.64	20227.02		5.237182	4.155932	4.305932
Paper (dry)		<	<	<		<	<	<

Supplementary Table 9-1. Measured $TCID_{50}$/mL values of the transferred virus to the skin. The "<" sign represents the titer measured was below the detection limit of the $TCID_{50}$ assay, which is at 90 $TCID_{50}$/ml. We used the value of 90 during statistical analysis, so this is an upper bound.

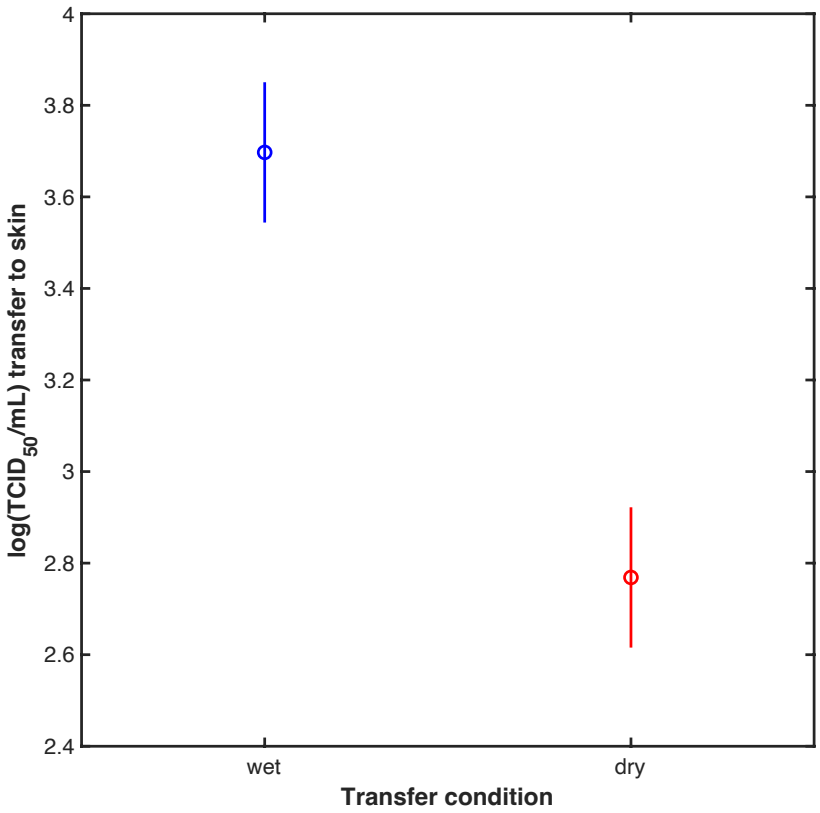
		TCID50/ml		
Nil (virus input control)		419371.2	160669	160669
Material				
Glass (wet)		5080.798	5080.798	160669
Glass (dry)		6927.034	5080.798	15587.41
Stainless steel (wet)		23582.98	23582.98	67753.53
Stainless steel (dry)		18694.83	4193.712	4929.173
Nil (virus input control)		160669	194654.9	372663.3
Material				
Glass (wet)		19465.49	109462.5	50807.98
Glass (dry)		4929.173	19465.49	16066.9

Supplementary Table 9-2. Values used for calculation of mass balance. R_{donor} for glass (wet) and glass (dry) are 0.905 and 0.307, respectively. That for stainless steel (wet) is 0.747. $R_{recipient}$ for skin (wet) and skin (dry) are 0.991 and 0.041, respectively.
The calculation were done as follow: the R's were applied to the raw TCID50 values, the values were calculated according to Supplementary Eq. 3, after which Supplementary Eq. 4 was used to do the mass balance.

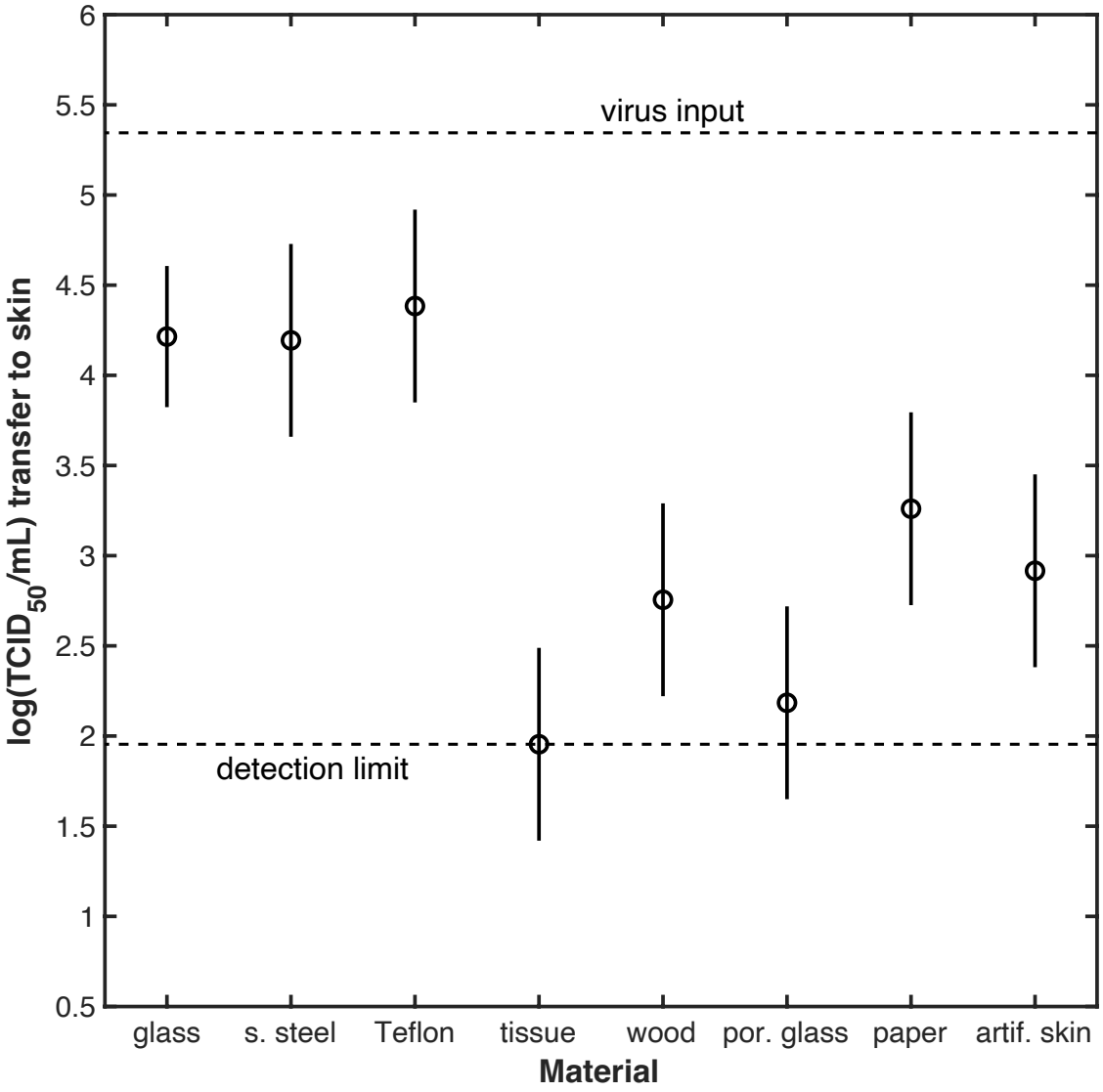
9.7.9. Additional figures



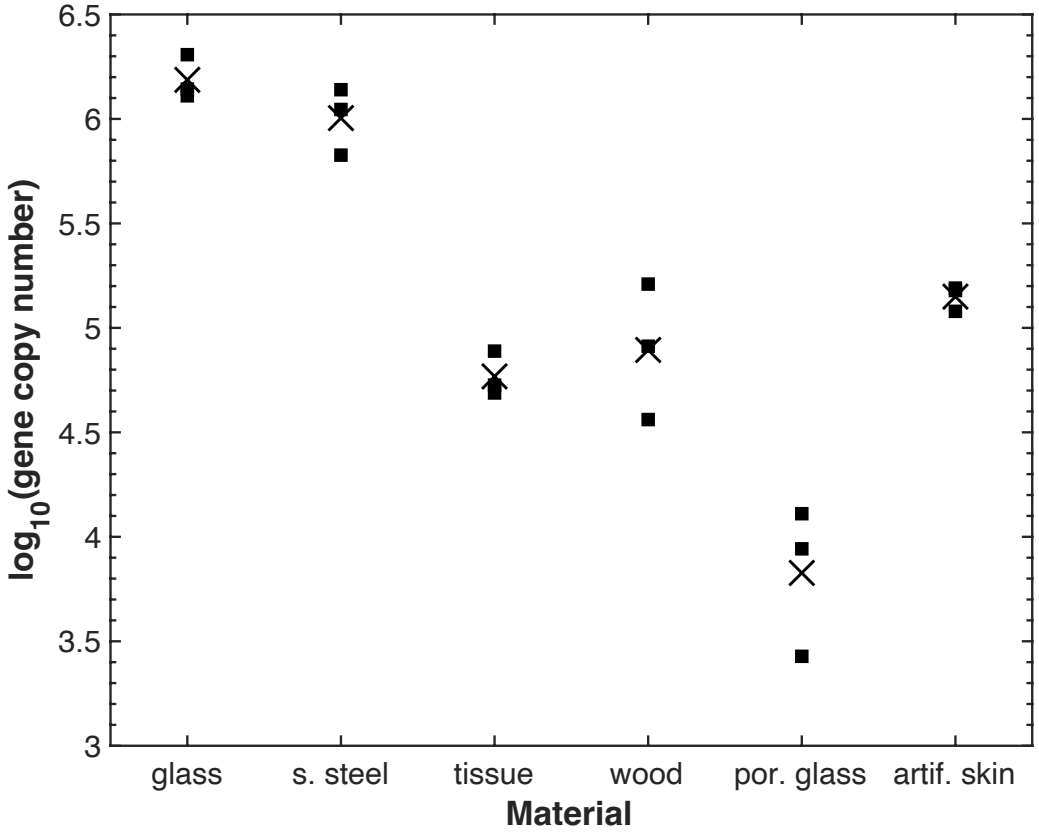
Supplementary Figure 9-7. Percentage of droplet mass transferred to a finger from artificial skin after the skin was contacted to various solids. The transfer experiment was repeated but, this time the test droplet was 2 mg of DMEM without any virus and the measurement was the mass instead of the $TCID_{50}$. This was to test whether the differences in transfer were entirely due to transfer of the liquid. Note that there is not a significant difference between the results for wet Teflon and wet glass, in spite of the large difference in receding contact angle. The very low percentage mass transferred in the dry experiments occurs because the droplet has evaporated and the mass of dissolved solid and suspended virus is minute. Clearly the wet samples transfer more virus and more water, the Pearson correlation coefficient between mass and transfer is R^2= 0.57. Considering only the wet experiments, the amount of water transferred is still not a great predictor of the virus transfer (R^2= 0.50), and the correlation is even lower if the porous glass is excluded.



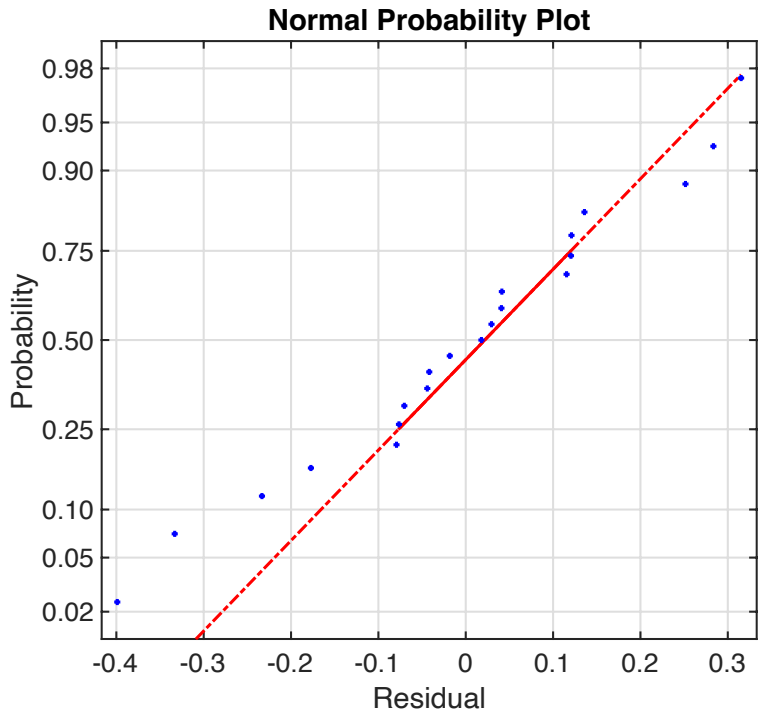
Supplementary Figure 9-8. Post Hoc comparison of log($TCID_{50}$/mL) for skin after contact when the droplet is wet and when it has evaporated (dry). More virus is transferred to skin when the droplet of virus suspension is wet.



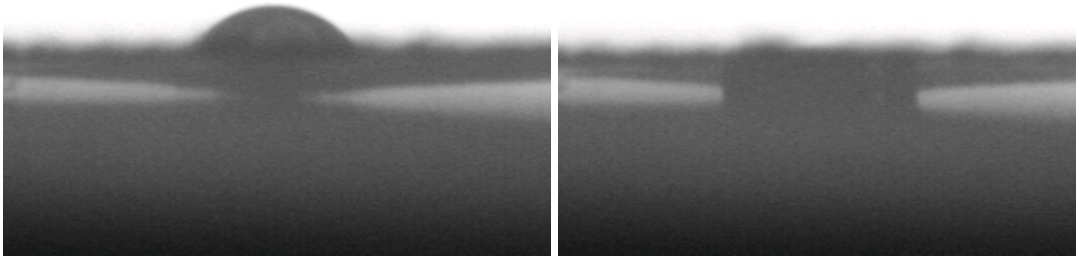
Supplementary Figure 9-9. Post Hoc comparison of log($TCID_{50}$/mL) transferred to skin after contact with different solid samples. The log($TCID_{50}$/mL) value includes results for both wet and dry conditions. The vertical bars represent comparison intervals; two groups are statistically different if their intervals do not overlap. Log($TCID_{50}$/mL) for each non-porous solid is greater than for each porous solids. We do not resolve a difference among the log($TCID_{50}$/mL) for the various impermeable solids.



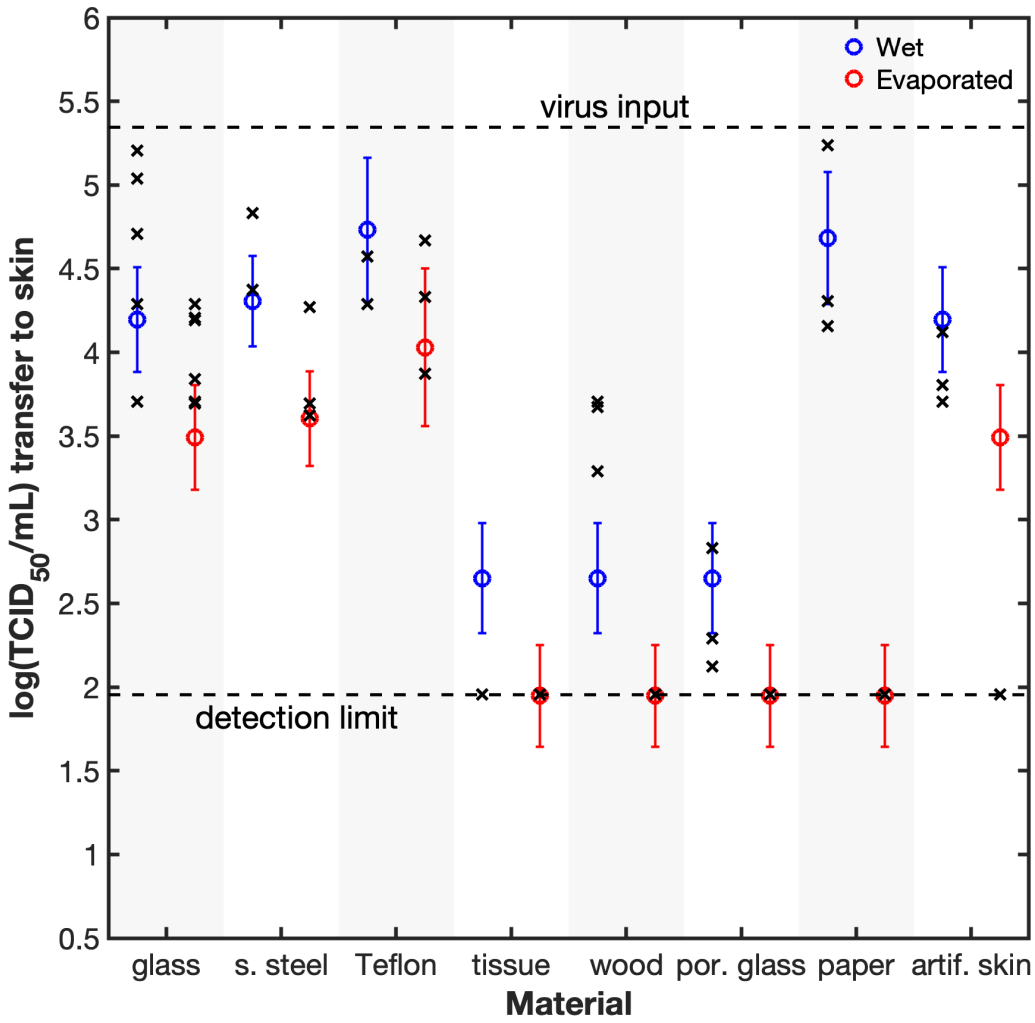
Supplementary Figure 9-10. RT-qPCR results for RNA that was eluted by liquid extraction (See 5.4.6) from various solids 30 min. after a 1 µL droplet was placed on the solid. Squares represent individual independent measurements and the X represent the mean of the log of three measurements. Supplementary Figure 9-11 explains the use of the log transformation. We know from prior work that steel and glass only slowly inactivate SARS-CoV-2[3], and the other materials do not have known active ingredients against the virus. We, therefore, interpret these results to be a test of the efficiency of liquid extraction of SARS-CoV-2. Comparing porous glass and glass, we see that it is more difficult to extract virus from a porous version of the same material. This is also generally true for other materials: recovery from all the porous solids is less than recovery of each of the non-porous solids. For the transfer experiments, "extraction" from the solid was done via solid-solid contact, which is distinct from liquid phase extraction, but the results here indicate that the virus enters the pores and therefore would not be available on the surface to be transferred.



Supplementary Figure 9-11. Normal probability plot (bottom) of residuals of qPCR data after a log10 transform. The residuals are approximately normally distributed, although deviations at large magnitude of residual are noted.



Supplementary Figure 9-12. Image of water droplet on paper sample. Freshly placed droplet (left) and after 2.5 minutes (right). The droplet initially sits on the surface, but after about 2.5 minutes it imbibes into the solid. The droplet volume is 1 μL.



Supplementary Figure 9-13. Predictive model of the transfer. Linear regression using the programming language, R, was used to make a predictive model for the $TCID_{50}$/mL, with the following factors: x = wet /dry (categorical), y = cos(advancing contact angle), and z = permeable/impermeable (categorical). Interaction terms were not found to be significant. The fitted equation was:

$$\text{Log}\,[TCID_{50}/mL] = 0.7025\,x - 0.4889\,y - 1.544\,z + 3.9808$$

And the p-values for the coefficients are 0.000113, 0.041, and 6.6×10^{-11}, respectively for wetness, contact angle and permeability, and $<10^{-6}$ for the intercept. The coefficient and p-value for contact angle were sensitive to our choice of the number to use for "undetectable". If we used 9.5 $TCID_{50}$/mL instead of 90, then the wettability coefficient became insignificant, so this coefficient may not be significant. Despite that, the model provides a good prediction of the $TCID_{50}$, as seen in the figure. One point of failure is the discrepancy for dry skin. Skin is rough so much of the virus in the dried state may be in crevices and therefore unavailable for transfer. If we were to include roughness as a factor, or broaden the concept of porosity to porosity or roughness, then clearly the model would perform better.

References

1 Chin, A. W. H. *et al.* Stability of SARS-CoV-2 in different environmental conditions. *The Lancet Microbe* **1**, e10, doi:10.1016/S2666-5247(20)30003-3 (2020).

2 Hosseini, M., Chin, A. W., Behzadinasab, S., Poon, L. L. & Ducker, W. A. Cupric oxide coating that rapidly reduces infection by SARS-CoV-2 via solids. *ACS Appl. Mater. Interfaces* **13**, 5919-5928 (2021).

3 Behzadinasab, S., Chin, A., Hosseini, M., Poon, L. & Ducker, W. A. A surface coating that rapidly inactivates SARS-CoV-2. *ACS Appl. Mater. Interfaces* **12**, 34723-34727 (2020).

4 Chan, K. *et al.* Analytical sensitivity of rapid influenza antigen detection tests for swine-origin influenza virus (H1N1). *J. Clin. Virol.* **45**, 205-207 (2009).

5 Malenovska, H. Virus quantitation by transmission electron microscopy, TCID50, and the role of timing virus harvesting: a case study of three animal viruses. *J. Virol. Methods* **191**, 136-140 (2013).

6 Reed, L. J. & Muench, H. A simple method of estimating fifty per cent endpoints. *Am. J. Epidemiol.* **27**, 493-497 (1938).

7 Chu, D. K. *et al.* Molecular diagnosis of a novel coronavirus (2019-nCoV) causing an outbreak of pneumonia. *Clin. Chem.* **66**, 549-555 (2020).

8 Flach, C. R. & Moore, D. J. Infrared and Raman imaging spectroscopy of ex vivo skin. *Int. J. Cosmet. Sci.* **35**, 125-135 (2013).

Chapter 10. The Viability of SARS-COV-2 on Solid Surfaces

Mohsen Hosseini[a], Saeed Behzadinasab[a], Zachary Benmamoun, William A. Ducker*

[a] These authors contribute equally to this article.

*Corresponding Author: William A. Ducker

Dept. of Chemical Engineering and Center for Soft Matter and Biological Physics, Virginia Tech, VA, 24061, USA

Email addresses of authors:

Saeed Behzadinasab: saeedb@vt.edu

William A. Ducker: wducker@vt.edu

Keywords: COVID-19, SARS-COV-2, Surface, Coating, Solid, Coronavirus

10.1. Abstract

The COVID-19 pandemic had a major impact on life in 2020 and 2021. One method of transmission occurs when the causative virus, SARS-CoV-2, contaminates solids. Understanding and controlling the interaction with solids is thus potentially important for limiting the spread of the disease. We review work that describes the prevalence of the virus on common objects, the longevity of the virus on solids, and surface coatings that are designed to inactivate the virus. Engineered coatings have already succeeded in producing a large reduction in viral infectivity from surfaces. We also review work describing inactivation on facemasks and clothing, and discuss probable mechanisms of inactivation of the virus at surfaces.

10.2. Introduction

Severe Acute Respiratory Coronavirus-2 (SARS-COV-2) is the virus that causes COVID-19 and has been responsible for more than 100 million cases and 2 million deaths as of February 2021 (COVID-19 Dashboard by the Center for Systems Science and Engineering (CSSE) at Johns Hopkins University (JHU), https://coronavirus.jhu.edu/map.html). SARS-CoV-2 is transmitted through infected respiratory droplets and aerosols generated by a diseased person [1, 2]. Respiratory droplets (5-10 μm) and aerosols (less than 5 μm) can be generated when a person sneezes, coughs, speaks or breathes [3]. An individual is infected by the virus through nasal or oral inhalation of the infected droplets or aerosols and then attachment of the virus to the epithelial membrane [2]. The pathway to infection is not fully understood but is thought to be via inhalation of either respiratory droplets or aerosolized virus (WHO Transmission of SARS-CoV-2: implications for infection prevention precautions, https://www.who.int/news-room/commentaries/detail/transmission-of-sars-cov-2-implications-for-infection-prevention-precautions). For this reason, health officials have advised that individuals should avoid poorly ventilated public places [4], wear a mask in public places, and increase distance between other individuals [3, 5].

The possibility of infection via solid surfaces has also been considered. In this scenario, a droplet that contains virus lands on and contaminates an inanimate object. The contaminated object is called a fomite. The next user touches the fomite, and the virus is transferred from the fomite to the user's hand. infection can occur if the person then touches their nose, mouth, eyes, or ears, (Figure 10-1). A preprint (Behzadinasab et al., medRxiv doi:

10.1101/2021.04.24.21256044) confirmed that SARS-CoV-2 can be transferred from fomites to artificial skin.

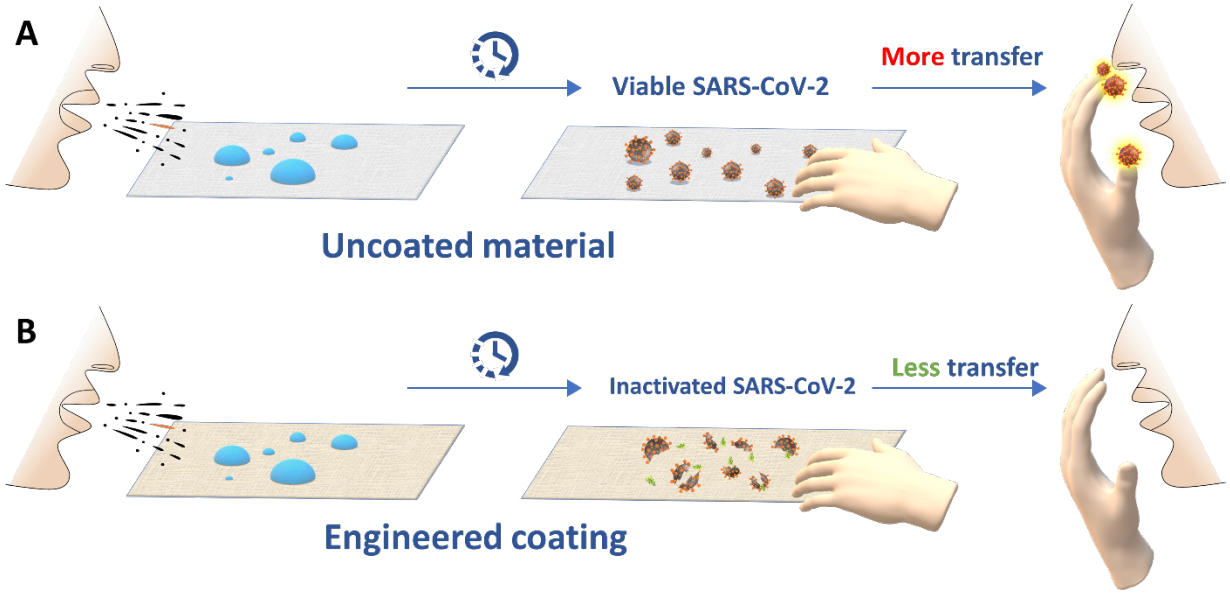


Figure 10-1. A. Infection via a fomite. B. Engineered coating to reduce infection.

A study on Golden Hamsters showed that the virus can be indirectly transmitted through fomites [6], but we are unaware of a study directly showing fomite transmission in humans. The WHO states that "fomite transmission is considered a likely mode of transmission for SARS-CoV-2" (WHO Transmission of SARS-CoV-2: implications for infection prevention precautions. https://www.who.int/news-room/commentaries/detail/transmission-of-sars-cov-2-implications-for-infection-prevention-precautions) but also notes that "People who come into contact with potentially infectious surfaces often also have close contact with the infectious person, making the distinction between respiratory droplet and fomite transmission difficult to discern" (WHO Transmission of SARS-CoV-2: implications for infection prevention precautions.

https://www.who.int/news-room/commentaries/detail/transmission-of-sars-cov-2-implications-for-infection-prevention-precautions). Modelling of outbreaks suggest that transmission via fomites may contribute up to 25% of deaths during periods of lockdown [7].

Infection via fomites depends on the longevity of SARS-CoV-2 on a solid because an infectious dose clearly must survive until following users contact the solid. The longevity of SARS-COV-2 depends on the solid material, but the virus can remain viable on some solids for up to seven days [8, 9]. According to the US Center for Disease Control (CDC), one method of reducing fomite transmission is washing of hands (CDC Cleaning and Disinfection for Household, https://www.cdc.gov/coronavirus/2019-ncov/prevent-getting-sick/cleaning-disinfection.html). Another method is the disinfection of common-touch objects such as door handles, railings, restaurant tables and keypads, using disinfectants such as 70% ethanol, bleach, or peroxide (CDC Cleaning and Disinfection for Household, https://www.cdc.gov/coronavirus/2019-ncov/prevent-getting-sick/cleaning-disinfection.html). However, these disinfectants do not provide ongoing protection from SARS-CoV-2. A thin film of ethanol evaporates rapidly at room temperature, so the solid can be contaminated again within minutes of disinfection. Thus conventional disinfection does not provide much protection on objects such as a subway handhold where cleaning may only be once per day whereas passengers may touch the handhold within minutes of each other. The labor cost of conventional disinfection is also high. Other methods can also be used to inactivate viable viruses on surfaces, including UV [10], sunlight [11] irradiation, cold plasma [12] and heat [13].

An alternative approach to disinfecting common-touch surfaces, and the main subject of this review, is surfaces that provide a continuous inactivation of the virus. By continuous, we mean that after application, the surface remains capable of inactivating the virus for at least a few

weeks. There are two timescales for such an approach: (1) the time to inactivate the virus, which should be as short as possible, preferably minutes, and (2) the longevity of the coating, which should be as long as possible, preferably months or even years. Such a surface can provide protection to users in heavily trafficked areas and preferably at a lower cost because of the lower labor cost.

An important distinction between viruses and bacteria is that viruses do not have a metabolism and cannot reproduce on their own. For this reason, many do not consider viruses to be alive. This is why one does not refer to killing viruses, but rather to inactivating them. An important consequence is that, even when there is no disinfection procedure, the virus loses activity over time, so any effort to inactivate the virus must be viewed against the natural decay of the viral population on surfaces. In this review, we compare the decay of the virus in some control situation without a deliberate disinfection of the surface to the decay on an engineered surface using the following metric:

$$\log \text{reduction} = \text{mean}\left[\log_{10}\left(\frac{\text{control titer}}{\text{sample titer}}\right)\right] \quad \text{(Equation 10-1)}$$

$$\% \text{ reduction} = \left(1 - 10^{-\log \text{reduction}}\right) \times 100\% \quad \text{(Equation 10-2)}$$

For example, the control could be an uncoated solid and the sample would be a coated solid. The ability of the virus to infect is most commonly quantified by $TCID_{50}$, which is a measure of the dilution required before a sample no longer infects cells. The most commonly used cell is a Vero cell [14, 15]. A greater value of $TCID_{50}$ (larger dilution) means that the sample of virus is more potent at infecting the cells.

A logical metric would be the ability to decrease the time required for the virus to reach some threshold level where it cannot infect mammalian cells or has some low probability of infecting cells. To date, however, the infective dose is not known, but less virus is obviously better. In the absence of a known infective dose, scientists either use their limit of detection of the virus, or a metric such as a 99.9% reduction in ability to infect. Because the range of concentrations of virus is so large, biologists usually consider the log reduction (Equation 10-1) where a 3 log reduction is the same as a 99.9% reduction.

The selection of active ingredient is an important step in preparation of surfaces that provide ongoing inactivation of SARS-CoV-2 [16]. Research to date has been guided by the reservoir of research on antiviral and other antimicrobial materials. In this connection, although the quaternary ammonium polymeric compounds [17, 18] and polyamine polymers [19] have previously shown antimicrobial activity, published work does not demonstrate a reduction in infection of SARS-CoV-2 [16, 20]. To date, copper, its compounds, and silver have shown promising antiviral activity against SARS-CoV-2 [16, 21-23] and were identified as potentially active elements.

The morphology of the surface can potentially play a role in inactivation of SARS-COV-2 [24]. Surface roughness or porosity can provide a greater surfaces area and affect wettability.

In this review article, we describe the effect of different surfaces and conditions in lowering the infectivity of SARS-CoV-2. First, we review the viability of the virus on common material surfaces and then the effect of environment conditions on the virus is assessed. A major section is devoted to the introduction of current anti-SARS-CoV-2 surfaces and coatings. Next, the current knowledge in antiviral face masks is reviewed. Finally, other methods of inactivating

SARS-CoV-2 on surfaces are discussed. There are two prior reviews of the surface stability of SARS-CoV-2 by Bueckert et al. [25] and Hasan et al. [26].

10.3. SARS-CoV-2 RNA ON PUBLIC SURFACES

RNA from SARS-CoV-2 has been found on surfaces in hospitals [27-32], laboratories [33], and public places [32, 34]. Here we summarize some of the results of sampling for viral RNA by the polymerase chain reaction technique (PCR). The result of this test does not discriminate virus that is able to infect cells from virus that has been inactivated, but simply gives the total RNA that is present. This compares to $TCID_{50}$ measurements (described above), which assay the ability of a sample to infect primate cells. Thus, the results of this section indicate that a viral component was present, not that it was able to infect humans.

Chia et al. [27] detected the SARS-CoV-2 RNA in hospital rooms where COVID-19 patients were kept (average temperature = 23 °C, relative humidity = 53–59%). Hospital surfaces were tested for SARS-CoV-2 RNA using polymerase chain reaction (PCR) techniques. The researchers tested 245 surfaces in 30 rooms. The most likely places to be contaminated were the floor (65%), followed by the air exhaust vent (60%), bed rail (59%), bedside locker (47%), cardiac table (~40%), electrical switch (~34%), chair (~34%), toilet seat and flush (~28%). Chia et al. found higher rates of contamination in the first week of illness compared to subsequent weeks.

Ong et al. [31] tested high-touch surfaces in the hospital rooms of three COVID-19 patients. The researchers tested 28 surfaces (from 26 solid types) for the SARS-CoV-2 RNA

using real-time reverse transcriptase-polymerase chain reaction (RT-PCR). Prior to cleaning, RNA was detected on 61% of the surfaces. Subsequent to cleaning with sodium dichloroisocyanurate, RNA was not detected on any surface. This showed the effectiveness of common disinfection methods. However, it is costly and time-consuming to routinely clean numerous objects. As explained in detail below, an alternative or supplemental process is to use surface coatings that can be applied to continuously inactivate SARS-CoV-2 without expensive and time-consuming cleaning routines.

Harvey et al. [34] explored the presence of virus in public places over 2 months (from April to June 2020). They checked door handles, gas pump handles, ATM keypads, garbage cans, crosswalk buttons in essential businesses (i.e., grocery stores, banks, gas stations, restaurants, laundromats, and a few more). Surfaces were samples using flocked polypropylene swabs to detect SARS-CoV-2 RNA with quantitative RT-PCR (RT-qPCR). Harvey et al. found that 8.3% of 348 tested objects had positive results, which is a large percentage for objects accessible to the public. The most contaminated surfaces were a trash can handle and a liquor store door handle. The percent of contaminated surfaces decreased when temperature increased (it has been shown that SARS-CoV-2 virus half-life shortens with increasing temperature. [35, 36]).

Fernández-de-Mera et al. [32] also reported the detection of viral RNA on high-touch items in public spaces. They investigated 14 surfaces in public sites, including pharmacies, post offices, supermarkets, a police station, a city hall, and a few more. The researchers[32] used Dry-Sponges (pre-hydrated with an isotonic surfactant and a virus-inactivating liquid) and RT-PCR to detect SARS-CoV-2 virus RNA. They reported that 21.4% (3 out of 14) of the tested surfaces had positive results.

In summary, the studies showed that there is evidence of widespread distribution of SARS-CoV-2 (where active or not) on public surfaces during the pandemic.

10.4. Pioneering studies of the Longevity of SARS-CoV-2 on Solids

Two early and seminal papers by van Doremalen et al. [8] and by Chin et al. [9] started our understanding of the stability on solids. Each of these papers showed that the infective titer depended on the material type, and that the titer decayed approximately exponentially with time. Van Doremalen et al. examined the stability on copper, cardboard, stainless steel, and plastic. From our perspective, the most important findings were that (a) the half-life of SARS-CoV-2 was strongly dependent on the material, 1 hour for copper and 7 hours on plastic, which was our basis for thinking that a material or coating could be developed to minimize the longevity of the virus and (b) that the half-life was shortest on copper, which provided a starting point for choosing an active material. From the public perspective, the idea that the virus could last for days on surfaces led to increased fear of contracting COVID-19 from surfaces and led to widespread decontamination of surfaces.

At about the same time Chin et al., examined the stability of SARS-CoV-2 on paper, tissue paper, wood, cloth, glass, a Hong Kong banknote, stainless steel, plastic, and the inner and outer layer of a facemask (as well as several disinfectants). They also found a strong dependence of the viral titer on the material type. In particular, they found that the titer was low on fibrous materials, which we shall discuss later. One particularly interesting result, which has not been widely discussed, is that the stability in suspension at 60 minutes was independent of the suspension pH in the range 3–10, a range which spans the protonation of isolated carboxylates

and the deprotonation of amines. The infectivity of the virus is not sensitive to temporary changes in the charged state of the proteins on the exterior, showing a strong resilience to denaturation.

Chin et al. also showed that the virus was less stable at greater temperature, with the viral titer barely decaying over 14 days at 4 °C and yet becoming undetectable within 5 minutes at 70 °C. Clearly temperature has a much stronger influence than pH. The dependence on temperature not only points to a means of disinfection, it also signals the need to consider environmental conditions when comparing results on different solids.

The early studies focused on viral stability on everyday objects, presumably with a view to providing immediate public health information, and not on well-characterized surfaces to enable elucidation of structure-activity relationships. Subsequently, there has been a move to study well-characterized solids to elucidation structure-activity relationships.

10.5. Effect of Environmental Conditions

Later work by Biryukov et al. [35], Matson et al. [37] and Riddell et al. [36] confirmed Chin et al.'s result showing the loss of stability at high temperature. Biryukov et al. and Matson et al. demonstrated that the virus was less stable on solids that were kept at higher humidity. The effect of humidity is a curious result. Higher humidity should hasten evaporation of the droplet and therefore hasten the large change in viral environment that occurs when the virus is dehydrated. We would have expected a higher humidity to preserve the virus, but this is clearly not observed.

Matson et al. showed that other chemical components in the droplet affected the longevity. The virus was more stable in nasal mucous than in sputum at 21°C and 27 °C. Pastorino et al. [38] evaluated the stability of the virus on addition of 10g/L bovine serum albumin (BSA). They added BSA to change the culture medium in order to mimic the protein present in the human mucus and other respiratory fluids. Although the virus was inactivated on glass and aluminum after 44 hr. and 4 hr. respectively, its stability was prolonged when moderate BSA concentration was added to the medium, to the point that the virus remained viable on all the surfaces even after 100 hours.[38] The medium was not found to be important [37] in an unpublished study by Szpiro et al (Szpiro et al., medRxiv doi: 10.1101/2020.08.22.20180042).

10.6. Stability on Common Solids

In this section, we focus on the stability of SARS-CoV-2 on common solids. Riddell et al. [36] investigated brushed stainless steel, an Australian polymer banknote, paper banknotes, glass, vinyl, and cotton cloth in the dark to eliminate the potential effect of UV inactivation. Their experiments showed that although infectivity from cotton was poor, the virus remained detectable for 28 days on other surfaces at 20 C. Conversely, this duration declined to 1 day at 40 ^{o}C. Another study [39] also verified the effect of temperature by evaluating the stability of SARS-COV-2 on swine skin, cloth (35% cotton and 65% polyester), 1 USD and 20 USD bank note at 4C, 22 C and 37 C. Harbourt et al. [39] illustrated that at 4 C, the virus remain viable on swine skin and bank notes more than 336 hours and 96 hours respectively, while this duration is reduced to 72 hours for cloth. Moreover, the virus was detected on swine skin, bank notes and clothing after 24 hours, 8 hours and 4 hours respectively at 22 C. In contrast, the stability of

SARS-COV-2 was reduced when the samples were incubated at 37 C, reducing the stability to 4 hr. for skin and bank notes, and less than four hours for clothing. Pastorino et al. [38] evaluated the stability of the virus on poly styrene, glass and aluminum with and without the addition of 10g/L bovine serum albumin (BSA). Biryukov et al. [35] did not find a significant difference in the longevity of the virus on stainless steel, acrylonitrile butadiene styrene (ABS) plastic, or a nitrile glove (NG).

Kasloff et al. [40] examined the viability of SARS-COV-2 on various porous and non-porous personal protective equipment (PPE) and found that the virus loses its infectivity (more than 3 log viral tier reduction) on stainless steel, PVC face shield, nitrile gloves, Tyvek, N95 mask and N-100 mask after 4-7 days while cotton and reinforced nitrile gloves were able to rapidly inactivate the virus, where the infectivity on them diminished after 1 hour and 4 hours respectively. However, the virus remained detectable on stainless steel, PVC face shield, N95 and N100 masks and Tyvek for 14-21 days, on nitrile gloves for 7-14 days, on reinforced nitrile gloves for 7 days and on cotton for only 24 hours. Kasloff et al. believed that the rapid loss of the virus viability on cotton is related to its porous nature, providing a large surface area to evaporate the infected droplet and causing a decrease in viable virus accordingly while maintaining the RNA level over the test period. This is in agreement with Kratzel et al. findings [41]. They observed that the infectivity of the virus is greatly reduced up to 100-fold upon drying. Riddell et al. [36] also demonstrated a rapid loss of viable virus on cotton.

Our overall summary of the work on common materials is that (1) the virus can last for a long time, as much as several weeks, (2) the recovery of virus depends on the type of material (3) there is low recovery from porous materials, and (4) recovery from metallic copper is particularly poor, suggesting that it is an active material.

10.7. Stability on Antimicrobial Coatings

The long persistence of SARS-COV-2 on surfaces and the need for frequent disinfection of common touch surfaces have given rise to the development and fabrication of anti-SARS-CoV-2 materials. The implementation of such surfaces could greatly reduce the risk of indirect transmission of the virus through surfaces. Given the recent discovery and impact of SARS-COV-2, there are only a few studies showing the design and fabrication of coatings that are active against SARS-COV-2 to date. All of the work on coatings are based on copper materials, but we also describe work on the effect of other particles in suspension.

Behzadinasab et al. evaluated the anti-SARS-COV-2 properties of cuprous oxide coated glass and stainless steel [16]. They applied a thin layer of polyurethane (PU) as the adhesive layer and then applied a 10 wt.% Cu_2O suspension in ethanol followed by a 2-hour drying at 120 °C, and then argon plasma treatment. The viral tests were done with 5 µL droplets of SARS-CoV-2 culture with a TCID of 7.8 log unit ($TCID_{50}$/mL). This coating inactivated more than 99.9% of the virus within one hour. The half-life of the virus was 3-4 minutes. The coating remained identically potent after 5 cycles of exposure to the virus and the following disinfection with 70% ethanol. Additionally, the coating still showed identical ability to inactivate SARS-CoV-2 after being kept under water for 2 weeks, which showed that this coating can endure any level of humidity in all climates. The ASTM D3359B adhesion test showed a high degree of peel resistance. This was the first published coating to specifically target SARS-CoV-2. This group also assessed the anti-SARS-COV-2 activity of polyallylamine and polydiallyldimethylammonium chloride coated on glass [16]. Though these polymers have

previously shown to have potential antimicrobial activity [19, 42, 43], they were unable [16] to inactivate the novel coronavirus.

Hutasoit et al. [22] assessed the activity of cold spray copper coatings. They coated 5–60 μm copper particles on two stainless steel plates using a Lightspee3D spray system, where a stationary nozzle deposited particles on a moving substrate at 500 °C and air pressure of 3 MPa. A post-fabrication heat treatment annealing was applied to one of the plates and then both plates were polished by a motor-driven steel brush to yield a uniform surface with 0.45 mm thickness. They applied 50 μL of SARS-COV-2 in culture medium containing $10^{5.5}$ $TCID_{50}$/mL on each surface and studied the reduction of viral titer versus time and found that the annealed and as-deposited samples are able to reduce the infectivity by 96% and 92% respectively. When the virus was left on the surface for 5 hours, the reduction increase to 99.2% and 97.9% respectively. Hutasoit et al. hypothesized that the release of Cu(I) from the surface and contact killing caused inactivation occurs through their coatings. Manto et al., in a preprint paper (Mantlo et al., medRxiv doi: 10.1101/2020.07.05.20146043), write that there is a plateau of 99% inactivation on a copper alloy between 2 and 8 h.

Hosseini et al. [44] fabricated a porous coating of CuO. The idea was to create a hydrophilic, porous surface so that suspensions of SARS-CoV-2 would be rapidly drawn into the porous interior where diffusion distances are short, there is a large surface area of active material, and the active material can be protected from abrasion. The CuO coating was produced by heat treatment of cuprous oxide particles at 700 ºC, which oxidized the particles to CuO and caused early-stage sintering to produce a robust coating without the use of a polymer . They examined this coating's potential against SARS-COV-2 by incubating a 5 μL of viral culture containing 7.8 log unit $TCID_{50}$/mL. Their experiments showed that a 30 μm coating of cupric

oxide is able to reduce the virus infectivity by 99.8% in 30 minutes and below the detection limit after one hour. When a droplet was placed on a thicker layer (about 50 μm) the droplet was completely imbibed and infectivity was reduced by 99.7% in less than one minute. At half an hour, the infectivity was below the detection limit (about 99.99%). The coating resisted peeling (ASTM D3359B test) and was unaffected by 70% ethanol or 3% bleach. Their experiments revealed that the infectivity of the virus is reduced by contact with this surface, and that the leachate (ions) does not have any antiviral activity. This group also discussed that the drying time on this coating is reduced compared to a flat surface, which probably aids in the reduction of infection of SARS-COV-2 on this CuO coating.

Hasan et al. [24] studied the anti-SARS-COV-2 property of nanostructured aluminum (Al 6063) and found that the surface roughness is another factor in the viability of the virus on surfaces. The aluminum was etched by 2 M NaOH to produce ridges that were about 23 nm wide. The etching increased the root mean squared roughness from 0.6 nm to 995 nm, and the static contact angle from 96.3° to 17.7°. Although not a coating, we have included it here as a surface modification. Nanoscale surface texturing has previously shown to improve the antimicrobial activity of surfaces [45]. The longevity of SARS-COV-2 in culture medium (10^5 $TCID_{50}$/mL) from a 10 μL droplet was compared on the roughened and the smooth surface. Their experiments demonstrated that the etched sample is able to produce a 5-log (99.999%) reduction in SARS-COV-2 on the surface in 6 hours and more than 2-log (99%) reduction in 3 hours, while this duration on control flat aluminum took 48 hours. This could be due to the adsorption or trapping the virions within the nanostructure texture [24]. They also reported that not only the roughness increased from 0.6 nm to 995 nm, but the wettability of aluminum changed when it was etched, reducing the static contact angle from 96.3° to 17.7°.

10.8. Mechanism of action against SARS-CoV-2

The literature currently lacks studies that explore mechanism of actions specifically against the SARS-CoV-2 virus. In this section, we summarize mechanisms of active ingredients against other viruses. Of course, the mechanism of action depends on both the specific microbe and the active ingredient, so the results are only a guideline for the mechanism for SARS-CoV-2. Most of the surface coatings that inactivate the SARS-CoV-2 virus are made from copper or its oxide states, so we focus copper mechanisms of action against other viruses.

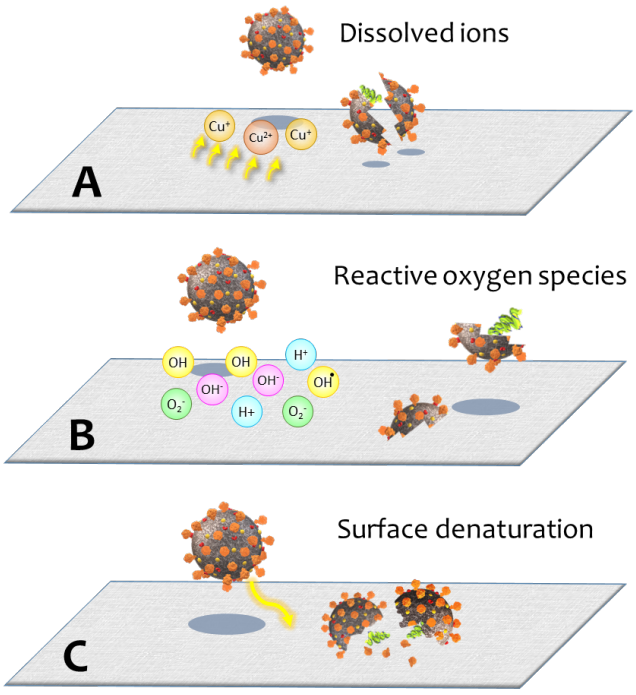


Figure 10-2. Possible mechanisms of inactivation of SARS-COV-2 on solids.

The antiviral mechanism of copper surfaces can have three potential routes: via ion release from copper solids, via generation of reactive oxygen species (ROS), and contact killing.

10.8.1. Attack of the virus by dissolved Cu(I) or Cu(II) species.

The speciation of copper in aqueous solutions that have salts and other chemicals is complex [46]. The dissolved species include the bare ions (Cu^{+} and Cu^{2+}) and potentially oxides and/or hydroxides of the copper ions. These ions can affect the virus in two ways. First, the dissolved ions affect the range of electrostatic interactions though the Debye-length or bind to charged groups and by either action alter the self-assembly of viral structures. At present it is unknown whether the copper species can permeate through SARS-COV-2 viral envelope, but if that is possible, binding to the (anionic) phosphate groups of the viral RNA is a possibility. If not, the binding will only affect the viral envelope proteins. A second effect is that the ions can participate in redox reactions, which is particularly important for copper species. Cu^{2+} is somewhat unusual for a bare metal ion in that it has a positive standard electrode potential ($Cu^{2+}_{(aq)} + 2e^{-} \rightarrow Cu_s$, E = 0.34 V and $Cu^{2+}_{(aq)} + e^{-} \rightarrow Cu^{+}_{(aq)}$, E = 0.15 V) and therefore is a mild oxidizing agent. It may be able to reduce come components in a virus. The converse is that Cu and Cu^{+} are mild reducing agents. Warnes et al. [47] explored the inactivation of murine norovirus on copper and they found release of copper ions, particularly cuprous ion (Cu^{+}), is an important factor for the virus inactivation.

10.8.2. Generation of reactive oxygen species (ROS) at the solid–liquid interface or by dissolved species

ROSs, which include the radicals, superoxide ($O_2^{-\bullet}$) and hydroxyl radicals ($^{\bullet}OH$), and hydrogen peroxide (H_2O_2), are extremely active species. They can interact with and oxidize different biomolecules of a virus, such as different proteins of SARS-CoV-2, its envelope, or the

RNA. Starting with reactions between copper ions and superoxide/hydrogen peroxide, the species undergo a series of redox reactions that lead to generation of hydroxyl radicals. Superoxide and hydrogen peroxide are produced by bacteria, but viruses do not have active metabolism to generate these. Thus, existing literature suggests that generation of ROS is not important for the inactivation of viruses. For example, Warnes et al. [47] found generation of ROS does not seem to play a role in the inactivation of norovirus by copper. Additionally, a study by Sunada et al. [48] concluded that ROS generation does not contribute to inactivation of bacteriophage viruses by Cu_2O particles.

10.8.3. Contact-killing

This mechanism is distinct from the other two in that it is dependent on the virus coming into direct contact with the solid. Here we include interaction with the electrostatic double-layer as contact killing. When the virus engages with the surface potential and also with short range intermolecular forces arising from the solid, the conditions for self-assembly change. It is well known that proteins can denature when they adsorb [49, 50], and that lipid vesicles can deposit as bilayer or monolayer structures depending on the solid interface [51], so it is reasonable that the native self-assembly of the virus could be undone by surface contact. This interaction would also depend on the surface roughness. The electrostatic interaction depends on the charges on both the solid and SARS-CoV-2. The spike protein has 10 cationic amino acids, 7 anionic amino acids and one histidine [52], giving a net charge of about + 3.5 at pH 7.4; the M protein has 8 cationic and 2 anionic amino acids, giving a net charge of +6. The envelope (E) protein has 3 of each charge [53]. Because there is a variety of both charges, the proteins could be attracted to

charges of either sign on the surface, but the preponderance of cationic groups suggests that adsorption will best on anionic solids [44]. The virus may also be disrupted by hydrophobic surfaces. Hydrophobic domains of proteins and lipid tails may assemble on hydrophobic surfaces (as is observed for vesicles) leading to loss of viral integrity.

Sunada et al. concluded that direct contact between the cuprous oxide particles and the virus was the primary method for viral inactivation [48]. This was based on experiments where the activity of suspended Cu_2O particles against bacteriophage viruses was reduced by blocking the surface with a passivating agent This experiment is difficult to interpret because surface passivation also reduces the dissolution of Cu species. Pezzotti et al. [54] have recently described work where suspensions of both silicon nitrite (Si_3N_4) and aluminum nitride (AlN) were shown to inactivate SARS-CoV-2. They hypothesize a similar method for inactivation via the reactive nitrogen species (RNS), ammonia, generated as the surface of the particles. The mechanism of contact killing is yet to be fully understood [55].

In addition to inactivation, there are other effects which may lead to reduced infectivity of a sample:

10.8.4. Adsorption

The assays that assess viral inactivation by solids have two stages: recovery of the virus from the solid, and an assay of the activity of the virus on cells. If the virus is not recovered from the solid, whether or not it is active, then the assay will not register activity. Irreversible adsorption (trapping) will therefore reduce the infectivity of a viral suspension, whether or not

the virion is still intact. Trapping of virus not only affects the assays, it also has an effect of the ability of a surface to infect individuals. In contrast to bacteria, which can live and reproduce on solids, viruses cannot reproduce on their own and undergo a natural decay of activity with time. It is enough to trap them, even if they are intact. This adsorption will be affected by intermolecular and surface forces that were described above.

10.8.5. Surface Wettability

Serval studies have suggested that a hydrophilic surface facilitates the inactivation by providing a higher contact area between the infected droplet and the active surface and maximize the use of antiviral surface [16, 24, 44]. In this connection, porous hydrophilic surfaces can act as the extreme for maximizing the contact between the surface and the droplet. Several studies have shown the correlation between porosity and efficacy for inactivating SARS-COV-2 inactivation time [36, 40, 41, 44], which might be either through the contact killing or capturing the virus within the porosity. Hosseini et al. [44] recently developed and tested a porous CuO that may operate partially on the trapping mechanism.

10.8.6. Drying of the respiratory droplet in contact with the solid

The inactivation of the virus increases with time and with the temperature of the contaminated droplet on an active surface [36] (Figure 10-3). All of the mechanisms discussed would be enhanced if the droplet size were reduced, thereby more quickly bringing the virus into contact with the active ingredient and so the drying of the droplet is likely to be important and

beneficial. An increase in wettability through roughening a surface may also help to spread the droplet on the surface to a higher extent. This will accelerate the evaporation and reduce transport distances and hasten virus inactivation accordingly.

An extreme version of roughening is to create a porous coating to accelerate the drying time by infiltrating the liquid as well as spreading it on the surface to have a more area for evaporation [44, 56]. The phenomenon by which a droplet spreads into a porous medium through capillary forces is called imbibition [57]. This phenomenon depends on the size, contact angle, geometry, tortuosity, and thickness of the pores [58-60] and drying is faster when the porous media has a broad pore size distribution [61].

So porous surfaces have a number of advantages: more surface area for an active ingredient, shorter diffusion times, greater adsorption area and faster drying time [44]. It may not even be necessary to have an active ingredient on a porous surface; if the virus is trapped in the pores, and preferably dried on to the interior space, it will become inactivated with time and is not in a position to infect another person.

An additional action of the drying action is that drying will lead to the air-water interface passing over adsorbed virions. At this time, the interfacial tension may damage adsorbed virus.

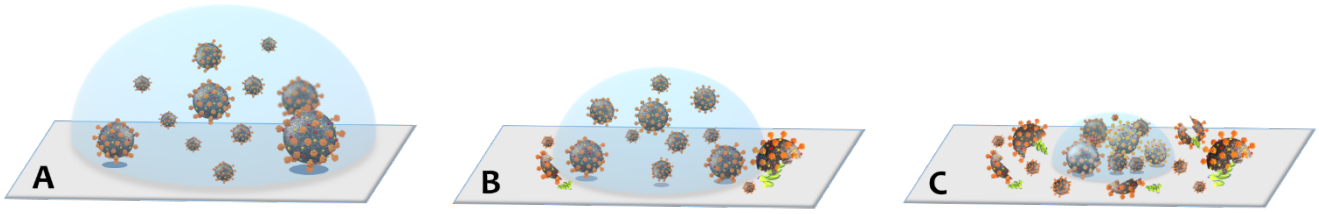


Figure 10-3. The effect of droplet drying on the surface. The concentration of dissolved species increases, and diffusion times get shorter. Passage of the air-liquid interface subjects adsorbed virus to a tension that may damage the virus.

10.9. INACTIVATION OF THE SARS-COV-2 VIRUS IN SUSPENSIONS

In addition to the inactivation of SARS-CoV-2 on surface coatings, there has been interest in inactivation of virus in suspensions. Jeremiah et al. [23] examined the effect of silver nanoparticles (AgNPs) on inactivation of SARS-CoV-2. The authors noted that silver cytotoxicity (i.e., toxic effects on cells rather than virus) only occurred if the nanoparticle concentration was above a threshold of 20 ppm, so their experiments were conducted at 2 ppm. They performed 3 experiments: (a) mixing virus suspension with AgNPs (for 1 hour at 37C), (b) infecting cells with the virus and later incubation with 10 nm polyvinylpyrrolidone (PVP)-coated AgNPs (48 hours at 37C), or (c) incubation of 10 nm PVP coated AgNPs in cells (3 hours at 37C) and later infection with SARS-CoV-2. The first two experiments showed complete inhibition of virus while the third showed less inactivation of the virus. Thus, the researchers note that silver has very strong anti-SARS-CoV-2 properties.

In a preprint, Ornstein et al. (Ornstein et al., medRxiv doi: 10.1101/2020.10.01.20204214) provided a preliminary study of the anti-SARS-CoV-2 effect of

metal organic frameworks (MOFs). They tested microporous crystalline titanium dicarboxylate MIL-125(Ti)-NH_2 MOF nanoparticles with 100 µL of $1x10^5$ TCID50/mL SARS-CoV-2 culture. Based on the details of their method, we calculated the concentration of MOF nanoparticles to be ~50 w/w% in the viral culture. After mixing the nanoparticles with the virus liquid, the researchers exposed UV-C light on the liquid for 30 minutes. Additionally, they tested a MIL-127(Fe) MOF with the same method and found that both MOFs have anti-SARS-CoV-2 activities. The authors did not provide statistical evaluation and noted that the results cannot be separated from the effect of UV-C alone. UV-C can be harmful to humans, thus the researchers tested two MOFs (MIL-125(Ti)-NH_2 and MIL-177-HT) with the virus and exposed them to room light for 30 minutes. They reported MIL-177-HT inactivated 50% of the SARS-CoV-2, while MIL-125(Ti)-NH_2 didn't show anti-SARS-CoV-2 effect.

Pezzotti et al. [54] measured the activity of silicon nitride (Si_3N_4), copper (Cu), and aluminum nitride (AlN) microparticles (average size = ~0.5-2 µm) in vivo. They added 15 w/w% of each powder to PBS, in addition to adding SARS-CoV-2 suspension that contained $2x10^5$ $TCID_{50}$. After slow rotation of the two suspensions for 1 or 10 min, the microparticles were separated by centrifugation and filtration with 0.2 µL filter. Subsequently, the supernatant was used to determine the inactivation of the virus by $TCID_{50}$ method. The authors reported 100% viral reduction with only 1 min of virus exposure to either Si_3N_4, Cu, or AlN.

A related pre-print by Lehman et al. (Lehman et al., bioRxiv: 10.1101/2020.08.29.271015) also reported that in vivo Si_3N_4 can inactivate the virus. The researchers incubated similar-size particles of Si_3N_4 to Pezzotti et al.'s study [54] with a viral culture that contained $2x10^4$ PFU/mL. They employed Si_3N_4 concentration from 5 up to 20 w/v%. To provide contact between the virus and active particles, the suspension was vortexed for

30 sec, followed by slow rotation using a tube revolver from 1 to 10 minutes. The results depended on both concentration and incubation duration, as one might expect: with 1 minute incubation, the virus was reduced 85% and 98% when using 5% Si_3N_4 and 20% Si_3N_4, respectively. Longer incubation periods led to increased inactivation of the virus. The authors showed that ~91% and 99.6% reduction of SARA-CoV-2 can be achieved when 5% Si_3N_4 and 20% Si_3N_4 are utilized, respectively.

10.10. Other Methods for Inactivating SARS-CoV-2 at Surfaces

SARS-CoV-2 can be inactivated by other methods, such as light-activated coatings[62], ultraviolet (UV) light [63-65], atmospheric cold plasma [12], heat treatment [66], and ozone [67].

Micochova et al. [62] evaluated the efficacy of TiO_2 and TiO_2-Ag coatings on lowering the infectivity of SARS-CoV-2 while a surface is illuminated with light. They described that radicals are initiated by photons on the TiO_2 surface, and that these radicals inactivate the virus. A spray gun was used to coat TiO_2 or TiO_2-Ag on ceramic tiles. Micochova et al. showed that the percentage of the infected SARS-CoV-2 after one hour was only 15% on the illuminated coating compared to 80% on polystyrene. They also reported that the introduction of silver into their coatings did not improve the antiviral activity.

Inagaki et al. [64] reported a dramatic reduction in SARS-CoV-2 viability by utilizing a deep UV-emitting diode (DUV-LED) with a wavelength of 280 ± 5 nm. They placed 150 µL of 2 x 10^4 PFU/mL virus stock on a petri dish (the material was not described) and irradiated it for

various times (intensity of 3.75 mW/cm^2 from a 2 cm height). This resulted in 87.4% (1s), 99.9%, (10s) and >99.9% (20 s) reduction in infection titer of SARS-CoV-2 compared to control (i.e., no UV irradiation). These results are impressive, however, the UV wavelength that the researchers used is on the boundary of UV-C region (UV-C wavelength = 100-280 nm) and UV-C light is known to be harmful to humans. This may limit application to situations where humans are not present or protected by shielding. Additionally, Inagaki et al. used a low concentration of virus (only 2 x 10^4 PFU/mL), however, in the publication by Heilingloh et al. [63] a 5 x 10^6 TCID50/mL viral stock was employed.

Heilingloh et al. [63] compared the ability of UV-A vs UV-C lights for the inactivation of SARS-CoV-2. UV-A has a wavelength of 320-400 nm while UV-C wavelength is between 100-280 nm. The researchers added 600 µL of 5 x 10^6 TCID50/mL virus stock (i.e., much more concentration than Inagaki et al.) in well plates and fixed the UV lamp at a distance of 3 cm (UV-C and UV-A intensities of 1940 and 540 mW/cm^2, respectively). UV-C irradiation resulted in complete inactivation of virus in 9 minutes while UV-A light was much less impactful. The authors noted that the required UV dose for complete inactivation of virus is 1048 mJ/cm^2. Additionally, they investigated the effect of combined UV-A and UV-C light combined, and as one might expect, by this method SARS-CoV-2 was inactivated the fastest. This resulted in 100% reduction in virus viability within 3 minutes.

Chen et al. [12] reported that cold atmospheric plasma can rapidly inactivate SARS-CoV-2 on solids. They used argon plasma (flow rate: 6.4 L/min, distance from surface: 15 mm, discharge voltage of 16.8-16.6 kV (peak-peak) at 12.9 kHz frequency) and achieved complete inactivation of virus in less than 180 seconds. The surfaces they tested were plastic, metal, cardboard, a football, a basketball, and a baseball. The researchers did not specify which type of

plastic, metal, cardboard etc. they used. Chen et al. also investigated similar goal using helium-fed argon with a flow rate of 16.5 L/min (distance from surface: 15 mm, discharge voltage of 16.8-16.6 kV (peak-peak) at 12.7 kHz frequency) and found that it is much less effective for inactivation of SARS-CoV-2. They were not able to reach complete inactivation of the virus in 5 minutes on plastic or metal. The researchers noted the surface that was Ar-plasma treated reached a high of 32 °C, while that of He-plasma reached 29 °C. The results by Chen et al. [12] are significant.

Thermal treatment is also highly effective. For example, Daeschler et al. [66] used heat to disinfect PPEs (personal protective equipment). They used high temperature to inactivate SARS-CoV-2 virus on 4 models of commercial N95 masks. The researchers incubated 5 µL of 7.8 Log units $TCID_{50}$/mL virus stock on both unprocessed and 10 times heat processed N95 masks and found that thermal treatment at 70C and 0% relative humidity for 60 minutes disinfects the masks from SARS-CoV-2. Daeschler et al. [66] also tested the properties of the mask after the disinfection treatments and reported no impact of the heat treatment on the mask. Thus, heat treatment, which is a low cost and simple method, for disinfecting surfaces, but compared to a coating, it requires active intervention and power.

10.11. Facemasks and Clothing

Facemasks are another area where ingredients have been added to inactivate SARS-CoV-2. This research has much in common with antiviral surface coatings, but in this case, the active ingredient is incorporated into a fabric. A normal facemask has two main tasks: to reduce the density of respiratory droplets transmitted from the person wearing the mask, and to reduce the

density of other people's respiratory droplets that are inhaled by the wearer. The former is the main goal of hand-made and basic surgical masks that are being worn during the COVID-19 pandemic. Masks worn to protect others should mainly contain microbes that already infect the user and can be handled by the user but not others. Masks that are worn to protect the user are more problematic because they may infect the user during handling. Particularly in this case, it would be useful to have mask materials with an active material that continuously inactivates SARS-CoV-2. An additional hazard for mask-wearers is that bacteria, unlike viruses, can colonize and reproduce on masks, and therefore bacterial numbers from the environment and the user can increase with time.

There exist two broad methods of designing self-cleaning textiles. One is by hydrophobizing a surface so that droplets have weak adhesion and roll off at a low tilt angle. This is aided by the fact that many surfaces are worn in near vertical orientation. The other approach is to modify the fabric to incorporate biocidal properties. Both approaches will be discussed. A key element of textiles is that they usually consist of fibers, which are essentially porous materials. If hydrophilic, the textiles can imbibe droplets of viral suspension.

Examples of poorly-wetting fabrics were in existence before the COVID-19 pandemic and include the work of Chauhan et al. who designed a superhydrophobic cotton textile that displayed antibacterial properties [68]. Galante et al. [69] designed a hydrophobic coating on nonwoven polypropylene textile that displayed reduced infection by two nonenveloped virions. This technology could be applied to the exterior of masks or other PPE to reduce the imbibition of droplets containing viral suspension.

Biocidal fabrics can be created by coating or impregnating fabric with a biocide such as copper, silver, or zinc particles. Again, these fabrics were studied before the COVID-19 pandemic. For example, in 2010, Borkow et al. designed an antiviral face mask by impregnating N95 face masks with copper oxide particles [70]. This mask was able to inactivate influenza A within 30 minutes, and maintained its filtration properties even after impregnation. During 2020, researchers have specifically targeted SARS-CoV-2. Hewawaduge et al. [71] designed 3-layer 70 Denier (D) nylon, 75 D polyester, and 20 D spandex facemasks impregnated with copper sulfide that inactivate SARS-CoV-2 within 30 minutes. Additionally, the masks were fabricated to maximize particle entrapment. Kumar et al. designed a facemask that was spray-coated with copper nanoparticles, and shellac – a hydrophobic biopolymer – that inactivated virus-like particles (VLP) that were sprayed on the mask [72]. Copper is a known biocide, but here the photocatalytic properties were examined as well, with the mask showing better antibacterial properties when exposed to sunlight. Marti et al. [73] designed coated face mask filters from non-woven spunlace fabric filters that were dip coated with benzalkonium chloride that inactivated 99% of deposited SARS-CoV-2 particles within one minute. As well as inactivating SARS-CoV-2, the coated masks also inactivated methicillin-resistant Staphylococcus aureus (MRSA) and Staphylococcus epidermidis (MRSE), both very contagious and hazardous. In a preprint, Zinn et al. (Zinn et al., bioRxiv doi: 10.1101/384040) designed cellulose/polyester fabrics coated with a copper-based metallic gel called “ActiveCopper” (aCu). They showed that aCu inactivated 99.9% of deposited SARS-CoV-2 virus within 30 seconds. aCu also inactivated a wide range of microbes, and was shown to be very robust, displaying no change in antimicrobial capability even after 14 days of repeated use. In a preprint, Tremiliosi et al. (Tremiliosi et al., bioRxiv doi: 10.1101/152520) designed polyester/cotton fabrics impregnated

with silver nanoparticles using a pad-dry-cure method that inactivated 99.99% of deposited SARS-CoV-2 virus after 2 minutes. The treated fibers also showed no irritating, photoirritating, or photosensitizing responses when applied, and can be considered hypoallergenic, which is very important for a textile. In another preprint, De Maio et al. (De Maio et al., medRxiv doi: 10.1101/2020.09.16.20194316) attached graphene (G) and graphene oxide (GO) into cotton and non-woven polyurethane, although the method of attachment was not described. The authors report that these functionalized materials were able to significantly increase the percentage of viable VERO cells within two hours on incubation. They also showed that their materials cause a 0.5-log reduction in the number of Escherichia coli (E. coli) after two hours and found that neither G nor GO demonstrate any cytotoxicity effect against A549 pulmonary tumor cells. In another preprint, Gopal et al. (Gopal et al., bioRxiv doi: 10.1101/365833) showed that polyamide 6.6 fibers embedded with zinc oxide during the polymerization process inactivated SARS-CoV-2 within 30 minutes. Additionally, the biocidal ability of the fabrics remained after 50 washes using a standardized home laundry test protocol.

These modified textiles have been shown the ability to be very robust, long lasting, breathable, and capable of inactivating a wide array of microbes very quickly. Since users inhale though the mask, a key element of these active masks will be showing the lack of toxicity of the active material.

10.12. Future Perspectives

10.12.1. Characterization of Surfaces

A large fraction of stability studies of SARS-CoV-2 to date have been on common substances like paper and steel. These previously conducted studies are undoubtedly valuable sources of information, but we suggest that future studies should contain a thorough description and characterization of the test solids. The inclusion of such information would help to understand the mechanism. At minimum, the exact source of the test surface and the cleaning procedure should be specified.

The surface chemistry can be measured by surface-selective techniques such as X-ray photoelectron spectroscopy (XPS) and energy-dispersive X-ray spectroscopy (EDX) and Fourier-transform infrared spectroscopy (FTIR), which are widely available in collaborative efforts or in service centers. Surface morphology studies can be carried out through scanning electron microscopy (SEM), optical microscopy, and atomic force microscope (AFM). The shape and size of particles and porous nature of the samples can be revealed by studying of surface topology. If the solid is porous, Brunauer–Emmett–Teller (BET) analysis can specify the surface area associated with the porosity.

The contact angle measurements also provide useful information on the wettability of the droplet on the surface. One complication here is that a natural viral suspension produced by an infected individual may contain many different ingredients depending on its source, and that these ingredients may affect the wettability. Surface characterization in future studies will enable discovery of the correlation between surface properties and inactivation and help to determine

the mechanism. It will lead the way to the design of optimal surfaces to reduce the half-life of the virus on the solid.

10.12.2. Porosity

In general, porosity is very important for future coatings because it (1) can trap the virus, (2) allows for a greater area of active ingredient, and (3) the internal structure is protected by the overlying structure from damage by abrasion, and (4) diffusion distances between the active ingredient and the virus can be made very small with small pore sizes. Several papers have noted the correlation between effectiveness and porosity. At this point only one, by Hosseini et al. , has shown that an increased pore volume of CuO led to a decrease in the viral titer of SARS-COV-2 [44].

10.12.3. Active ingredients

To date, active ingredients have been based mainly on prior work on other viruses. There have been no specific active ingredients that have been targeting specifically at SARS-CoV-2. Given the efforts to find drugs that target specific portions of SARS-COV-2, we may expect that some of these will be incorporated into future surface coatings.

10.12.4. Multiple Organisms.

The deployment of vaccines the COVID-19 pandemic will, hopefully, mean that SARS-CoV-2 will have less impact on life beyond 2021. But the lessons learned from coatings can still

be applied to other organisms, such as bacteria, fungi, and other viruses. We expect that multi-microbe coatings will continue to be fruitful areas of research following public sensitivity to microbial diseases.

10.12.5. Transfer from Surfaces to Humans

To date, the focus has been on surfaces that inactivate SARS-CoV-2, but to cause infection, the virus must be transferred to the respiratory tract. To reach the respiratory tract, there needs to be contact transfer from the solid to hands and from hands to the face. Transfer of virus through this chain of contacts is an interesting future area of research.

10.12.6. The mechanism of the inactivation of SARS-CoV-2

Studies of the mechanism of action of new antiviral materials should provide valuable insight into the selection of new antimicrobial agents and the design and fabrication of improved antimicrobial surfaces.

10.13. SUMMARY

SARS-CoV-2 has been found on many public surfaces during the pandemic and the lifetime of infective virus on solids is as long as a week under laboratory conditions. To diminish the window of opportunity for infection from surfaces, several researchers, including those from

our group have sought to prepare coatings that rapidly inactivate SARS-CoV-2. Such surfaces are already capable of causing a 99.9% reduction in 1 hour [16] or cause almost immediate loss of infectivity through adsorption into porous coatings [44].

Acknowledgments

This work was supported by the National Science Foundation under Grant No. CBET-1902364.

Competing interests

WD declares part ownership in a startup company to produce surface coatings.

REFERENCES

[1] Lai C-C, Shih T-P, Ko W-C, Tang H-J, Hsueh P-R: Severe acute respiratory syndrome coronavirus 2 (SARS-CoV-2) and coronavirus disease-2019 (COVID-19): The epidemic and the challenges. International journal of antimicrobial agents 2020, 55:105924.

[2] Cevik M, Kuppalli K, Kindrachuk J, Peiris M: Virology, transmission, and pathogenesis of SARS-CoV-2. bmj 2020, 371:m3862.

[3] Prather KA, Wang CC, Schooley RT: Reducing transmission of SARS-CoV-2. Science 2020, 368:1422-1424.

[4] Somsen GA, van Rijn C, Kooij S, Bem RA, Bonn D: Small droplet aerosols in poorly ventilated spaces and SARS-CoV-2 transmission. The Lancet Respiratory Medicine 2020, 8:658-659.

[5] Wang Q, Yu C: The role of masks and respirator protection against SARS-CoV-2. Infection Control & Hospital Epidemiology 2020, 41:746-747.

**[6] Sia SF, Yan L-M, Chin AW, Fung K, Choy K-T, Wong AY, Kaewpreedee P, Perera RA, Poon LL, Nicholls JM: Pathogenesis and transmission of SARS-CoV-2 in golden hamsters. Nature 2020, 583:834-838.

Demonstrated transmission via fomites

**[7] Meiksin A: Dynamics of COVID-19 transmission including indirect transmission mechanisms: a mathematical analysis. Epidemiology & Infection 2020, 148:E257.

Modelling to show the importance of transmission via fomites

**[8] Van Doremalen N, Bushmaker T, Morris DH, Holbrook MG, Gamble A, Williamson BN, Tamin A, Harcourt JL, Thornburg NJ, Gerber SI: Aerosol and surface stability of SARS-CoV-2 as compared with SARS-CoV-1. New England Journal of Medicine 2020, 382:1564-1567.

One of the first two papers to show the longevity of SARS-CoV-2 on fomites

**[9] Chin A, Chu J, Perera M, Hui K, Yen H-L, Chan M, Peiris M, Poon L: Stability of SARS-CoV-2 in Different Environmental Conditions. Lancet Microbe 2020, 1:e10.

One of the first two papers to show the longevity of SARS-CoV-2 on fomite

[10] Hadi J, Dunowska M, Wu S, Brightwell G: Control Measures for SARS-CoV-2: A Review on Light-Based Inactivation of Single-Stranded RNA Viruses. Pathogens 2020, 9:737.

[11] Ratnesar-Shumate S, Williams G, Green B, Krause M, Holland B, Wood S, Bohannon J, Boydston J, Freeburger D, Hooper I: Simulated sunlight rapidly inactivates SARS-CoV-2 on surfaces. The Journal of infectious diseases 2020, 222:214-222.

[12] Chen Z, Garcia Jr G, Arumugaswami V, Wirz RE: Cold atmospheric plasma for SARS-CoV-2 inactivation. Physics of Fluids 2020, 32:111702.

[13] Abraham JP, Plourde BD, Cheng L: Using heat to kill SARS-CoV-2. Reviews in Medical Virology 2020, 30:e2115.

[14] Malenovska H: Virus quantitation by transmission electron microscopy, TCID50, and the role of timing virus harvesting: A case study of three animal viruses. J Virol Methods 2013, 191:136-140.

[15] Chan K, Lai S, Poon L, Guan Y, Yuen K, Peiris J: Analytical sensitivity of rapid influenza antigen detection tests for swine-origin influenza virus (H1N1). J Clin Virol 2009, 45:205-207.

**[16] Behzadinasab S, Chin A, Hosseini M, Poon LL, Ducker WA: A Surface Coating that Rapidly Inactivates SARS-CoV-2. ACS applied materials & interfaces 2020, 12:34723–34727.

FIrst paper to demonstrate a coating that inactivates SARS-CoV-2

[17] Gottenbos B, van der Mei HC, Klatter F, Nieuwenhuis P, Busscher HJ: In vitro and in vivo antimicrobial activity of covalently coupled quaternary ammonium silane coatings on silicone rubber. Biomaterials 2002, 23:1417-1423.

[18] Isquith A, Abbott E, Walters P: Surface-bonded antimicrobial activity of an organosilicon quaternary ammonium chloride. Applied microbiology 1972, 24:859-863.

[19] Iarikov DD, Kargar M, Sahari A, Russel L, Gause KT, Behkam B, Ducker WA: Antimicrobial surfaces using covalently bound polyallylamine. Biomacromolecules 2014, 15:169-176.

[20] Monge FA, Jagadesan P, Bondu V, Donabedian PL, Ista L, Chi EY, Schanze KS, Whitten DG, Kell AM: Highly Effective Inactivation of SARS-CoV-2 by Conjugated Polymers and Oligomers. ACS applied materials & interfaces 2020, 12:55688–55695.

*[21] Sousa BC, Cote DL: Antimicrobial Copper Cold Spray Coatings and SARS-CoV-2 Surface Inactivation. MRS advances 2020, 5:2873-2880.

A coating that inactivates SARS-CoV-2

*[22] Hutasoit N, Kennedy B, Hamilton S, Luttick A, Rashid RAR, Palanisamy S: Sars-CoV-2 (COVID-19) inactivation capability of copper-coated touch surface fabricated by cold-spray technology. Manufacturing Letters 2020, 25:93-97.

A coating that inactivates SARS-CoV-2

*[23] Jeremiah SS, Miyakawa K, Morita T, Yamaoka Y, Ryo A: Potent antiviral effect of silver nanoparticles on SARS-CoV-2. Biochemical and biophysical research communications 2020, 533:195-200.

Shows effect of particles on SARS-CoV-2

**[24] Hasan J, Pyke A, Nair N, Yarlagadda T, Will G, Spann K, Yarlagadda PK: Antiviral Nanostructured Surfaces Reduce the Viability of SARS-CoV-2. ACS Biomaterials Science & Engineering 2020, 6:4858-4861.

Shows effect of surface structure on inactivating SARS-CoV-2

**[25] Bueckert M, Gupta R, Gupta A, Garg M, Mazumder A: Infectivity of SARS-CoV-2 and Other Coronaviruses on Dry Surfaces: Potential for Indirect Transmission. Materials 2020, 13:5211.

A useful review.

[26] Hasan MA, Carmel Mary Esther A, Dey A, Mukhopadhyay AK: A review on coronavirus survivability on material's surfaces: present research scenarios, technologies and future directions. Surface Engineering 2020, 36:1226-1239.

*[27] Chia PY, Coleman KK, Tan YK, Ong SWX, Gum M, Lau SK, Lim XF, Lim AS, Sutjipto S, Lee PH: Detection of air and surface contamination by SARS-CoV-2 in hospital rooms of infected patients. Nature communications 2020, 11:1-7.

Shows the existence of SARS-CoV-2 RNA in the human environment

*[28] Razzini K, Castrica M, Menchetti L, Maggi L, Negroni L, Orfeo NV, Pizzoccheri A, Stocco M, Muttini S, Balzaretti CM: SARS-CoV-2 RNA detection in the air and on surfaces in the COVID-19 ward of a hospital in Milan, Italy. Science of The Total Environment 2020, 742:140540.

Shows the existence of SARS-CoV-2 RNA in the human environment

[29] Dargahi A, Jeddi F, Vosoughi M, Karami C, Hadisi A, Mokhtarie SA, Alighadri M, Haghighi SB, Sadeghi H: Investigation of SARS CoV-2 virus in environmental surface. Environmental Research 2021:110765.

[30] Zhou J, Otter JA, Price JR, Cimpeanu C, Garcia DM, Kinross J, Boshier PR, Mason S, Bolt F, Holmes AH: Investigating SARS-CoV-2 surface and air contamination in an acute healthcare setting during the peak of the COVID-19 pandemic in London. Clinical Infectious Diseases 2020:ciaa905.

[31] Ong SWX, Tan YK, Chia PY, Lee TH, Ng OT, Wong MSY, Marimuthu K: Air, surface environmental, and personal protective equipment contamination by severe acute respiratory syndrome coronavirus 2 (SARS-CoV-2) from a symptomatic patient. Jama 2020, 323:1610-1612.

[32] Fernández-de-Mera IG, Rodríguez del-Río FJ, de la Fuente J, Pérez-Sancho M, Hervás D, Moreno I, Domínguez M, Domínguez L, Gortázar C: Detection of environmental SARS-CoV-2 RNA in a high prevalence setting in Spain. Transboundary and Emerging Diseases 2020, 00:1-6.

[33] Lv J, Yang J, Xue J, Zhu P, Liu L, Li S: Detection of SARS-CoV-2 RNA residue on object surfaces in nucleic acid testing laboratory using droplet digital PCR. Science of The Total Environment 2020, 742:140370.

*[34] Harvey AP, Fuhrmeister ER, Cantrell ME, Pitol AK, Swarthout JM, Powers JE, Nadimpalli ML, Julian TR, Pickering AJ: Longitudinal monitoring of SARS-CoV-2 RNA on high-touch surfaces in a community setting. Environmental Science & Technology Letters 2020, 8:168–175.

Shows the existence of SARS-CoV-2 RNA in the human environment

*[35] Biryukov J, Boydston JA, Dunning RA, Yeager JJ, Wood S, Reese AL, Ferris A, Miller D, Weaver W, Zeitouni NE: Increasing temperature and relative humidity accelerates inactivation of SARS-CoV-2 on surfaces. MSphere 2020, 5:e00441-00420.

Shows effect of environmental conditions on the longevity of SARS-CoV-2 on surfaces

*[36] Riddell S, Goldie S, Hill A, Eagles D, Drew TW: The effect of temperature on persistence of SARS-CoV-2 on common surfaces. Virology journal 2020, 17:1-7.

Shows effect of environmental conditions on the longevity of SARS-CoV-2 on surfaces

*[37] Matson MJ, Yinda CK, Seifert SN, Bushmaker T, Fischer RJ, van Doremalen N, Lloyd-Smith JO, Munster VJ: Effect of environmental conditions on SARS-CoV-2 stability in human nasal mucus and sputum. Emerging infectious diseases 2020, 26:2276-2278.

Shows effect of environmental conditions on the longevity of SARS-CoV-2 on surfaces

*[38] Pastorino B, Touret F, Gilles M, de Lamballerie X, Charrel RN: Prolonged infectivity of SARS-CoV-2 in fomites. Emerging infectious diseases 2020, 26:2256-2257.

Shows effect of solution conditions on the longevity of SARS-CoV-2 on surfaces

*[39] Harbourt DE, Haddow AD, Piper AE, Bloomfield H, Kearney BJ, Fetterer D, Gibson K, Minogue T: Modeling the stability of severe acute respiratory syndrome coronavirus 2 (SARS-CoV-2) on skin, currency, and clothing. PLoS neglected tropical diseases 2020, 14:e0008831.

Demonstrates longevity of SARS-CoV-2 on skin

[40] Kasloff SB, Leung A, Strong JE, Funk D, Cutts T: Stability of SARS-CoV-2 on critical personal protective equipment. Scientific reports 2021, 11:1-7.

[41] Kratzel A, Steiner S, Todt D, V'kovski P, Brueggemann Y, Steinmann J, Steinmann E, Thiel V, Pfaender S: Temperature-dependent surface stability of SARS-CoV-2. Journal of infection 2020, 81:452-482.

[42] Dos Santos RLO, Sarra G, Lincopan N, Petri DFS, Aliaga J, Marques MM, Dias RB, Coto NP, Sugaya NN, Paula CR: Preparation, Antimicrobial Properties, and Cytotoxicity of Acrylic Resins Containing Poly (diallyldimethylammonium chloride). The International Journal of Prosthodontics 2020, doi: 10.11607/ijp.6506.

[43] Muñoz-Bonilla A, Fernández-García M: Polymeric materials with antimicrobial activity. Progress in Polymer Science 2012, 37:281-339.

**[44] Hosseini M, Chin AW, Behzadinasab S, Poon LL, Ducker WA: Cupric Oxide Coating That Rapidly Reduces Infection by SARS-CoV-2 via Solids. ACS applied materials & interfaces 2021, 13:5919–5928.

Second paper to show a coating designed to inactivate SARS-CoV-2. Explains importance of porosity.

[45] Hasan J, Xu Y, Yarlagadda T, Schuetz M, Spann K, Yarlagadda PK: Antiviral and antibacterial nanostructured surfaces with excellent mechanical properties for hospital applications. ACS Biomaterials Science & Engineering 2020, 6:3608-3618.

[46] Moffett JW, Zika RG: Oxidation kinetics of Cu (I) in seawater: implications for its existence in the marine environment. Marine chemistry 1983, 13:239-251.

[47] Warnes SL, Keevil CW: Inactivation of norovirus on dry copper alloy surfaces. PloS one 2013, 8:e75017.

**[48] Sunada K, Minoshima M, Hashimoto K: Highly Efficient Antiviral and Antibacterial Activities of Solid-State Cuprous Compounds. Journal of hazardous materials 2012, 235:265-270.

Demonstrated effect of Cu_2O on a virus and explores mechanism

[49] Haynes CA, Norde W: Globular proteins at solid/liquid interfaces. Colloids and Surfaces B: Biointerfaces 1994, 2:517-566.

[50] Perevozchikova T, Nanda H, Nesta DP, Roberts CJ: Protein adsorption, desorption, and aggregation mediated by solid-liquid interfaces. Journal of pharmaceutical sciences 2015, 104:1946-1959.

[51] Kalb E, Frey S, Tamm LK: Formation of supported planar bilayers by fusion of vesicles to supported phospholipid monolayers. Biochimica et Biophysica Acta (BBA)-Biomembranes 1992, 1103:307-316.

[52] Liu Z, Xiao X, Wei X, Li J, Yang J, Tan H, Zhu J, Zhang Q, Wu J, Liu L: Composition and divergence of coronavirus spike proteins and host ACE2 receptors predict potential intermediate hosts of SARS-CoV-2. Journal of medical virology 2020, 92:595-601.

[53] Bianchi M, Benvenuto D, Giovanetti M, Angeletti S, Ciccozzi M, Pascarella S: Sars-CoV-2 Envelope and Membrane Proteins: Structural Differences Linked to Virus Characteristics? BioMed Research International 2020, 2020:4389089.

[54] Pezzotti G, Ohgitani E, Shin-Ya M, Adachi T, Marin E, Boschetto F, Zhu W, Mazda O: Instantaneous “catch-and-kill” inactivation of SARS-CoV-2 by nitride ceramics. Clinical and translational medicine 2020, 10:e.

[55] Bleichert P, Santo CE, Hanczaruk M, Meyer H, Grass G: Inactivation of bacterial and viral biothreat agents on metallic copper surfaces. Biometals 2014, 27:1179-1189.

[56] Gimenez R, Soler-Illia GJ, Berli CLA, Bellino MG: Nanopore-Enhanced Drop Evaporation: When Cooler or More Saline Water Droplets Evaporate Faster. ACS nano 2020, 14:2702-2708.

[57] Cai J, Yu B: A discussion of the effect of tortuosity on the capillary imbibition in porous media. Transport in porous media 2011, 89:251-263.

[58] Prat M: On the influence of pore shape, contact angle and film flows on drying of capillary porous media. Int J Heat Mass Transfer 2007, 50:1455-1468.

[59] Prat M: Pore network models of drying, contact angle, and film flows. Chemical engineering & technology 2011, 34:1029-1038.

[60] Metzger T, Irawan A, Tsotsas E: Influence of pore structure on drying kinetics: A pore network study. AIChE Journal 2007, 53:3029-3041.

[61] Metzger T, Tsotsas E: Influence of pore size distribution on drying kinetics: A simple capillary model. Drying Technology 2005, 23:1797-1809.

[62] Micochova P, Chadha A, Hesseloj T, Fraternali F, Ramsden JJ, Gupta RK: Rapid inactivation of SARS-CoV-2 by titanium dioxide surface coating. Wellcome Open Research 2021, 6:56.

[63] Heilingloh CS, Aufderhorst UW, Schipper L, Dittmer U, Witzke O, Yang D, Zheng X, Sutter K, Trilling M, Alt M: Susceptibility of SARS-CoV-2 to UV irradiation. American journal of infection control 2020, 48:1273-1275.

[64] Inagaki H, Saito A, Sugiyama H, Okabayashi T, Fujimoto S: Rapid inactivation of SARS-CoV-2 with deep-UV LED irradiation. Emerging Microbes & Infections 2020, 9:1744-1747.

[65] Khaiboullina S, Uppal T, Dhabarde N, Subramanian VR, Verma SC: Inactivation of Human Coronavirus by Titania Nanoparticle Coatings and UVC Radiation: Throwing Light on SARS-CoV-2. Viruses 2021, 13:19.

[66] Daeschler SC, Manson N, Joachim K, Chin AW, Chan K, Chen PZ, Tajdaran K, Mirmoeini K, Zhang JJ, Maynes JT: Effect of moist heat reprocessing of N95 respirators on SARS-CoV-2 inactivation and respirator function. Cmaj 2020, 192:E1189-E1197.

[67] Clavo B, Córdoba-Lanús E, Rodríguez-Esparragón F, Cazorla-Rivero SE, García-Pérez O, Piñero JE, Villar J, Blanco A, Torres-Ascensión C, Martín-Barrasa JL: Effects of ozone treatment on personal protective equipment contaminated with SARS-CoV-2. Antioxidants 2020, 9:1222.

[68] Chauhan P, Kumar A, Bhushan B: Self-cleaning, stain-resistant and anti-bacterial superhydrophobic cotton fabric prepared by simple immersion technique. Journal of Colloid and Interface Science 2019, 535:66-74.

[69] Galante AJ, Haghanifar S, Romanowski EG, Shanks RMQ, Leu PW: Superhemophobic and Antivirofouling Coating for Mechanically Durable and Wash-Stable Medical Textiles. ACS Applied Materials and Interfaces 2020, 12:22120-22128.

[70] Borkow G, Zhou SS, Page T, Gabbay J: A Novel Anti-Influenza Copper Oxide Containing Respiratory Face Mask. PLOS 2010, 5:e11295.

[71] Hewawaduge C, Senevirathne A, Jawalagatti V, Kim JW, Lee JH: Copper-impregnated three-layer mask efficiently inactivates SARS-CoV2. Environmental Research 2021, 196:110947.

[72] Kumar S, Karmacharya M, Joshi SR, Gulenko O, Park J, Kim GH, Cho YK: Photoactive Antiviral Face Mask with Self-Sterilization and Reusability. Nano Letters 2021, 21:337-343.

[73] Martí M, Tuñón-Molina A, Lillelund Aachmann F, Muramoto Y, Noda T, Takayama K, Serrano-Aroca Á: Protective Face Mask Filter Capable of Inactivating SARS-CoV-2, and Methicillin-Resistant Staphylococcus aureus and Staphylococcus epidermidis. Polymers 2021, 13:207.

Chapter 11. Conclusions and Future Work

11.1. Conclusions

Seven antimicrobial coatings were prepared using simple methods and low-cost materials. For widespread applicability of the coatings, the methodologies were developed so that the final implementation by the consumer required little technical knowledge. The coatings had a variety of properties: they were porous or non-porous, transparent or opaque, and hydrophilic or hydrophobic, while they were all highly antimicrobial, robust, and easy-to-prepare. A wide range of desired properties were achieved with this suite of coatings.

To fabricate each coating, an organic adhesive layer was used along with inorganic antimicrobial ingredients. The adhesive layer was polyurethane or polydopamine and the active ingredients were copper, cuprous oxide (Cu_2O), or zinc oxide (ZnO). The coatings kill or inactivate drug-resistant bacteria, fungi, mycobacteria, and viruses rapidly.

This dissertation also investigated the transfer of COVID-19 virus from inanimate surfaces to fingers. Also, the opportunities and challenges in the field of antimicrobial surface coatings were discussed in detail.

11.2. Future Work

This work is composed of research that showed a porous antimicrobial coating kill 99.9% of drug-resistant bacteria in 3 minutes. Naturally, further improvement of the kill period is an interesting subject matter. The author of this dissertation suggests researching other methods to kill bacteria more rapidly. In brief, a porous coating with different pore sizes than what was used in this dissertation has a high potential to achieve a shorter kill time of than three minutes. Other porous coatings can be easily fabricated using heat treatment of PMMA particles as was shown in this work.[1] Different particles sizes can be used to achieve various pore sizes, and other polymer particles, such as polystyrene (PS) or polyethylene (PE), are available for this purpose.

Another effective method for preparing various porous scaffolds involves combining elastomers with sacrificial particles, curing the elastomer via heat treatment, and then dissolving the sacrificial particles with an appropriate solvent. Several commercially available elastomers, including SYLGARD 184 or 527,[2] can be easily incorporated, and inorganic materials are a suitable choice for the sacrificial particles. Inorganic particles with a range of nano- or micro-sized diameters can be obtained commercially. The author suggests using salt particles such as NaCl crystals because they are inexpensive, widely available, safe, and rapidly soluble in water.

Additionally, antimicrobial coatings can be made by utilizing other antimicrobial ingredients. Iodine, for example, is known to possess excellent antimicrobial properties that can be exploited against a wide range of bacteria, fungi, viruses, and more. Through addition of polyvinylpyrrolidone-idodine (PVP-I) to porous scaffolds, an effective and easily prepared antimicrobial coating can be fabricated. As this dissertation demonstrated,[1] the presence of porosity will greatly increase antimicrobial activity of an active ingredient. Therefore, it is

anticipated that the addition of iodine to a porous scaffold will increase its effectivity. For further practicality, iodine can be incorporate into a porous wrap in a manufacturing environment where the adhesive backing of the wrap simplifies the process of creating antimicrobial surfaces.[3]

Furthermore, the contact killing mechanism of action of copper or cuprous oxide surfaces can be further investigated. In particular, in-situ and time-resolved killing of pathogens by surface coatings are missing from the current literature. Therefore, such characterization of the interaction between bacterial or viral cells and an active surface (such as copper) is an exciting avenue of experiments and it can further improve our understanding of the mechanism. Such experiments will demonstrate how different parts of bacterial cells are affected by an antimicrobial coating. In-situ imaging techniques, such as SEM, along with EDS, and other X-ray-based elemental analyses methods can be beneficial for this goal.

Pathogens that contaminate water sources can pose a significant threat to human health. *Escherichia coli (E. coli)*, for example, is a bacterium that commonly spreads via contaminated drinking water. Also, it has been reported[4] that non-tuberculous mycobacteria (NTM) infections occurred in patients in some operation rooms where heater-cooler units were employed during the surgery. The bacteria biofilms were traced to the water reservoir of the machines. An antimicrobial filter has the potential to rapidly inactivate or kill pathogens in various circumstances, including those mentioned above. As this dissertation discussed, copper or cuprous oxide are excellent antimicrobials with a broad range of activity against various types of germs.[1, 3, 5-7] Copper can be added to a stainless-steel filter using the same process that was employed in producing antimicrobial porous coatings in this work. This process involves preparing a polydopamine (PDA) layer followed by electroless deposition of copper,[1, 7] which will result in the development of a highly effective antimicrobial filter.

REFERENCES

(1) Behzadinasab, S.; Williams, M. D.; Aktuglu, M.; Falkinham III, J. O.; Ducker, W. A. Porous Antimicrobial Coatings for Killing Microbes within Minutes. *ACS Appl. Mater. Interfaces* **2023,** *15* (12), 15120–15128, DOI: https://doi.org/10.1021/acsami.2c22240.

(2) Behzadinasab, S.; Chin, A. W. H.; Hosseini, M.; Poon, L. L. M.; Ducker, W. A. Sars-Cov-2 Virus Transfers to Skin through Contact with Contaminated Solids. *Sci. Rep.* **2021,** *11* (1), 22868, DOI: https://doi.org/10.1038/s41598-021-00843-0.

(3) Behzadinasab, S.; Williams, M. D.; Falkinham III, J. O.; Ducker, W. A. Facile Implementation of Antimicrobial Coatings through Adhesive Films (Wraps) Demonstrated with Cuprous Oxide Coatings. *submitted* **2023**.

(4) Falkinham III, J. Disinfection and Cleaning of Heater–Cooler Units: Suspension-and Biofilm-Killing. *J. Hosp. Infect.* **2020,** *105* (3), 552-557.

(5) Behzadinasab, S.; Chin, A.; Hosseini, M.; Poon, L.; Ducker, W. A. A Surface Coating That Rapidly Inactivates Sars-Cov-2. *ACS Appl. Mater. Interfaces* **2020,** *12* (31), 34723-34727, DOI: https://doi.org/10.1021/acsami.0c11425.

(6) Behzadinasab, S.; Hosseini, M.; Williams, M.; Ivester, H.; Allen, I.; Falkinham III, J.; Ducker, W. Antimicrobial Activity of Cuprous Oxide-Coated and Cupric Oxide-Coated Surfaces. *J. Hosp. Infect.* **2022,** *129*, 58-64, DOI: https://doi.org/10.1016/j.jhin.2022.07.022.

(7) Behzadinasab, S.; Williams, M. D.; Hosseini, M.; Poon, L. L.; Chin, A. W.; Falkinham III, J. O.; Ducker, W. A. Transparent and Sprayable Surface Coatings That Kill Drug-Resistant

Bacteria within Minutes and Inactivate Sars-Cov-2 Virus. *ACS Appl. Mater. Interfaces* **2021,** *13* (46), 54706-54714, DOI: https://doi.org/10.1021/acsami.1c15505.